

EVEN-D CARBON NANOSTRUCTURES
FOR SENSING AND ENERGY
APPLICATIONS

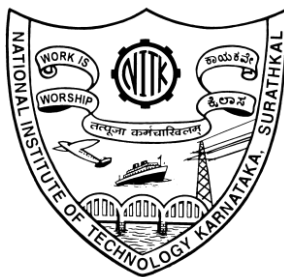
Thesis

Submitted in partial fulfilment of the requirements for the
degree of

DOCTOR OF PHILOSOPHY

by

PRAVEEN MISHRA



DEPARTMENT OF CHEMISTRY
NATIONAL INSTITUTE OF TECHNOLOGY KARNATAKA
SURATHKAL, MANGALURU – 575025
JANUARY, 2020

This Thesis is dedicated

to my family, Naniji



...In the memory of my Dadaji

DECLARATION

I hereby *declare* that the Research Thesis entitled **Even-D Carbon Nanostructures for Sensing and Energy Applications** which is being submitted to the **National Institute of Technology Karnataka, Surathkal** in partial fulfilment of the requirements for the award of the Degree of **Doctor of Philosophy in Chemistry** is a *bonafide report of the research work carried out by me*. The material contained in this Research Thesis has not been submitted to any University or Institution for the award of any degree.

Praveen Mishra

Reg. No.: 155111CY15F05

Department of Chemistry

Place: NITK, Surathkal

Date:

C E R T I F I C A T E

This is to *certify* that the Research Thesis entitled **Even-D Carbon Nanostructures for Sensing and Energy Applications** submitted by **Praveen Mishra (Register Number: 155111CY15F05)** as the record of the research work carried out by him, is *accepted as the Research Thesis submission* in partial fulfilment of the requirements for the award of degree of **Doctor of Philosophy**.

Research Guide

Chairman – DRPC

ACKNOWLEDGEMENT

This journey to realize a life-long dream of obtaining Ph.D. degree would not have been possible without the support of many individuals who have been there in my thick and thin. In that sense, this journey has also been theirs as it is mine. In this short space, I wish to acknowledge that support which made this dream possible for me.

As it is said that a great teacher makes good student. The role of a research supervisor is of paramount importance for shaping the Ph.D. degree. Therefore, it is my duty to acknowledge the ever supporting and generous Prof. B. Ramachandra Bhat for being a constant source of everlasting support and inspiration. His insightfulness, guidance, patience and thoughtfulness have always been conveyed and induced positively by our research group. It has been a fortune to have him as an advisor and to have freedom to explore and evaluate the ideas. I have great admiration towards him for being a wonderful teacher and above all a great human being.

I am grateful to my RPAC members Prof. A. Vasudeva Adhikari, Dept. of Chemistry, Prof. Subba Rao, Dept. of Applied Mechanics, and Prof. M. K. Nagaraj, Dept. of Applied Mechanics. Their encouragement, perceptive comments and fruitful discussions throughout the progress of my research work have been success driving factors towards accomplishment of my objectives.

I would like to thank Prof. A. M. Isloor and Prof. D. Krishna Bhat who have extended administrative facility for my Ph.D. work in their tenure as the Head of the Department of Chemistry.

I am thankful to the National Institute of Technology Karnataka, Surathkal for providing an opportunity to conduct my research work and faculty members of the chemistry department for their good wishes.

I am thankful to the kind assistance of IUAC New Delhi, IISc Bengaluru, MNIT Jaipur, Sharda University Greater Noida, Dept. of Physics and Dept. of Metallurgy and Materials Engg. NITK Surathkal, for extending their sophisticated experimental and characterization facilities.

I am grateful to the all the non-teaching staff of the Dept. of Chemistry, NITK Surathkal for extending their kind assistance and made the time spent in the department comfortable. I wish to state special gratitude to Mrs. Shamila Nandini for her care and help in all the official matter without fail.

The research tenure can be hectic if not for the enthusiastic team of lab mates to cheer you up. I would acknowledge a very supportive team of fellow research scholars, Dr. Pooja Bhat, Dr. Raghavendra Prasad, Dr. Lolakshi Mahesh Kumar, Dr. Ansari Rashida Bano Maqbool Hasan, Ms. Anuma Saroja, and Mr. Madhu N. Nimbalkar for their company during my Ph.D. tenure and being steady support throughout the course of Ph.D. I cannot leave to thank my supportive friends within and outside the department, and few more for being there as constant source of joy and support.

I would like to express an extreme sense of gratefulness to my family members, especially my parents.

Finally, I conclude with an abundance of thanks to all those who have helped me directly or indirectly in making this dissertation a possibility.

A handwritten signature in cursive script that reads "Praveen". The signature is written in black ink and is positioned above the printed name.

PRAVEEN MISHRA

ABSTRACT

The thesis titled “*Even-D Carbon Nanostructures for Sensing and Energy Applications*” encompass the work on Even-D carbon nanostructures, particularly graphene and graphene quantum dots for the prospective use as materials for sensors and photovoltaic devices. A new route to obtain the quantum dot by bombarding the graphene oxide (GO) sheets with the swift heavy ions is discussed. The graphene quantum dots (GQD) in their native state were found to be highly useful in determining the metal cations like Ca^{2+} , Cu^{2+} , and Co^{2+} . The determination of Ca^{2+} ions in the water was quantitatively possible in the presence of interfering ions such as Al^{3+} , Na^+ , and K^+ . However, the detection of transition metals with GQD remains only qualitatively feasible, because transition metals non-selectively quench the PL of GQD. The amine functionalized GQD ($\text{NH}_2\text{-GQD}$) made the quantitative determination of glucose possible via aggregation induced photoluminescence enhancement with an accuracy of 98%. The $\text{NH}_2\text{-GQD-GO}$ composite proved to be an active material for the electrochemical determination of oxalic acid within 0.5 mM to 55 mM and a limit of detection of 50 μM . The $\text{NH}_2\text{-GQD}$ were also demonstrated to be an excellent co-sensitizer for the hybrid quantum dot solar cell when used in conjunction with anthocyanin dye. The photosensitizer combination improved the photon conversion efficiency by ~50%. Significant raise in other parameters was also observed. The work presented in this thesis demonstrates the utilization of the excited electron resulted by the electromagnetic irradiation on the GQD. It is evident that the energy emitted by the electron returning to the ground state is utilized for photoluminescent detection of various analytes. The extraction of excited electron through electrochemical means resulted in making GQD based electrochemical sensors and co-sensitizers in the photovoltaic devices.

Keywords: Analytical Chemistry, Carbon Nanostructures, Sensors, Photovoltaics, Electrochemistry, Photoluminescence.

TABLE OF CONTENTS

LIST OF FIGURES	vii
LIST OF TABLES	xiii
LIST OF ABBREVIATIONS	xv
CHAPTER 1	1
INTRODUCTION	1
1.1 NANOMATERIALS	1
1.2 CARBON NANOSTRUCTURES	2
1.2.1 2D Carbon Nanostructures	3
1.2.2 1D Carbon Nanostructures	6
1.2.3 0D Carbon Nanostructures	8
1.3 APPLICATIONS OF CARBON NANOSTRUCTURES	10
1.3.1 Sensors	10
1.3.2 Devices for Energy Applications	15
1.4 VISION	22
CHAPTER 2	25
STATE OF THE ART	25
2.1 ADVANCES IN GRAPHENE	27
2.1.1 Graphene as Sensors:	28
2.1.2 Graphene in Photovoltaics	31
2.2 ADVANCES IN GRAPHENE QUANTUM DOTS	34
2.2.1 Synthesis of GQD	34
2.2.2. GQD as Sensors	38
2.2.3 GQD in Photovoltaics	43
2.3 SUMMARY OF LITERATURE REVIEW	47

2.4 PROPOSED WORK.....	48
2.4.1 Motivation.....	48
2.4.2 Objectives	49
CHAPTER 3	51
SYNTHESIS AND CHARACTERIZATION OF GRAPHENE QUANTUM DOTS AND THEIR SIZE REDUCTION USING SWIFT HEAVY ION BEAM.....	51
3.1 INTRODUCTION	53
3.2 EXPERIMENTAL.....	54
3.2.1 Materials	54
3.2.2 Synthesis of Graphene Quantum Dots.....	54
3.2.3 Characterizations.....	55
3.3 RESULTS AND DISCUSSION.....	55
3.4 CONCLUSIONS.....	61
CHAPTER 4	63
ELECTROCHEMICAL REDUCTION OF AMINO-FUNCTIONALIZED GRAPHENE QUANTUM DOTS IMMOBILIZED ON GRAPHENE OXIDE FOR THE DETECTION OF OXALIC ACID	63
4.1 INTRODUCTION	65
4.2 EXPERIMENTAL.....	66
4.2.1 Synthesis of amino functionalized GQDs.....	66
4.2.2 Fabrication of Electrode.....	67
4.2.3 Material Characterization.....	67
4.3 RESULTS AND DISCUSSIONS.....	68
4.3.1 Characterization of GO and GQDs.....	68
4.3.2 Electrochemical sensing of oxalic acid:.....	74
4.3.3 Determination of Oxalic acid in Real Sample	86

4.4 CONCLUSIONS.....	86
CHAPTER 5	89
PHOTOLUMINESCENCE QUENCHING IN METAL ION (Cu^{2+} , Co^{2+}) INTERACTED GRAPHENE QUANTUM DOTS	89
5.1 INTRODUCTION	91
5.2 EXPERIMENTAL.....	91
5.2.1 Synthesis of Graphene Quantum Dots (GQD)	91
5.3 RESULTS AND DISCUSSION	92
5.4 CONCLUSIONS.....	97
CHAPTER 6	99
CALCIUM-INDUCED PHOTOLUMINESCENCE QUENCHING OF GRAPHENE QUANTUM DOTS IN HARD WATER: A QUICK TURN-OFF SENSING APPROACH.....	99
6.1 INTRODUCTION	101
6.2 EXPERIMENTAL SECTION	102
6.2.1 Synthesis of GQD:	102
6.2.2 Determination of Ca^{2+} in aqueous media.....	102
6.3 RESULTS AND DISCUSSION	103
6.4 CONCLUSIONS.....	116
CHAPTER 7	117
GRAPHENE QUANTUM DOTS WITH NITROGEN-RICH EDGES AS PL-TURN- ON SENSOR FOR GLUCOSE	117
7.1 INTRODUCTION	119
7.2 EXPERIMENTAL.....	120
7.2.1 Synthesis of NH_2 - GQD.....	120
7.2.2 Material Characterization.....	121

7.2.3 Determination of Glucose	121
7.3 RESULTS AND DISCUSSION	122
7.3.1 Characterization of GQD and NH ₂ -GQD	122
7.3.2 Mechanism of Aggregation induced photoluminescence emission in glucose-NH ₂ -GQD system	130
7.3.3 A Comparison of UV-Vis Absorbance and PL Emission Method on Determination of Glucose	131
7.3.4 Accuracy of the Determination of Glucose	138
7.3.5 Selectivity of Sensing methods	140
7.3.6 Determination of Glucose in Real Samples	142
7.4 CONCLUSIONS.....	143
CHAPTER 8	145
SYNTHESIS AND CHARACTERIZATION OF AMINE FUNCTIONALIZED GRAPHENE QUANTUM DOTS AS CO-SENSITIZER FOR HYBRID QUANTUM DOT SOLAR CELLS	145
8.1. INTRODUCTION	147
8.2. Experimental	148
8.2.1 Synthesis of NH ₂ -GQD.....	148
8.2.2 Extraction of Dye and Formulation of Sensitizer	148
8.2.3 Fabrication of the QDSC	148
8.3 RESULTS AND DISCUSSION	150
8.3.1 Characterization of NH ₂ -GQD.....	150
8.3.2 Absorbance and Emission spectra of Sensitizers.....	152
8.3.3 Characterization of Photovoltaic Cells	154
8.4 CONCLUSIONS.....	156
CHAPTER 9	157

SUMMARY AND CONCLUSIONS	157
9.1 SUMMARY OF RESEARCH WORK.....	159
9.2 CONCLUSIONS.....	165
9.3 FUTURE WORK.....	166
REFERENCES	167
PUBLICATIONS.....	191
LIST OF JOURNAL PUBLICATIONS	191
LIST OF CONFERENCES	192
LIST OF WORKSHOPS	193
CURRICULUM VITAE.....	195

LIST OF FIGURES

CHAPTER 1

Figure 1.1 Graphene as primary building block of carbon nanostructures (Geim and Novoselov 2007).....	4
Figure 1.2 Single and multi-walled carbon nanotubes.....	7
Figure 1.3 Schematic diagram of an electrochemical Sensor device.....	14
Figure 1.4 Band gaps of conventional semiconducting materials.	17
Figure 1.5 Efficiencies of Existing PV cells (Source: NREL, USA).....	19
Figure 1.6 Band diagram of the components of quantum dot solar cell.	21
Figure 1.7 A typical construction of quantum dot solar cell.....	21

CHAPTER 3

Figure 3.1 Synthesis of Graphene Quantum Dots using Swift Heavy Ion Beam.	54
Figure 3.2 XRD spectrum of graphene oxide	56
Figure 3.3 XRD spectrum of graphite.....	56
Figure 3.4 Transmission electron microscopic image of graphene oxide.....	57
Figure 3.5 Transmission electron microscopic image of HGQD.....	57
Figure 3.6 Transmission electron microscopic image of IGQD	58
Figure 3.7 FTIR spectra of graphite, HGQD and IGQD	59
Figure 3.8 UV-Vis spectra of HGQD and IGQD.....	59
Figure 3.9 PL spectra of HGQD and IGQD.....	60

CHAPTER 4

Figure 4.1 XRD spectrum of graphene oxide	68
Figure 4.2 Transmission electron microscopic image of graphene oxide.....	69
Figure 4.3 FTIR spectra of graphite, graphene oxide, and GQD	69
Figure 4.4 FTIR spectra of GQD and NH ₂ -GQD-GO	70
Figure 4.5 Raman spectrum of GQD obtained at incident wavelength of 514 nm.....	72
Figure 4.6 Transmission electron microscopic image of NH ₂ -GQD	73

Figure 4.7 Particle size analysis of NH ₂ -GQD (Inset: Particle size of distribution of NH ₂ -GQD from TEM).....	74
Figure 4.8 Cyclic voltogram of GQD, NH ₂ -GQD, and NH ₂ -GQD-GO	75
Figure 4.9 Cyclic voltogram of GQD with and without the addition of 0.2 M oxalic acid.....	75
Figure 4.10 Cyclic voltogram of NH ₂ -GQD with and without the addition of 0.2 M oxalic acid.....	76
Figure 4.11 Cyclic voltogram of GO with and without the addition of 0.2 M oxalic acid.....	76
Figure 4.12 Cyclic voltogram of NH ₂ -GQD/GO with and without the addition of 0.2 M oxalic acid.....	77
Figure 4.13 Plausible mechanism of binding between NH ₂ -GQD and oxalic acid and subsequent electro-reduction at E _{red} = -0.6 V	79
Figure 4.14 Cyclic voltogram of NH ₂ -GQD-GO with addition of variable concentration of oxalic acid.....	80
Figure 4.15 Variation of cathodic current density within 0.01 - 2 mM of oxalic acid.....	81
Figure 4.16 The linear variation of the current density between 0.5 – 2.0 mM of oxalic acid.....	82
Figure 4.17 Variation of cathodic current density within 0.01 - 55 mM of oxalic acid	82
Figure 4.18 The linear variation of the current density between 2.0 - 55 mM concentration of oxalic acid.....	83
Figure 4.19 Chronoamperometric response of NH ₂ -GQD-GO on addition of 0.2 mM oxalic acid.....	84
Figure 4.20 Variation in cathodic current density on addition of oxalic acid, uric acid, and glucose.....	85

CHAPTER 5

Figure 5.1 A graphical representation of synthesis procedure.....	92
Figure 5.2 XRD spectrum of graphene oxide (Inset: XRD spectrum of graphite)	93

Figure 5.3 FTIR spectra of GQD, Co ²⁺ interacted GQD, and Cu ²⁺ interacted GQD..	94
Figure 5.4 Fingerprint region of GQD, Co ²⁺ interacted GQD, and Cu ²⁺ interacted GQD.	94
Figure 5.5 UV-Vis spectra of GQD, Co ²⁺ interacted GQD, and Cu ²⁺ interacted GQD.	95
Figure 5.6 PL spectra of GQD, Co ²⁺ interacted GQD, and Cu ²⁺ interacted GQD at 365 nm excitation.....	96
Figure 5.7 GQD, Co ²⁺ interacted GQD, and Cu ²⁺ interacted GQD under 365 nm.	96

CHAPTER 6

Figure 6.1 A schematic of the synthesis of graphene quantum dots and its subsequent quenching of photoluminescence in hard water.....	104
Figure 6.2 XRD spectrum of graphene oxide	105
Figure 6.3 FTIR spectra of graphite, graphene oxide, and GQD	105
Figure 6.4 FTIR spectra of the fingerprint region of GQD and Ca-GQD	106
Figure 6.5 Raman spectrum of GQD.	106
Figure 6.6 Transmission electron microscopic image of GQD and their size distribution (inset)	108
Figure 6.7 UV absorbance spectra of GQD and Ca-GQD.....	108
Figure 6.8 PL emission spectra of GQD and Ca-GQD.....	109
Figure 6.9 The variation of photoluminescence of GQD in solutions containing 0 μM to 250 μM Ca ²⁺ ions under 375 nm irradiation.....	111
Figure 6.10 Variation of the photoluminescence intensities of GQD at different concentrations of Ca ²⁺ ions.....	111
Figure 6.11 Linear variation of the photoluminescence quenching of GQD at different concentrations of Ca ²⁺	112
Figure 6.12 The expected and observed photoluminescence of various test samples of Ca ²⁺ ion as detected by GQD under 375 nm irradiation.....	113
Figure 6.13 The selectivity of photoluminescence quenching of GQD towards Ca ²⁺ in the presence of other common cations found in hard water.	114

CHAPTER 7

Figure 7.1 FTIR spectra of GQD and NH ₂ -GQD.	123
Figure 7.2 Deconvoluted peaks of N-H and O-H stretching in NH ₂ -GQD.	123
Figure 7.3 Raman spectrum of NH ₂ -GQD.....	124
Figure 7.4 XPS survey scan of NH ₂ -GQD.....	125
Figure 7.5 XPS C specific scan of NH ₂ -GQD.	126
Figure 7.6 XPS N specific scan of NH ₂ -GQD.....	126
Figure 7.7 XPS O specific scan of NH ₂ -GQD.....	127
Figure 7.8 Transmission electron microscopic image of NH ₂ -GQD (Inset: Size distribution).....	128
Figure 7.9 Transmission electron microscopic image of NH ₂ -GQD aggregated along glucose (Inset: Size distribution).	128
Figure 7.10 UV-Vis and photoluminescence spectra of NH ₂ -GQD recorded within 250 - 650 nm and 420 - 650 nm, respectively. The photoluminescence spectrum was recorded for incident electromagnetic wave of wavelength 380 nm.	129
Figure 7.11 The plausible mode of interaction between NH ₂ -GQD and glucose in 2:1 stoichiometric ratio in aggregated quantum dot.....	131
Figure 7.12 The variation on the UV-Vis absorbance spectra of NH ₂ -GQD at varying concentrations of glucose (0.1 mM to 500 mM).....	133
Figure 7.13 The variation of UV-Vis absorbance at 260 nm for varying concentrations of glucose (0.1 mM to 500 mM).....	133
Figure 7.14 The variation of UV-Vis absorbance at 260 nm for varying concentrations of glucose (0.1 mM to 10 mM).....	134
Figure 7.15 The variation of UV-Vis absorbance at 260 nm for varying concentrations of glucose (50 mM to 500 mM).....	134
Figure 7.16 The variation on the photoluminescence spectra of NH ₂ -GQD at varying concentrations of glucose (0.1 mM to 500 mM).....	136
Figure 7.17 The variation of photoluminescence intensity at 480 nm for varying concentrations of glucose (0.1 mM to 500 mM).....	136
Figure 7.18 The variation of photoluminescence intensity at 480 nm for varying concentrations of glucose (0.1 mM to 10 mM).....	137

Figure 7.19 The variation of photoluminescence intensity at 480 nm for varying concentrations of glucose (50 mM to 500 mM).....	137
Figure 7.20 Determination of C_{glucose} in test sample 1 (3 mM), test sample 2 (7 mM) and test sample 3 (9 mM) using UV-Vis absorption calibration curve and PL intensity calibration curve.....	139
Figure 7.21 Determination of C_{glucose} in test sample 4 (90 mM), test sample 5 (180 mM), and test sample 6 (400 mM) using UV-Vis absorption calibration curve and PL intensity calibration curve.....	139
Figure 7.22 Average % Error for determination of C_{glucose} using UV-Vis absorption calibration curve and PL intensity calibration curve within the range of 0.1 – 10 mM and 50 – 500 mM.	140
Figure 7.23 Relative absorbance of glucose in comparison to various sugars (10 mM).	141
Figure 7.24 Relative photoluminescence intensity of glucose in comparison to various sugars (10 mM).	141

CHAPTER 8

Figure 8.1 Schematic representation of the use of anthocyanin dye and $\text{NH}_2\text{-GQD}$ as photosensitizer in a hybrid quantum dot sensitized solar cell.....	149
Figure 8.2 XRD Spectrum of graphene oxide.....	150
Figure 8.3 TEM image of $\text{NH}_2\text{-GQD}$ (Inset: SED of $\text{NH}_2\text{-GQD}$, Particle size distribution, Image of Blue emission of $\text{NH}_2\text{-GQD}$).	150
Figure 8.4 FTIR spectra of graphite, graphene oxide, GQD, and $\text{NH}_2\text{-GQD}$	151
Figure 8.5 Cyclic voltogram of GQD and $\text{NH}_2\text{-GQD}$	151
Figure 8.6 Absorbance spectra of dye, GQD, $\text{NH}_2\text{-GQD}$, and $\text{NH}_2\text{-GQD/Dye}$ mixture.	153
Figure 8.7 PL spectra of dye, GQD, $\text{NH}_2\text{-GQD}$, and $\text{NH}_2\text{-GQD/Dye}$ mixture	154
Figure 8.8 JV and output power curve of DSSC and $\text{NH}_2\text{-GQD/dye}$ sensitized hybrid QDSC.....	155

CHAPTER 9

Figure 9.1 A schematic representation of synthesis of GQD using swift heavy ions.	160
Figure 9.2 Photoluminescent quenching of the GQD on interaction with metal ions.	161
Figure 9.3 The detection of Ca^{2+} in presence of interfering ions using GQD.	161
Figure 9.4 Intensification of photoluminescence of $\text{NH}_2\text{-GQD}$ by aggregation in presence of glucose.	162
Figure 9.5 A schematic representation of oxalic acid sensing using $\text{NH}_2\text{-GQD-GO}$ composite.	163
Figure 9.6 Anthocyanin and $\text{NH}_2\text{-GQD}$, a co-sensitization approach to hybrid quantum dots solar cells.	164

LIST OF TABLES

CHAPTER 4

Table 4.1 The parameter of NH₂-GQD-GO/GC electrode for electrochemical determination of oxalic acid in comparison to other electrodes reported in literature. 84

CHAPTER 6

Table 6.1 The photoluminescence measurements and the calculated strength of the test samples of Ca²⁺ ions. 114

Table 6.2 Comparison of the reported sensing method for Ca²⁺ ions with other methods. 115

CHAPTER 7

Table 7.1 Graphene Quantum Dots for PL detection of glucose. 142

CHAPTER 8

Table 8.1 Photoemission parameters of NH₂-GQD 153

Table 8.2 Solar cell parameters. 155

CHAPTER 9

Table 9.1 Performance of GQD and modified GQD composites as sensors for various analytes. 163

LIST OF ABBREVIATIONS

AFM	: Atomic Force Microscopy
ATR	: Attenuated Total Reflectance
BCP	: Block Co-polymer
B-GQD	: Boron doped graphene quantum dots
BHJ	: Bulk Heterojunction
BSA	: Blood Serum Albumin
CA	: Chronoamperometry
Ca-GQD	: Calcium bound graphene quantum dots
CCE	: Carbon Ceramic Electrode
CNT	: Carbon Nanotubes
CQD	: Carbon Quantum Dots
CV	: Cyclic Voltammetry
CVD	: Chemical Vapor Deposition
DFT	: Density Functional Theory
DMF	: Dimethylformamide
DNA	: Deoxyribonucleic Acid
DSSC	: Dye Sensitized Solar Cell
E_{Red}	: Reduction Potential
FET	: Field Effect Transistor
FF	: Fill Factor
FLG	: Few Layer Graphene
FTIR	: Fourier Transformed Infra-red
GCE	: Glassy Carbon Electrode

GNR	: Graphene Nanoribbons
GO	: Graphene Oxide
GOx	: Glucose Oxidase
GQD	: Graphene Quantum Dots
HGQD	: Hydrothermally obtained Graphene quantum dots
HOMO	: Highest Unoccupied Molecular Orbital
HOPG	: Highly Oriented Pyrolytic Graphite
IGQD	: Ion beam irradiated Graphene quantum dots
I _{sc}	: Short Circuit Current
ITO	: Indium Tin Oxide
LUMO	: Lowest Unoccupied Molecular Orbital
MLG	: Multi-layer Graphene
MWCNT	: Multiwalled Carbon Nanotubes
NADH	: Nicotinamide adenine dinucleotide
N-GQD	: Nitrogen doped graphene quantum dots
NH ₂ -GQD	: Amine functionalized Graphene Quantum Dots
NH ₂ -GQD-GO	: Amine functionalized Graphene Quantum Dots and Graphene Oxide Composite
NIR	: Near Infra-red
NP	: Nanoparticles
NREL	: National Renewable Energy Laboratory
P3HT	: poly(3-hexylthiophene)
PBASE	: pyrene buanoic acid succidymidyl ester
PCBM	: [6, 6]-phenyl-C ₆₁ -butyric acid methyl ester
PCE	: Photon Conversion Efficiency

PEDOT	: poly(3,4-ethylenedioxythiophene)
PL	: Photoluminescence
P_{\max}	: Maximum Power Output
PSS	: poly(styrene sulfonate)
PV	: Photovoltaic
QD	: Quantum Dots
QDSC	: Quantum Dot Solar Cell
rGO	: Reduced Graphene Oxide
R_s	: Sheet Resistance
S-GQD	: Sulphur doped Graphene Quantum Dots
ssDNA	: Single-strand Deoxyribonucleic Acid
STM	: Scanning Tunneling Microscopy
SWCNT	: Single-walled Carbon Nanotubes
TCE	: Transparent Conductive Electrodes
TEM	: Transmission Electron Microscopy
TiO_x	: Titanium Suboxide
TNA	: TiO_2 Nanotube Arrays
UV	: Ultraviolet
UV-Vis	: Ultraviolet-Visible
V_{\max}	: Maximum Voltage Output
V_{OC}	: Open Circuit Voltage
XPS	: X-ray Photoelectron Spectroscopy
XRD	: X-ray Diffraction
ϕ_G	: Work-function of Graphene

CHAPTER 1

INTRODUCTION

Abstract: This chapter provides a brief introduction of carbon nanomaterials and their applications in sensors and photovoltaic devices

1.1 NANOMATERIALS

“There is plenty of room at the bottom”

- Richard Feynman

When Richard Feynman spoke these words at Caltech in an American Physical Society Meeting held on December 29, 1959, he laid foundation to the investigation of world of smalls.

The word “nano” originated from the Greek word “nanos” meaning dwarf. The word “nano” in science and technology indicate the number 10^{-9} , i.e., one billionth of any unit. To really appreciate the field of nanotechnology, we need to have a look at the scale being discussed in the thesis.

Nanomaterials are materials with size in any one spatial direction within 1-100 nm and their property being markedly different from that of bulk.

There are Web sites like <http://htwins.net/scale2/> that allow the user to zoom in from astronomical scales to subatomic scales by stepping through factors of 10.

The invention of the scanning tunneling microscope (STM) in the year 1981 sprang the field of nanoscience and technology into motion. This invention enabled us to image and manipulate atoms. A great challenge thus far was that existing nanoscale imaging techniques were limited to the conducting material. In 1986, the invention of Atomic Force Microscopy (AFM) extended reach to insulating materials as well.

Based on above information, assuming nanomaterials came into existence only recently would be erroneous. Nanomaterials have been around us since the time we are on earth as a species and even before. They can be found in various forms in nature be it biomolecules like deoxyribonucleic acid (DNA), Proteins, and lipids to minerals like zeolites. Even before the concept of nanomaterials, we were using it. Few such examples are the ancient artefact like Lycurgus cup from 4th century Rome and Michael

Faraday's colloidal gold. It took recent advances in imaging technology which revealed the true nature of those materials.

A major distinction between various types of nanomaterials is their dimensionality. As the name suggests, the properties of nanomaterials are caused due to their dimensions. Hence, it is logical to characterize nanomaterials based on their dimensionality. In this context, we can characterize nanomaterials in three categories:

- 0D Nanomaterials
- 1D Nanomaterials
- 2D Nanomaterials

Dimensionality of the nanomaterials are determined under various criteria depending on the intended use. For simplicity, we will limit the discussion with respect to the electronic or to be more precise excitonic (exciton is an electron-hole pair in semiconductor) applications of the nanomaterials. Thus, dimensionality of the nanomaterials is the number of dimensions, electrons or excitons can move. Hence, it becomes more akin a particle in a box situation. Thus, we can define nanoparticles as:

1. 0D Nanomaterials: Nanomaterials in which electronic or excitonic movement is restricted in all the three-translational dimension.
2. 1D Nanomaterials: Nanomaterials in which electronic or excitonic movement is restricted in any two of the three-translational dimension.
3. 2D Nanomaterials: Nanomaterials in which electronic or excitonic movement is restricted in any one of the three-translational dimension.

Carbon nanostructure in such reference are no different and can well be defined under the same guidelines. Different carbon nanostructures which are of specific concern to the proposed work are explored in further sections.

1.2 CARBON NANOSTRUCTURES

Carbon is the second and fourth most abundant element (by mass) in the human body and universe, respectively. Carbon is also the chemical basis of all the known life forms on earth. Therefore, carbon-based materials can be an ecological friendly and sustainable solution for countless applications. Outstanding properties of carbon such

as chemical and physical stability, diverse hybridizations, catenation, ability to form strong covalent bond, and ease of compounds formation has attracted widespread scientific interest. Last 3 decades have witnessed exponential advances in the study of carbon compounds and nanostructures. Discovery of Fullerenes in 1985 (Kroto *et al.* 1985) and publications by the Sumio Iijima on single-wall carbon nanotubes in 1993 (Iijima and Ichihashi 1993) took the research into a “new era” for nanostructures materials. Kroto was awarded the 1996 Nobel Prize in Chemistry for the discovery of fullerene. With the isolation of an atomically thick carbon monolayer (which was deemed to be improbable up until then) called graphene (Novoselov *et al.* 2004), the family of carbon nanostructures looked almost synonymous to the classification of nanomaterials. With remarkable properties and flat structure, which was elusive to start with, graphene led its discoverers to the 2010 Nobel Prize in Physics.

1.2.1 2D Carbon Nanostructures

Graphene is the most common 2D carbon nanostructures. Graphene is a thin layer of pure sp^2 hybridized carbon having a bond length of 0.142 nm, neatly packed in a hexagonal honeycomb lattice. Multiple layers of graphene stacked one over other form graphite having 0.335 nm inter-planar spacing. It is also deemed as mother of all carbon nanostructures as theoretically these can be molded in all representative shapes as shown in Figure 1.1.

Graphene is the thinnest compound known to man with its thickness being equivalent to the diameter of a carbon atom. It is the lightest (density of 0.77 mg/m^2) and strongest material discovered (tensile stiffness of 150,000,000 psi). Graphene is an excellent conductor of heat at room temperature ($(4.84 \pm 0.44) \times 10^3$ to $(5.30 \pm 0.48) \times 10^3 \text{ W.m}^{-1}.\text{K}^{-1}$). Graphene is a good absorber of electromagnetic waves in visible spectrum with little dependence on its wavelength. The white light absorption capacity of graphene is $\sim 2.3\%$ which is useful in spin transport. This implies that graphene is visible to the naked eye. The absorption of visible light by graphene saturates above certain intensity (Bao *et al.* 2009). In addition, the refractive index of graphene changes with the applied electric field, which is also known as Kerr effect (Zhang *et al.* 2012a).

Graphene have very interesting properties suited for electronic applications. Graphene is a perfect atomic monolayer of carbon with infinite 2D expansion (Geim and

MacDonald 2007). The conduction and valence bands of graphene meet at a fixed energy-momentum coordinate known as Dirac Point. Hence, graphene is a zero-bandgap material. The room temperature electron mobility of graphene is reported to be $2,00,000 \text{ cm}^2 \cdot \text{V}^{-1} \cdot \text{s}^{-1}$ (Du *et al.* 2008) with very little dependency on temperature and zero effective mass of electrons (Geim and Novoselov 2007). The mobility of graphene is only hindered by defect scattering and not by phonon scattering. These properties means that graphene has a theoretical resistivity of $10^{-6} \Omega \cdot \text{cm}$, which is lowest for any material known at room temperature (Chen *et al.* 2008).

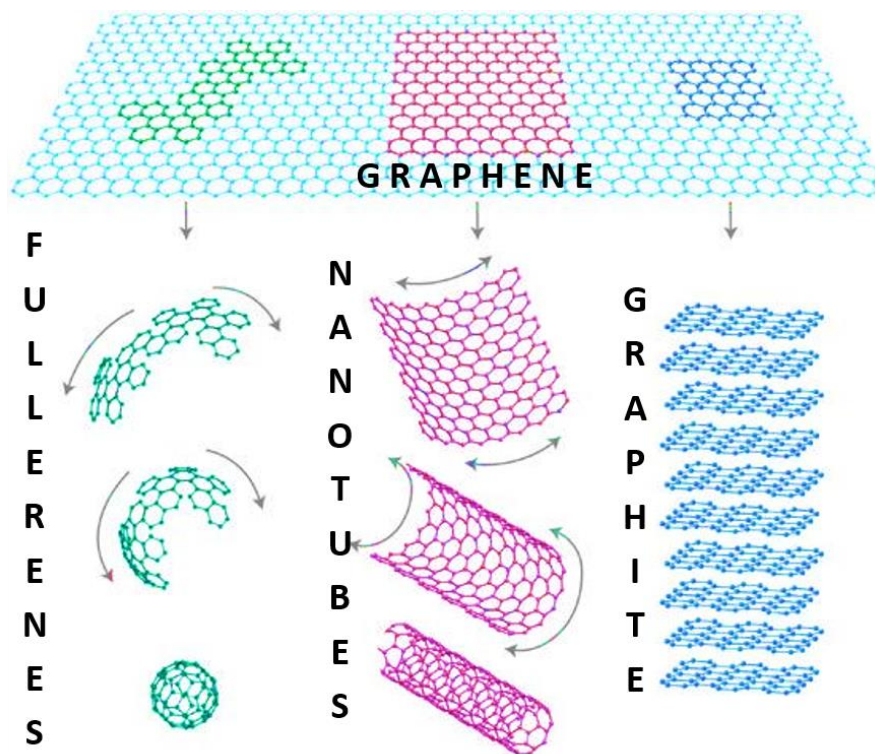


Figure 1.1 Graphene as primary building block of carbon nanostructures (Geim and Novoselov 2007)

The expensive and complex synthesis of high-quality graphene prevented them from being available for applied research and commercial uses. The chemical vapor deposition (CVD) of graphene involves using poisonous and volatile chemicals like ethylene and benzene over metallic catalysts such as platinum, nickel or titanium carbide high temperatures to grow graphene. Additionally, the growth of graphene

layers on a large scale using crystalline epitaxy on non-metallic substrate was previously impossible. Another problem with pure graphene has been its zero-band gap which limits its use as semiconductor. Creation of defects within the graphene is needed to obtain band structure of semiconductor. These challenges severely limited its use in electronics. It was difficult to separate graphene from the metallic substrate without harm to former's material integrity.

The key to efficient separation of graphene from its substrate is hidden in the analysis of graphene's interfacial adhesive energy (Yoon *et al.* 2012). The separation process reduces the toxic waste as the metallic board is reusable for future applications. Additionally, the quality of the graphene obtained after separation was excellent for creating molecular electronic devices. However, irrespective of the advances in the research, the quality of the graphene is still the limiting factor in its technological applications. Low temperature CVD are also explored to produce graphene over a very thin pieces of metal or other arbitrary surfaces (of tens of nanometers thick). The ripples, doping levels and domain size of graphene are controlled while separating it from the substrate. The separation also controls the relative crystallographic orientation and the number of the graphene layers. With such degree of assurance on the morphology of graphene makes them widely utilized, simplified and cost-effective.

However, graphene-based products are commercially available. One company already produces and offers conductive ink for consumer use. This ink is made by mixing tiny flakes of graphene with a suitable solvent. Conductive inks are used to directly print the electrodes onto paper. Graphene makes the printed material more conductive and efficient than the materials previously printed using organic semiconducting ink.

Another use for graphene is in paint formulation. Graphene is chemically inert and non-permeable. Hence, graphene acts as a barrier for oxygen and water diffusion, thereby preventing corrosion. Vehicles in future would be painted in corrosion resistant graphene-based paint or made up of graphene be grown metal surface. The excellent mechanical strength and low density of graphene makes is highly useful for protective armors and is currently under developed to replace Kevlar. Graphene will be used to make protective clothing, armored vehicle and building material in near future.

Graphene is more efficient in conducting electrons when compared to silicon, at much faster speeds (1000 km.s^{-1} , i.e. 30 times faster than silicon). The superior properties of graphene mean that in few years flexible, robust, and feather weight electronic products would be seen as common consumer products.

1.2.2 1D Carbon Nanostructures

1.2.2.1 Carbon Nanotubes

The discovery of carbon nanotubes (CNT) opened a new era in materials science. The credit due to the discoverers of CNT suffered some controversy (Pacios Pujadó 2012), Sumio Iijima is usually regarded as discoverer carbon nanotubes as his report in 1991 (Iijima 1991) initiated a flurry of excitement which took the field of carbon nanomaterials as whole, further. CNT have a range of fascinating electronic, magnetic and mechanical properties. Like graphene, CNT are also mechanically resilient (~ 100 times stronger than steel), and light weight. The fibers made up of nanotubes can strengthen many materials. The thermal and electrical conductivity of CNT is greater than copper.

CNT is a tube-shaped material, made of sp^2 hybridized carbon with diameter measuring in few nanometers. The uniqueness of CNT is due to the strong bonding within the carbon atoms leading to the tubes having extreme aspect ratios. CNT can few nanometers thin and hundreds of microns in length. These aspect ratio is similar to having a 40 m long hair strand.

CNT have various structures of different length, thickness, and number of layers. The characteristics of nanotubes varies on how the hypothetical graphene sheet was rolled to form the CNT. Depending on the structure, CNT can behave either like a metal or semiconductor. The hypothetical graphene layer that makes up the nanotube looks like rolled-up continuous hexagonal mesh having carbon molecules at the apexes of those hexagons.

CNT can be either single-walled carbon nanotubes (SWCNT) or multi-walled carbon nanotubes (MWCNT). SWCNT is like a regular straw. It is a single graphene layer rolled into a tube referred to as “wall”. MWCNT are a collection of concentric tubes of

increasing diameters. They can range from 2 to 100 tubes (walls) or more. The tubes are held at a distance by the repulsive interatomic forces.

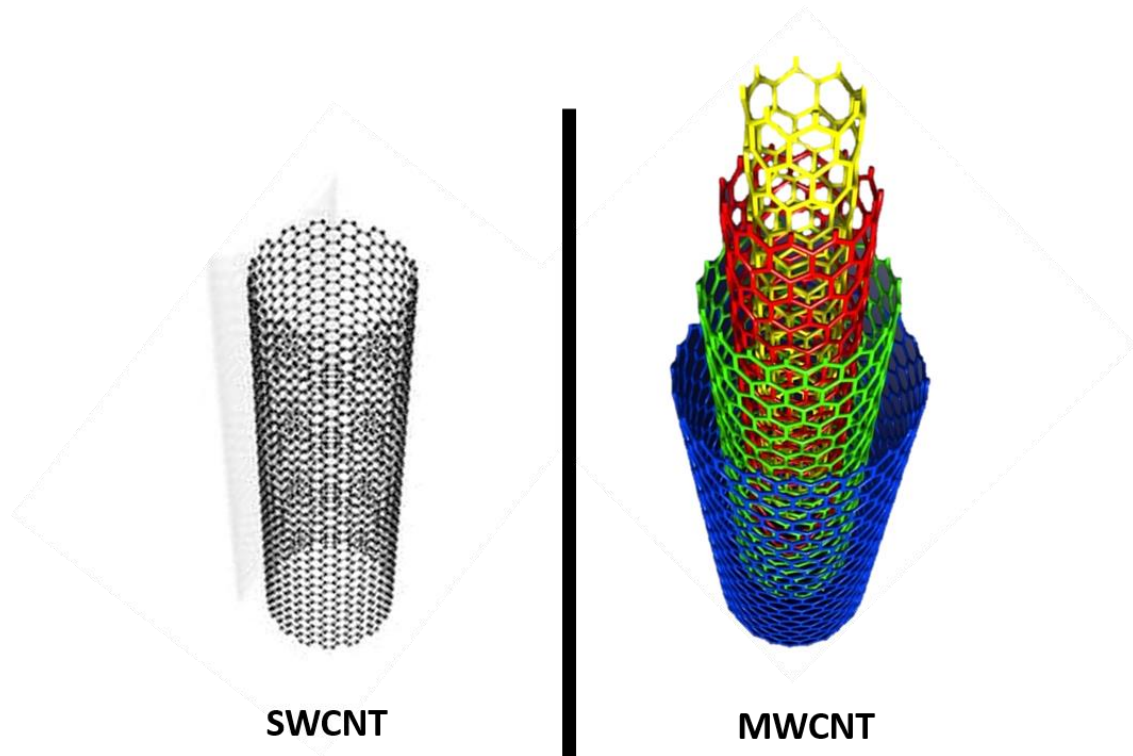


Figure 1.2 Single and multi-walled carbon nanotubes

CNT is most commonly used as structural reinforcement filler. They are readily added to the materials like rebar and cement for improving the compression and tensile strength of the building material. CNT are also explored to extract power from sunlight and even as a heat source. The thermal conductivity of CNT are available along the length and thickness of the tube. Therefore, CNT play a role on either sides of thermal insulation. The excellent electrical conductivity of CNT makes them an exceedingly cost effective replacement of metal wires. CNT can be easily doped to impart semiconducting properties for the next generation computer chips. Among other applications, CNT can be used as a chemical carrier for drug delivery. Selected drugs can be easily attached to or encapsulated in CNT with markers. These can target and attack only specific of cells (e.g. cancer cells) making the drug delivery highly specific and efficient.

The CVD growth of CNT always requires catalyst. The catalyst is generally deposited on the surface on which the CNT will be grown. Another approach of the use of catalyst is to suspend it in a hot stream of gas for the formation of nanotube. However, the later approach is very inefficient method for synthesizing CNT. Another possibility in CVD synthesis of CNT is to simultaneously inject precursor (hydrocarbon) and catalyst bearing compound in the set-up. This method involves the growth of CNT without patterning the substrate. Injecting toluene and ferrocene simultaneously for growing CNT using CVD is one such example. This mode of CNT growth is called a two-source process and require two injection mechanisms being operating concurrently with a carrier gas injection assembly. Compared to this method, the single source CVD is simpler, inexpensive and more reliable to use.

1.2.2.2 Graphene Nanoribbons

Graphene nanoribbons (GNR), are strips of graphene with width less than 50 nm. GNR were introduced as a theoretical model by Mitsutaka Fujita to examine the edge and nanoscale size effect in graphene (Fujita *et al.* 1996). Although now they are not just of theoretical importance but are things of reality with major research going on for its various potential application (Celis *et al.* 2016).

1.2.3 0D Carbon Nanostructures

1.2.3.1 Fullerene

Researchers at Rice University discovered fullerenes in 1985 (Kroto *et al.* 1985). They were awarded with the 1996 Nobel prize in Chemistry for their discovery. They are a member of the carbon allotropes family and were named after Buckminster Fuller, architect of Geodesic dome with which the shape of molecule bear resemblance. Fullerene molecules are entirely composed of carbon forming hollow ellipsoid, sphere, or tube. C₆₀ is the most commonly known variant of fullerene with spherical shape. C₆₀ are referred as buckyballs owing its structural resemblance to a typical white and black soccer ball. Cylindrical fullerenes are called buckytubes. Structure of fullerenes are like graphite. Fullerenes are composed of hexagonal rings containing pentagonal (or heptagonal) rings preventing the shape from being planar.

1.2.3.2 Carbon Dots

Carbon quantum dots (CQD) are surface passivated carbon nanoparticles having size generally < 10 nm, exhibiting fluorescence (Li *et al.* 2012). CQD were first discovered in 2004 accidentally during the purification of SWCNT (Xu *et al.* 2004). CQD possess the attractive properties like good conductivity and stability, low toxicity, and environmental friendliness. CQD are easy to synthesize and exhibit optical properties comparable to quantum dots. The discovery of CQD prompted widespread research to exploit the fluorescence of CQD, leading to their applications in biomedicine, optoelectronic, catalysis, and sensing (Lim *et al.* 2015). Significant advances were made in the synthesis, properties, and applications of CQD (Wang and Hu 2014).

The fundamental mechanisms behind the fluorescence of CQD are highly debated. The size-dependent fluorescence properties of the CQD are thought to be due to the emissions rising from the electronic transitions with the core of the dots influenced by quantum confinement effects. However, few works attribute the characteristic fluorescence to recombination of surface-trapped charges, or to the coupling between core and surface electronic states (Li *et al.* 2015b). The excitation-dependent fluorescence of CQD resulting in the tenability of their characteristic emission is mostly linked to their inhomogeneous distribution (Sciortino *et al.* 2016; Demchenko and Dekaliuk 2016) due to polydispersity. Few reports explain it as a violation of Kasha's rule caused by an unusually slow solvent relaxation.

1.2.3.3 Graphene Quantum Dots

Graphene quantum dots (GQD) are the single to few-layers graphene fragments of a size 30 nm or less. Spectral studies have determined that the GQD are generally but multi-layer graphene domains containing up to 10 layers of reduced graphene oxide (rGO) within the size of 10 to 60 nm (Razbirin *et al.* 2014). Due to the properties such as chemical stability, photoluminescence, pronounced quantum confinement effect, and low toxicity, GQD are considered as a capable material for various applications. The unique electronic, optical, photoelectric and spin properties of GQD are induced by the quantum confinement effect and edge effect due to their smaller size and functional groups present on their edges, respectively (Chen *et al.* 2010; De Raedt and Katsnelson 2009; Güçlü *et al.* 2011; Ritter and Lyding 2009; Wang *et al.* 2014c; Shen *et al.* 2012).

Currently, several techniques are available to prepare GQD. Few of the noted techniques include chemical and electrochemical synthesis, electron beam lithography, reduction of graphene oxide (GO), catalytic cage opening of C₆₀ (Lu *et al.* 2011), microwave assisted hydrothermal route (Tang *et al.* 2012), Soft-Template method (Tang *et al.* 2013), solvothermal and hydrothermal techniques (Li *et al.* 2013a), and the ultrasonic exfoliation.

GQD have various important applications in bio-imaging, drug delivery, LEDs, photodetectors, solar cells, and a fluorescent material, biosensors fabrication (Benítez-Martínez and Valcárcel 2015; Bacon *et al.* 2014; Guo *et al.* 2010; Kim *et al.* 2014). Detailed advances in GQD are discussed in chapter 2.

1.3 APPLICATIONS OF CARBON NANOSTRUCTURES

Carbon Nanostructures have found applications in various fields among which electronics, sensors, energy, reinforced materials, hybrid biomaterials, drug delivery systems, adsorbents, and membrane are few noted ones. In the proposed work, we are focusing on the intended use of the synthesized materials for sensors and photovoltaic applications.

1.3.1 Sensors

In simple terms, a sensor is a device which response to selected environment stimuli and produce a quantitative or qualitative output. The sensor consists of 3 major components:

- A receptor which is sensitive to the stimuli.
- The detector element (works in a physicochemical way; optical, piezoelectric electrochemical, thermometric, and magnetic).
- A Transducer which converts received stimuli signal from detector to observable information.

Sensors are used in various common objects for innumerable applications, many of which are not known by most people. Analog sensors like potentiometers and force-sensing resistors are still widely utilized in consumer products. Their applications include machineries, air carriers, cars, pharmaceutical sensing, robotics and many other products used in our daily life.

Here, we will focus our attention on two major class of sensors which are of special interest for a practitioner of chemistry or material science. Chemical sensor and biosensors are two very closely related devices considering the use of nanomaterials and mechanism that guide the device. But to keep up with the traditional definition we will discuss about them separately and look for the advances in the field when concerned with applications of carbon nanomaterials

1.3.1.1 Chemical Sensor

A chemical sensor is a standalone analytical device capable of providing information about the chemical make-up of its environment, i.e., in a liquid or a gas phase. The information is provided as a quantifiable physical signal which is then correlated to the concentration of a desired chemical (called as analyte). Recognition and transduction are the two main steps involved in the functioning of a chemical sensor. The analyte molecule interacts selectively with the receptor (A specific molecule or the sites included in the structure of the recognition element of the sensor) in the recognition step. As a result, the variation in the physical parameters of the receptor is reported by means of an integrated transducer generating the output signal. The later step is known as the transduction step.

1.3.1.2 Biosensor

A biosensor is essentially a chemical sensor used for the recognition of the materials of biological nature. In biomedicine and biotechnology, sensors which are able to detect analytes with the aid of biological components, such as biomimetic polymers, cells, nucleic acids, or proteins, are known as biosensors. The increasing development of synthetic biomimetic materials ready to substitute few of the existing biomaterials makes the distinction between a biosensor and chemical sensor that much inaccurate. Molecularly imprinted polymers and aptamers are few of the typical biomimetic materials used in development of the biosensors. Whereas a non-biological sensor used for the detection of biological analytes is termed as sensor or Nano sensor (when receptor is a nanomaterial). This terminology is applicable for both *in-vitro* and *in-vivo* applications. The encapsulation of the biological component in a biosensor, presents a different challenge than the ordinary sensors. The encapsulation can be either be done by employing a semipermeable barrier, such as a dialysis membrane or a hydrogel, or

by using a 3D polymer matrix. These encapsulation techniques either physically constrain the sensing macromolecule or chemically bind the macromolecule to the scaffold.

Carbon nanostructures owing to their versatility have already made way into upcoming sensing materials. The amount of work that has been accomplished in the field is truly exhaustive. The ease of preparation and properties of these materials make them an ideal choice for such applications. We will look up more in detail about work pertaining to such carbon nanostructures as sensing materials and resulting devices in the literature survey section.

On the basis of sensing mechanism, these sensors are classified under various categories, of which two major ones are:

- Photoluminescence Sensors
- Electrochemical Sensors

1.3.1.3 Photoluminescence Sensors

Photoluminescence (PL) sensors are basically materials which take help of the photoluminescence for the detection of analytes. They can be further classified in two categories:

- a) **Turn On Sensors:** Wherein the material exhibits PL upon binding with the analyte of choice. They are primarily of qualitative type when used in a device but in assay analysis, the intensity of luminescence is a direct indication of the amount of analyte present in the desired environment, and hence can be used for quantitative estimation as well.
- b) **Turn Off Sensors:** In such kind of sensors, a sensing molecule which already exhibits PL, has its PL quenched when bound or reacted to the analyte, thereby showing reduced intensity. These are mainly used for quantitative assay analysis but can be employed for qualitative estimation where the quenching is drastic. QGD can majorly be employed for Turn Off Sensor use.
 - **Qualitative Estimation with Turn Off Sensors:** A qualitative estimation can be at best done via visual observation. For this purpose, a change in color is the best indication. A very common example is the indicators used

in titrations. They give an instant account of the state of titrating mixture. For a photoluminescent material, the loss of PL can be such indicator. Thus, when photoluminescent material interact with a suitable analyte in such a way that it relaxes the excitonic boundary and facilitates energy transfer, the PL of the material is lost. This phenomenon is very well utilized for qualitative detection of such analytes.

- **Quantitative Estimation with Turn Off Sensors:** For a quantitative estimation using turn off sensing, assay method is utilized. In a typical assay method, standard solutions of analytes are interacted with the photoluminescent materials. The loss in intensity of PL emission is directly proportional to the concentration of analyte. After obtaining the standard plot, the concentration of analyte in the unknown sample is determined. In QD, the incubation time for assay is very short, hence the time for analysis is substantially reduced.
- c) **Shift Sensor:** There is a possibility of shift in emission wavelength towards blue side or red side of spectrum with the binding of analyte. In such case, there will be an additional emission peak present in the spectrum indicative of binding, and this can well be employed for sensing application.

As mentioned, among the three type of PL sensors, QD based sensors are at large Turn Off Sensors. Here, the photoluminescence of QD gets quenched which interacts with analyte molecules. This quenching is being utilized for both qualitative and quantitative estimations. GQD have shown to have remarkable potential as turn off sensing material for a wide range of analytes.

1.3.1.4 Electrochemical Sensors (EC Sensors)

Electrochemical Sensor is a class of sensors that utilize a chemical/biochemical reaction leading to an electrical response to determine a specific compound. These sensors conform to self-containing, stand-alone device which are capable of providing specific quantitative or semi-quantitative analytical information using a chemical recognition element which is in contact with a transduction element". In simple terms, "an EC Sensor is a device which is used to detect and/or quantify a particular component in a

desired sample through an electrochemical response”. Figure 1.3 shows a schematic of EC Sensor.

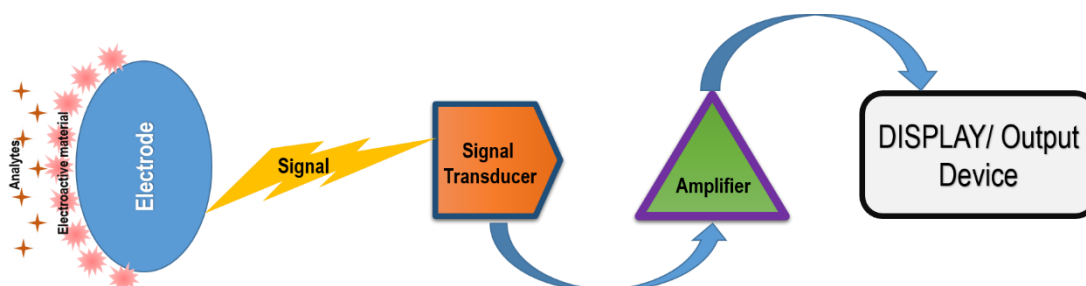


Figure 1.3 Schematic diagram of an electrochemical Sensor device.

In an electrochemical sensor, there are three major components of device, which are:

1. **Electrode:** Electrode is that part of device which come in direct contact of media in which analyte is to be sensed. These electrodes are traditionally made up of inert material like glassy carbon to avoid the loss of electrode material in the analysis media. Based on the analyte of interest, electrode is coated with electroactive material which reacts with analyte molecules to give electric response. Careful selection or design of the electroactive material is of utmost importance to an EC sensor as it governs the selectivity of device. A device which cannot be selective to analyte and gives signal from interfering species is of no practical use. This response is then received by a signal transducer.
2. **Signal Transducer:** A signal transducer is the component of sensor which registers the electronic response sent through electrode. In electrochemical setup, it may be a simple potentiostat which can observe the change in current occurring due to analyte and electroactive material interaction.
3. **Amplifier:** Amplifier is added to the setup to boost the mild response to an observable one. It may be connected to a signal processor in order to improve the signal to noise ratio for having better sensing.

1.3.2 Devices for Energy Applications

Over the past few decades, researchers have been seeking to develop new and improved technologies to harvest, store, and transfer energy with the capability of improving the quality of life all over the world. The application of nanotechnology needs to be employed in the development of energy applications to take the next leap forward from the current generation of technology.

Nanofabrication is an important part of nanotechnology for the development of energy devices. Nanofabrication involves designing and creating devices on the nanoscale. Producing devices which are smaller than 100 nm presents new alternatives for the capture, storage, and transfer of energy. The inherent level of control that nanofabrication delivers to scientists and engineers is critical in providing them with capability of solving many of the problems that the world is facing today related to the current generation of energy technologies.

People in the fields of science and engineering have already begun to develop ways of utilizing nanotechnology for the improvement of consumer products. Benefits already observed from the design of these products are an increased efficiency of lighting and heating, increased electrical storage capacity, and a decrease in the amount of pollution. These benefits make the investment of capital in the research and development of nanotechnology a top priority. These advances again warrant special interest for chemical science researchers as there is still room to improve on the materials used in such devices. When concerned with the energy we can broadly classify them as either energy generating, or energy storage devices and carbon nanostructures have found applications in all of them. Here we discuss about photovoltaic devices used for energy generation.

1.3.2.1 Photovoltaics devices

Energy generation has been a prime necessity for humans from the dawn of civilization. From generating energy from combustion to mechanical and now electronics, we have indeed come a long way ahead in related technologies. The problem with energy generation is, it requires some resource from where we can extract energy all due to the fundamental rule of energy that it can neither be created nor destroyed but only

transferred through various forms. Speaking of resources, we have limitations associated with them. Few of them will be not consistently available, may be expensive, can have a higher mechanical cost associated with conversion, could be toxic or damaging to humans and other natural beings, polluting, or will deplete over time etc. One such resource which can avoid pity much all these limitations within acceptable limits and be available for eternity of the human civilization is that ball shining in the sky all through the daytime.

Solar-generated electricity has potential to serve people living in the most isolated spots on earth as well as in the center of our biggest cities. From their first used in the space program, photovoltaic (PV) systems are now generating electricity to pump water, light up the night, activate switches, charge batteries, supply the electric utility grid, and more. Whether you are a homeowner, farmer, planner, architect, or just someone who pays electric utility bills, PV may already touch your life in some way.

A typical photovoltaic system employs solar panels, each comprising several solar cells, which generate electrical power. The first step is the photoelectric effect followed by an electrochemical process where atoms, ionized in a series, generate an electric current. PV installations may be ground-mounted, rooftop mounted, or wall mounted. They may be mounted in a permanent orientation to maximize production and value or they may be mounted on trackers that follow the sun across the sky.

Solar PV generates no pollution. The direct conversion of sunlight to electricity occurs without any moving parts. Photovoltaic systems have been used for fifty years in specialized applications, standalone and grid-connected PV systems have been in use for more than twenty years. The numerous types of photovoltaic cells, but our interest lies in a Quantum dot solar cells (QDSC). QDSC originated from a relatively more familiar PV cell type viz. Dye sensitized Solar Cells (DSSC). The difference between the two being the sensitizer element which is Quantum dots in case of QDSC against the organic dyes used in DSSC.

As known, the future of technology is when it reaches to the most deprived section of society. This is the primary reason for relentless pursuit in this field even when we have cells with much higher efficiency and stability than those mentioned above. The limitations with them are that they are not very cost effective. Silicon solar cells though

are well used for most commercial applications still is expensive in an initial installation which turns off many potential users. In such context developing materials for cells which are easy to synthesize and give decent enough performance is what we aim for society. Before moving any further, we will have a brief introduction about PV cells and what Quantum dots adds to their development.

Types of PV Cells

PV cells (or Solar Cells, which is most common form) are device which to put in simple terms generate voltage when exposed to photons of suitable energy, hence the name photovoltaic cells. PV cells have been under development for over 71 years now with first patent by Russell Ohl in 1946. First Working solar cell was produced by Bell Laboratories in just six year of the patent. The first major application of solar cells came in Space race with Vanguard satellite being the first one to use them in 1958 as an alternative to primary batteries used before. There are wide number of solar cells of different kinds which are developed since then. Here we will have a look at the different types of cells as classified by National Renewable Energy Laboratory (NREL), USA.

PV cells can be classified in following groups:

- Single Junction PV Cells: Which have only one p-n junction in heart of the PV device. As shown in Figure 1.4, GaAs leads the efficiency race in this class owing to its band gap which equivalent to mid-range of the energies of visible spectrum.

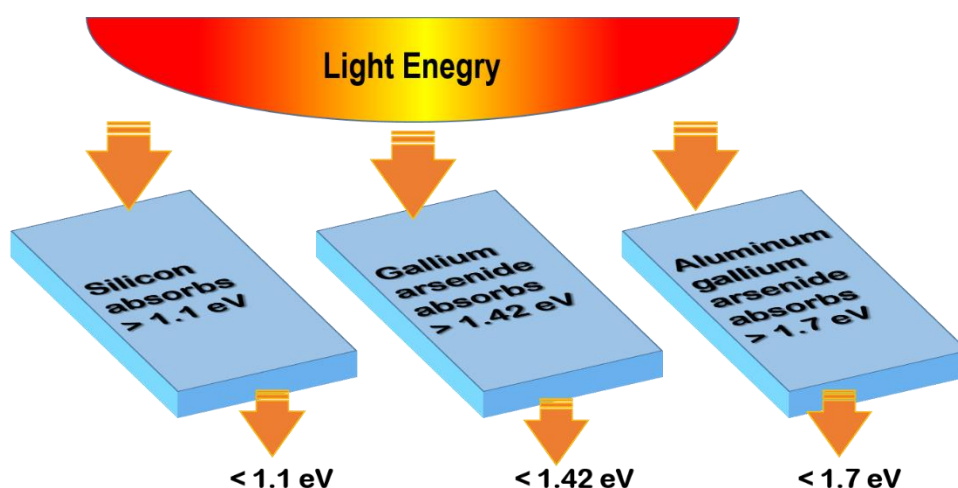


Figure 1.4 Band gaps of conventional semiconducting materials.

- Multi Junction PV Cell: In such kind of cell assembly two or more p-n junctions are used to absorb photons. This leads to the wider absorption of photons of visible spectrum and in turns provide even better efficiency than single junction cells.
- Silicon PV cells: Silicon by large holds a major share of commercial PV market. They have achieved so due to lower cost of production and better stability (viz for Crystalline silicon solar cell). Hence, they command to be mentioned in separate category. There are two major types of Si PV cells which are:
 - Crystalline silicon cells are the most common among the existing range of solar cells both commercially and research
 - Amorphous silicon cells, which have higher efficiency than its crystalline counterpart, but suffers from poor stability to maintain that performance for longer durations.
- Thin Film Solar Cells (2nd Generation): These cells are second generation solar cells that is made by depositing one or more thin layers, or thin film of photovoltaic material on a substrate, such as glass, plastic or metal. Thin-film solar cells are commercially used in several technologies, including cadmium telluride, copper indium gallium diselenide, and amorphous silicon. These cells are different from the earlier described First generation cells because, they part away from the wafer-based design to more modular and easier to use design.
- Emerging Cells (3rd Generation): NREL classifies a number of thin-film technologies as emerging PV (often called third generation PV cells) - most of them are yet to be commercially applied and are still in the research or development phase. Many use organic materials, often organometallic compounds as well as inorganic substances. Despite the fact that their efficiencies had been low and the stability of the absorber material was often too short for commercial applications, there is a lot of research invested into these technologies as they promise to achieve the goal of producing low-cost, high-efficient solar cells. Few of these cells are:
 - Copper zinc tin sulfide solar cell (CZTS), and derivatives
 - Dye-sensitized solar cell (DSSC), (or Grätzel cell)
 - Organic solar cell

- Perovskite solar cell
- Polymer solar cell
- Quantum dot solar cell (QDSC)

The achievements in the research of perovskite cells have received tremendous attention in the public, as their research efficiencies recently soared above 20 %. They also offer a wide spectrum of low-cost applications.

These cells in addition also use light concentrating technique through combination with optical lenses and a tracking system. Such cells are called concentrator PV and they often use currently available high-efficiency PV cells for even better performance. Figure 1.5 shows a recent comparison of the reported efficiencies of existing PV cells.

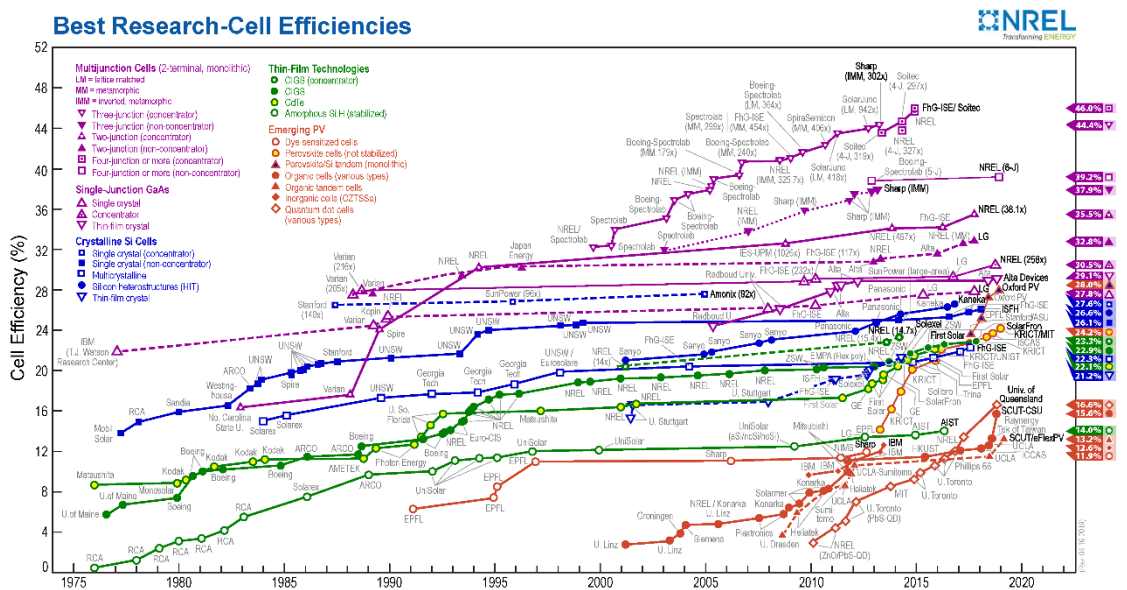


Figure 1.5 Efficiencies of Existing PV cells (Source: NREL, USA).

Limitations of existing PV Cells

Currently available PV cells are highly efficient device. But irrespective of such high performance, need to look for alternative cells are ever growing. If we put thought to it, the existing cells show quite many limitation, common among which are:

- **Price:** Usually the high efficiency cells are very costly to produce and hence not an affordable solution for many. The initial cost of installation usually drives many consumers away.

- **Stability:** Few cells among the listed ones are very stable but then they are costly (for e.g. Multi/single junction cells or silicon cells). Others are simply not stable for longer use. This again pose a longevity issue when these cells are applied for commercial use.
- **Modularity:** With the development of modern electronics both for commercial and personal use, requirement for power source which run these devices is ever increasing. Currently secondary cells (rechargeable) are used to power such device but it will be more efficient to install a PV module in such device. Hence, the modularity of the cells becomes important. This virtually kicks out all the first-generation solar cells out of game. This opens the field for second and third generation of PV cells among which third generation ones are with real potential to be a part of electronic device which are holographic or transparent in nature.

1.3.2.2 Quantum Dot Solar Cells

QDSC are new and upcoming class of third generation PV cells which makes use of QD as sensitizers. This is the fundamental difference between a QDSC and DSSC. To successfully substitute the sensitizer in DSSC with a semiconducting QD, we need to consider the characteristic energetics of each cell component. Figure 1.6 shows the energetics of the QD sensitizer, the TiO_2 scaffold, and the electrolyte solution, along with the working and counter electrodes. The position of conduction band, valence bands, and the electrolyte oxidation potential are relative to each other to promote the cell operation. The phrase “*electrons sink and holes float*” can summarize the mechanism of QDSC, which means that the electrons are energetically drawn to transfer to states as low in energy as possible, and holes to states as high as possible.

In order for all of the reactions to take place as described above the two relative energy requirements must be met: the QD conduction band must lie above the TiO_2 conduction band, and the electrolyte potential must lie between the QD valence band and the TiO_2 conduction band. The maximum voltage is then defined as the energetic difference between the TiO_2 conduction band and the electrolyte oxidation potential. Figure 1.7 depicts a basic construction of QDSC.

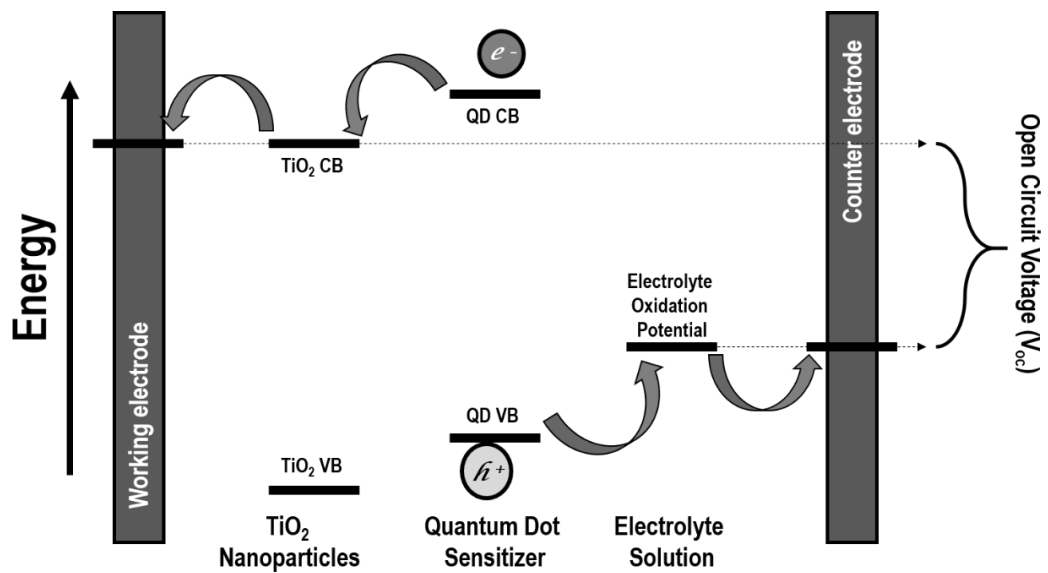


Figure 1.6 Band diagram of the components of quantum dot solar cell.

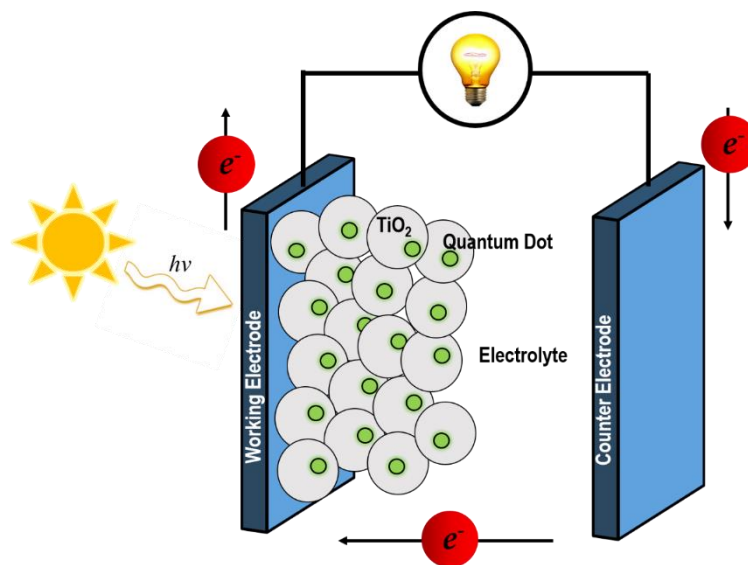


Figure 1.7 A typical construction of quantum dot solar cell.

As discussed earlier, Graphene have been attempted for their use in PV cells and with good success. Use of GQD as sensitizer for PV applications is very new and much work is to be done in this. A detailed account of the literature reports for both these materials in photovoltaics have been presented in Chapter 2.

1.4 VISION

Carbon is among the most abundant material found around us. Carbon nanostructure have been present with us since the time we learnt to make fire and its real potential have been unearthed only in couple of decades. Even-D carbon nanostructures have been used in wide range of applications. Their properties and ease of modification make them ideal choice for many electronic and excitonic based applications. When we examine the benefits of carbon nanostructures, it is very natural that we develop future devices which are based on these materials. Among the various applications of carbon nanostructures, sensors and energy are the most promising ones. Various literature reports have emphasized the compatibility of these materials towards such devices.

With each progressive step taken in science and technology, we are also risking our environment with variety of pollutants and hazardous materials. This makes the importance of chemical/biosensors even more evident. Today we are surrounded with hazardous materials such as heavy metals, radioactive substances, toxic gases, particulate pollutants, biological parasites to name a few. Detection of such entities are very important for well-being of humans. Sensors also are very vital to medical science. They provide the primary information about the state of human body with respect to level of biomolecules of concern and other infectious agents. Even-D carbon nanostructures have shown to be very prominent sensing material of all the above-mentioned target analytes. Their high surface area and excitonic properties enables them to be used for sensing of these molecules with exceptional efficiency.

Progression in technology also means we need more energy to sustain our future generations. Along with the conventional source of energy, which are going to be major resource for our energy consumption, alternative forms of energy are also required to meet the raising demand. Among the alternative resources available, light (visual electromagnetic spectrum) is one which is available in endless amount. Tapping this resource mean in coming years, we will be generating a competitive amount of energy compared to conventional fuels and this form is much clean compared to any conventional resource available to date. Again, the use of even-D carbon nanomaterials is at the forefront in terms of research pertaining to photovoltaic devices. They have shown applicability in all the components of PV cells. With the finding of GQD, a

carbon nanostructure as sensitizer is also a possibility. Much research has been done since 2010 to see the applicability of GQD as sensitizer for QDSC. Therefore, the properties of even-D carbon nanostructures towards the sensing and energy applications are explored.

CHAPTER 2

STATE OF THE ART

Abstract: This chapter summarizes the current state of research pertaining to the graphene and graphene quantum dots, two of the most versatile even-D carbon nanostructures for their intended use in sensor and PV devices.

2.1 ADVANCES IN GRAPHENE

Graphene - a single atomic thick layer of graphite piqued the interest of scientists as early as 1947, with the theoretical study of the properties of graphene (in the context of graphite) (Wallace 1947). The first transmission electron microscopy (TEM) image of isolated rGO was reported in 1948 (Ruess and Vogt 1948). rGO was prepared by the thermal reduction of GO in a stream of hydrogen. Another such attempt to graphene by reducing GO with hydrazine was reported in 1962 (Boehm *et al.* 1962). The term graphene was first coined in 1987 (Mouras *et al.* 1987; Bacon *et al.* 2014). But it took almost 17 years from then on to obtain a stable monolayer graphene sheet observed with all its properties (Novoselov *et al.* 2004). Their work fetches them Nobel prize in Physics 2010.

A major challenge which limits the use of graphene is the unavailability of pure graphene. At one point in 2008, graphene was the most expensive material in the world, costing an eye-watering \$100,000,000/cm². The mechanical exfoliation method (Scotch tape method) to peel of single layer of graphene from Highly Pyrolytic Oriented Graphite (HPOG) was a major breakthrough in the history of nanotechnology (Novoselov *et al.* 2004). The inability to utilize this method to produce large quantity of graphene is its major limitation, however, the graphene obtained as such are of high quality. American chemist James Tour's group in 2010 reported another method of preparing GO (Marcano *et al.* 2010) which was an improvement over age old know method to produce graphitic oxide (Hummers and Offeman 1958). This method gave a good yield of GO which were a highly defective sheets of graphene with oxide linkages, and therefore offered poor conductivity. Although this seems a very method for the synthesis of graphene, it is by far the most commonly used one in laboratories to produce GO, followed temperature assisted reduction (Tkachev *et al.* 2012) or reagent assisted reduction (Ghosh *et al.* 2013) to give rGO which is not a pristine graphene by any measure but still usable for many applications. CVD is another very commonly

used method for the synthesis of high quality graphene (Reina *et al.* 2009) but again these methods require very high temperature and a pure substrate to synthesize graphene. The quality of graphene obtained is not as pristine as those obtained using mechanical exfoliation. However, CVD grown graphene are usable for most of the electronic applications. Unzipping of CNT is another way of producing one-dimensional graphene sheets i.e. GNR (Shinde *et al.* 2011). Kang and group have compiled other methods to synthesis graphene in a critical review (Choi *et al.* 2010).

Potential uses of graphene are expected to affect everyone's lives in near future. Flexible, thin, mechanically resilient, and chemically diverse graphene is suitable for flexible electronic screens, integrated electric circuits, sensors, and PV devices etc. (Allen *et al.* 2010). Few other noted applications of graphene are in biomedical research, desalination of waters, and composite materials etc. Graphene will be common to the consumers as glass or plastic, and perhaps more useful soon.

2.1.1 Graphene as Sensors:

Graphene and graphene based nanomaterials are seen as replacement of CNTs in sensor applications (Cooper *et al.* 2012), due to excellent ability to adsorb materials (Gadipelli and Guo 2015). Graphene is utilized as electrochemical sensor for various kinds of analytes (Razzino *et al.* 2019; Justino *et al.* 2017). Graphene is employed in two major types of sensors as discussed below.

2.1.1.1 Graphene as Chemical Sensors:

Graphene have superior electrochemical response compared to other electrodes such as glassy carbon electrodes (GCE) (Shang *et al.* 2008), graphite (Shan *et al.* 2009), and CNT (Alwarappan *et al.* 2009; Wang *et al.* 2009b). Graphene exhibits an electrochemical potential window of ~ 2.5 V in 0.1 M phosphate-buffered saline solution (PBS) at pH 7.0 (Zhou *et al.* 2009). Small organic molecules like dopamine, ascorbic acid, and uric acid have reportedly been simultaneously detected using graphene (Shang *et al.* 2008). Few reports discussed the electrochemical activity of rGO and graphene-based nanomaterials in determining analytes such as nucleic acids, potassium ferricyanide, dopamine, and acetaminophen (Wang *et al.* 2009b; Zhou *et al.* 2009). Graphene-based sensors have also shown to detect gaseous analytes such as CO,

H₂O, NO₂, and NH₃. These sensors operate by measuring a variation in resistivity caused due to the adsorption of gas molecules on the graphene based electrode (Schedin *et al.* 2007; Arsat *et al.* 2009; Qazi *et al.* 2007). A rGO based sensor is shown to be competent of identifying toxic gases with ppb sensitivity (Robinson *et al.* 2008). rGO offers similar performance as CNT-based sensor with significantly less electronic noise. Graphene has been employed in identifying organic vapors like nonanol, octanoic acid, and trimethyl amine (Dan *et al.* 2009). Furthermore, the researchers achieved single molecule detection with an electrical sensor made of few-layered graphene (Shinde *et al.* 2011). The transfer of electrons to graphene increases the resistance of the device and vice-versa. Schedin and co-workers unintentionally functionalized their device with a residual polymer layer from lithographic resist and managed to detect single molecule with pure graphene. The response of the sensor was measured before and after the removal of polymer resist. Without the resist, the sensitivity of the device dropped by few orders of magnitude (Dan *et al.* 2009). Impurities and defects also affect the response of the sensor towards the gas adsorption onto graphene (Ao *et al.* 2008; Zhang *et al.* 2009).

2.1.1.2 Graphene as Biosensors

Like the trait of graphene in chemical sensors, graphene and its derivatives are used in biosensors. The electrochemical response of hydrogen peroxide (H₂O₂) on an rGO electrode has been studied which resulted in improved performance compared to GCE, graphite, and CNT (Zhou *et al.* 2009). A similar effect was observed in the electrochemical behavior of nicotinamide adenine dinucleotide (NADH) on graphene-modified electrodes (Tang *et al.* 2009). In both the cases, the higher electrochemical activity of graphene was attributed to the presence of high density of edge-plane-like defective sites. The improvement of the activity of graphene-modified electrodes towards NADH was affirmed when the results were compared with the unmodified edge plane pyrolytic graphite electrode. High density of the defective edges of graphene contributes to enhance the redox behavior of biomolecules (Banks *et al.* 2004). A multilayer graphene nanoflake film electrode was successfully used in the simultaneous detection of uric acid, ascorbic acid, and dopamine with the detection limit as low as 0.17 μM (Zhou *et al.* 2009). Graphene reportedly exhibits better sensitivity towards

dopamine than CNT to distinguish between ascorbic acid, dopamine, and serotonin (Alwarappan *et al.* 2009). The sensitivity of graphene was found to be high within the linear range of 5–200 μM towards dopamine (Wang *et al.* 2009b). The excellent selectivity towards is assumed to be the result of high conductivity, large surface area, and π interaction between dopamine and graphene. Paracetamol was determined quantitatively using an electrochemical sensor based on functionalized graphene (Kang *et al.* 2010). The electrochemical behavior of paracetamol on graphene modified GCE was studied using cyclic voltammetry (CV) and square wave voltammetry. A composite material designed using graphite platelets, Nafion, glucose oxidase served as a glucose biosensor (Fu *et al.* 2009). An enzyme free glucose sensor with NiO/CNT/rGO ternary composite for the detection of glucose shows the versatility of the material to be used as a biosensing component (Prasad *et al.* 2016). Both the studies show the excellent support graphene as a substrate provides for the electrical writing of the redox centers of various metalloproteins without altering their structural integrity or biological activity. The π stacking graphene reportedly adsorbs monolayers of single strand DNA (ssDNA) which leads to their isolation from the biological matter (Patil *et al.* 2009). The method used for isolation involved vigorous sonication of a suspension of ssDNA and hydrophilized graphene. Graphene have been incorporated into functionalized bio systems integrated with aptamers, DNA, peptides, proteins, and cells. Graphene-electrolyte field effect transistor was used to detect dissolved bovine serum albumin (BSA), which is an important protein for biochemical applications (Ohno *et al.* 2009). The sensor was prepared by using mechanically exfoliated single-layer graphene supported on a silicon dioxide wafer. The circuit was completed with an electrolyte solution and reference electrode. The electrical response of this device towards the adsorption of BSA from standard solutions was observed. The detection limit of BSA was reported to be as low as 0.3 nM. The same research group fabricated an aptamer-modified graphene-FET immunosensor. Functionalization of the graphene-FET with aptamers was also developed by the same group to be used as an immunosensor (Ohno *et al.* 2010). The structure of aptamers functionalization of the graphene-FET was confirmed by the AFM.

2.1.2 Graphene in Photovoltaics

Among the very first use of graphene was shown by integrating graphene with silicon wafers. Deposition of graphene sheet onto n type silicon created a Schottky junction had a lower forward voltage drop which resulted in a faster switching speeds and better efficiency (Li *et al.* 2010). Graphene functions both as transparent upper electrode and antireflection coating. Graphene owing to its intrinsic electric field properties, aids in charge separation and hole transport. The opportunities for optimizing the use of graphene in conjunction with silicon are apparent. One such example is the passivation of the silicon to improve the interface. Typically, deposition of an oxide forms a protective surface, prevents corrosion, and reduce reactivity. One way of increasing the efficiency of devices having graphene films is to match the work function of the graphene to its neighboring components. Several attempts have been made to engineer the work function of graphene (ϕ_G). Designing a simple FLG/Si heterojunction device is done considering the direct relationship between the number of layers in the FLG and the resulting V_{OC} . FLG containing 4 layers of graphene have found to be the best matching despite having disordered stacking (Ihm *et al.* 2010). The V_{OC} is determined by the work function of the CVD-grown graphene layers when the Si substrate is unchanged. The work function of graphene matches with silicon as the number of layers are increased. The ϕ_G approaches the silicon work function (ϕ_{Si}) from a lower value. Organic cells are manufactured at a lower cost, but they are yet achieving the efficiency comparable to that of silicon based solar cells. An organic polymer dispersion consisting of a narrow-band electron donating poly(3-hexylthiophene) (P3HT), and a fullerene derivative in form of [6, 6]-phenyl-C₆₁-butyric acid methyl ester (PCBM) being an electron acceptor is a popular active layer for the proof-of-concept devices. Cells with such donor/acceptor blend constituting the active layer are called bulk heterojunction (BHJ) cells. The work on the development of graphene based PV is largely at an early stage and does not compete with the best performance obtained from similar organic solar cells made with ITO electrodes. The graphene based PV barely reach a photon conversion efficiency (PCE) of 2%. In comparison, the PV made using ITO can have PCE in excess of 6%. The design considerations and challenges in the optimization of parameters associated with a simple graphene modified BHJ cell is well illustrated in the literature (Wang *et al.* 2009a). CVD grown FLG films function as the

anode in their device, filling the role of ITO (or other transparent conductive electrodes (TCE)). The films varied in thickness from 6 - 30 nm, with R_s from 1350 to 210 ΩW^{-1} and T from 91% to 72%. The complete device structure is FLG/graphene/PEDOT:PSS/P3HT:PCBM/LiF/Al. The device is mounted on glass, which provides protection and structural integrity and permits light, which passes through the FLG layer to be absorbed by the P3HT:PCBM active layer, generating the charge that will be collected by the FLG and LiF/Al electrodes. With a simple substitution of unmodified FLG film for ITO, 30 times reduction in the device efficiency was observed. This efficiency reduction was associated to several factors. First, the hydrophobicity of graphene precludes uniform coating of the PEDOT:PSS layer, which is essential as a planarizing buffer layer for reducing surface roughness, as well as the hole injection barrier between P3HT and graphene. To address this, the graphene was modified by UV/ozone treatment, which improved wettability by introduction of OH and C=O groups to the surface. This resulted in improved short-circuit current (I_{SC}) and open-circuit voltage (V_{OC}) values, with slightly reduced fill-factor (FF) for an overall improvement to PCE of 0.74%. The decrease in FF was attributed to increased series resistance of the cell, as disruption of the aromatic structure by surface groups results in decreased conductivity. To circumvent this effect, the graphene was modified instead by noncovalent functionalization with pyrene butanoic acid succidimidyl ester (PBASE). This resulted in the same improvement in V_{OC} and further improvement in both I_{SC} and FF, resulting in overall PCE of 1.71%, reaching slightly more than half of the ITO version of the device. The effect of PBASE modification was multifaceted; in addition to avoiding π -conjugation disruption and maintaining conductivity, ϕ_G was increased from 4.2 eV to 4.7 eV, increasing the open circuit potential as well as resulting in better matching between the Fermi level of FLG and the HOMO of PEDOT for more efficient hole collection. Many improvements to graphene BHJ cell designs have appeared recently, including using metals for doping or blocking. By immersing CVD-grown graphene films into $AuCl_3$, Shi et al. showed formation of Au particles on the graphene surface by spontaneous reduction of metal ions. The extent of the metal doping, controlled by immersion time, effectively tunes the surface potential, over a range of ~ 0.5 eV (Shi *et al.* 2010). The introduction of graphene to TiO_2 -nanostructured films have reported to alter the properties of the film (Ng *et al.* 2010). rGO scaffolds

were used to harvest photogenerated charge and increased the photocurrent by 90% over pristine TiO₂ under UV illumination. While pristine TiO₂ films yield a maximum PCE of 7.4%, the rGO-TiO₂ nanocomposite films yield maximum PCE of 13.9% for in situ rGO (photocatalytic reduction) and 11.4% for hydrazine rGO (chemical reduction using hydrazine). In these devices, graphene serves as an efficient collector of generated electrons and prevents recombination. It has also been shown that the introduction of a thin sol-gel processed titanium suboxide (TiO_x) layer for hole blocking can improve device efficiency 2 folds (Choe *et al.* 2010). In this device with CVD graphene/PEDOT:PSS/P3HT:PCBM/TiO_x/Al construction, the I_{SC} and V_{OC} values closely match those for ITO, with only the lower FF preventing the overall efficiency from being comparable. An interfacial dipole layer (consisting of WPF-6-oxy-F, a synthesized polymer) in an inverted-structure organic solar cell can reduce the work function, increase built-in potential, and improve charge extraction (Jo *et al.* 2010). CVD-grown graphene films were used as the device cathode for design flexibility and the ability to build stacked devices. The ionic or polar groups of the WPF-6-oxy-F form interface dipoles, better matching ϕ_G to the LUMO of PCBM (4.2 eV). Untreated MLG film has $\phi_G = 4.58 \pm 0.08$ eV, close to HOPG at 4.5 eV. It was reduced by 0.05 ± 0.03 eV using poly(ethylene oxide), 0.22 ± 0.05 eV with Cs₂CO₃, and 0.33 ± 0.03 eV with WPF-6-oxy-F. Though graphene finds a natural function as a TCE, it also presents potential for additional utility by virtue of its chemical structure. Its aromatic skeleton can function as a nucleating agent for the self-assembly of organic nanostructures. Using rGO flakes as a seeding agent for planar aromatic molecules (which tend to self-assemble), “hybrid” wires were formed through noncovalent hydrogen bonding and π - π stacking interactions (Wang *et al.* 2010). By choosing a photoluminescent molecule (in this case N,N'- dioctyl-3,4,9,10-perylene dicarboximide) which is effectively “wrapped” in graphene, a photovoltaic active material can be produced. Incorporating photoactive quantum dots and GO is another reported method to improve the current density under photo illumination for solar energy conversion (Jagtap *et al.* 2016).

These were the few important reports available in the field of sensors and photovoltaic with graphene (a 2D carbon nanostructure) as central material. As discussed in introduction, when graphene is cut into smaller fragments of suitable size, it leads to the formation of GQD having properties absent in graphene. In later section, we will

see the advances made in research of GQD for both sensory and photovoltaic applications.

2.2 ADVANCES IN GRAPHENE QUANTUM DOTS

History of GQD is rather recent. With the discovery of graphene, people started contemplating the possibility of existence of quantum dots in graphene with theoretical studies made as early as 2007 (Silvestrov and Efetov 2007). Various physical properties of GQD have been studied which range from spin qubits (Trauzettel *et al.* 2007), Dirac Billiard (Ponomarenko *et al.* 2008), electron localization (Hewageegana and Apalkov 2008), effect of magnetic field (Guttinger *et al.* 2010) and edge effect (Romanovsky *et al.* 2009) due to quantum confinement to name a few. Among all the properties of GQD, its PL catches the eye of the researchers worldwide. Therefore, GQD are often the choicest material for sensors and bio imaging. Due to infinite Bohr's radius of excitons, the GQD shows remarkable size dependent energy absorbance, making it a potential candidate for photovoltaic applications.

Like any nanomaterials, synthesis of GQD can again be described in either Top Down or Bottom Up approach.

2.2.1 Synthesis of GQD

2.2.1.1 Top Down Method

The conversion of a graphite to graphite oxide sheets is an essential step in the Top Down approach. The improved hummer's method is by far the most common approach to obtain GO (Marcano *et al.* 2010). Furthermore, majority of the top-down methods differ in their means to convert GO sheets to quantum dots. These means are usually how the methods are given their name.

Hydrothermal Cutting

Among the most used method to prepare GQD is the hydrothermal cutting method which yields blue-luminescent quantum dots of diameter 5–13 nm that can be easily dispersed in water (Pan *et al.* 2010). The method broadly involves the thermal reduction of GO to rGO sheets, oxidation of rGO sheets in acid media followed by their hydrothermal cutting to obtain the GQD. The mechanism involved in the cleavage of GO is similar to the breakdown of CNT into smaller tubes and nanoribbons in acid

media. The evidence of these mechanism are well documented in the literature having support of XRD, FTIR, XPS, and UV-vis measurements (Kosynkin *et al.* 2009). The oxidation of rGO in the acidic conditions creates epoxy (–C–O–C–) groups. These groups have tendency to be formed in a line along a carbon lattice causing the C–C bonds to break. Further, the epoxy chain is oxidized into epoxy pairs and are then converted to more stable carbonyl pairs. These carbonyl groups remain on the edges of the GQD after the alkaline hydrothermal treatment and makes the quantum dots dispersible in water. The linear defects cause further disruption in the GO during the hydrothermal reduction from where the oxygen atoms are removed. The temperature of the thermal reduction had a major impact on the cutting of the graphene sheets. The low-temperature process produced poorly ordered GQD. However, the high-temperature thermal treatment resulted in well-crystallized GQD of 3.6 nm average diameter (Pan *et al.* 2012). These particles also exhibited strong green photoluminescence. These GQD were used as fluorescence probes for cellular imaging. The original blue-luminescence of the GQD in alkaline conditions are almost completely quenched in the acidic media (Shen *et al.* 2011). The work was inspired by the luminescence studied in the visible and NIR regions of single layer nanographene oxide sheets which were surface-passivated by polyethylene glycol (PEG) (Sun *et al.* 2008). Hydrazine hydrate was used for the reduction method GO under hydrothermal conditions to produce GQD of 5 - 13 nm diameter having their surface-passivated by PEG. These GQD exhibited frequency upconverted emission. This method involved multiple steps where the key ones were the treatment of small graphene oxide sheets with an oligomeric PEG diamine and their subsequent reduction with hydrazine hydrate during the hydrothermal cutting. A much shorter one-pot hydrothermal cutting method to produce PEG-passivated GQD was also reported in which GO sheets were reduced to GQD while simultaneously coupling the hydroxyl groups of PEG to the carboxyl groups of GQD (Shen *et al.* 2012). The quantum yield of the GQD-PEG at 360 nm emission was found to be ~ 28.0%, which was twice of the GQD with no surface passivation. These PEG-passivated GQD also exhibit up-conversion photoluminescence. The functionalized GQD also exhibited the PL-shifting or bandgap tuning ability (Jin *et al.* 2013). The amine-functionalized GQD was observed to have a red-shift in the PL when compared with the non-functionalized GQD. The DFT

calculations was used to study effect of the electron withdrawing or donating properties of the functional groups on the bandgap. The quantum dots were synthesized by a two-step process: oxidation of graphene oxide in a mixture of $\text{H}_2\text{SO}_4/\text{HNO}_3$ followed by reduction by hydrazine. The modified QD were produced using a step in between the oxidation and reduction where diamine-terminated PEG was attached to the GQD by a ring opening reaction of the epoxy groups generated in alkaline conditions.

Solvothermal Cutting

In the pioneering work involving the solvothermal cutting, DMF was used in capacity of both as a solvent and reducing agent to synthesize GQD by the one-step solvothermal method (Zhu *et al.* 2011; Zhu *et al.* 2012). The cutting and reduction of GO was a one step process. The GQD were separated using column chromatography. Therefore, the GQD with different degrees of oxidation and PL were separated.

Electrochemical Cutting

GQD of size 3 - 5 nm were produced using an electrochemical method that involved the fragmentation of a graphene film pre-treated with oxygen plasma to increase hydrophilicity (Li *et al.* 2011). These QD were incorporated into a PV device with a PCE of 1.28%. The particles were found to be stable for in water for several months. Water-soluble GQD with uniform size and high yield were synthesized by electrochemically exfoliating graphite and their reduction by hydrazine in room temperature (Zhang *et al.* 2012b). This was the first report of a yellow PL observed in GQD, which was attribute to the hydrazide groups on the surface of GQD produced during the low-temperature reduction step. The effect of low temperature on the PL of GQD was verified by the control experiment done in higher temperatures. The reducing ability of hydrazine is deemed to be limited at ambient temperature, therefore, predominantly reducing the epoxide and hydroxyl groups. It is also expected to undergo amidation with the carboxylic groups present at the edges of graphene leading to the formation of the hydrazide groups and phthalhydrazide like groups when two neighboring carboxylic groups join.

Nanolithography

GQD are also carved by the use of ultra-high-resolution electron beam lithography to cut graphene to desired sizes (Ponomarenko *et al.* 2008). The process is highly precise

in producing uniform GQD with very small defects, however, offers a very low yield. Another instance of a production of the size-controlled GQD was using self-assembled block copolymers (BCP) as an etch mask on graphene films grown by CVD (Lee *et al.* 2012). The method again offers a low yield, but very uniform particles for probing the effect of size and functionalization on the properties of GQD.

Microwave-Assisted Cutting

Microwave is another energy source used for fragmentation of graphene to GQD. A glucose-derived GQD were produced through a microwave assisted hydrothermal approach (Tang *et al.* 2012). The fast and homogeneous heating, and size uniformity of the GQD produced are the major advantages of a microwave assisted method. This method does not require passivating agent. Size of the GQD obtained can be changed by varying duration of the microwave irradiation. The GQD obtained had an average diameter of 3.4 ± 0.5 nm, were tunable from 1.65 - 21 nm by increasing duration of irradiance. The GQD exhibit deep ultraviolet emission of (303 nm) 4.1 eV, which is reported as the shortest emission wavelength among all the solution based GQD. This method is versatile in terms of carbon source in that most of the carbohydrates which contain C, H, and O in the ratio of 1:2:1 may be used as the carbon source to prepare GQD provided that H and O exist in the forms of hydroxyl, carboxyl, or carbonyl groups that may dehydrate under hydrothermal conditions.

Nanotomy-Assisted Exfoliation

Nanotomy assisted exfoliation was reported to produced graphene nanostructures with various predetermined shapes with controlled dimensions (Mohanty *et al.* 2012). They achieved this by diamond-edge-induced nanotomy (nanoscale-cutting) of graphite into graphite nanoblocks, which were then exfoliated.

Ultrasonic Shearing

A simple ultrasonic route for producing GQD with excitation independent up- and down-converted emission was reported in the literature (Zhuo *et al.* 2012). They used the GQD as photosensitizers for rutile and anatase photocatalyst systems.

2.2.1.2. Bottom Up Method

Synthesis of GQD from hexa-peri-hexabenzocoronene, a polycyclic aromatic hydrocarbon was among the first reported attempt to synthesize GQD from bottom-up route (Liu *et al.* 2011a). The monodispersed disk-like GQD of ~60 nm and 2 - 3 nm thickness having nanoscale fragments of graphene stacked via π interactions were produced. A step wise organic synthesis was employed to produce large colloidal GQD (Yan *et al.* 2010b). The QD were made up of 132, 137, and 168 conjugated carbons produced by the oxidation of polyphenylene dendritic precursors. These QD were stabilized by 2',4',6'-trialkyl phenyl groups. The group then extended their work to make the GQD dispersible in water (Yan *et al.* 2010a). They noted that as the size of the quantum dot increases, although there is more edge available to attach flexible chains to, there is also higher inter-graphene attraction leading to stacking. To prevent the stacking, they attached the trialkyl phenyl groups such that the quantum dots were enclosed in 3D and could no longer stack.

2.2.1.3. Side Way Method

Researchers have also shown a unique side way approach to synthesized GQD by means of the cage opening of fullerenes (Chua *et al.* 2015). The work was similar to the an earlier report where very small GQD were formed by the ruthenium catalyzed cage-opening of C₆₀ (Lu *et al.* 2011). The ruthenium surface interacts strongly with the C₆₀ molecules, leading to surface vacancies on the ruthenium, which helps the C₆₀ molecules to embed in the surface. The fragmentation of the embedded molecules at elevated temperatures then produces carbon clusters that undergo diffusion and aggregation to form GQD. The shape of the GQD can be tailored by optimizing the annealing temperature.

2.2.2. GQD as Sensors

In recent years, GQD have various applications in analytical chemistry due to their unique photophysical properties. GQD have emerged as a potential tool for designing and tuning their PL for chemical sensors and biosensors. In the past decade, many efforts were made in the development of nanoparticle (NP) based sensors and biosensors. In this context, CNT and graphene are the most sought-after materials for

the development of sensors. They have been employed in developing electrochemical sensors and also optical sensing (Pérez-López and Merkoçi 2012). QD have attracted significant interest over the past decade due to their exceptional optical and electronic properties. They have shown potential usage in the development of PL and electrochemical sensors. However, most of the QD suffers the issue of acute toxicity towards humans and therefore renders them biologically incompatible. In addition, they are colloids and their coupling to chemicals is difficult and causes problems with the colloidal stability in some applications (Kuang *et al.* 2011). Few of the sensor systems based on CNT, graphene, and QD have been applied for sensing biomolecules, DNA, proteins, pesticides, heavy metals and gas (Pérez-López and Merkoçi 2012; Kuang *et al.* 2011). When compared to the existing materials for sensing, GQD have been utilized in the determination of a various chemical entities with comparable sensibility and selectivity. The GQD based sensors have even exhibited improvement in certain aspects, such as the better dispersibility as compared to CNT and graphene in polymeric matrices and aqueous solutions (Pérez-López and Merkoçi 2012). Additionally, GQD are non-toxic, easy to handle and possess excellent optical and electrical properties expected from QD. The exceptional properties of GQDs have fostered the development of different types of sensors using conventional, doped or functionalized NP for detecting metal ions, small organic molecules, and biomaterials with improved sensitivity, selectivity, and specificity. There still exists enormous potential for their development as sensing materials due to their recent emergence.

2.2.2.1 Photoluminescence sensors

Photoluminescence (PL) sensors based on GQDs have so far been used mainly to detect ionic species, small organic molecules or biomaterials. GQD-based probe sensors have been used to determine Fe^{3+} , Cu^{2+} , Al^{3+} and the hazardous species like Hg^{2+} , Cr^{6+} , and Ni^{2+} (Benítez-Martínez and Valcárcel 2015; Wang *et al.* 2017; Xu *et al.* 2017). Analytical applications of these sensors are largely focused on Fe^{3+} , due to its prominent role in biological systems.

The selective detection of Fe^{3+} ions in water samples was achieved by the use of Nitrogen-doped GQD (N-GQD) PL sensor (Xu *et al.* 2015). N-GQD and amine functionalized GQD (NH_2 -GQD) were used to determine Fe^{3+} in tap water by

attenuating the PL emission of the dots (Li *et al.* 2015a). Nitrogen atoms in these cases acts as chelating sites for Fe^{3+} ions. N-GQD was also synthesized by a green and inexpensive route for highly sensitive and selective sensing Fe^{3+} (Tam *et al.* 2014). A PL probe based on the N-GQD obtained by hydrothermal treatment in the presence of hydrazine of GQD previously prepared by pyrolyzing citric acid was reported as a label-free detection platform for Fe^{3+} in real water samples (Ju and Chen 2014). The quenching of PL in such cases was thought to be the formation of hydroxides, when metal ions coordinate with hydroxyl groups present at the edges of N-GQD, and restrain recombination of excitons by facilitating charge transfer. Similarly, Sulphur-doped GQD (S-GQD) were also used as an PL probe for the selective detection of Fe^{3+} in serum samples (Li *et al.* 2014). The incorporation of S atoms into the GQD skeleton tunes the local electronic density of the QD and promotes the coordination of phenolic hydroxyl groups at the edges of S-GQD to Fe^{3+} . This is a highly specific interaction responsible for the PL quenching in the S-GQD. Ionic Liquids (IL) were also used to synthesize IL-modified GQD for the determination of Fe^{3+} (Ananthanarayanan *et al.* 2014). Incorporation of IL led to the aggregation of IL-modified GQD, with ferric ions acting as coordinating sites to bridge several functionalized QD. This aggregation led to the PL quenching of the QD. A similar quenching effect of GQD obtained by carbonizing pyrene was also used for the sensitive detection of Fe^{3+} (Zhou *et al.* 2013). The selectivity for ferric ions was credited to their specific coordination with hydroxyl groups present at the edges of GQD.

Copper, another essential trace element for plants, animals and humans have been largely attempted to be determined or detected by the modified GQD based PL sensors. Cu^{2+} ions can be easily absorbed on pristine GQD (Liu *et al.* 2014). A sensing platform based on the PL quenching owing to the complexation of Cu^{2+} by GQD was reported for the highly efficient detection of Cu^{2+} (Wang *et al.* 2014b). Addition of Biothiol cysteine to the Cu^{2+} -GQD complex in aqueous solution recovered the PL fraction which was quenched by complexation of Cu^{2+} ions with GQD (Liu *et al.* 2014). This facilitated the development of a turn-on method for the quantification of Cu^{2+} . NH_2 -GQD were also employed to sense Cu^{2+} (Sun *et al.* 2013). The PL quenching effect for these sensors was possibly due to the non-radiative electron/ hole recombination annihilation via an effective electron transfer process.

Al^{3+} is another cation which pose a sever health hazard towards human health. A boron functionalized GQD (B-GQD) based sensor was reported for the detection of Al^{3+} (Fan *et al.* 2014). B-GQD with green PL were prepared electrochemically using a graphite rod (anode) and a Pt foil (cathode) immersed in a borax aqueous solution. The sensor exploited the PL intensity enhancement of B-GQD upon interaction with Al^{3+} .

Heavy-metal ions Hg^{2+} , Cr^{6+} , Ni^{2+} and Cd^{2+} are hazardous, pervasive pollutants with high toxicity and adverse impacts on human health. In this light, various GQD-based sensors have been developed for their detection and quantification. Thus, Wang *et al.* developed a GQD-based sensing probe for Hg^{2+} (Wang *et al.* 2014a). Another GQD-based sensor for the determination of Hg^{2+} in aqueous solution was reported by Chakraborti *et al.* (Chakraborti *et al.* 2013). The interaction between Hg^{2+} ion and GQD results in an aggregate-induced quenching due to the affinity of Hg^{2+} towards carboxyl groups present at the edges of GQD. Deep blue colored PL N-GQD was reported to determine Cr^{6+} in water samples (Cai *et al.* 2014). The quenching of PL was due to the reduction of Cr^{6+} to Cr^{3+} , promoted by hydroxyl groups and nitrogen in the QD. Huang *et al.* reported a metal-ion sensor based on a quenching-recovery strategy for Ni^{2+} detection (Huang *et al.* 2013). Dimethylglyoxime was introduced as a competitive chelator for Ni^{2+} and afforded the selective detection of nickel ions. This sensing strategy is also proved useful for the detection of Mn^{2+} , Co^{2+} , and Cu^{2+} ions. The PL quenching effect was ascribed to facilitated non-radiative electron/hole recombination annihilation through effective electron transfer quenching.

A combination of GQD and the $\text{Fe}^{2+}/\text{Fe}^{3+}$ redox couple was used as a label-free GQD-sensor for colorimetric detection of H_2O_2 (Wu *et al.* 2013). The sensor was used to detect the color change observed in a GQD solution containing peroxidase substrate from yellow to green due to the reduction of H_2O_2 catalyzed by GQD.

The monitoring of anionic species in environmental matrices with GQDs was a subject of some interest in recent years. The presence of ClO^- ions hypochlorite ions results in a proportional increase in PL of GQD which was used for analytical purposes (Hallaj *et al.* 2015). Hypochlorite ions oxidize the QD, thereby enhancing their PL. It is an assumption, that the sensing mechanism involves a chemical reaction between GQD and ClO^- . Dong *et al.* constructed another free-chlorine sensor based on surface-

passivated blue GQD (Dong *et al.* 2012). The oxidation of self-passivated layer of GQD in the presence of ClO^- ions quenches its PL. N-GQD are also found sensitive to pH in the range 1.81– 8.96, thus providing a general pH sensor with a wide range of applications from determinations of species in real water sample to the quantification of intracellular contents (Wu *et al.* 2014). A fast, sensitive, specific, and pH-dependent PL off-on sensor based on GQD was reported by Bai *et al.* for the determination of phosphate ions (Bai *et al.* 2013). The PL quenching observed in the Eu^{3+} ion aggregated GQD is due to the energy transfer caused by the complexation. The recovery of GQD to its native state restores the PL, as the Eu^{3+} ions binds to phosphate. Therefore, the use of Eu^{3+} ions aggregated GQD acts as an off-on sensor for the detection of phosphate ions. GQD were also successfully used to detect alkaline phosphatase by coordinating Cu^{2+} with GQD (Zhu *et al.* 2015).

Glucose is among the most important biomolecules. There is widespread research available for the sensors developed to determine glucose in different media. B-GQD prepared by hydrothermal cutting of boron-doped graphene was realized as a PL probe for the selective sensing of glucose (Zhang *et al.* 2014). The mode of determination is based on the aggregation-induced PL enhancement of the QD brought about by the reaction of the two cis-diol units in glucose with the two boronic acid groups on B-GQD. This reaction restricts the intramolecular rotation and increase the PL of the formed aggregate. The 3-aminobenzeneboronic acid functionalized GQD is another boronic GQD sensor reported for the determination of glucose (Qu *et al.* 2013). This is a PL turn off sensor as the presence of glucose leads to the formation of a negatively charged boronated complex between glucose and the functionalized QD. The formation of complex leads to the coulombic charge transfer results in the loss of PL. Various other monosaccharides were also reportedly detected by using GQD in combination with a boronic acid-substituted bipyridinium salt (Li *et al.* 2013b). This sensor system was sensitive to other saccharides in the following order:

Fructose > Galactose > Glucose.

The increasing use of NP have created a need for a check on the human and environmental exposure to nanomaterials. Development of effective methods to monitor the presence of nanomaterials is indispensable for detecting relevant

concentrations of NP, separating NP, and removing potential interferents from samples. A GQD-based sensor for the determination of GO in environmental samples, which is among the largest used form of graphene, was developed as the presence of GO quench the PL of the GQD (Benitez-Martinez *et al.* 2014). GO was retained in a cellulose membrane from spiked river-water samples and recovered by sonicating the membrane. Attenuation of the PL was ascribed to energy transfer between the two types of carbon NP (non-covalent interactions and π - π stacking, mainly).

2.2.2.2 Electrochemical sensors

The application of GQD as PL sensors and biosensors by virtue of their stable luminescence and unique optical properties is widespread. On the contrary, GQD have rarely used to construct electrochemical sensors despite their known properties as electron carriers and acceptors. However, there are few reports concerning the use of GQD as electrochemical sensor. Among the very first reports of such sensors is a GQD-modified gold electrode used to detect H₂O₂ (Zhang *et al.* 2013). Chronoamperometry (CA) measurements was found to be suitable for assessing the catalytic response of the GQD/Au electrode to H₂O₂. In another report, a carbon ceramic electrode (CCE) modified with GQD as a glucose oxidase (GOx) substrate for the electrochemical sensing of glucose was presented (Razmi and Mohammad-Rezaei 2013). The GOx catalyzed the reduction of oxygen was studied by the group using CV measurements. The reduction in current was proportional to the concentration of glucose. Roushani *et al.* reported an electrochemical sensor based on GQDs for the detection of persulfate (S₂O₈²⁻) (Roushani and Abdi 2014). The electrochemical performance of the sensor was examined by CV and CA. In another use of GQD as an electrochemical sensor, a molecularly imprinted polypyrrole/GQDs composite for detection of bisphenol A was reported (Tan *et al.* 2016).

2.2.3 GQD in Photovoltaics

Photovoltaic devices are perhaps the most exciting avenue for GQD. The prospect of exploiting the tunable electronic properties and ability of graphene to absorb a high percentage of incident light, GQD-based PV shows great potential. Unlike graphene, this material has potential to be a sensitizer material for PV cells. A straightforward electrochemical method for producing GQD from free standing graphene was reported

(Li *et al.* 2011). Hydrophilic and monodisperse GQD of 3 - 5 nm in diameter was prepared by the treatment of graphene with O₂ and using it further as a working electrode in a cyclic voltammetry setup. As mentioned in earlier section, the GQD displayed an excitation-dependent emission wavelength and intensity which was distinct from other QD compositions. The presence of hydroxyl, carbonyl, and carboxylic acid groups on the surface of the as-prepared GQD was determined using high-resolution XPS. These groups made the GQD water soluble, and paved the way for potential conjugation with other molecules. GQD were also soluble in some organic solvents which makes them suitable to be used in the non-aqueous phase of devices. GQD were integrated into polymer PV cells, with a composition of ITO/PEDOT:PSS/P3HT:GQD/Al to form a metal-insulator-metal device, giving PCE of 1.28% after some optimization, outperforming the GQD free assembly.

The photoelectrical properties of colloidal GQD are expressed differently when orientated differently on polar surfaces (Hamilton *et al.* 2011). The orientation of molecular devices on surfaces can change their efficiency and even functionality. Therefore, the control on the orientation of colloidal GQD on a water and mica substrate led to the inference about the effect the orientation of GQD have on the photo electric properties of colloidal GQD in a solution. The alignment of the GQD on the substrate (water) was determined by the strength of the molecule-water interaction, and the co-facial molecule-water interaction. Colloidal GQD used by Hamilton were produced via the synthetic approach reported by Pan *et al.*, which results in carboxylate GQD (Pan *et al.* 2010). Three types of GQD were synthesized to get differing degrees of carboxylic acid modification, differing numbers of alkyl chains attached (2',4',6'-trialkyl phenyl) and sizes. The aggregation of the GQD has been prevented by the alkyl chains, which, due to steric constraints, twist in all 3D creating a cage around the graphene core. The photoinduced charge injection could potentially be tuned by these alignment effects for increased cell performance.

GQD have been explored for use is in DSSC as a supplement or replacement of dyes as it has the potential to increase the efficiency of DSSC. GQD can be used as both photoanode sensitizers (Li *et al.* 2011; Pan *et al.* 2013), and composite materials in counter electrodes (Chen *et al.* 2013b). It is the size and synthesis-dependent optical

properties, efficient multiple carrier generation, high PL quantum yields, tunable band gaps, high electronic mobilities, and high specific surface areas that make GQD ideal for use in DSSC.

A large GQD core with 168 conjugated carbon was synthesized for photovoltaic applications having showed maximum absorbance at 591 nm (Yan *et al.* 2010a). The GQD had a molar absorption coefficient an order of magnitude larger than metal complexes used in DSSC ($1.0 \times 10^4 \text{ M}^{-1}$). The photoelectrical properties of these GQD on a TiO_2 photoanode was studied, which was constructed by the immersion of nanocrystalline thin films of TiO_2 on conducting glass in a toluene/ethanol mixture containing GQD. The HOMO (5.3 eV) and LUMO (3.8 eV) of the GQD, when compared to the relative bands of TiO_2 , and reduction potential of the I^{3-}/I^- electrolyte allowed the sensitization of the TiO_2 . An open current–voltage of 0.48 V was produced. It was noted that the efficiency of the cell can be increased by tuning the functionalization and surface chemistry GQD. The increase in the affinity of the GQD to the TiO_2 surfaces through similar modifications also effects the properties of the resulting PV device.

GQD-sensitized nanotube arrays were used to fabricate photo electrocatalysts (Pan *et al.* 2013). TiO_2 nanotube arrays (TNA) were chosen by the authors due to their high n-type photoconductivity (excess free electrons), large internal surface area, excellent stability, and environmental friendliness. The GQD were prepared by a hydrothermal method and were complexed with the TNA via vacuum-assisted filling and electrophoretic filling, with the latter being preferred due to poor GQD deposition on the TNA when using the former (Chen *et al.* 2013b). The GQD-TNA heterojunctions showed enhanced photoelectrochemical activity over unfilled TNA, and that reported for CdS filled arrays. The researchers reported that visible light excitation of GQD resulted in electron transfer to the TiO_2 and inferred that the mechanism for electron transfer would lead to highly active holes on the surface of the GQD, which would oxidize water, producing hydroxyl radicals. The production of a $\bullet\text{OH}$ radical may be useful for decomposing organic pollutants in the water to CO_2 and H_2O_2 (Pan *et al.* 2013).

Green-luminescent GQD and poly(3-hexylthiophene) (P3HT) were used to construct a bulk heterojunction polymer (Li *et al.* 2011). They constructed a photovoltaic cell, where an electron transport cascade results in an electric current, (where PEDOT:PSS stands for poly(3,4-ethylenedioxythiophene):poly(styrene sulfonate)). They showed that the addition of GQD to the active layer (P3HT) improved the performance of the cell, which showed an open circuit voltage of 0.67 V (PCE = 1.28%). As per the authors, while the increased performance is probably due to the high electron mobility within the GQD, the low fill factor (conversion efficiency) can be attributed to the lack of device optimization common with novel constructions. Publication by Kim *et al.* shows a similar system with significantly improved performance (Kim *et al.* 2013a).

GQD-doped polypyrrole counter electrode were fabricated with the GQD synthesized via the oxidation of carbon black and then being added to a pyrrole/lithium perchlorate solution (Chen *et al.* 2013b). This complex was doped onto fluorine-doped tin oxide (FTO) glass, by electrochemical deposition. For the fabrication of the DSSC, an I³⁻/I⁻ electrolyte was sandwiched between the CE and a TiO₂ photoanode. Doping the polypyrrole with GQDs afforded a more porous structure, with more active sites and higher charge transfer rate for electrolyte reduction. A 10% doping with GQD gives the highest PCE, close to that afforded by a platinum CE.

GQD/polymer blends were used to improve the optoelectronic properties of photovoltaic devices containing graphene-based materials (Gupta *et al.* 2011). Their focus was the development of low-cost donor/acceptor materials for photovoltaic applications. They showed that GQD-polymer blends performed better than graphene-sheet-blended polymers. GQDs were synthesized via a hydrothermal method and were then functionalized with aniline (ANI-GQD). Two types of cells were constructed; cells with the blended ANI-GQD-functionalized polymers (P3HT/ANI-GQD), and cells with graphene-sheet aniline-functionalized polymers (P3HT/ANIGS). The peak performance for the P3HT/ANI-GQD was for a device consisting of 1 wt% ANI-GQD. The researchers investigated the morphology of the blends using AFM. The GQD blend showed uniform morphology and nanoscale phase separation, while the graphene sheet blend showed large-scale phase separation. This difference in morphologies increased the resistance for exciton migration and reduced the device performance.

A zinc oxide/GQD solid-state solar cell was also reported in the literature (Dutta *et al.* 2012). The GQD were synthesized by a top-down approach, which were used to infiltrate and cover ZnO nanowire (NW) arrays grown on aluminum doped ZnO (AZO) thin films, by repeated spin-casting of an ethanolic suspension of GQDs on the NWs. They then deposited a 60–70 nm layer of N,N'-diphenyl-N,N'-bis(3-methylphenyl)-1,1'-biphenyl)-4,4'- diamine (TPD) to act as a hole transporting layer. The deposited materials were then annealed, and a gold electrode sputtered on the TPD layer. The researchers verified the charge transfer at the interface between the photo-excited GQDs and ZnO NWs by emission spectroscopy and photovoltaic measurements. The open circuit voltage reported was 0.8 V without any optimization. N-GQD synthesized by hydrothermal method also proves to be an efficient green sensitizer with ZnO nanorod based photoanodes for solar energy conversion when compared to pristine GQD (Majumder and Mondal 2016).

2.3 SUMMARY OF LITERATURE REVIEW

Graphene and GQD, both have shown voluminous advances in field of sensors and PV. Both being different types of nanomaterials often have different roles to play in such applications.

Graphene being a continuous 2D nanomaterial having large surface area proves to be a very good substrate to sensing reagents in sensors. Additionally, they show a change in electronic conductivity upon interacting of analytes and change often is selective. Therefore, Graphene have been used as sensor for various kinds of analyte among which, gases are prime ones. On the other hand, GQD being more discreet 0D nanomaterials have only been used as sensing agent. The presence of functional groups on the edge and excitonic confinement, leads them to be used both as EC sensors and PL sensors respectively. We have discussed the sensing ability of both in details, with suitable references and the various mechanism making the sensing of analyte possible.

The properties of graphene and GQD make them ideal candidate of PV applications. Graphene here again leads the range of use in PV cells from being substrate for sensitizer, to hole transport to electrode. Potential in modification of graphene have opened doors to variety of ideas to make use of it in PV cells. On the other hand, GQD and their modified version have been tried as sensitizers for PV cells and replace

existing inorganic quantum dots in QDSC. Very little amount of work has been done in the field and this gives us an opportunity to explore the use of these materials in the stated applications.

2.4 PROPOSED WORK

2.4.1 Motivation

Even-D carbon nanomaterial is a class material that warrants more insight to understand about their properties. They are new in the game and this excites the curiosity to explore the material for their properties and various potential applications. Widespread research in Graphene led to the discovery of a very interesting materials, which is just a fragment of Graphene called GQD due to the properties which are present in typical quantum dots. These properties of GQD make it widely useful for variety of purposes, among which sensing and photovoltaic applications at the forefront. It is so because the fate of electron after excitation in GQD decide whether it can be used as a sensor (observed PL when excited electron return to ground state) or a photosensitizer (when excited electron is extracted to produce current via photosensitization).

In recent years, both graphene and GQD have shown profound applications as sensors. The sensing ability of these ranges from hazardous cations to anions, from biomolecules to oxidants, and from toxins to explosives. The mode of sensing studied ranges from electrochemical sensor, photo-luminescent/fluorescent sensors, colorimetric sensors and hybrid sensors to something called as immunosensors and aptasensors as well. These nanomaterials have shown immense potential in sensing biomolecules, like DNA, proteins, Amino acids, Uric Acid, Glucose and even virus. This shows promising potential of these materials to be employed as a choicest material for various sensing applications.

Photovoltaic is another very promising area for even-D carbon nanomaterials. Most used form of PV cells is made of silicon and germanium semiconducting material and although have good efficiency and stability but are also expensive. Thus, a continuous search for a more economical photovoltaic device is underway. This constant vigil to explore new type of photovoltaic device has given us a variety of cells.

Thin film solar cells are greatly explored for having relatively economical construction and transparent appearance. Among various hybrid thin film solar cells, two major categories are Dye-sensitized solar cell (DSSC) and Quantum dot solar cells (QDSC). QDSC promise more potential over DSSC owing to better quantum efficiency and band gap tunability of Quantum Dots (QD) as opposed to dyes.

Major drawbacks of QDSCs have been the toxic nature of QD (Cd is chief material in such cells) used in its construction. There have been efforts to produce relatively low toxicity Quantum dots (eg. Indium (In) based QD) but source of Indium as such is much expensive rendering the device less cost effective. GQD thus provide a novel and exciting material for the construction QDSC because of low toxicity of carbon, and more economical source.

2.4.2 Objectives

In current proposal, we aim to achieve following objectives:

- To synthesize functionalized even-D carbon nanomaterials with suitability for chemical sensing material.
- To characterize the as synthesized product by TEM, XRD, and spectroscopic techniques such as FTIR, UV-Vis, PL and Raman Spectroscopy.
- To construct suitable PL sensing for glucose and metals ions
- To construct suitable electrochemical sensing material for oxalic acid.
- To synthesize functionalized GQD for photosensitization.
- To construct a GQD sensitized QDSC.

CHAPTER 3

**SYNTHESIS AND CHARACTERIZATION OF GRAPHENE
QUANTUM DOTS AND THEIR SIZE REDUCTION USING
SWIFT HEAVY ION BEAM**

Abstract: This chapter includes a discussion over the synthesis of GQD by swift ion beam irradiation over graphene oxide.

3.1 INTRODUCTION

The synthesis of GQD is possible by various routes (Bacon *et al.* 2014). As is the case with any nanoparticle, the steps to achieve it is one among the top down approach or bottom up approach. The synthesis can also be classified as chemical or physical methods. In terms of yield, the chemical synthesis always is a beneficial route to follow. This mode of synthesis also enables researchers to chemically modify the GQD to obtain the desired properties, for e.g. (Jang *et al.* 2015) reported that the oxidation of GQD results in the red shift the PL from blue to green. However, a major limitation of the chemical route is the production of non-regular sized GQD. This in turns limits their usability as it dilutes the property of the GQD. Physical route of producing GQD also have shown better control over the shape and size of the end product. Ultra-high-resolution electron beam lithography was used for cutting graphene to desired size fragments (Ponomarenko *et al.* 2008). The block copolymer were used as etch mask for the size controlled fabrication of GQD (Lee *et al.* 2012). However, low absolute yield was a major drawback in such methods.

The effect of ion beam over graphene is well-studied. Graphene has shown remarkable stability in high density 150MeV Au ion irradiation (Kumar *et al.* 2014a). Graphene was shown to have defects at higher fluence with appreciable retainment of crystallinity. The swift heavy ion irradiation of 100 MeV Ag ion may also be utilized as a tool for defect annealing in graphene (Kumar *et al.* 2014b). A fluence of Ag ion irradiation above 1×10^{13} ions/cm² reduced the number of graphene layers. The focused ion beam was used to cut graphene sheet (Kotakoski *et al.* 2015). Ga⁺ focused ion beam was employed to carve out random patterns from pristine graphene showing how ion beam can be utilized in cleaving the graphene sheet to smaller sizes. However, the effect of ion beam irradiation on graphene oxide was less explored. The structural changes may be brought about by exposing graphene oxide to electron beam (Tyagi *et al.* 2016). The reduction of graphene oxide in 25 eV electron beam with varying fluence was studied as well. Here, a two-step process of producing size controlled GQD made possible using both chemical and physical process is presented. Additionally, the

method is a quintessential top down approach of synthesis, which produce blue luminescence GQD.

3.2 EXPERIMENTAL

3.2.1 Materials

Graphite was procured from Sigma Aldrich. Sulphuric acid, nitric acid, phosphoric acid, hydrogen peroxide, hydrochloric acid and sodium hydroxide were purchased from Finar Chemicals and used without further purification.

3.2.2 Synthesis of Graphene Quantum Dots

In a typical synthesis procedure (Figure 3.1), GO was prepared using Improved Hummer's method (Marcano *et al.* 2010). In a typical procedure, 100 mL of 9:1 ratio of H_2SO_4 and H_3PO_4 was added to a beaker containing 1 g of graphite and 6 g $KMnO_4$. This mixture was stirred for 12 h at 50 °C over a magnetic stirrer. The mixture was then brought to room temperature and added with 3mL 30% H_2O_2 . The resultant mixture neutralized using NaOH, centrifuged and the precipitate was washed thoroughly with dil. HCl, methanol and distilled water to obtain graphene oxide and dispersed in 500 mL distilled water. Further, as prepared GO was put in a Teflon-lined autoclave in alkaline medium and reaction was kept for 16 hours at 150 °C which is in accordance to hydrothermal synthesis (Pan *et al.* 2010). This yielded a suspension of GO fragments and GQD. The as obtained fragmented GO and GQD were spin coated onto glass substrate and then exposed to Ni ion beam of 80 MeV at a fluence of 1×10^{12} ions/cm² available from the 15 UD tandem pelletron accelerator at IUAC, New Delhi, India. The resultant GQD were dispersed in water using ultrasonic bath.

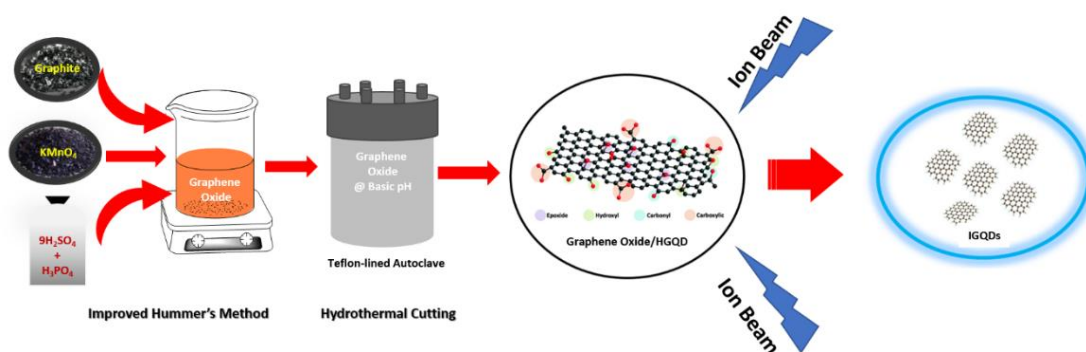


Figure 3.1 Synthesis of Graphene Quantum Dots using Swift Heavy Ion Beam.

3.3.3 Characterizations

The GO was characterized using Rigaku miniflex X-ray diffractometer using Cu-K α radiation of 1.54Å operating at 40 kV and 15 mA with a scan rate of 2° sec⁻¹. GQDs were characterized using Transmission electron microscopy (JEM-2100Plus Transmission Electron Microscope), Bruker Alpha Eco-ATR FTIR in ATR mode with scan range of 4000-600 cm⁻¹ and 24 scans, Analytik Jena Specord S600 UV-Vis Spectrophotometer, and Horiba Fluoromax Spectrofluorometer.

3.3 RESULTS AND DISCUSSION

GO as synthesized was analysed using powder X-ray diffraction. GO represents itself in the XRD with its characteristic broad peak corresponding to (002) plane found at diffraction angle (2 θ) of 9.98° (Figure 3.2). The graphitic sharp peak occurring at 2 θ of 26° (Figure 3.3) is absent in XRD pattern of GO which indicates the complete loss in graphitic staking of 2D carbon layers. These assignments of peaks are well established (Stobinski *et al.* 2014). Moreover, the presence of trace graphene in graphene oxide is not observed in the conventional XRD and can be seen only with synchrotron XRD (Kumar *et al.* 2014a). A further inspection of GO by TEM (Figure 3.4) shows a very clear sheet with usual creases found in a typical 2D structure.

After the hydrothermal treatment of GO, we obtained a mixture of fragmented GO and GQD. The presence of GQD was confirmed by the faint blue PL which was observed when the obtained mixture was seen under a longwave UV lamp. The hydrothermally obtained GQD (HGQD) and ion beam irradiated GQD (IGQD) were further studied under the TEM to understand the changes brought upon by the irradiation process over their sizes (Figure 3.5 and 3.6). HGQD under TEM showed larger fragment size of 100 nm (which is supported by Particle size analysis given as inset). However, as per the hypothesis, the beam irradiation significantly reduced the size of GQD as the average size of IGQD was approximately 30 nm (inset from particle size analysis).

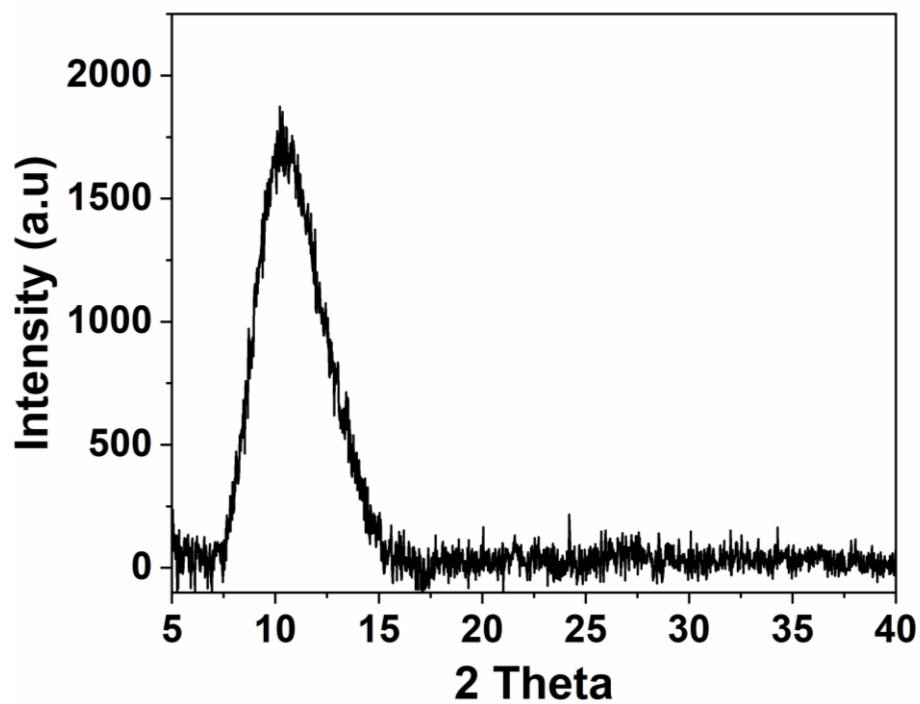


Figure 3.2 XRD spectrum of graphene oxide

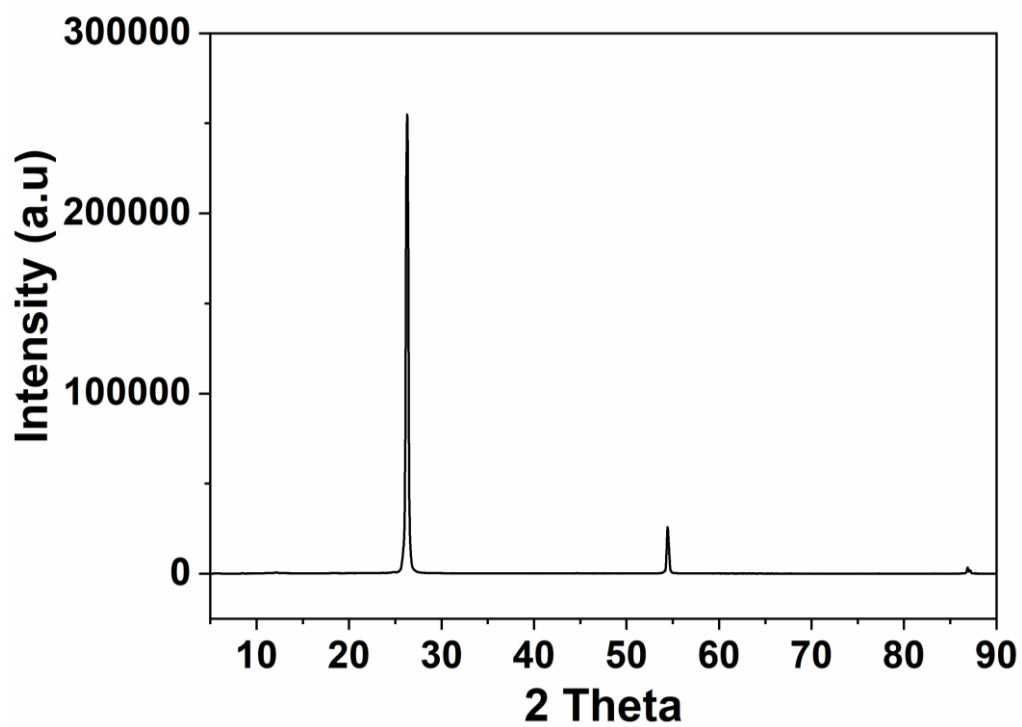


Figure 3.3 XRD spectrum of graphite

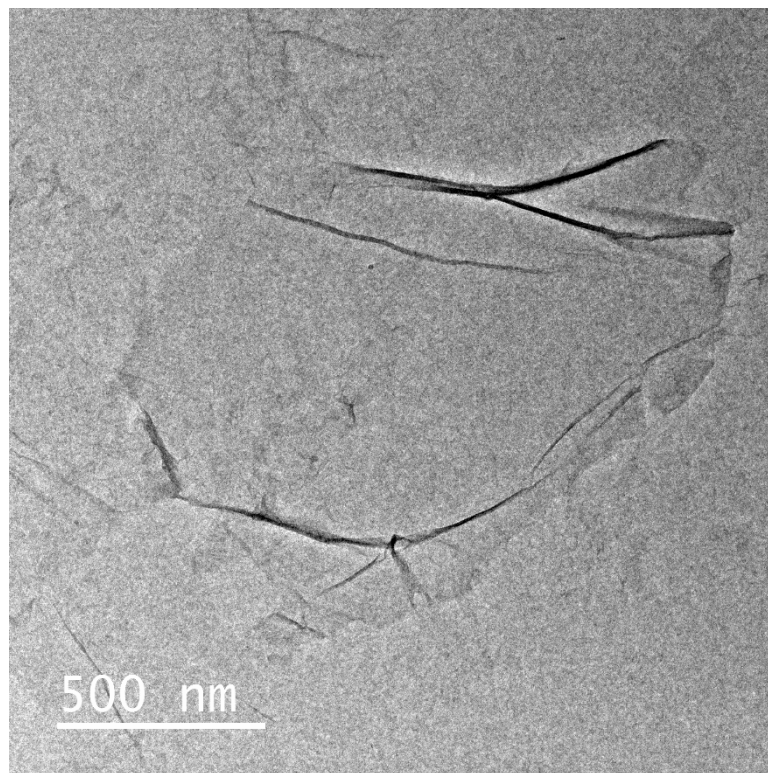


Figure 3.4 Transmission electron microscopic image of graphene oxide

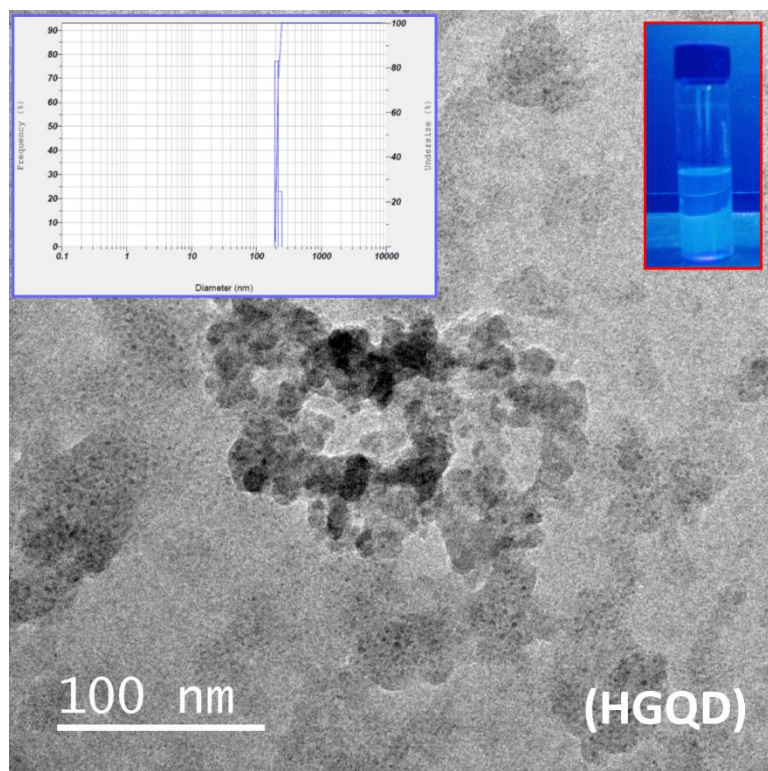


Figure 3.5 Transmission electron microscopic image of HGQD

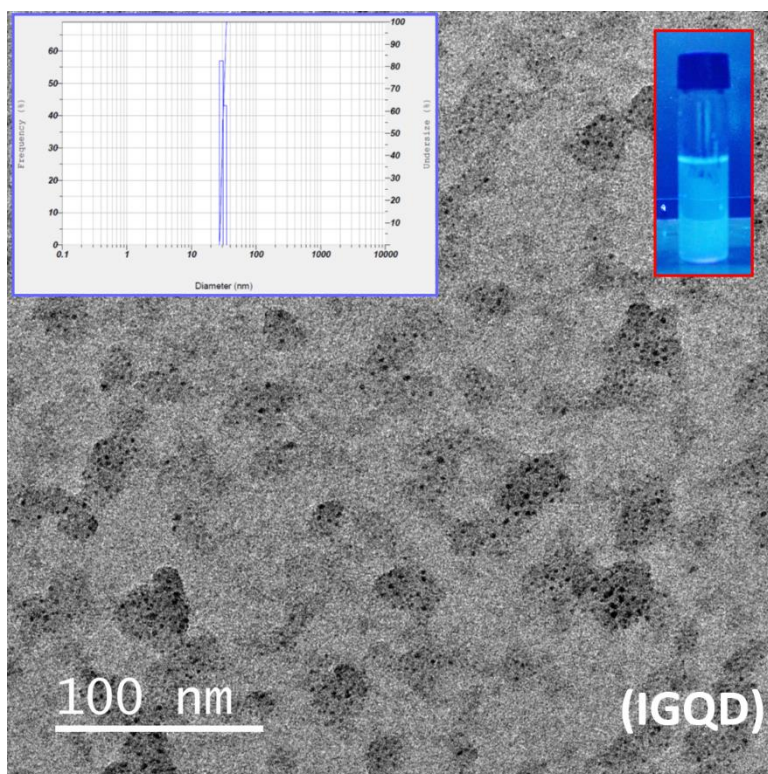


Figure 3.6 Transmission electron microscopic image of IGQD

The reduction in size is brought about due to the cleaving of C-O-C bonds present on the HGQD and GO when irradiated with the beam. This was well understood by the study of FTIR spectra obtained for graphite, HGQD, and IGQD (Figure 3.7). Graphite being devoid of any functional group, showed no peak in FTIR spectrum. The HGQD spectrum presented with characteristic peaks corresponding to the -O-H stretching at $3200-3600\text{ cm}^{-1}$, -C=O stretching at 1634 cm^{-1} , -C-O- stretching at $1000-1300\text{ cm}^{-1}$, and aromatic -CH substitution at 850 cm^{-1} which are the usual bonds present in GO and HGQD. However, on irradiating with ion beam, the -CO- bond cleaved to yield smaller sized IGQD, which is evident from the absence of peak corresponding to -C-O- stretching at $1000-1300\text{ cm}^{-1}$ and aromatic CH substitution at 850 cm^{-1} in its FTIR spectrum. The cleaving of graphene oxide sheet is supposed to be taking place along -C-O-C- bond (Pan *et al.* 2010). However, the fragmentation of graphene oxide sheet along -C-O-C- bond takes place where C is substituted with additional H instead of in oxirane configuration as -C-C- bond cleavage is shown to be highly stable in presence of high energy irradiation (Kumar *et al.* 2014a). Additionally, there was no trace peaks

corresponding to Ni-O bond in the FTIR spectra which lead us to the conclusion that Ni was not present in the IGQD and was probably removed as oxide of nickel.

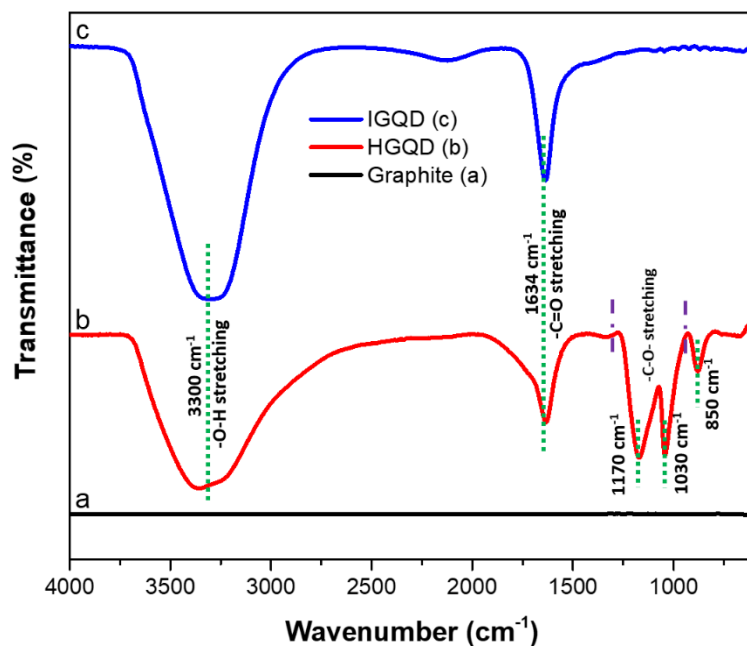


Figure 3.7 FTIR spectra of graphite, HGQD and IGQD

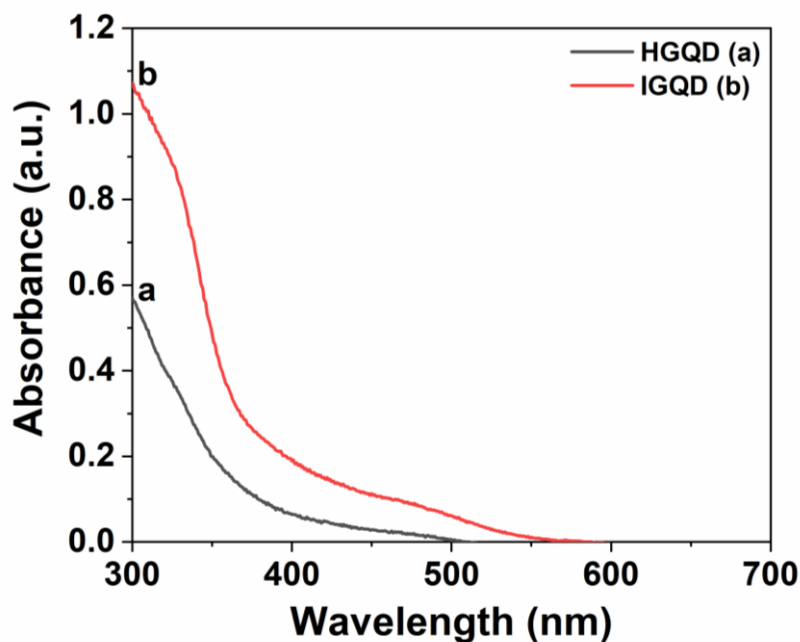


Figure 3.8 UV-Vis spectra of HGQD and IGQD

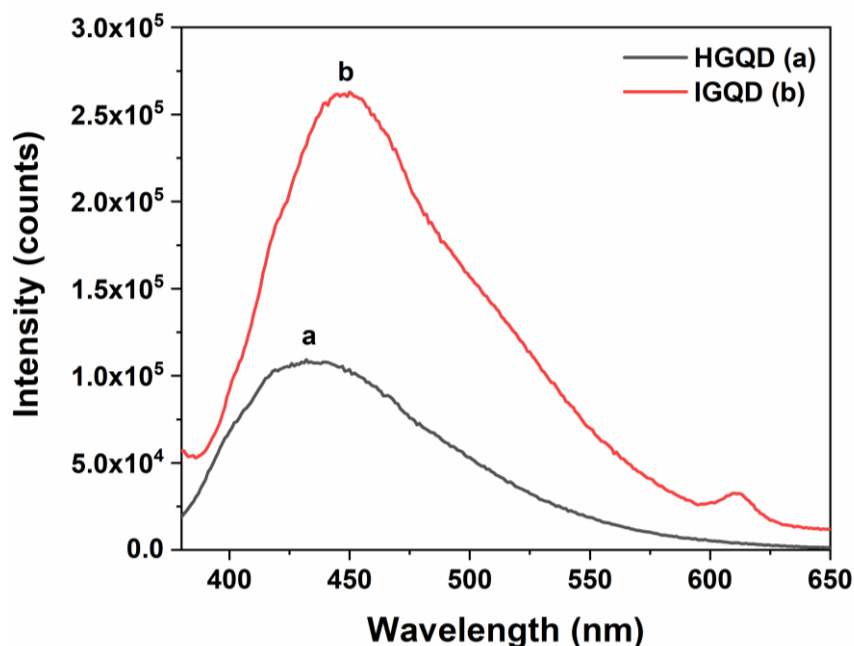


Figure 3.9 PL spectra of HGQD and IGQD

Photoluminescence is an important property of GQD as discussed earlier in the introduction. GQD exhibits PL behaviour when the size is reduced below 35nm. This is because the mobility of exciton is restricted in all the direction under 35 nm such that the energy released on the electron hole recombination is in the visible region. However, the energy requirement for the generation of exciton is 3.39 eV which is calculated from the UV-vis spectrometer where GQD showed the absorbance at 365 nm (Figure 3.7). It was expected that IGQDs should emit the higher intensity PL on excitation with 365 nm monochromatic wavelength than that of HGQDs. This is because, the PL is observed due to the presence of graphene quantum dots, and hence, the intensity of PL increase with the increase in the number of quantum dots. The PL spectra of HGQD and IGQD agrees with this assumption (Figure 3.8). Moreover, a closer inspection shows a very faint red shift in the emission within the PL from HGQD from IGQD. This is due to the better size regularization of GQD from HGQD to IGQD. The size of fragments in HGQD were very large and not controlled. They had huge variation which was evident from their transmission electron micrograph. As the PL emission varies with the size of quantum dots, the variation in size leads to a wide band of emission spectrum. However, in case of IGQD, the ion beam irradiation not only reduce the size of the quantum dots, the homogenous nature of fluence of the radiation

means the size of the dots are well regularized thereby giving a comparatively narrower emission spectrum. It must be noted along with this, that the regularization of size of GQD by ion beam also depends on the distribution of ethoxy linkage over the GO and HGQD frame which is not well controlled in the chemical route. Hence the overall nature of emission peak is still very wide as a result. Therefore, the results obtained from PL spectroscopy and TEM analysis suggest that treatment of GO and HGQD with swift heavy ion beam lead to a successful reduction in the size of the quantum dots.

3.4 CONCLUSIONS

In this study we have synthesized GQD via hydrothermal cutting of GO sheets which were further reduced in size by means of Ni²⁺ ion beam irradiation. High energy Ni ions were responsible for the cleaving of ethoxy bond present in GO and HGQD which led to the reduction in size of the GQDs there by increasing its PL intensity. The PL of the GQDs is a result of excitonic entrapment due to its size reduction. The controlled size distribution of ion beam irradiation of GQDs is evident from the TEM and particle size analysis. Hence, ion beam irradiation can be sought as a suitable technique to reduce the size of GQD.

CHAPTER 4

**ELECTROCHEMICAL REDUCTION OF AMINO-
FUNCTIONALIZED GRAPHENE QUANTUM DOTS
IMMOBILIZED ON GRAPHENE OXIDE FOR THE DETECTION
OF OXALIC ACID**

Abstract: This chapter presents a detailed account for the synthesis and characterization of NH₂-GQD-GO composite for the electrochemical determination of oxalic acid.

4.1 INTRODUCTION

Oxalic acid is commonly found molecules in various organisms like fungi, plants and animals. High concentration of oxalic acid is found to remove calcium from blood, which in turn have severe disturbances in the activity of heart and neural system. Normal range of oxalic acid in human body is 10-40 mg.24h⁻¹ in urine, and 0.8-2.50 μmol.L⁻¹ in blood plasma. However, in case of individuals with a metabolic disorder called hyperoxaluria, the amount of oxalic acid in their urine can be as high as 53-654 mg.24h⁻¹ (Koch and Strong 1969). This condition is often associated with kidney stone. Therefore, it is important to determine oxalic acid in biofluids (Tadi and Motghare 2013). There are very few methods reported for the determination of oxalic acid or the oxalates in biological systems. In 1929 the first method was presented to parallel the volumetric method to measure the oxalic acid by quantitative estimation of CO₂ by treating with KMnO₄ (Van Slyke and Sendroy 1929). This method is often used in conjunction with isolation of oxalic acid (Zarembski and Hodgkinson 1962). A reaction between oxalic acid and indole also led to the photometric determination of oxalic acid (Bergerman and Elliot 1955). Another related technique to determine oxalic acid in the biological system is fluorometric, colorimetric and spectrometric methods (Zarembski and Hodgkinson 1965; He and Gao 1997; Costello *et al.* 1976). Chromatography is another suitable techniques which was explored for the determination of oxalic acid (Fry and Starkey 1991; Pfeiffer *et al.* 1997). Electrophoresis is another reported technique for determination of oxalic acid (Trevaskis and Trenerry 1996). However, these methods require preparation of assays and thus are usually time consuming. A much more capable and fast sensors are thus needed in the modern age. Electrochemical sensors can meet this requirement, however, a major challenge is the lack of enzyme free electrochemical sensors (Pundir and Sharma 2010). Among the reported electrodes, bare platinum electrode and platinum nanoparticles decorated GCE have shown by far the best sensitivity towards oxalic acid (Ma *et al.* 2016). Bare platinum showed LOD of 0.38 μM whereas platinum nanoparticles decorated GCE could detect oxalic acid as low as 0.28 μM. The graphene modified carbon ionic liquid electrode

have shown to detect oxalic acid till 0.48 μM with a linear range of 8.00 μM to 6.00 mM (Wang *et al.* 2015). Palladium nanoparticles loaded carbon nanofibers modified carbon paste electrode have shown a detection limit of 0.2 mM with linear ranges of 0.2-13 mM and 13-45 mM (Liu *et al.* 2010). Similarly, platinum nanoparticles immobilized on polypyrrole nanofibers also presented as field-effect transistor type sensors for the determination of oxalic acid to femtomolar-level (Kim *et al.* 2018). Irrespective of showing appreciable sensitivity towards the detection of oxalic acid, these electrodes are very expensive to fabricate given the use of rare earth metal or the stability and synthesis of ionic liquid. Another common precedence in electrochemical detection is the use of the variation in anodic current (oxidative cycle) for the determination of analyte. Here we report a two-step synthesis of amino functionalized GQDs, which when forms suspension with graphene oxide (GO), can sense oxalic acid, which can be determined by electrochemical method. Graphene oxide is a 2-dimensional nanostructure which is loaded with oxygen rich functional group which makes its chemical modification possible (Pan *et al.* 2018). The GO provides high surface area to adsorb the analyte, thus was selected as substrate for the composite. The presence of oxygen rich group in the system also enables us to utilize the cathodic current (reduction cycle) for analysis. This enables the electrode to be very responsive towards the presence of analyte. This method is developed to offer a potential alternative to the existing enzyme-based sensors. An enzyme free sensor offers a better operating range and durability over enzyme based sensors (Chen *et al.* 2013c).

4.2 EXPERIMENTAL

4.2.1 Synthesis of amino functionalized GQDs

Graphite was procured from Sigma Aldrich. All the other reagents used in the experiment were purchased from Merck India. Graphene oxide (GO) was synthesized by the improved Hummer's method (Marcano *et al.* 2010) as described in earlier in Chapter 3. GQD were prepared using well reported hydrothermal cutting method (Pan *et al.* 2010), wherein, the as-prepared GO dispersed in water was adjusted to pH 10 using NaOH. Further, 18 ml of this mixture was autoclaved at 200 $^{\circ}\text{C}$ for 12 h. The resultant dispersion was filtered. The observance of photoluminescence at 365 nm confirms the synthesis of GQD. GQD were functionalized using

hexamethylenetetramine. GQD in hexamethylenetetramine solution was refluxed at 80 °C for 4 h to yield amino functionalized GQD (NH₂-GQD). NH₂-GQD-GO composite was synthesised by dispersing NH₂-GQD in GO suspension. GQD-GO composite was synthesised similarly by dispersing GQD in GO suspension.

4.2.2 Fabrication of Electrode

The NH₂-GQD-GO composite suspension was drop casted over the glassy carbon electrode ($\phi = 4.0$ mm) followed by 4 h of drying in hot air oven at 60 °C to form the working electrode. This electrode was further used to study its suitability for the electrochemical determination of oxalic acid. For a comparison, GQD, NH₂-GQD and GO drop casted glassy carbon electrodes were also fabricated.

4.2.3 Material Characterization

The X-ray diffraction pattern of Graphene oxide was characterized using Rigaku Mini Flex X-ray Diffractometer. Graphene oxide and GQD were examined under the Transmission electron microscopy (JEM-2100PlusTransmission Electron Microscope) for their morphology and size determination. The FTIR spectra of the samples were obtained using BRUKER FTIR spectrometer with Eco-ATR accessory. Raman spectra of the samples were obtained using a Renishaw Raman microscope using 514 nm laser excitation at room temperature.

All the electrochemical measurements were performed using Metrohm Autolab PGSTAT-30 electrochemical workstation using a three-electrode setup. Platinum wire was used as counter electrode and saturated calomel electrode (SCE) was reference electrode. The 0.2 M phosphate buffer (pH = 7.4) was used as electrolyte, which matches the pH of average urine sample. Scan rate for the all the measurement was 50 mV.s⁻¹. The voltage ranges for the cyclic voltammetry sweep from -1.0 V to 0 V with the start and end voltage of 0 V. For the electrochemical determination of the sample, 2 ml of sample (oxalic acid or urine) was added to the 20 ml of electrolyte. All the solutions were prepared using deionized water.

4.3 RESULTS AND DISCUSSIONS

4.3.1 Characterization of GO and GQDs

The GO synthesized by improved Hummer's method was analysed for its X-ray diffraction pattern to confirm its successful synthesis. Presence of the characteristic broad peak at $2\theta = 11.5^\circ$ corresponding to the (001) plane of graphene oxide (Figure 4.1) (Marcano *et al.* 2010). The peaks at $2\theta = 26.5^\circ$ and 54.5° are of (002) and (004) planes of graphitic carbon sheets respectively (JCPDS Card No.75-1621). These peaks suggest that some of the layered graphite like structure have been retained in the GO. This is further confirmed by TEM of $\text{NH}_2\text{-GQD}$ in Figure 4.6. Additionally, the graphitic peak may also be due to traces of nanographite which are retained with the graphene oxide. However, the small intensity of the graphitic peak suggests very low percentage of graphitic impurity in the GO. The accompanying transmission electron micrograph shows a typical sheet of GO with varying layers (Li *et al.* 2016) (Figure 4.2). Small ruptures in the sheets are also typical of GO, as they are indicative of the strong oxidation of graphene.

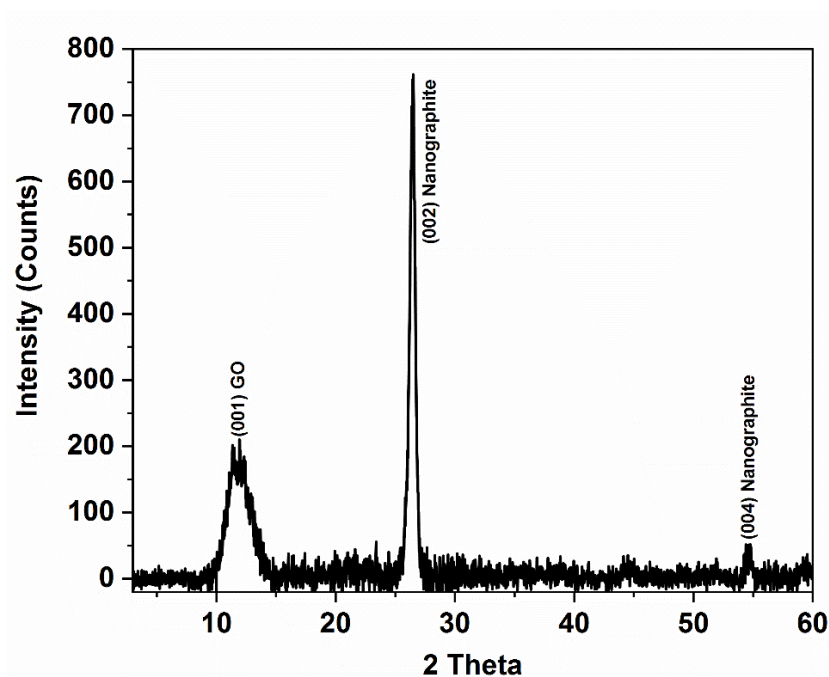


Figure 4.1 XRD spectrum of graphene oxide

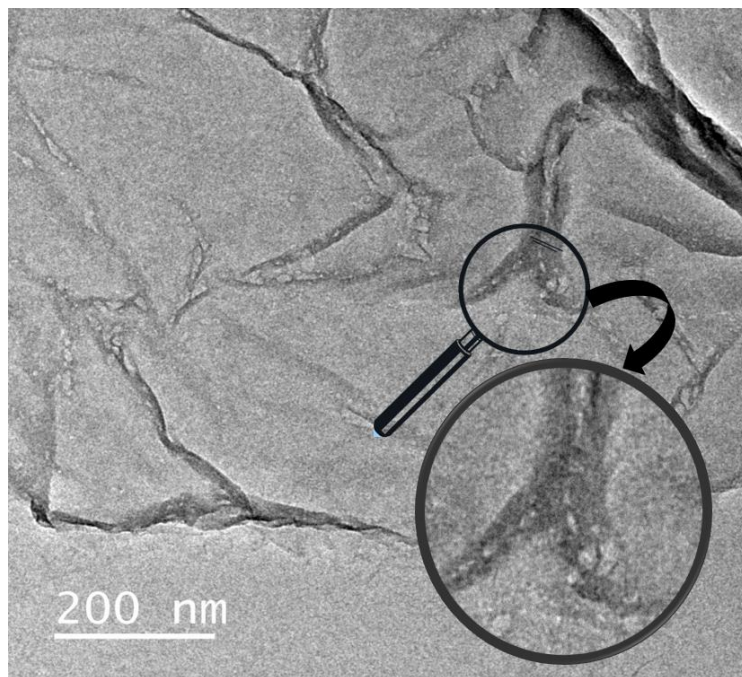


Figure 4.2 Transmission electron microscopic image of graphene oxide

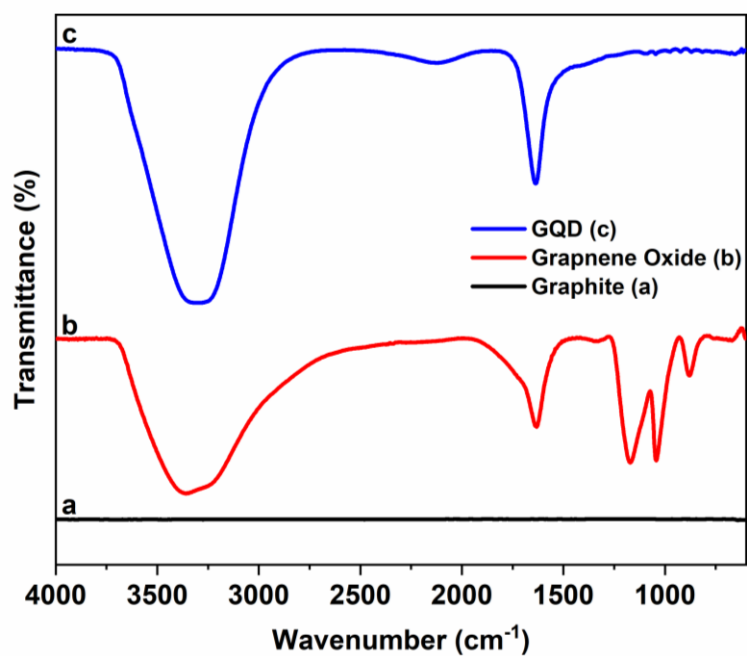


Figure 4.3 FTIR spectra of graphite, graphene oxide, and GQD

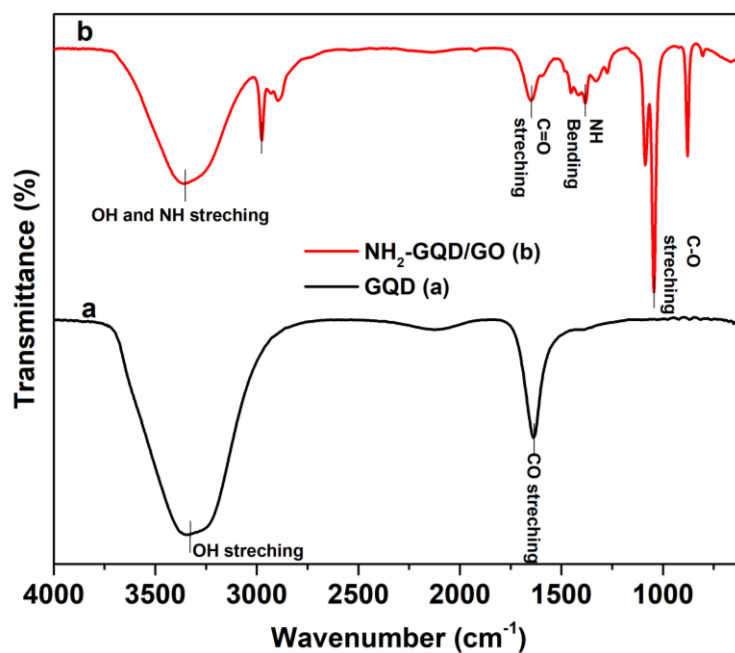


Figure 4.4 FTIR spectra of GQD and NH₂-GQD-GO

Figure 4.3 represents the FTIR spectra of graphite, graphene oxide and GQD as recorded within wavenumber from 4000-600 cm⁻¹. Generally, the spectra reveal the presence of oxygen containing functional groups attached to the all carbon honeycomb core. In the presented spectra, there are no peaks for graphite, which is obvious as graphite is devoid of any functionality. Graphite being the starting material presents a good reference point as how step by step the functionality is introduced with the successive step to synthesize GQD. Graphene oxide, which was synthesized from graphite by oxidative exfoliation. Characteristic peaks corresponding to the -OH at 3200-3600 cm⁻¹, C=O (1670-1820 cm⁻¹), -COC at 1000-1300 cm⁻¹ was observed. These are the usual defects which are introduced by oxidative exfoliation in the graphitic and graphene plane (Hummers and Offeman 1958). GQD are synthesized by hydrothermal cutting of GO sheets along the ethoxy functionality as discussed by Pan et. al.(Pan *et al.* 2010) This leads to the formation of smaller size quantum dots with excitonic entrapment in all the three spatial dimension. What it also does is introduce an edge with certain functional groups which may be seen in the FTIR spectrum of GQD. As the GOQ is formed due to the breaking of -COC- linkage, we only observe peaks

corresponding to the -OH at $3200\text{-}3600\text{ cm}^{-1}$, C=O ($1670\text{-}1820\text{ cm}^{-1}$). These peaks indicate the presence of -COOH , -CO and -OH terminating edges of GQDs. Further, these groups play an important role in binding with nitrogen during the amination step which leads to the formation of $\text{NH}_2\text{-GQD}$. Figure 4.4 compares the FTIR spectra of GQDs and $\text{NH}_2\text{-GQD-GO}$. Broad -OH peak at 3450 cm^{-1} in the spectra of GQD widens further and shift towards 3500 cm^{-1} in $\text{NH}_2\text{-GQD-GO}$ due to merging with -NH stretching peak which is indicative of amino functionalization of GQD by forming -CONH_2 bonds over the surface of GQDs (Zhu *et al.* 2014). This is further strengthened by the presence of -NH bending peak at 1382 cm^{-1} . These results hence help us understand a clear pathway which is being followed to obtain $\text{NH}_2\text{-GQD}$ from graphite. Additionally, the role of edge become even more important in both GQD and $\text{NH}_2\text{-GQD}$ because they dominate the properties of their graphene core. This dominance of the edges over the core is much more evident when the Raman spectra of GQDs was observed in correlation to the information obtained by the TEM. Raman analysis (Figure 4.5) of GQD presented the characteristic D band and G band associated with graphene at 1350 cm^{-1} and 1580 cm^{-1} respectively. The D band arise due to the disordered C atoms at the edges of the GQD, whereas the G band is observed due to the in-plane vibration of sp^2 -bonded C atoms, respectively (Hu *et al.* 2013). The 1:1 intensity of both bands indicates the appreciable loss of graphitic layered structure and could be interpreted as the GOQ synthesized is either single or few layers (mostly bi- or tri-) in nature. However, it will be later revealed in TEM, that the core of the GQD are much dark for it be of such few layers. This anomaly is because the GQD are more defective than the graphene sheets owing to their dominating edge effect, and hence, the intensity ratio may not be the ideal indication to estimate the number of layers of the quantum dots (Kim *et al.* 2013b).

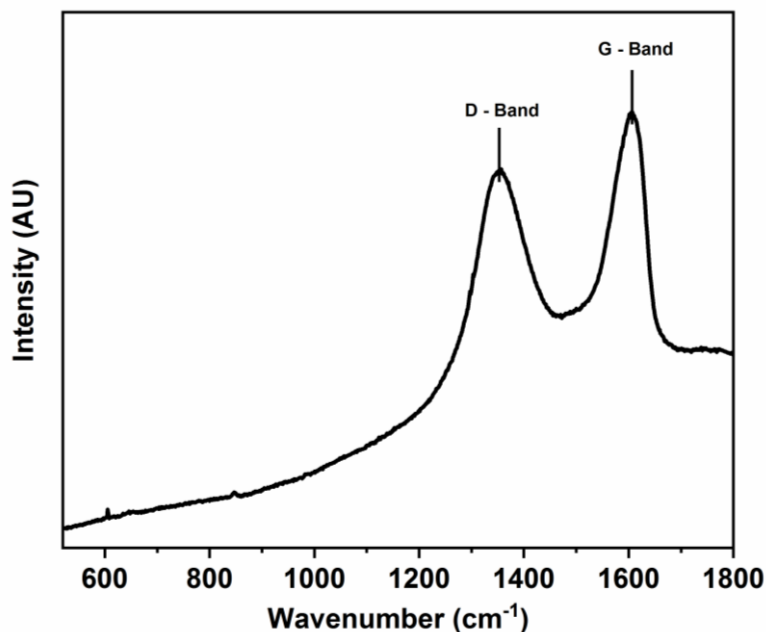


Figure 4.5 Raman spectrum of GQD obtained at incident wavelength of 514 nm.

The NH₂-GQD synthesized via hydrothermal cutting of GO can be visualized in the TEM micrograph (Figure 4.6). The average particle size of the NH₂-GQD determined by the particle size analyser with the quantum dots dispersed in ethanol was found to be 30 nm (Figure 4.7). Particle size of NH₂-GQD was also determined by TEM after the image analysis by ImageJ software developed by Wayne Rasband. The average size of the QD from TEM was found to be 22 nm (Inset Figure 4.7). The result reflects data collected from 25 QD in the image with the minimum size of 12 nm, maximum of 37 nm and standard deviation of 7.2. Many of the NH₂-GQD also presents very dark core. This is due to the multiple graphitic layers which constitute the QD. Moreover, the larger size of QD in the particle size analyser is the result of the solvent barrier formed around the dots due to H-bonding between the solvent molecule and the QD. The reason for this interaction is the presence of oxygen containing functional groups on the edge of the GQD. This is also evident from the FTIR spectra of the quantum dot (Figure 4.4). Moreover, this edge effect is later shown to play an important role in the electrochemistry of NH₂-GQD.

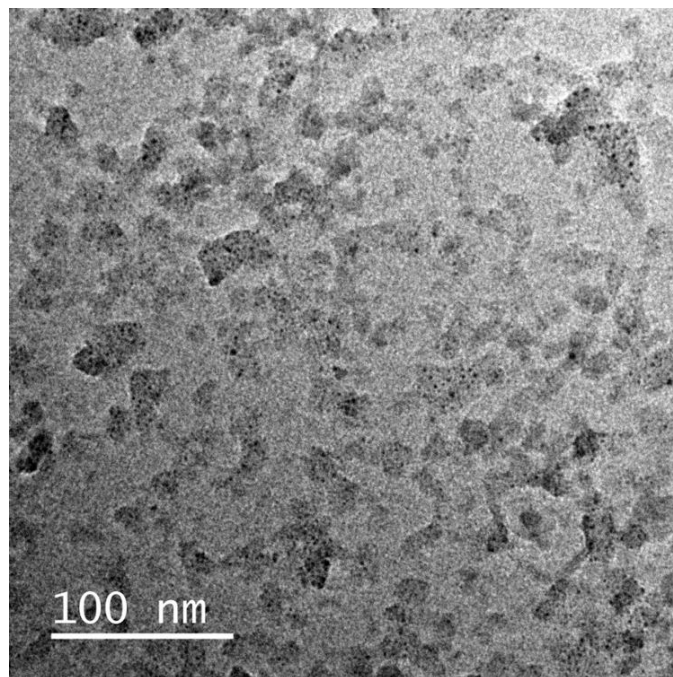


Figure 4.6 Transmission electron microscopic image of NH₂-GQD

Therefore, on close characterization of GQD and NH₂-GQD, it was observed that the quantum dots are well covered with functional groups bearing electronegative centres (i.e. either O or N) on the edges. This in turn lead to the hypothesis that they should exhibit their electrochemical property in the reductive cycle or the cathodic sweep of the cyclic voltammetry. In subsequent section, a discussion is made on how these quantum dots express themselves in the cathodic cycle, and how this property may be used to detect oxalic acid in the aqueous media.

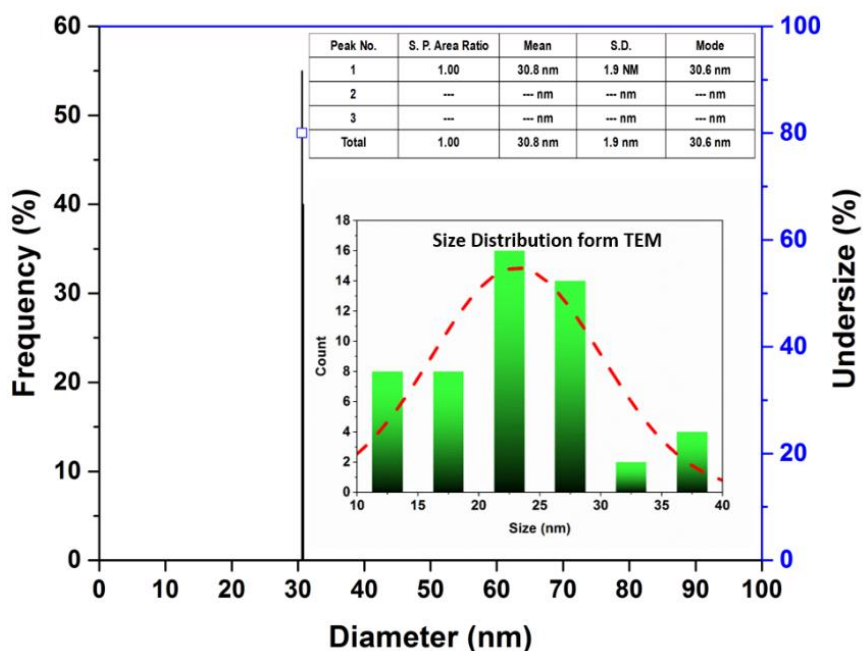


Figure 4.7 Particle size analysis of NH₂-GQD (Inset: Particle size of distribution of NH₂-GQD from TEM)

4.3.2 Electrochemical sensing of oxalic acid:

Electrochemical properties of NH₂-GQD, and NH₂-GQD-GO composite are evaluated using cyclic voltammetry, with the potential range of -1.2 V to 0.5 V. The oxidation and reduction potentials were determined by plotting a graph of current density against the applied voltage. As seen in Figure 4.8, GQD, NH₂-GQD, and NH₂-GQD-GO shows distinct cathodic peak at -0.6 V. This is due to the reduction of carboxyl and carbonyl groups present over the edge of the quantum dots. The reduction in the cathodic current density observed in the CV curve as we go from GQD to NH₂-GQD is due to the availability of lesser number of carboxylic groups per gram of the overall nanostructure, which is in the following order:

$$\text{NH}_2\text{-GQD-GO} < \text{NH}_2\text{-GQD} < \text{GQD}$$

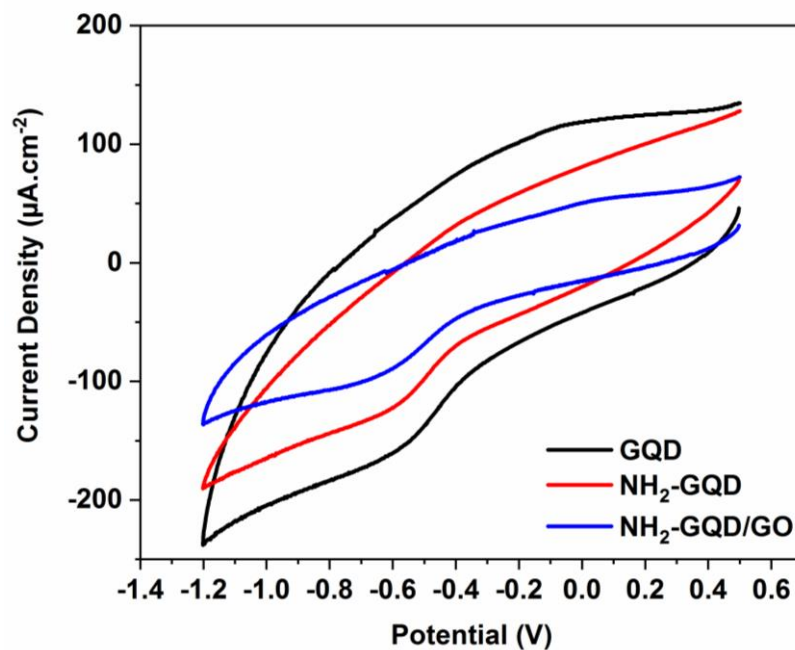


Figure 4.8 Cyclic voltammogram of GQD, $\text{NH}_2\text{-GQD}$, and $\text{NH}_2\text{-GQD/GO}$

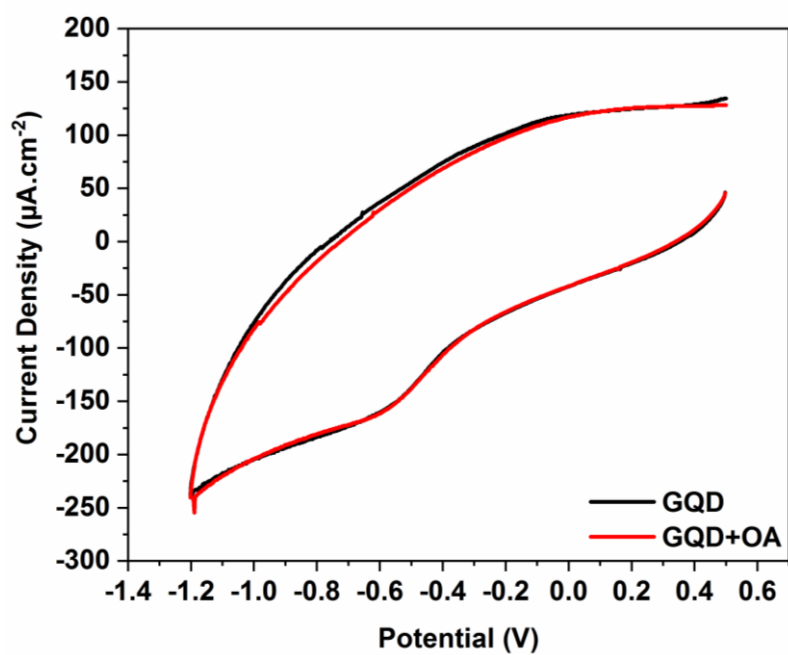


Figure 4.9 Cyclic voltammogram of GQD with and without the addition of 0.2 M oxalic acid

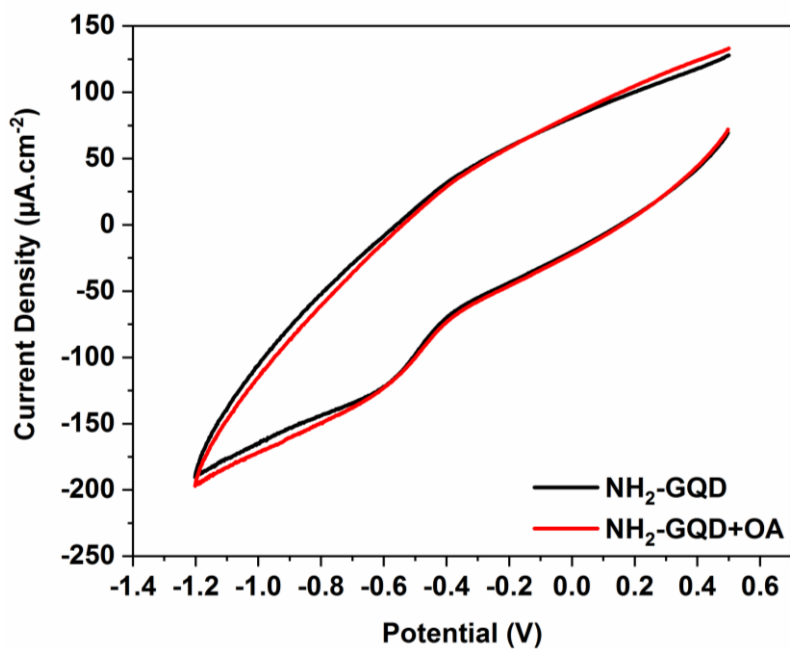


Figure 4.10 Cyclic voltammogram of NH₂-GQD with and without the addition of 0.2 M oxalic acid

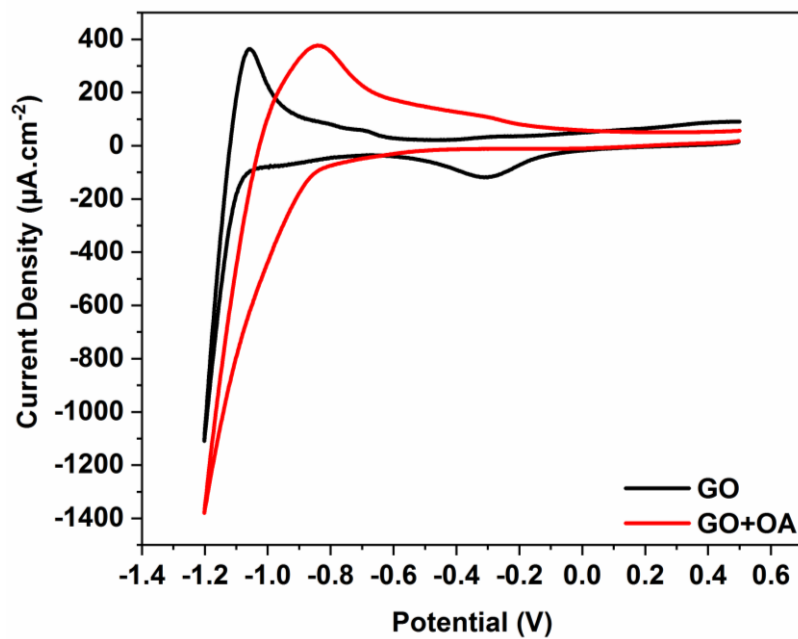


Figure 4.11 Cyclic voltammogram of GO with and without the addition of 0.2 M oxalic acid

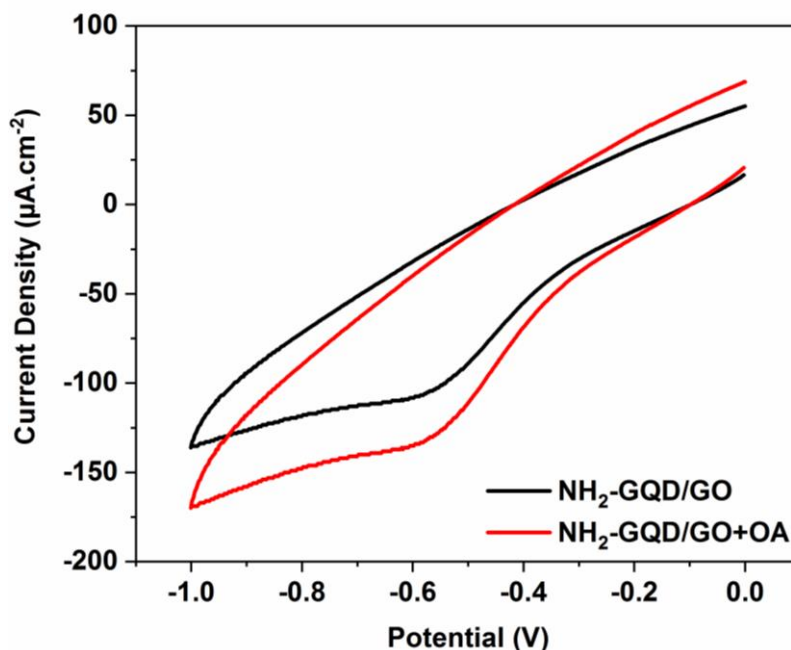


Figure 4.12 Cyclic voltammogram of NH₂-GQD/GO with and without the addition of 0.2 M oxalic acid.

The dependence of the cathodic current density on the availability of carboxylic group is further strengthened by the fact that GO, although has a large number of carbonyl and ethoxy groups, fails to improve the cathodic current density when composited with NH₂-GQD. This is further seen in the CV of GO that there is no cathodic peak observed at -0.6 V (Figure 4.11). Therefore, it may be understood that the increase in the number of carboxylic groups in the GQD system is directly related to the increase in the cathodic current density observed at the said potential. This information prompted the attempt to use the NH₂-GQD-GO composite for the determination of oxalic acid.

Figure 4.9 – Figure 4.12, shows the variation in the cathodic current density observed for the GC electrode deposited with GQD, NH₂-GQD, GO, and NH₂-GQD-GO, respectively, with and without the addition of 0.2 M oxalic acid. As evident from the cyclic voltammogram, there is no significant change in the observed currents at the applied potential range for GQD and NH₂-GQD. In case of GO, there is no cathodic peak observed when oxalic acid was added to the electrolyte. The cathodic peak observed in GO without oxalic acid is due to the reduction of GO to graphene (Yang *et al.* 2011).

However, in case of NH₂-GQD-GO, the addition of oxalic acid showed a significant increase in the cathodic current density. This highlights the need of amination of GQD. The potential sweep window was shortened for the composite after it was established that the cathodic peak occurs at -0.6 V to have better resolution of the two voltogram. The edges of GQDs are saturated with oxygen rich groups which results in no significant raise in the cathodic current density when oxalic acid is added as it does not get binding sites on the edge and additionally the low amount of binding which occur is not enough to induce a variation in the current density. The amination of the GQD edges reduce the oxygen rich groups on the edge and therefore NH₂-GQD-GO composite showed lower cathodic current density of all as evident in Figure 4.8. Additionally, the presence of NH₂ groups on the edges of the quantum dots help in binding with oxalic acid thereby increasing the number of acid groups on the edges available for reduction which increase the reduction current density. The mechanism for the change in cathodic current may be visualized from Figure 4.13. As oxalic acid is a dicarboxylic acid, it forms an amide linkage with the amino groups present in NH₂-GQD while also leading to on free carboxylic group available for reduction at -0.6 V. Therefore, it is a case where, the oxalic acid increases the number of carboxylic groups on the edge of the NH₂-GQD. However, this is not observed to happen in NH₂-GQD deposited GC electrode as either there is no substrate available to facilitate the formation of amide linkage. This is where the need of forming NH₂-GQD-GO composite is highlighted. GO owing to its large surface area provides the platform for the formation of amide linkage between amino groups of NH₂-GQD and carboxylic group of oxalic acid. Hence, in a nutshell, the presence of oxalic acid provides extra carboxylic groups when bonded to NH₂-GQD which further undergo deprotonation at the said potential leading to an increase in the cathodic current density. This dependence of cathodic current density observed in the NH₂-GQD-GO/GC electrode system on the concentration of oxalic acid led to the exploration of the system for the electrochemical determination of oxalic acid. This may be taken up as the foundation for the development of NH₂-GQD-GO based electrochemical sensor for oxalic acid.

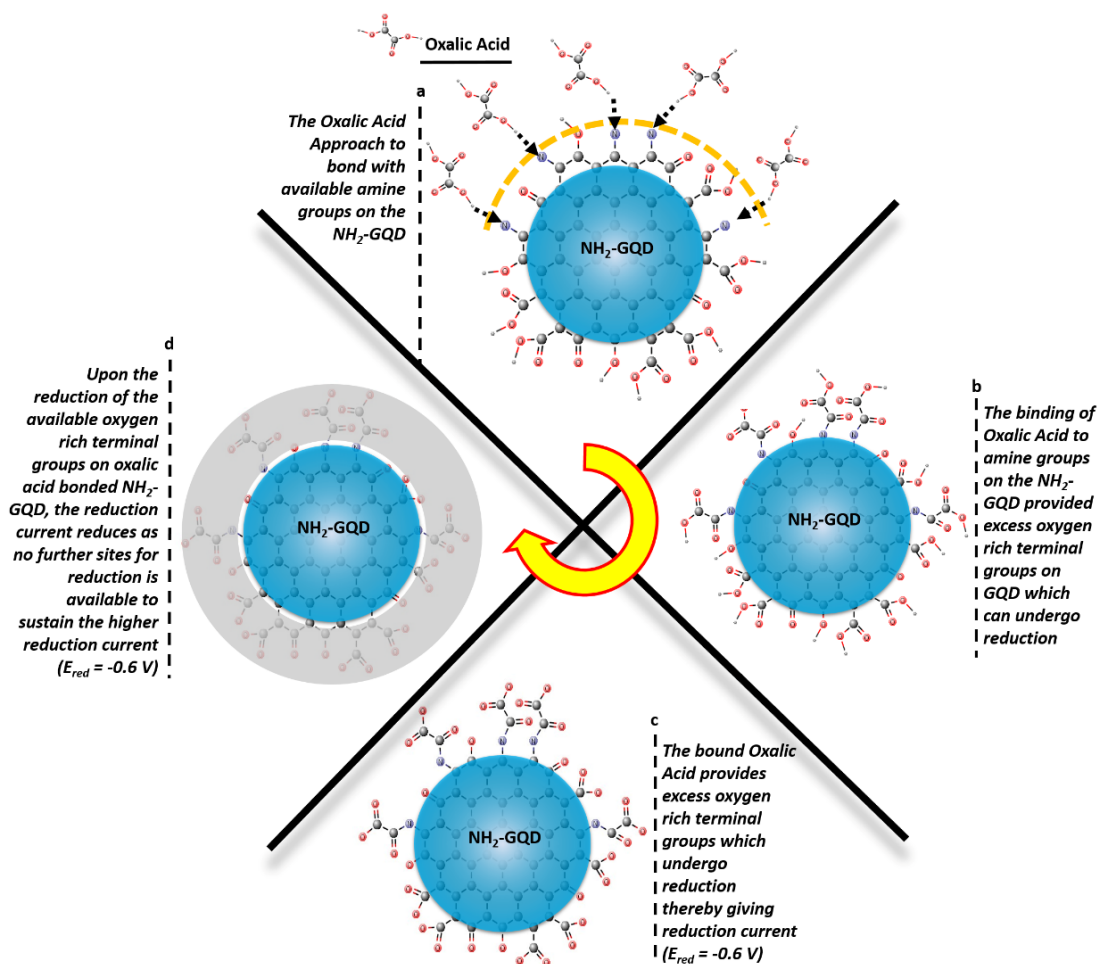


Figure 4.13 Plausible mechanism of binding between $\text{NH}_2\text{-GQD}$ and oxalic acid and subsequent electro-reduction at $E_{\text{red}} = -0.6 \text{ V}$

The suitability of an electrochemical sensor relies in its ability to quantitatively analyse the presence of the analyte. It was found that this increase in cathodic current density is also concentration dependent, which can be well visualized in Figure 4.14. The consecutive cyclic voltogram of $\text{NH}_2\text{-GQD-GO/GC}$ electrode with the addition of incremental concentration of oxalic acid shows that there is an increase in cathodic current density.

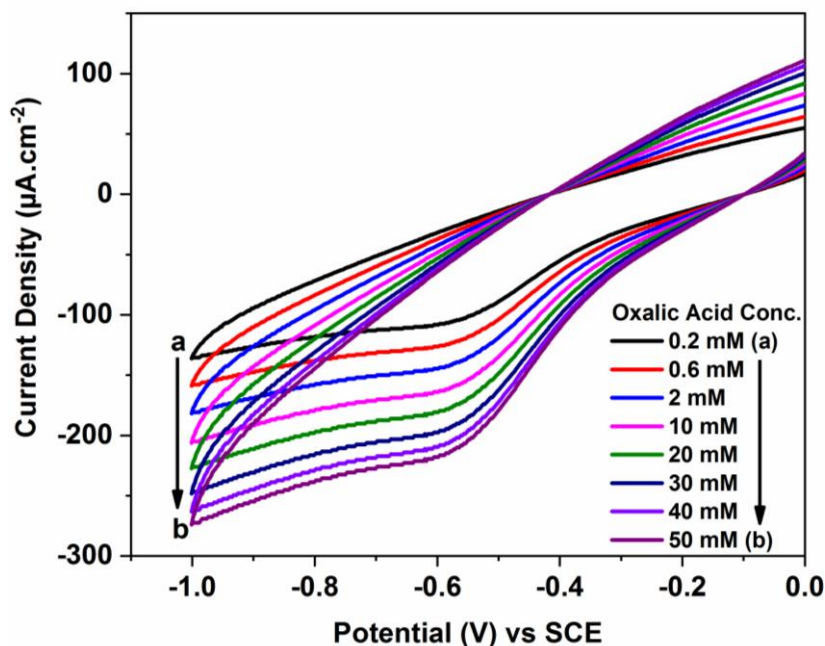


Figure 4.14 Cyclic voltammogram of NH₂-GQD-GO with addition of variable concentration of oxalic acid.

The nature of this variation is found to be linear with two different slopes which can be seen from Figure 4.15 and 4.16. Figure 4.15 represents the variation in cathodic current density with the concentration of oxalic acid from 0.01 mM to 2 mM. The Figure 4.16 shows that within this range of concentration of oxalic acid, the cathodic current density was found to be linearly increasing between 0.5 mM to 2 mM of oxalic acid with the goodness of fit (R^2) of 0.96 and standard deviation (SD) of 12.9. The sensitivity of the electrode for this range was calculated to be $129.502 \mu\text{A}\cdot\text{mM}^{-1}\cdot\text{cm}^{-2}$. Similarly, Figure 4.17 represents the variation in cathodic current density with the concentration of oxalic acid from 0.2 mM to 55 mM, with the linear variation of the cathodic current density within 2.0 mM to 55 mM of oxalic acid (Figure 4.18) having R^2 as 0.98 and SD of 38.05. The sensitivity of the electrode for this range was found to be $142.253 \mu\text{A}\cdot\text{mM}^{-1}\cdot\text{cm}^{-2}$. The limit of detection of oxalic acid for the electrode was found to be 0.05 mM, which is based on the lower limit of the oxalic acid which resulted in a variation of current density at -0.6 V by 12.9 μA (equivalent to SD of 12.9 for oxalic acid between 0.05 – 2.0 mM) after 3 trials. The shaded region of the curve resembles

the SD expanse for the data point with the darker region (confidence range) being the limit of \pm SD and the lighter region (prediction range) corresponds to the limit of \pm 3SD. The determination of the current densities w.r.t the concentration of the oxalic acid considered to be statistically accepted as all the data points lie within the prediction range (i.e. follow the 3SD rule, whereby 95% of all the data should lie between the \pm 3SD from the mean).

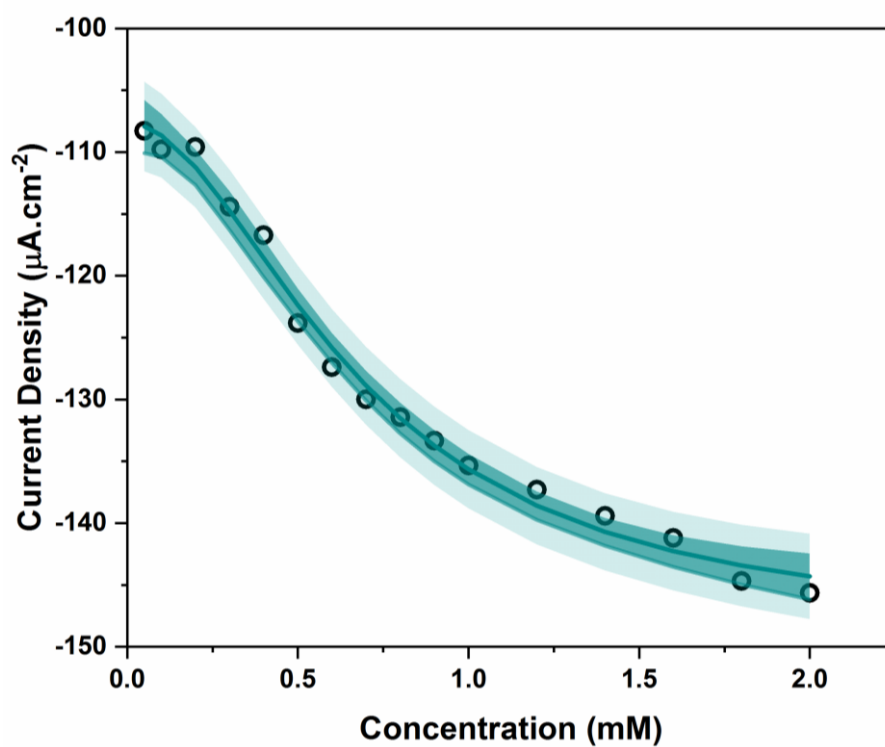


Figure 4.15 Variation of cathodic current density within 0.01 - 2 mM of oxalic acid.

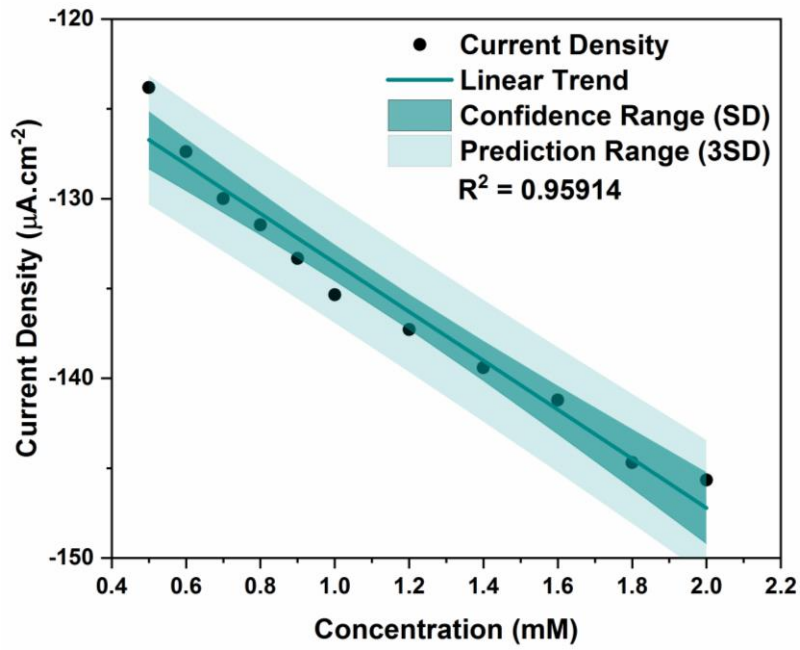


Figure 4.16 The linear variation of the current density between 0.5 – 2.0 mM of oxalic acid.

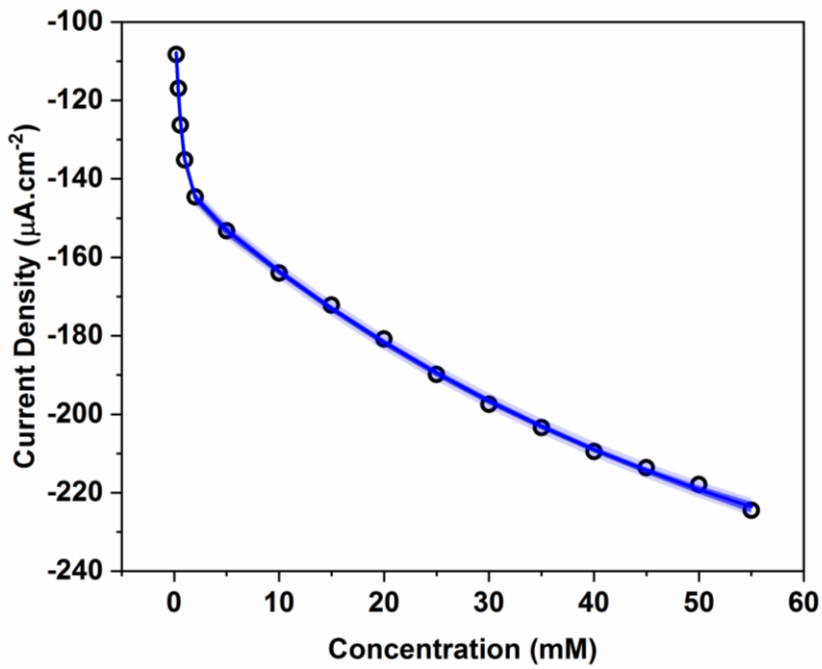


Figure 4.17 Variation of cathodic current density within 0.01 - 55 mM of oxalic acid

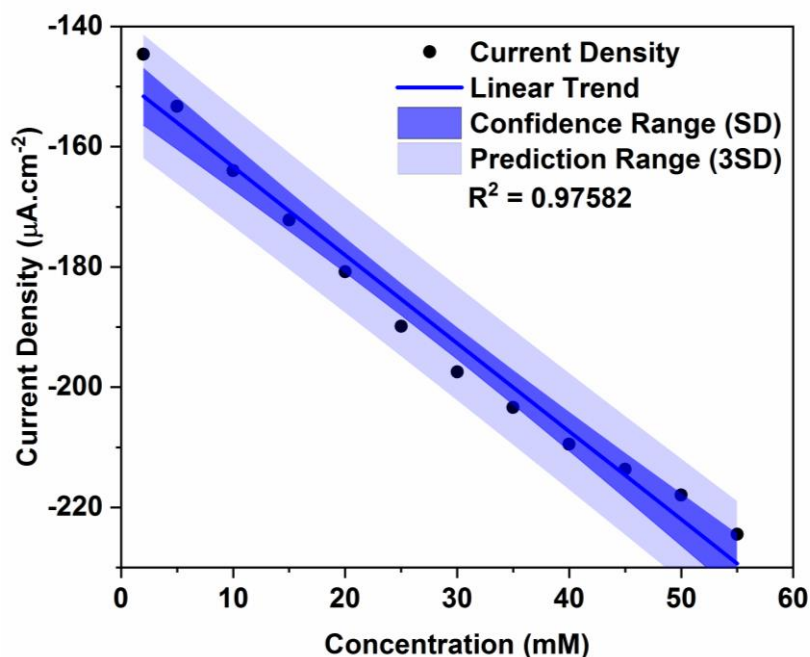


Figure 4.18 The linear variation of the current density between 2.0 - 55 mM concentration of oxalic acid.

Table 4.1 gives a comparison of presented electrode with other electrodes reported in the literature. NH₂-GQD-GO/GC electrode have widest linear range among all the electrodes. Moreover, the all carbon architecture makes its most economical among all the other reported electrodes for the electrochemical determination of oxalic acid. Another first for this electrode is the use of cathodic current density (reductive cycle) for the determination oxalic acid. To the best of our knowledge, all the other electrochemical methods of determination of oxalic acid is cathodic current density (Oxidative cycle) based. This opens the possibility to determine the analytes with materials which have predominately electron rich centres. In the present study, oxalic acid (analyte) and active sensing material (NH₂-GQD) are have O and N centres. Oxalic acid being dicarboxylic acid have two protons available to be released. The NH₂-GQD have edges laden with NH₂, CO and -COOH group. Among this the -NH₂ moiety binds to one carboxylic group oxalic acid to form amide linkage. The other carboxylic group of the bonded oxalic acid is free to undergo deprotonation. Therefore, in presence of

oxalic acid there is an increase in -COOH group on NH₂-GQD-GO which undergoes deprotonation at the said potential, thereby giving a rise in cathodic current density.

Table 4.1 The parameter of NH₂-GQD-GO/GC electrode for electrochemical determination of oxalic acid in comparison to other electrodes reported in literature.

Electrode	Sensitivity ($\mu\text{A}\cdot\text{mM}^{-1}\cdot\text{cm}^{-2}$)	Linear Range (up to, mM)	LOD (μM)	Potential (V)	Ref.
Bare Pt electrode	NA	0.57×10^{-3} - 104.01×10^{-3}	0.38	0.9	(Ma <i>et al.</i> 2016)
Pt-nanoparticles/GC	NA	104.01×10^{-3} - 228.75×10^{-3} 342.80×10^{-3} - 548.92×10^{-3}	0.28	0.95	
Graphene modified carbon ionic liquid electrode	NA	8×10^{-3} - 6.0	48	1.34	(Wang <i>et al.</i> 2015)
Pd-CNF/CPE	NA	0.2-13 13-45	20	1.10	(Liu <i>et al.</i> 2010)
NH ₂ -GQD-GO/GC	129.502 142.253	0.5 - 2.0 2.0 - 55.0	50	-0.65	This work

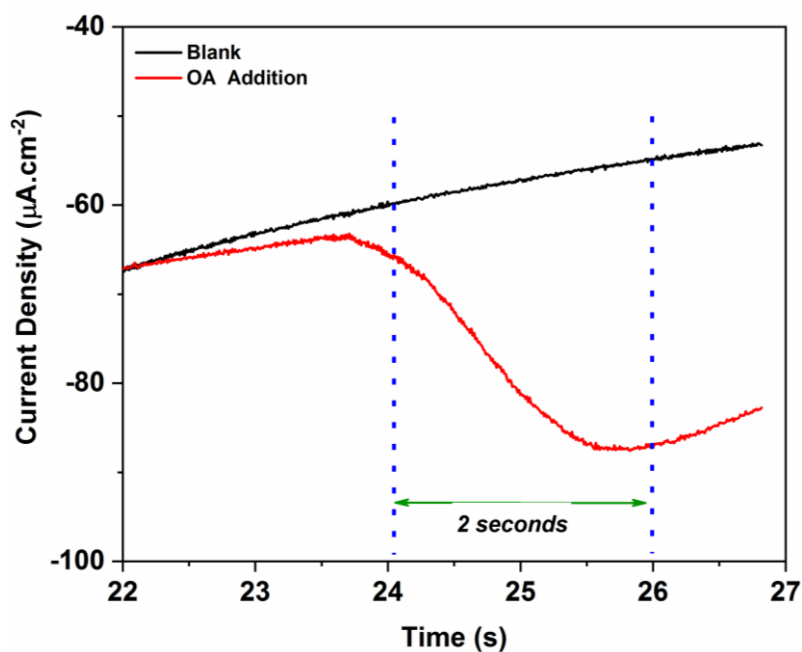


Figure 4.19 Chronoamperometric response of NH₂-GQD-GO on addition of 0.2 mM oxalic acid

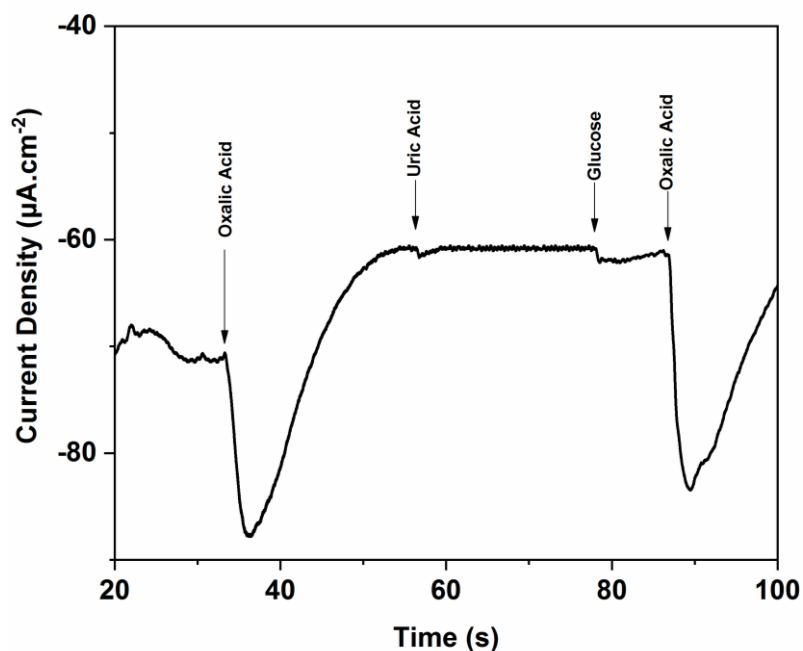


Figure 4.20 Variation in cathodic current density on addition of oxalic acid, uric acid, and glucose.

The quickness of the electrode to determine the presence of the analyte also contribute towards the sensitivity of the sensor to ascertain its efficiency. Apart from sensitivity, the selectivity of the electrode, i.e. its ability to only determine the targeted analyte in presence of other possible interfering agents is also a desired property. To study these, the chronoamperometric behaviour of $\text{NH}_2\text{-GQD-GO}$ was studied with the addition of oxalic acid during the scan to calculate the response time (Figure 4.19), and with the addition of oxalic acid, glucose and uric acid during the scan (Figure 4.20) for the interference study. Glucose and uric acid were selected as interfering agents as they are the other components which are usually present in urine sample which are analysed for the determination of oxalic acid (or oxalate) in humans. This study reveals that the electrode is very responsive towards the presence of oxalic acid with a response time of mere 2 seconds. The interference study shows that the observed change in cathodic peak on addition of oxalic acid is significantly very large compared to the addition of glucose or uric acid. As the cathodic current density is dependent on overall number of carboxylate groups available for reduction, the cathodic current density starts to reduce as all the groups are reduced. This is the reason behind the current density observed

again retaining a stable value which is ionic current due to movement of electrolytic ion only.

4.3.3 Determination of Oxalic acid in Real Sample

The urine samples were studied to determine the oxalic acid content by collecting from a healthy human (Pan *et al.* 2018). Additionally, spinach extract was also studied for its oxalic acid content. This was done to study the practical applicability of the sensor. To confirm the practical applicability of the sensor, urine was used as a real sample and the experiment was conducted. The 2 mL urine sample was added to the 20 mL 0.1M NaOH electrolyte, to which the NH₂-GQD-GO/GC electrode was dipped as working electrode with Pt wire as counter electrode and saturated calomel electrode as reference electrode. The estimation of the sample was done by substituting the current density obtained at -0.6 V in the calibration curve depicted in Figure 4.17. The concentration of oxalic was found to be 0.55 mM which is equivalent to 49 mgL⁻¹ of oxalic acid the urine sample which is around the average limit of oxalic acid in urine. In a separate experiment, the spinach extract was prepared by crushing 100 g spinach leaves in mortar pestle and then dissolving them in water followed by filtration. The aliquot was used for further analysis. 2 mL aliquot was added to 20 mL 0.1M NaOH and was studied under the protocol. The content of oxalic acid was found to be 1.5mM which is equivalent to 135 mgL⁻¹ oxalic acid in the aliquot.

Therefore, the obtained results using NH₂-GQD-GO/GC electrode for the determination of oxalic acid in wide concentration range of 0.5 mM to 55 mM was ascertained to be quick and accurate. It is also relatively non-responsive towards other interfering molecules that might be present in certain chemical and biological samples. This phenomenon can be utilized in generating a non-enzymatic sensor for oxalic acid.

4.4 CONCLUSIONS

Graphene quantum dots are unique with respect to their structural and optoelectronic properties. However, here we demonstrated that they possess some interesting electrochemical properties as well. The NH₂-GQDs-GO composite exhibit good electrochemical response in cathodic sweep of cyclic voltammetry. It was also established that the cathodic current density observed at -0.6 V is dependent on the

carboxylic group present on the quantum dots. The NH₂-GQD-GO composite was found sensitive towards the oxalic acid in condition of average urine pH (i.e. 6 to 8 using a phosphate buffer) at the said potential. The variation in the current density was linear across the range of 0.5 mM to 2.0 mM and 2.0 mM to 55 mM oxalic acid. The limit of detection was found to be 0.05 mM oxalic acid. This material was also very sensitive towards the analyte with the response time to be as quick as 2 seconds. Additionally, the reported electrode was found resistant to significant change in current density due to certain interfering molecules. Moreover, we have also illustrated the possibility of utilizing the cathodic current density for quantitatively determining the analyte in chemical and biological samples for the first time. This can be extended to further develop a non-enzymatic biosensor for the determination of oxalic acid in food, vegetables and other biological samples.

CHAPTER 5

**PHOTOLUMINESCENCE QUENCHING IN METAL ION (Cu^{2+} ,
 Co^{2+}) INTERACTED GRAPHENE QUANTUM DOTS**

Abstract: The excellent photoluminescent property of GQD is highly sought for analytical applications. This chapter presents the effect of transition metal ions over the photoluminescence of GQD.

5.1 INTRODUCTION

Heavy metals (or Transition Metals) are among the most toxic pollutants found in water. Exposure to metal ions has been related to various disorders in humans which include respiratory problem, carcinogenicity, nervous system failure and poisoning. However, few are also essential for healthy functioning of human body. Copper and Cobalt are two of those metals. Copper is essential in forming red blood cells and to maintain healthy nerve cells and immune system. It also assists in the formation of collagen found in bones and connective tissue. The adverse effects of excessive copper intake include vomiting, diarrhea, stomach cramps, and nausea. It has also been associated with liver damage and kidney disease. Cobalt is another essential metal which is an important component of vitamin B₁₂. These metals are a common occurrence in environment and water and with an increase in applications of nanoparticles makes this problem even more severe (Lauwerys and Lison 1994; Chen *et al.* 2006). Various methods developed to sense these elements involve primarily the use of complex organic molecules, or peptides via electrochemical determination (Yang *et al.* 2003; Liu *et al.* 2006; Gupta *et al.* 2006; Singh *et al.* 2006). Organic ligands have also been used for fluorometric determination Cu²⁺ and Co²⁺ ions (Maity *et al.* 2011; Song *et al.* 2013). Although these sensors being efficient, usually involve the use of molecules which are not readily available, and their synthesis makes them expensive. Here, we demonstrated how PL of GQD can be utilized in the possible qualitative determination of Cu²⁺ and Co²⁺ metal ions. Preparation of these GQD are facile and offers very fast qualitative detection.

5.2 EXPERIMENTAL

5.2.1 Synthesis of Graphene Quantum Dots (GQD)

In a typical synthesis procedure (scheme represented in Figure 5.1) GO was prepared using Improved Hummer's method (Marcano *et al.* 2010) as described in Chapter 3.

Further, as prepared GO were put in a Teflon-lined autoclave in alkaline medium and reaction was kept for 16 hours at 200 °C which is in accordance to hydrothermal synthesis (Pan *et al.* 2010). This step was a the modification of the synthesis procedure reported in chapter 4 for GQD. Aqueous GQDs thus synthesized were reacted in separate batchs with copper (II) nitrate and cobalt (II) nitrate respectively. GQD were characterized using Bruker Alpha Eco-ATR FTIR, Analytik Jena Specord S600 UV-Vis Spectrophotometer, and Horiba Fluoromax Spectrofluorometer.

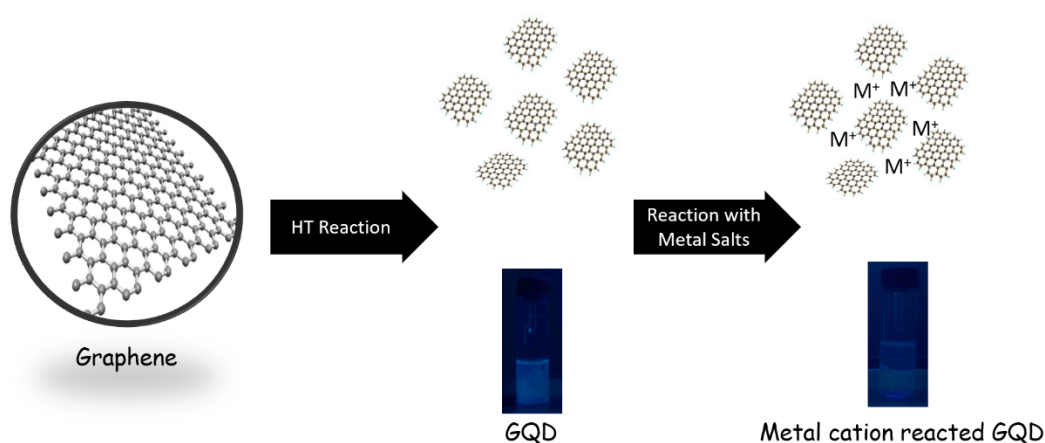


Figure 5.1 A graphical representation of synthesis procedure

5.3 RESULTS AND DISCUSSION

Graphene oxide as synthesized was analyzed using X-ray diffraction. The presence of the characteristic broad peak at 2θ of 7.5-15 degree corresponding to the (002) plane of graphene oxide (Figure 5.2) instead of the usual sharp peak at 26 degrees for graphite suggest a synthesis of high purity graphene oxide.

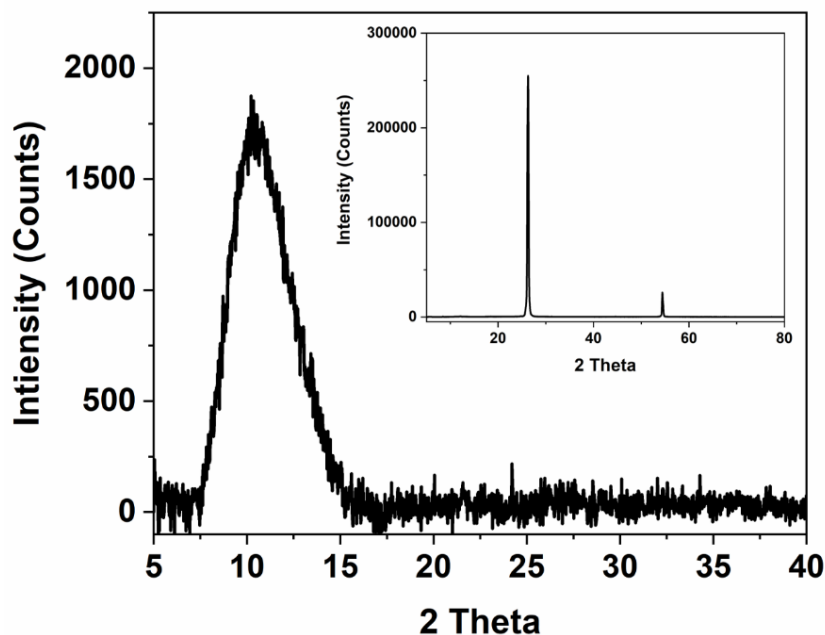


Figure 5.2 XRD spectrum of graphene oxide (Inset: XRD spectrum of graphite)

Figure 5.3 represents the FT-IR spectra of Graphite, graphene oxide and GQD as recorded between 4000 - 600 cm^{-1} . The spectra reveal the presence of oxygen-containing functional groups attached to the all carbon structure. In the present graph, there are no peaks for graphite, which confirms the absence of oxygenated functional groups from the starting material.

In graphene oxide, we observe characteristic peaks corresponding to the $-\text{OH}$ at 3200-3600 cm^{-1} , $\text{C}=\text{O}$ at 1670-1820 cm^{-1} and $-\text{COC}$ at 1000-1300 cm^{-1} , which are the usual defects 2-dimensional sheet of graphene oxide. In GQD, we observe only peaks corresponding to the $-\text{OH}$ at 3200-3600 cm^{-1} , $\text{C}=\text{O}$ (1670-1820 cm^{-1}) which are indicative of $-\text{COOH}$ terminating edges of GQD. These $-\text{COOH}$ groups further play important role in binding with Co (II) and Cu (II) ions. Figure 5.4 shows the fingerprint region of IR for as prepared, Co interacted GQDs and Cu interacted GQDs. It clearly shows the presence of $\text{Co}-\text{O}$ at 610 cm^{-1} and 627 cm^{-1} and $\text{Cu}-\text{O}-\text{H}$ deformation vibrations at 685 cm^{-1} (sh, br) and 875 cm^{-1} (w, br) (Bertoluzza *et al.* 1985), which are absent in as prepared GQD. This indicates the successful binding of GQD to Co^{2+} and Cu^{2+} ions through oxo linkage.

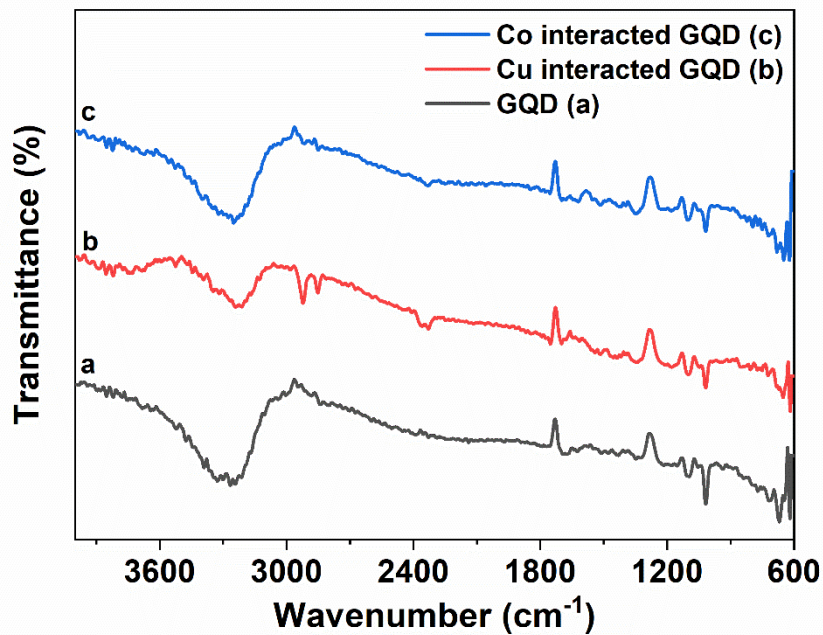


Figure 5.3 FTIR spectra of GQD, Co^{2+} interacted GQD, and Cu^{2+} interacted GQD.

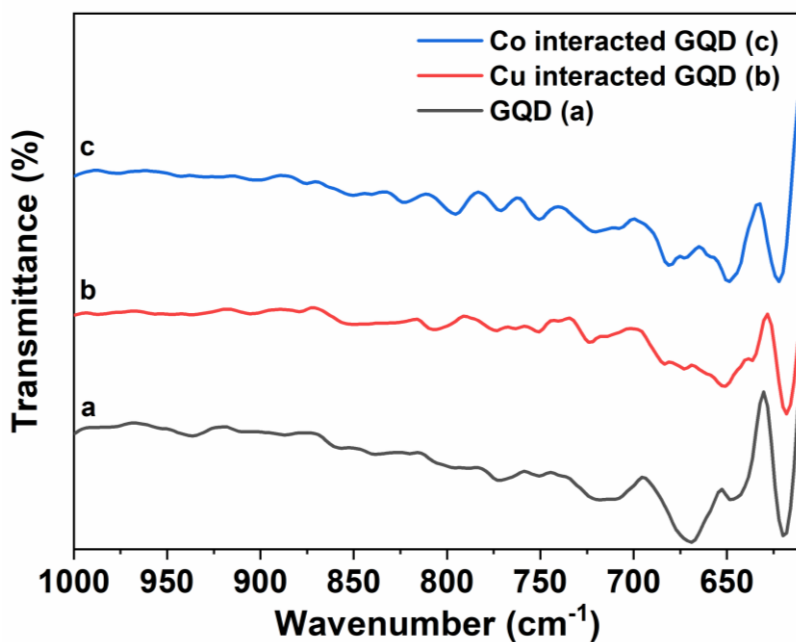


Figure 5.4 Fingerprint region of GQD, Co^{2+} interacted GQD, and Cu^{2+} interacted GQD.

As discussed earlier, Luminescence is a very important property for quantum dots. GQD prepared herewith showed typical blue luminescence. Figure 5.5 shows the UV-Vis absorption spectrum of GQD, Co^{2+} and Cu^{2+} interacted GQDs, absorbs at 365 nm which was used as excitation wavelength for PL studies. Figure 5.6 shows the PL spectra of as prepared GQD, and Co^{2+} and Cu^{2+} interacted GQD.

It is evident that luminescence of GQD has been drastically quenched due to interaction with metal ions. The apparent loss of intensity can be well visualized from Figure 5.7 which compares luminescence of GQD, Co-GQDs and Cu-GQDs under irradiation of 365nm. It is inferred that the long-range interaction of GQD around metal ions relieves the excitonic barrier which is responsible for this observed photoluminescence quenching. A schematic representation of which was earlier presented (fig. 1). The extent of photoluminescence quenching being different for both the metal ions are indicative that the selective determination of metal ions may be possible after careful optimization.

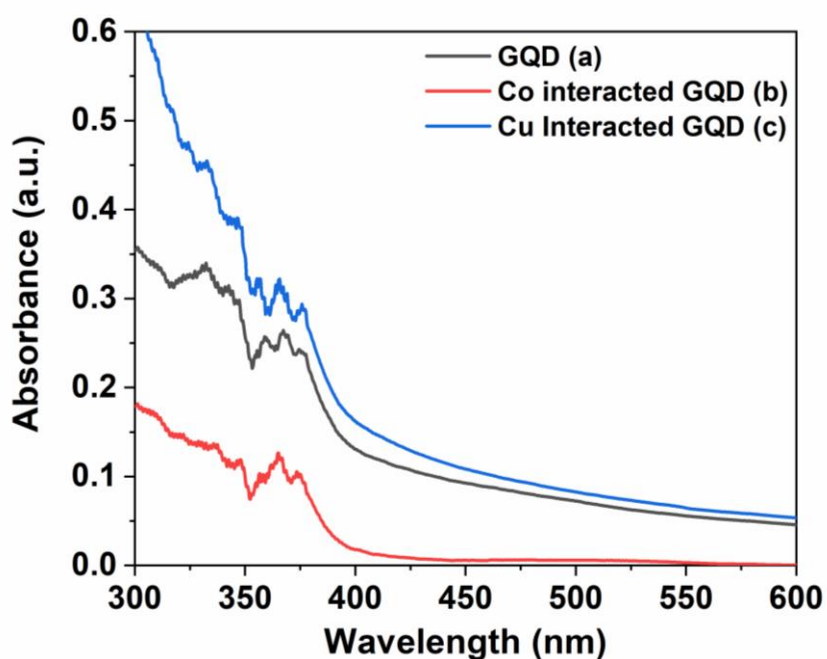


Figure 5.5 UV-Vis spectra of GQD, Co^{2+} interacted GQD, and Cu^{2+} interacted GQD.

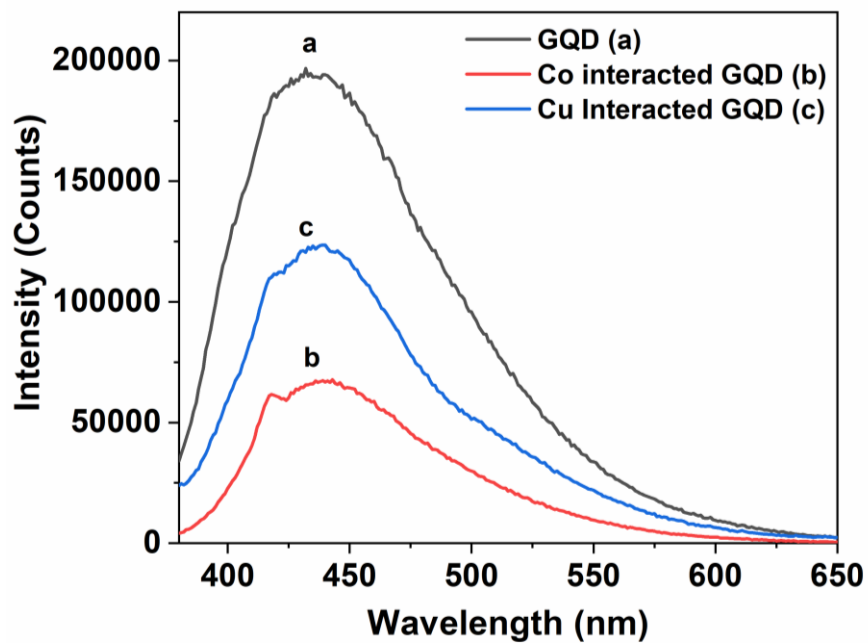


Figure 5.6 PL spectra of GQD, Co^{2+} interacted GQD, and Cu^{2+} interacted GQD at 365 nm excitation.

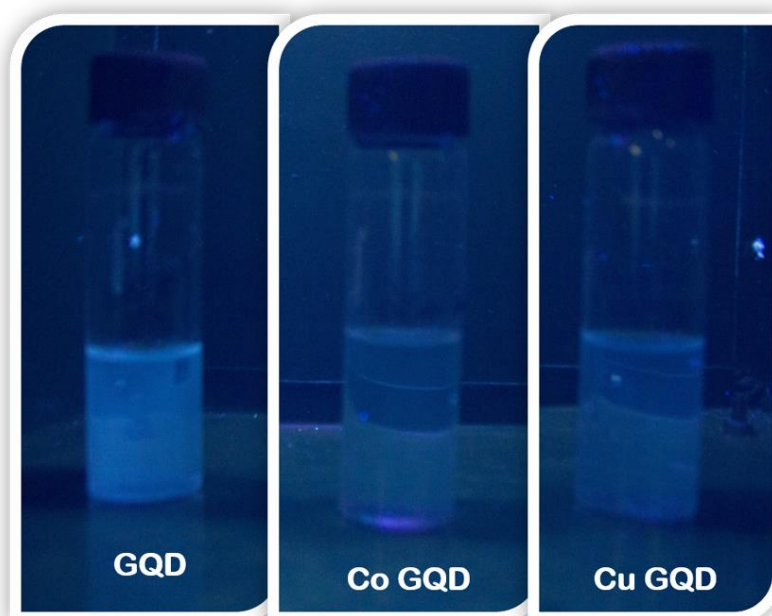


Figure 5.7 GQD, Co^{2+} interacted GQD, and Cu^{2+} interacted GQD under 365 nm.

5.4 CONCLUSIONS

GQDs are well synthesized via Hydrothermal cutting of GO sheets and this reduction in size leads to the excitonic entrapment within the GQDs structure leading to its semiconducting non-zero band gap and subsequent photoluminescence. Metal ion interacts with GQD core via oxo-linkage with dangling oxygen at the edge of GQDs. The quenching of PL observed in Co^{2+} and Cu^{2+} interacted GQDs is due to long range conjugation around metal ions which relax excitonic barrier. This PL quenching is well utilized in fast qualitative sensing of metal ions (Co^{2+} and Cu^{2+}) present in the aqueous medium. The reported PL quenching of GQDs in presence of metal ions can be further extended towards their quantitative determination.

CHAPTER 6

**CALCIUM-INDUCED PHOTOLUMINESCENCE QUENCHING
OF GRAPHENE QUANTUM DOTS IN HARD WATER: A QUICK
TURN-OFF SENSING APPROACH**

Abstract: Presence of calcium salts in water is primary reason for the hardness. Excess of calcium intake leads to various physiological ailments like fatigue, dizziness, kidney stones to name a few. Currently calcium is mostly determined by titration methods or with the help of sophisticated techniques like AAS. This chapter reports a facile fluorometric determination of Ca^{2+} ion in the aqueous solution using graphene quantum dots with very high accuracy.

6.1 INTRODUCTION

As discussed earlier, use of GQD as a fluorescent platform are reported with success for various metal ions (Benítez-Martínez and Valcárcel 2015) such as Al^{3+} (Fan *et al.* 2014), Fe^{3+} (Ananthanarayanan *et al.* 2014; Zhou *et al.* 2013; Li *et al.* 2014; Van Tam *et al.* 2014; Ju and Chen 2014; Li *et al.* 2015a; Xu *et al.* 2015), Cu^{2+} (Sun *et al.* 2013; Liu *et al.* 2014; Wang *et al.* 2014b; Huang *et al.* 2013), Cr^{6+} (Cai *et al.* 2014), Hg^{2+} (Wang *et al.* 2014a; Chakraborti *et al.* 2013), Ni^{2+} (Huang *et al.* 2013), Mn^{2+} (Huang *et al.* 2013), Co^{2+} (Huang *et al.* 2013), and Ce^{3+} (Salehnia *et al.* 2017). The detection of these metal ions is of industrial significance. However, in domestic use, water sample often does not contain these ions, and hence these probes may not be used in such cases. Most common ion present in domestic water samples is Ca^{2+} , which is directly responsible for the hardness of water.

Calcium is one of the most commonly found element in water and biological system. Calcium is an essential dietary supplement for the development of human body. It is directly involved in the growth of bones and cartilages. Presence of calcium in water is a measure of the hardness of water, and consumption of hard water is shown cause various health hazard (Jayasumana *et al.* 2014). The irregularities in the calcium intake, more specifically in large intakes can reportedly lead to ailments like prostate cancer, cardiovascular disease, preeclampsia, kidney stone, and weight loss.

The methods of determining calcium reported in the literature are very few and sophisticated. Determination of calcium using chromophores or molecules which can give visual aid are helpful for the process on the go. Biochromatic squaraine dye based foldamers were one such reported to selectively determine Ca^{2+} calorimetrically with

success (Arunkumar *et al.* 2005). The reported molecule showed a 1:1 binding with Ca^{2+} . The optical signal in this mode of detection is observed when the bichromophore fold around the Ca ion which leads to the excitonic coupling between the two squaraine chromophores. Fluorescent molecules specifically designed for determining the cation are proven and efficient platform for the quantitative determination which may offer quick sensing approach (Valeur and Leray 2000). Among the most popular known fluorescent probe for determining Ca^{2+} , an 8-coordinate tetracarboxylate chelating site with stilbene chromophores was employed by Gryniewicz *et al.* (Gryniewicz *et al.* 1985). The difficulty to synthesize these molecules is a major limitation for these sensing platforms. An interesting development was made in the fluorescent probes by fabricating a fibre optics probe based on a natural carboxylic polyether antibiotic (Suzuki *et al.* 1989). Other methods include state of the art techniques like wavelength dispersive X-ray fluorescence and laser-induced breakdown spectroscopy in the biological samples with success (Costa *et al.* 2019). Induced plasma atomic emission spectroscopy was used to determine the amount of calcium in rice varieties (Ozbek *et al.* 2019). These methods although able to estimate the content of Ca in trace amounts are not universally applicable. Due to very limited and available reports on the determination of Ca ions, there is a need to explore a much quick and economic way for determining calcium in the aqueous system. Here, we report a GQD based PL turn-off sensor for the determination of Ca^{2+} ions. Aim of the study is develop a very fast qualitative tool for the detection of Ca^{2+} in aqueous and biological samples.

6.2 EXPERIMENTAL SECTION

6.2.1 Synthesis of GQD:

Graphene oxide was prepared using Improved Hummer's method (Marcano *et al.* 2010), detailed in Chapter 3, followed by the synthesis of GQD in accordance to hydrothermal Synthesis (Pan *et al.* 2010) as described in Chapter 5.

6.2.2 Determination of Ca^{2+} in aqueous media

For determination of Ca^{2+} , 1 mL aqueous solution of CaCO_3 of varying concentration (0.5 μM to 250 μM w.r.t Ca^{2+} ions) was added to 19 ml GQD dispersion (1 mg/ml) containing glycine-sodium hydroxide buffer (0.08M, pH 10) and stirred for 10 min. PL

intensity of GQD was found to be highest at pH 10. These samples were collectively termed as calcium bound GQD (Ca-GQD).

6.3 RESULTS AND DISCUSSION

The schematic representation of the experimental procedure is given as Figure 6.1. The details of the procedure followed are provided in the experimental section. To summarize the process, the highly photoluminescent GQD were obtained from hydrothermal cutting of graphene oxide as reported elsewhere (Pan *et al.* 2010) with modifications. The PL quenching in GQD is a well-documented phenomenon for transition metals and lanthanides in literature (Ju and Chen 2014; Ananthanarayanan *et al.* 2014; Salehnia *et al.* 2017). Therefore, a similar approach was attempted for the quenching of deep blue photoluminescence by the introduction of Ca^{2+} ions. Calcium was selected as the primary analyte for this study due to it being the primary reason for hardness of water. The subsequent quenching of the PL observed in GQD dispersion on introduction of Ca^{2+} ions means they can be qualitatively determined. The observed effect further prompted an investigation for the quantitative determination of the Ca^{2+} ion in the hard water samples. As demonstrated in the Figure 6.1, the workflow of the experiment involves the synthesis of GQD with deep blue PL by the hydrothermal cutting (Pan *et al.* 2010) of graphene oxide (Marcano *et al.* 2010), which was subsequently was arrested by the introduction of Ca^{2+} ions. Another takeaway from the scheme is the fact that there is a plausible scenario where Ca^{2+} , owing to its divalent nature interacts with two GQD resulting in the relaxation of excitonic barrier. This relaxation leads to the photoluminescence quenching which is a common occurrence in case of transition metals (Ananthanarayanan *et al.* 2014). However, this phenomenon is not reported in the literature for the alkali and alkaline earth metals to best of our knowledge. The primary reason for this may be the smaller size of these cations. However, among the common cations present in the hard water, Ca have shown to exhibit excellent PL quenching phenomenon in the GQD dispersion. We will discuss the results obtained which lead to the conclusion about the possible use of GQD for quantitatively determining the amount of Ca^{2+} in the hard water samples and the intrinsic limitation which this system presents.

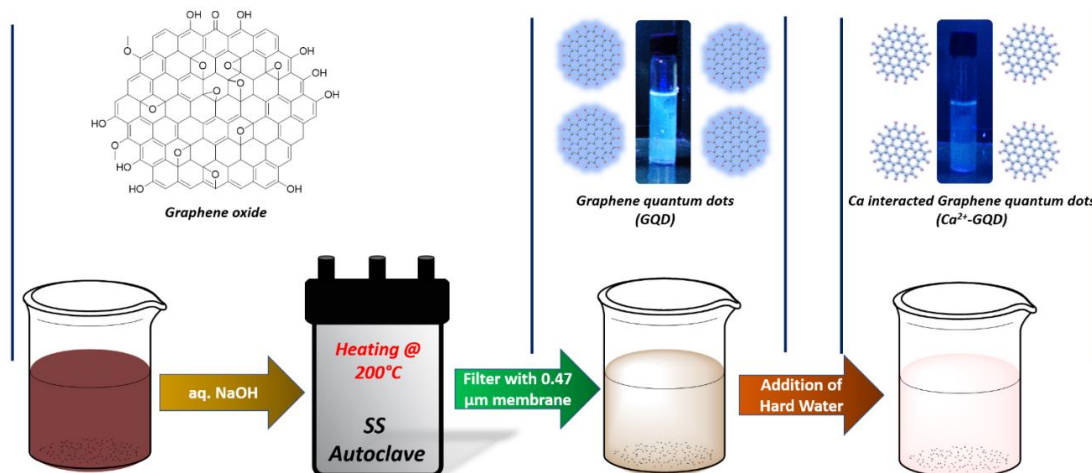


Figure 6.1 A schematic of the synthesis of graphene quantum dots and its subsequent quenching of photoluminescence in hard water.

Graphene oxide was used as the precursor for the synthesis of GQD. The quality of the precursor plays an important role in the properties of the GQD obtained. The graphitic stacks present in the precursor may lead to the improper fragmentation during the hydrothermal process. This as a result, means a highly stacked fragments of GQD would be obtained which have poor PL. Therefore, graphene oxide was analysed using X-ray diffraction to ascertain its physical characterization. The observed characteristic broad peak at diffraction angle (2θ) of 10.2° , corresponds to the (002) plane of graphene oxide (Chen *et al.* 2012) (Figure 6.2). The observed peak was significant departure from the highly intense and sharp peak at observed at 2θ of 26° for graphite. The complete absence of any peak at 26° or near about signifies that the highly pure graphene oxide was obtained. Additionally, there is a virtual absence of the graphitic stacking in the obtained graphene oxide which was a result of proper intercalation during the oxidation process. The oxidation of graphite also adds oxygen rich functional moieties in the graphene sheets which are the primary characteristic of graphene oxide. The purity of graphene oxide is also important as the formation of the GQD depends on the oxygen rich functional groups present in graphene oxide (Pan *et al.* 2010). As discussed by Pan *et. al.*, the cleavage of the graphene oxide sheets takes place at the ethoxy groups present due to the high pressure and temperature of the hydrothermal process. The role of oxygen containing functional groups can be visualized by the FTIR analysis.

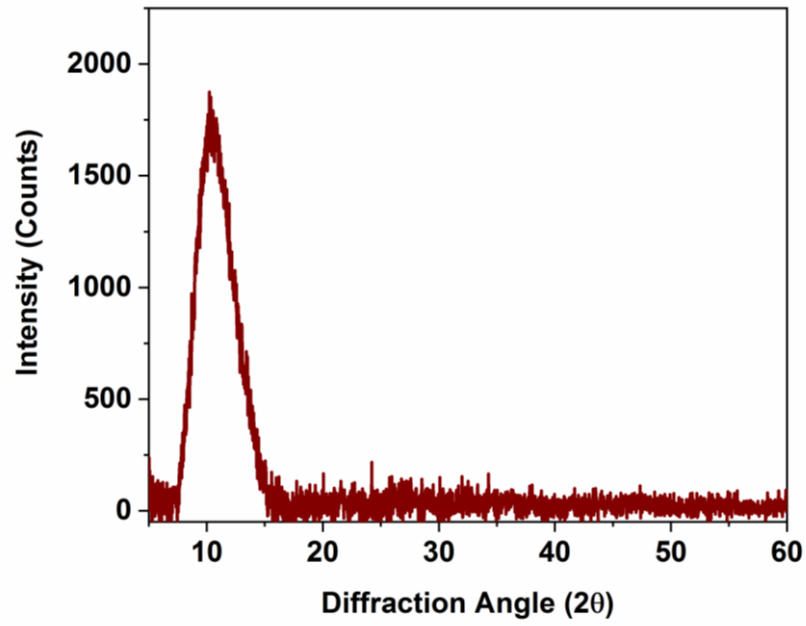


Figure 6.2 XRD spectrum of graphene oxide

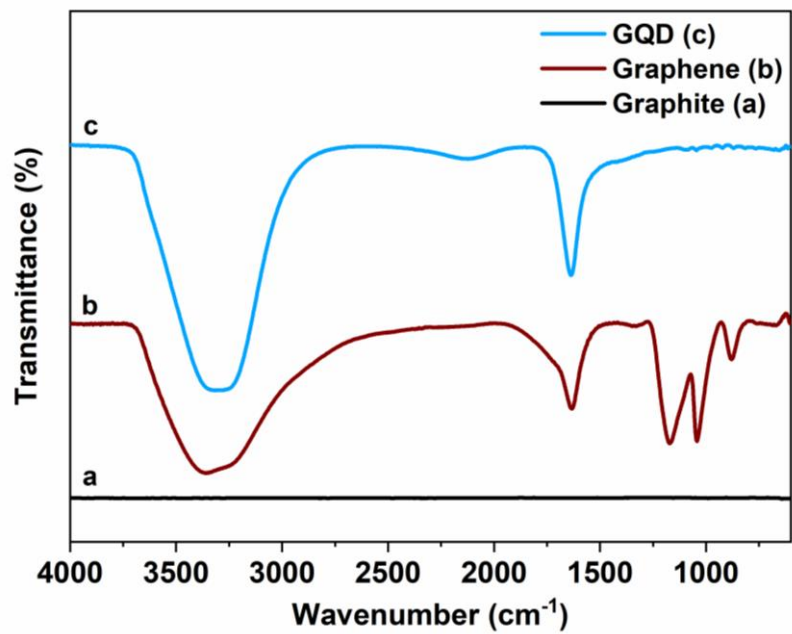


Figure 6.3 FTIR spectra of graphite, graphene oxide, and GQD

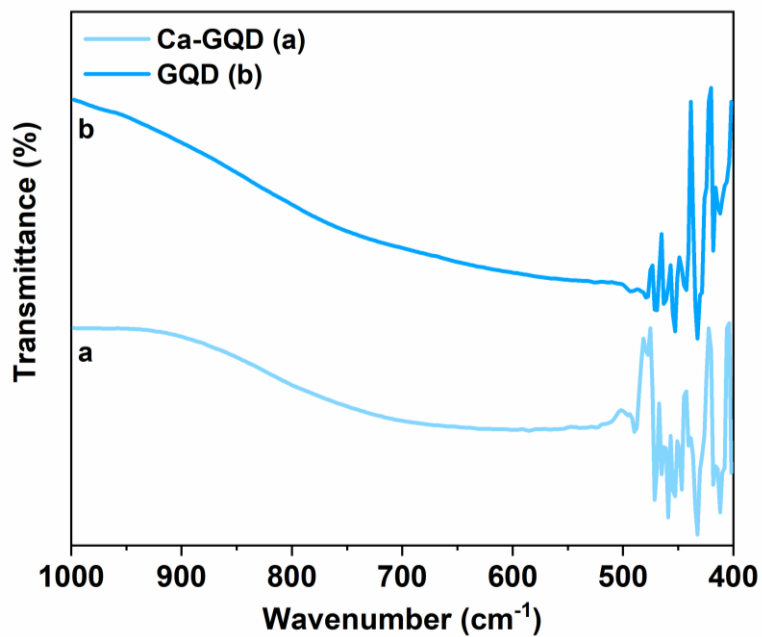


Figure 6.4 FTIR spectra of the fingerprint region of GQD and Ca-GQD

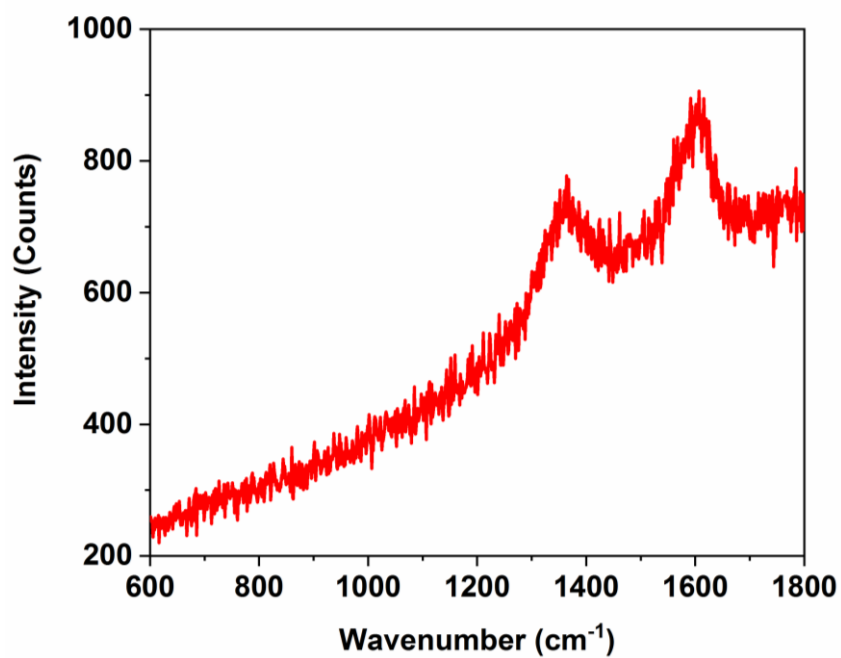


Figure 6.5 Raman spectrum of GQD.

The changes in the available functional groups in each of the stages were observed from the FTIR spectra of graphite, graphene oxide, and GQD (Figure 6.3). Graphite is a layered structure of sp^2 carbon arranged honeycomb lattice. The spectrum of graphite was observed as a straight line due to the absence of functional groups. Therefore, the spectrum of graphite was observed as a straight line. Graphene oxide is a functionally rich carbon nanostructure with various oxygen bearing functional groups namely carboxylic ($-COOH$; $-OH$ stretching 3300 cm^{-1} and $-C=O$ stretching 1700 cm^{-1}), hydroxyl ($-OH$ stretching 3500 cm^{-1}), carbonyl ($-C=O$ stretching 1680 cm^{-1}), ether ($-C-O-C-$ stretching 1250 cm^{-1}) and anhydride groups ($-CO-O-OC-$ stretching, 1080 cm^{-1}) were observed at their respective wavenumber. GQD is formed when the ether and highly unstable anhydride groups are cleaved. The fragmentation of these groups leads to the formation of additional carbonyl ($-C=O$) and hydroxyl ($-OH$) groups in the GQD. Therefore, the characteristic peaks corresponding to the ether and anhydrides are absent in the FTIR spectrum of GQD. Hence, the FTIR results ascertain the formation of GQD. On introduction of Ca^{2+} ion in the dispersion of GQD, the $-COOH$ groups play an important role in binding to the calcium ions (Bala *et al.* 2007; Ancillotti *et al.* 1977). Ca^{2+} binds strongly to the carboxylic groups with bond strength stronger than certain heavy metals (Bala *et al.* 2007). The binding of Ca^{2+} ions with carboxylic group of GQD was confirmed by comparing the fingerprint region FTIR of the GQD and Ca^{2+} interacted GQD (Ca-GQD) (Figure 6.4). It clearly shows the presence of Ca-O bending vibrations at 415 cm^{-1} (Choudhary *et al.* 2015), which is absent in the spectrum of GQD. Therefore, it was concluded that the Ca^{2+} binds to the carboxylic group of GQD. The Raman spectra of GQD was observed with characteristic D band and G band at 1350 cm^{-1} and 1580 cm^{-1} , respectively, commonly associated with graphene (Figure 6.5). The 1:1 ratio of the D and G band intensities signals towards the appreciable loss of graphitic layered structure. The ratio of intensities also means that the synthesized GQD are mostly bi-atomic layer or tri-atomic layer thick. This is the direct influence of the highly pure graphene oxide precursor used for the synthesis of GQD.

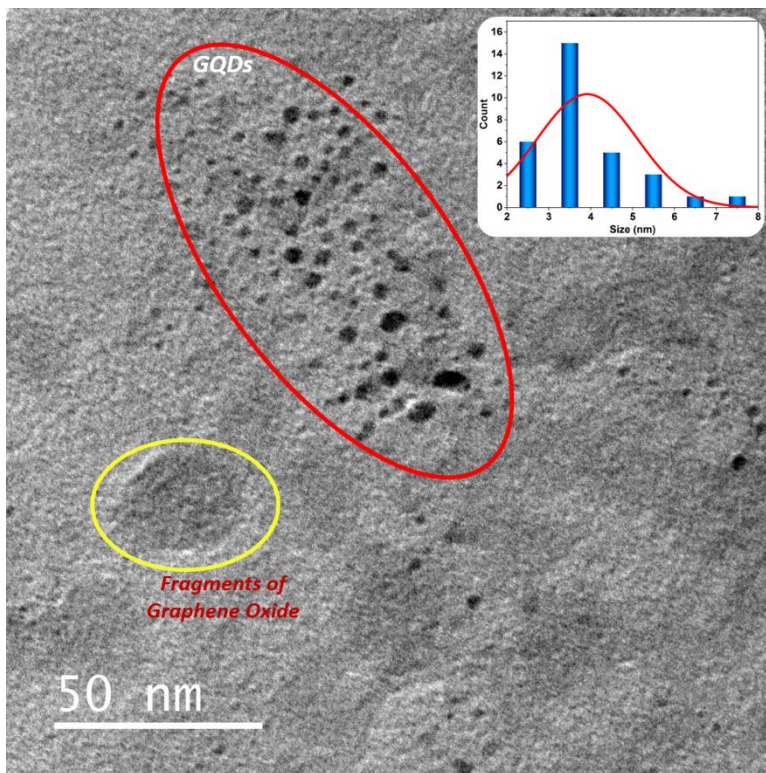


Figure 6.6 Transmission electron microscopic image of GQD and their size distribution (inset)

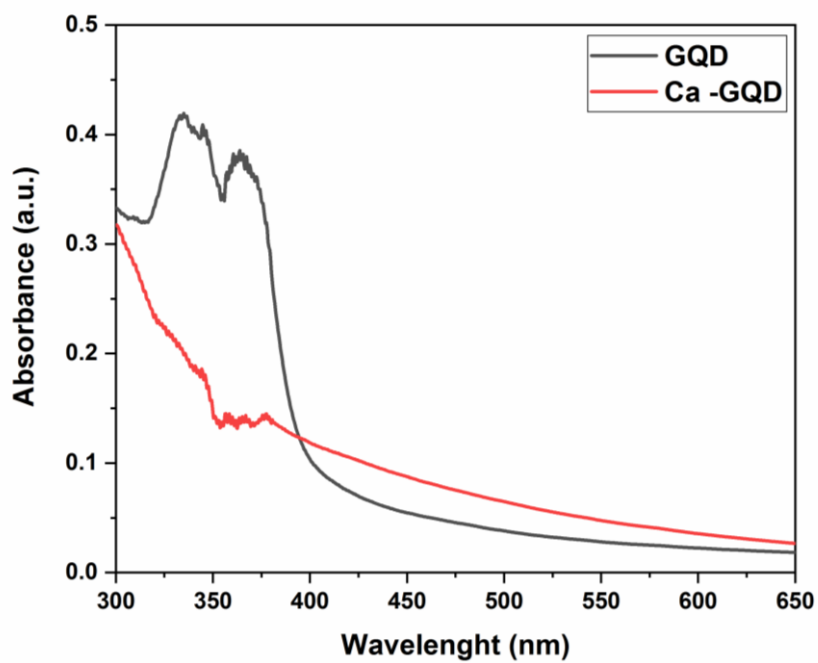


Figure 6.7 UV absorbance spectra of GQD and Ca-GQD.

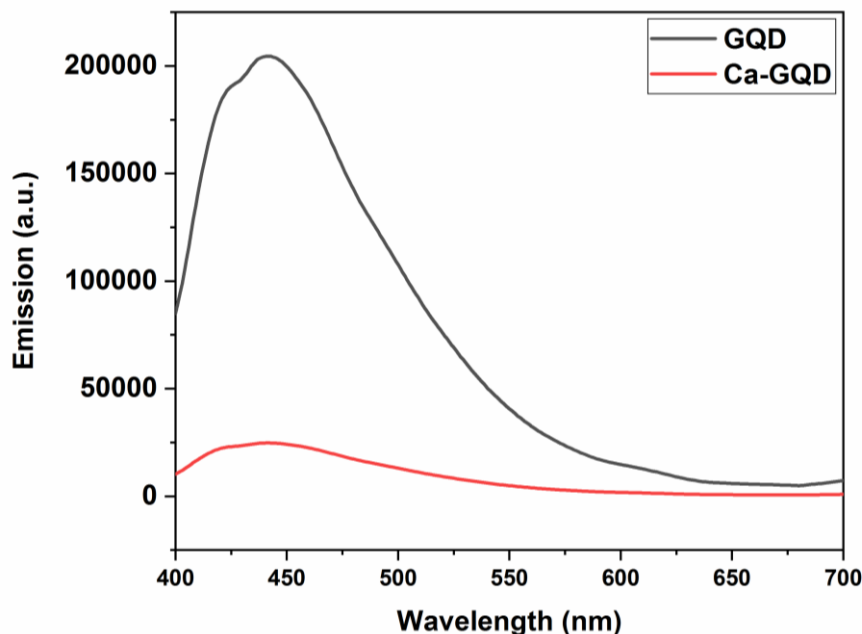


Figure 6.8 PL emission spectra of GQD and Ca-GQD

The transmission electron micrograph of the quantum dots reveals the visual cues about the size and the size distribution of GQD (Figure 6.6). The average size of GQD was observed to be approximately 3.5 nm in diameter. The size distribution of the GQD was also very narrow, with 93% of GQD being within the size of 3 to 5 nm. The narrow size distribution is highly essential for observing sharp PL. This is because the size of GQD has a direct effect on the PL (Kim *et al.* 2012). Hence, the as-synthesized GQD produced a deep blue luminescence. The UV-Vis absorbance spectra of GQD and Ca-GQD is presented as Figure 6.7. GQD absorbs electromagnetic radiation within the range of 320-400 nm with two absorbance peaks at 340 nm and 375 nm. The addition of Ca^{2+} ion to the GQD significantly reduces the absorbance, which is the case in the UV-Vis spectrum of Ca-GQD. This reduction in the absorbance is early signs of the eventual loss in PL in Ca-GQD. This is because the intensity of PL emission is also dependent on the absorbance in the UV-Vis region. The loss in absorbance and the relaxation of excitonic barrier cumulatively reduce the observed PL in the Ca-GQD. The absorbance at 375 nm results in the PL emission at 450 nm, which is corresponding to visible blue color (Figure 6.8).

The effect of Ca^{2+} on PL of GQD on a first glance seems similar to that mentioned for other metal ions (Benítez-Martínez and Valcárcel 2015) in the literature such as Al^{3+} (Fan *et al.* 2014), Transition metals like Fe^{3+} (Ananthanarayanan *et al.* 2014; Zhou *et al.* 2013; Li *et al.* 2014; Van Tam *et al.* 2014; Ju and Chen 2014; Xu *et al.* 2015; Li *et al.* 2015a), Cu^{2+} (Sun *et al.* 2013; Liu *et al.* 2014; Wang *et al.* 2014b; Huang *et al.* 2013), Cr^{6+} (Cai *et al.* 2014), Hg^{2+} (Wang *et al.* 2014a; Chakraborti *et al.* 2013), Ni^{2+} (Huang *et al.* 2013), Mn^{2+} (Huang *et al.* 2013), and Co^{2+} (Huang *et al.* 2013), and lanthanides like Ce^{3+} (Salehnia *et al.* 2017). The study involving cerium (a lanthanide) as an analyte reports the direct suppression in the PL intensity of GQD due to the redox reaction between Ce^{3+} ion on the GQDs surface. This is possible because Ce benefits with having 2 stable oxidation states of +3 and +4 which is actively involved in the process of PL quenching. Other transition metal ions such as Fe usually require the modification in the GQD with groups like 1-butyl-3-methylimidazolium (BMIM) (Ananthanarayanan *et al.* 2014) or heteroatom like nitrogen (Ju and Chen 2014). In such cases, the reason behind the apparent suppression of the PL intensity is deemed to be the relaxation in excitonic barrier which is caused by the metal ions. However, the GQD itself is not selective towards the heavier transition metal ions therefore the need of modification arises. GQD, however was observed to be selective in binding with Ca^{2+} ion (discussed later) with appreciable PL quenching. The mode of PL quenching here is not based on the redox behaviour, as was the case with Ce^{3+} ions due to a single stable oxidation state of Ca. The reason for the apparent PL quenching was the relaxation of the excitonic barrier as is the case with the modified GQD binding to transition metals, however, with the exception that the binding in present case is with the as-synthesized GQD without the need of any modification. Furthermore, the loss of absorption as near the excitation wavelength as evident in the Figure 6.7, also results in the reduced PL observed. Hence, the loss of PL intensity is a cumulative result of the lower absorbance of excitation wave and the relaxation of excitonic barrier due to the charge transfer capability of Ca^{2+} ions. Therefore, the reported mode of detection of Ca^{2+} ion is quite different from the similarly available literature.

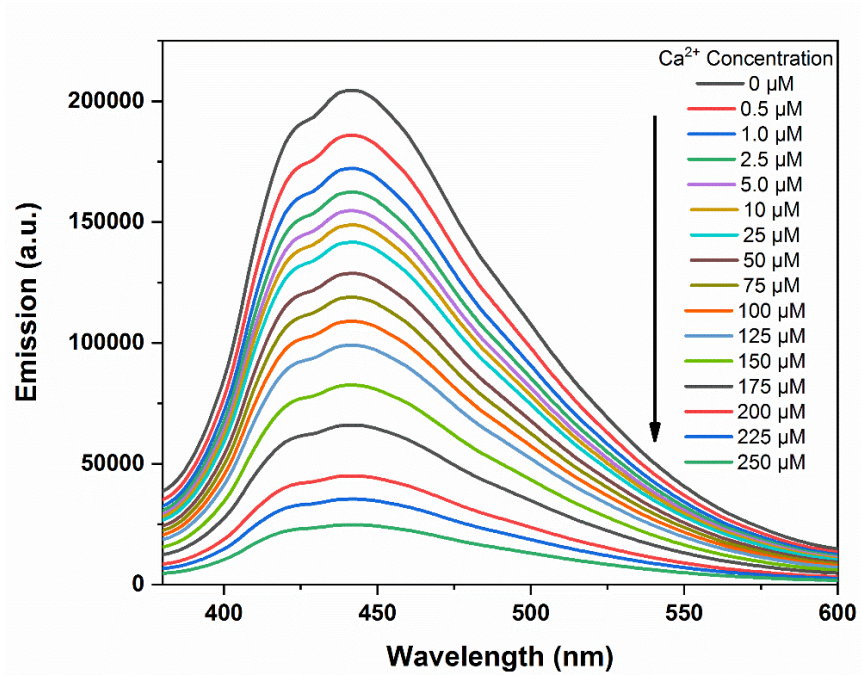


Figure 6.9 The variation of photoluminescence of GQD in solutions containing 0 μM to 250 μM Ca^{2+} ions under 375 nm irradiation.

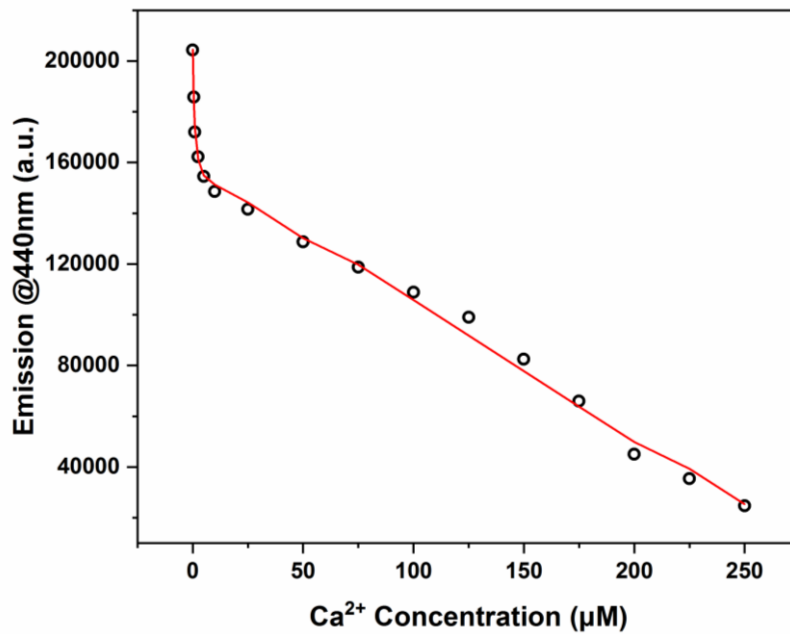


Figure 6.10 Variation of the photoluminescence intensities of GQD at different concentrations of Ca^{2+} ions.

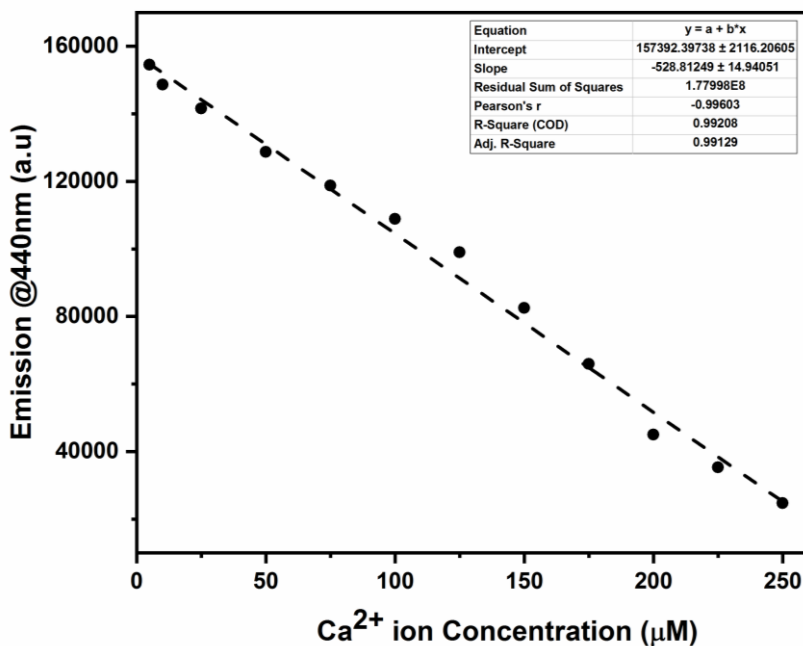


Figure 6.11 Linear variation of the photoluminescence quenching of GQD at different concentrations of Ca^{2+} .

As is evident with the discussion so far, photoluminescence is a significant property for GQD. They exhibit a typical blue luminescence when excited with an incident beam of 375 nm. This PL emission is further utilized to quantitatively determine the amount of Ca^{2+} ion in an aqueous media. The loss of absorbance in the UV-Vis spectra and earlier known phenomenon on excitonic relaxation in the metal interacted GQD, it is understood that the mode of detection will be based on the PL quenching which in simpler terms can be called as a “Turn-off” sensor. Figure 6.9 shows the observed quenching in the PL intensities of GQD at various concentration of Ca^{2+} in the solution. As is evident from the graph, the extent of the PL quenching is directly related to the concentration of Ca^{2+} in the solution. The quenching of the PL is a result of the combined effect of the reduced absorbance at the excitation energy, and the relaxation of excitonic boundaries in the Ca^{2+} interacted GQD which facilitates charge transfer among the GQD bound to the Ca^{2+} ion.

As observed from the Figure 6.9, the extent of PL quenching is gradual with the increase in the concentration of Ca^{2+} ions in the solution. The relation between the PL quenching and the concentration of Ca^{2+} ions is presented in Figure 6.10. The PL quenching was

found to be linear to the concentration of the Ca^{2+} ions with a coefficient of regression of 0.99129 (Figure 6.11). The linearity between the observed PL and concentration was valid till $5 \mu\text{M}$ Ca^{2+} ions in water. Therefore, it was concluded that the limit of detection (LOD) of Ca^{2+} ions is $5 \mu\text{M}$. The variable size and availability of the functionality on the edges of the GQD mean that the interaction between the Ca^{2+} ions and the GQD are not in a fixed stoichiometric ratio.

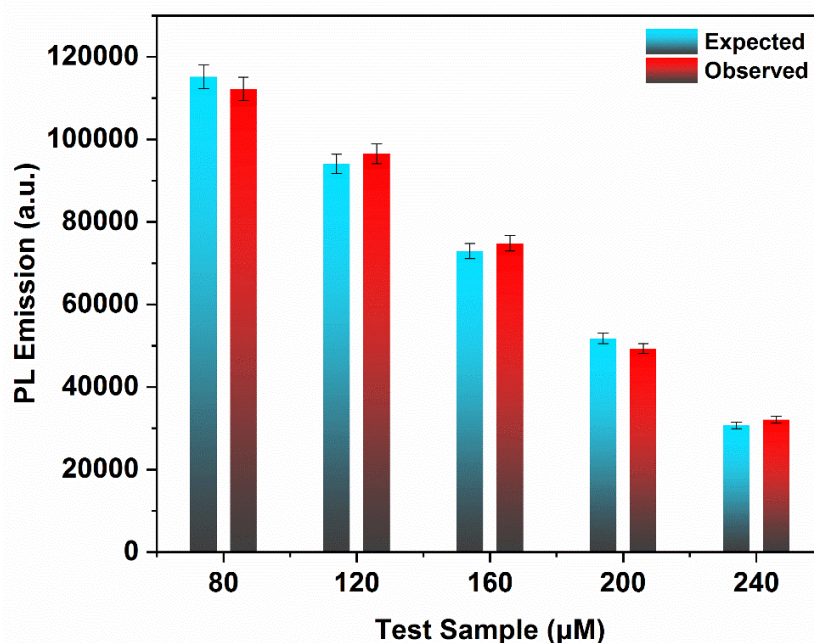


Figure 6.12 The expected and observed photoluminescence of various test samples of Ca^{2+} ion as detected by GQD under 375 nm irradiation.

The performance of the GQD as a Ca^{2+} sensing platform was evaluated using water samples having known concentrations (80, 120, 160, 200, and 240 μM). The expected PL values based on the calibration curve plotted in Figure 6.10 for the water samples are compared with the observed PL in Figure 6.12. Both expected and observed PL values were in close agreement, and the calculated concentrations of the test samples are given in Table 1. The observed intensity of PL was in good agreement with the expected intensity of PL as determined by the equation of the linear fit for the calibration plot as shown in Figure 6.11. The average accuracy was $96.56 \pm 3.44 \%$ for the measurement of PL intensity. Similarly, the concentrations of Ca^{2+} ions determined in the test samples were having an average accuracy of $96.74 \pm 3.26 \%$. These results

signify the potential of the reported method to determine the amount of Ca^{2+} ion in aqueous solutions.

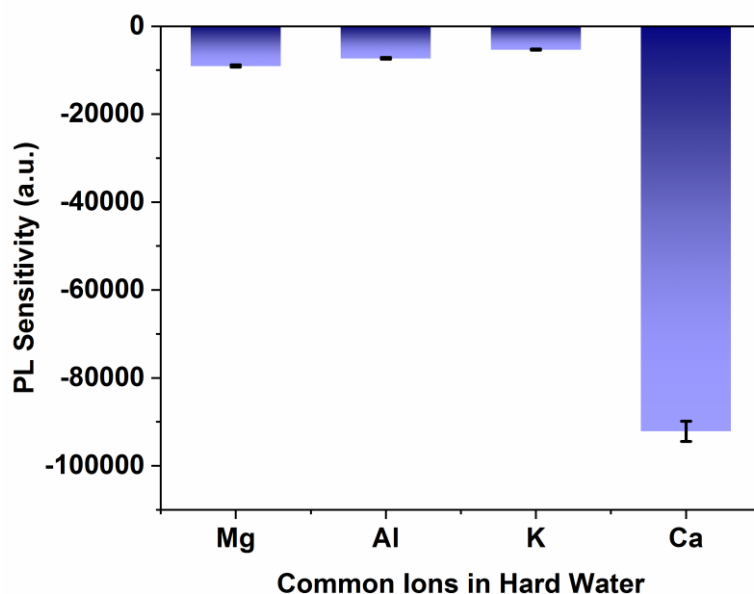


Figure 6.13 The selectivity of photoluminescence quenching of GQD towards Ca^{2+} in the presence of other common cations found in hard water.

Table 6.1 The photoluminescence measurements and the calculated strength of the test samples of Ca^{2+} ions.

S. No.	Actual Conc. (μM)	Expected PL (a.u)	Observed PL (a.u)	Determined Conc. (μM)	PL emission Accuracy (%)	Conc. Of Ca^{2+} Accuracy (%)
1	80	115152	112240	85	97.5 ± 2.5	93.7 ± 6.3
2	120	94032	96540	115	97.3 ± 2.7	95.8 ± 4.2
3	160	72912	74787	156	97.4 ± 2.6	97.5 ± 2.5
4	200	51792	49266	204	95.1 ± 4.9	98 ± 2.0
5	240	30672	32062	237	95.5 ± 4.5	98.7 ± 1.3
Average Accuracy in measurement (%)					96.56 ± 3.44	96.74 ± 3.26

Table 6.2 Comparison of the reported sensing method for Ca²⁺ ions with other methods.

S.No.	Mode of Determination	Detection Range	Limit of Detection	Accuracy	Reference
1	Bichromophoric Squaraine Foldamer	NA	NA	NA	(Arunkumar <i>et al.</i> 2005)
2	Fluorescent photoinduced electron transfer cation sensors	NA	NA	NA	(Valeur and Leray 2000)
3	Fluorescent Indicators	Only Qualitative	Few mM	NA	(Grynkiewicz <i>et al.</i> 1985)
4	Fibre Optic Sensor	10 ⁻⁷ M - 10 ⁻¹ M	10 ⁻⁷ M	NA	(Suzuki <i>et al.</i> 1989)
5	Wavelength dispersive X-ray fluorescence (WDXRF) and	NA	0.1 % (w/w)	99.9 %	(Costa <i>et al.</i> 2019)
6	Laser-induced breakdown spectroscopy (LIBS)	NA	0.1 % (w/w)	99.9 %	(Costa <i>et al.</i> 2019)
7	Microwave induced plasma atomic emission spectrometry	13 µg.L ⁻¹ - 10 g. L ⁻¹	13 µg.L ⁻¹	93.9 %	(Ozbek <i>et al.</i> 2019)
8	GQD	5 µM – 250 µM	5 µM	96.74%	This Work

The common cations found in the potable water samples apart from Ca^{2+} are Mg^{2+} and Al^{3+} . The GQD were highly sensitive towards Ca^{2+} ions as compared to the Mg^{2+} and Al^{3+} ion (Figure 6.13). This is possibly due to the larger size of Ca^{2+} ions as compared to the Mg^{2+} and Al^{3+} ions, which facilitate higher PL quenching. However, the presence of transition metals may interfere in proper detection of Ca^{2+} ions due to the competing PL quenching of GQD.

Table 6.2 compares the results obtained for the use of GQD as a sensory platform for the Ca^{2+} ions with the other techniques used for the determination of the said cation in literature. As it is evident, the accuracy of the presented mode of determination is comparable to that of highly sophisticated techniques like WDXRF, LIBS, and Microwave induced plasma AES within the linear range of $5\ \mu\text{M} - 250\ \mu\text{M}$. The method is more suitable than various others, owing to ease of preparation of GQD and its availability in humblest of the setups.

6.4 CONCLUSIONS

In conclusion, the hydrothermal cutting of GO sheets was used to synthesize GQD, which lead to the reduction in the size of the GO sheet. This size reduction is responsible for the excitonic entrapment within the GQD structure, which is the cause of observed photoluminescence. The observed interaction between Ca^{2+} and GQD core was due to the bond formation between Ca^{2+} ion and carboxylic groups on the edges of GQD. This interaction leads to the quenching of PL in GQD. The reason for the quenching was the apparent reduction in the absorption of UV irradiation at 375 nm and because of the long-range conjugation around Ca^{2+} ions which relax excitonic barrier. This “turn-off” mechanism of PL quenching can be employed to determine Ca^{2+} ions in the aqueous media. The reported method was able to determine the strength of Ca^{2+} ions with an accuracy of $96.74 \pm 3.26\%$ and limit of detection being $5\ \mu\text{M}$. Therefore, the reported method may be used as a quick and economic alternative to determine the amount of Ca^{2+} ion in potable water samples.

CHAPTER 7

**GRAPHENE QUANTUM DOTS WITH NITROGEN-RICH EDGES
AS PL-TURN-ON SENSOR FOR GLUCOSE**

Abstract: Quantitative determination of glucose is essential in biomedical, food, and beverages industry. This chapter reports the preparation of one step in-situ synthesized amino-functionalized GQD for aggregation induced PL determination of Glucose.

7.1 INTRODUCTION

Glucose, owing to its role and importance in dietary supplements and biological system, could be argued to be most important analyte among all. The comprehensive work have already been undertaken in terms of quantitative estimation of glucose in biological assays (Oliver *et al.* 2009). Most of these sensors are electrochemical sensors which can be either enzymatic (Lee *et al.* 2019; Kim *et al.* 2019) or non-enzymatic (Li *et al.* 2019; Du *et al.* 2019; Diouf *et al.* 2019; Wang *et al.* 2019). Electrochemical sensors benefit from very low limit of detection (LOD) intrinsically due to the very high precision (Wang 2008). Therefore, such sensors are often used in determination of analytes in biological systems with accuracy in ppm levels (Chen *et al.* 2013a). However, the ultra-low concentration sensitivity means that these sensors are not suitable for detecting glucose in higher concentrations as is the case in food samples. Another limitation of the electrochemical sensors is the complex fabrication of electrodes. Therefore, a PL emission-based sensing approach for glucose can be a looked upon as a complimentary method of analysis. Additionally, such sensors are also reaching LOD as low as 16 nM (Ngo *et al.* 2019). However, as is the case with electrochemical sensors, the linear range of detection is very low thereby limiting their applications to clinical diagnostics and biomedical applications.

The PL based sensors are usually able to detect glucose in concentration range of 0.1 – 1000 mM (Benítez-Martínez and Valcárcel 2015). This range is perfectly suited for testing food samples and other samples where higher concentration of glucose are expected. Syshchyk *et. al.* reported an enzyme biosensor on porous silicon for PL determination of glucose within concentration range of 0 - 3.0 mM (Syshchyk *et al.* 2015). Yi *et. al.* reported a label free silicon quantum dot PL probe for determining the concentration of glucose in μM range with high specificity (Yi *et al.* 2013). However, the sensing in mM region was not possible using this method. PL carbon dots are looked upon as viable PL sensor for various analytes including glucose (Roy *et al.*

2015). Carbon dots with reduced graphene oxide are shown to be able to detect glucose concentration as low as 140 nM with linear range of determination being 1-60 μM (Yeh *et al.* 2013). Qin *et al.* reported a low cost synthesis of PL carbon dots for determining glucose within linear range of 2 – 18 mM with LOD being 45 μM (Qin *et al.* 2013). Zhnag *et al.* reported B-GQD with linear range of detection being 0.1 – 10 mM and LOD as 0.03 mM (Zhang *et al.* 2014). Another boron rich GQD was reported with same linear range of detection but lower LOD of 5 μM (Qu *et al.* 2013). Few other reports of GQD as PL sensing probe for determination of glucose are available (Liu *et al.* 2013; Abdel-Fattah *et al.* 2016).

In present report, we discuss the one-pot synthesis and characterization of amine-functionalized GQD ($\text{NH}_2\text{-GQD}$) and its applicability for the quantitative detection of glucose. A comprehensive study utilizing both UV-Vis absorbance and PL emission as a tool for the determination of glucose is provided. A stringent error analysis of the determination for both methods is also given. Additionally, commercial samples used to determine the glucose content and a comparative study of reported PL sensor with similar sensor from literature is reported. $\text{NH}_2\text{-GQD}$ owing to its easy preparation and wide linear range with LOD as low as 0.01 mM makes then suitable to complement already available sensors for diverse applications.

7.2 EXPERIMENTAL

7.2.1 Synthesis of $\text{NH}_2\text{-GQD}$

The amine functionalized GQDs were synthesized using Graphene oxide (GO) as precursor obtained from improved Hummer's method (Marcano *et al.* 2010) detailed in Chapter 3. The preparation of $\text{NH}_2\text{-GQD}$ was carried out using hydrothermal method (Pan *et al.* 2010) with modifications. In a typical procedure, the as-prepared GO dispersed in water was brought to pH 10 using NaOH. Further, 18 ml of this mixture with 2 ml hexamethylenetetramine (HMTA) was taken in an autoclave with Teflon lining and heated at 200 °C for 12 h. The resultant dispersion was then filtered followed by dialysis in a dialysis bag (retained molecular weight: 3500 Da) overnight to yield strongly fluorescent quantum dots. The concentration $\text{NH}_2\text{-GQD}$ obtained was ~ 1 mg/ml. The PL was observed in UV Cabinet with the irradiation of 365 nm which was

indicative of the synthesis of quantum dots. Same method was followed without the addition of HMTA to synthesize GQD.

7.2.2 Material Characterization

The FTIR spectra of the quantum dots were obtained on BRUKER FTIR spectrometer with Eco-ATR accessory. Raman spectra of the samples were obtained using a Renishaw Raman microscope using 514nm laser excitation at room temperature. Quantum dots were examined under the transmission electron microscope (JEM-2100 Plus Transmission Electron Microscope) for their morphology and size determination. UV-Vis spectra were recorded on Analytik Jena Specord S600 UV-Vis spectrophotometer. All the PL measurements were made on Horiba Fluoromax Spectrofluorometer.

7.2.3 Determination of Glucose

The determination of glucose was carried out using standard solutions of glucose with varying concentrations (from 0.1 mM to 500 mM) for obtaining calibration curve. The concentration of NH₂-GQD used was 1 mg/ml with glycine-sodium hydroxide buffer to maintain pH 10 during the estimation. Few test solutions of glucose were prepared to check the error in determination. The commercial glucose instant mix were dissolved in distilled water in predetermined amount. The resulting solutions were filtered through 47 μm membrane filter to undissolved and other colloidal matter followed by further dilution to check the suitability of method for real samples.

The % error in determination was calculated using formula:

$$\% \text{ Error} = \frac{(\text{Observed Value} - \text{Actual Value}) \times 100}{\text{Actual Value}}$$

The relative UV-Vis absorbance of for the monosaccharide and disaccharide interacted NH₂-GQD was calculated using formula:

$$\text{Relative Absorbance} = \frac{\text{Absorbance of Sample (A)} - \text{Absorbance of Blank (A}_0\text{)}}{\text{Absorbance of Glucose (A}_g\text{)} - \text{Absorbance of Blank (A}_0\text{)}}$$

The relative PL emission of for the monosaccharide and disaccharide interacted NH₂-GQD was calculated using formula:

$$\text{Relative PL Emission} = \frac{\text{PL emission of Sample (I)} - \text{PL emission of Blank (I}_0\text{)}}{\text{PL emission of Glucose (I}_g\text{)} - \text{PL emission of Blank (I}_0\text{)}}$$

7.3 RESULTS AND DISCUSSION

7.3.1 Characterization of GQD and NH₂-GQD

The distinction between GQD and NH₂-GQD was ascertained using FTIR spectroscopy (Fig. 7.1). FTIR spectrum of GQD was observed with characteristic peaks at 3500 cm⁻¹ (broad) and 1700 cm⁻¹ (sharp) corresponding to -OH stretching and -C=O stretching, respectively. In the spectrum of NH₂-GQD, the presence of additional side peak at 3300 cm⁻¹ due to NH stretching along with 3500 cm⁻¹ for -OH stretching is clear evidence for the amine functionalization of GQD (Figure 7.2). There was a slight shift in -C=O stretching peak to 1680 cm⁻¹ in spectrum of NH₂-GQD indicated the presence of amide groups on NH₂-GQD as well. The Raman spectrum of NH₂-GQD was recorded to assess the nature of edges (Figure 7.3). NH₂-GQD showed characteristic D band and G band associated at 1350 cm⁻¹ and 1580 cm⁻¹, respectively. The disordered carbon atoms at the edges of NH₂-GQD generate D band in the Raman spectrum, whereas the G band is result of to the in-plane vibration of sp²-bonded carbon atoms. There is an appreciable loss of graphitic layered structure as evident from 1:1 ratio of D and G band intensities. Conventionally, the intensity ratio hints towards the formation of single to few atomic layer (bi- or tri-) thick NH₂-GQD. However, the D band in NH₂-GQD is of higher intensity than graphene, as the fraction of carbon atoms present on the edge with respect to those in the core is higher than the graphene. Therefore, intensity ratio is not the ideal indicator of the number of layers in the GQD (Kim *et al.* 2013b). This can be emphasized by TEM of NH₂-GQD, where the NH₂-GQD appears darker than expected which means that there are more than bi- or tri- atomic layers thick (Figure 7.8).

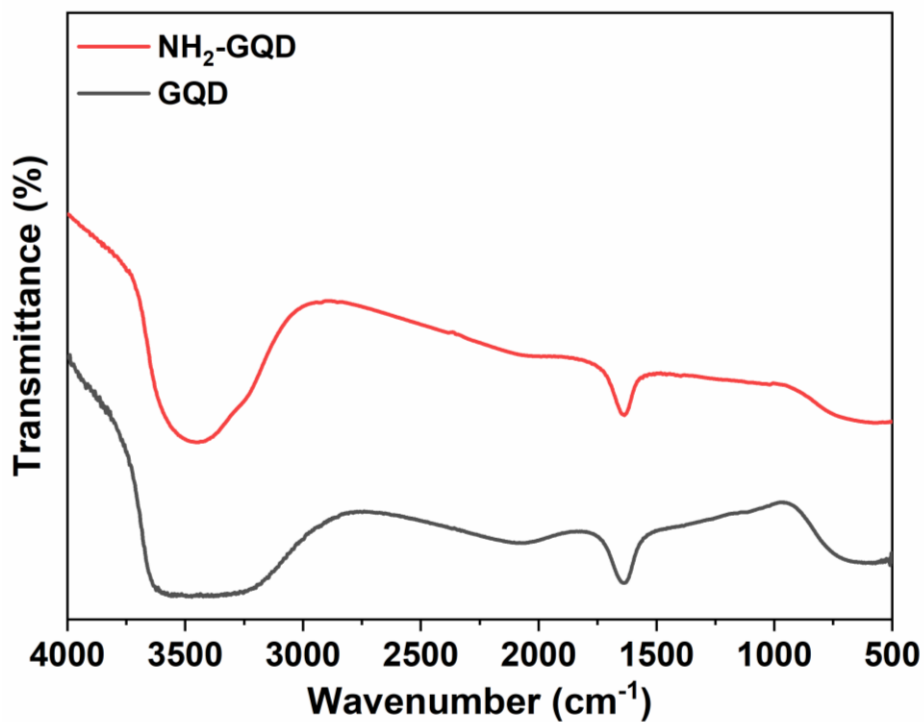


Figure 7.1 FTIR spectra of GQD and NH₂-GQD.

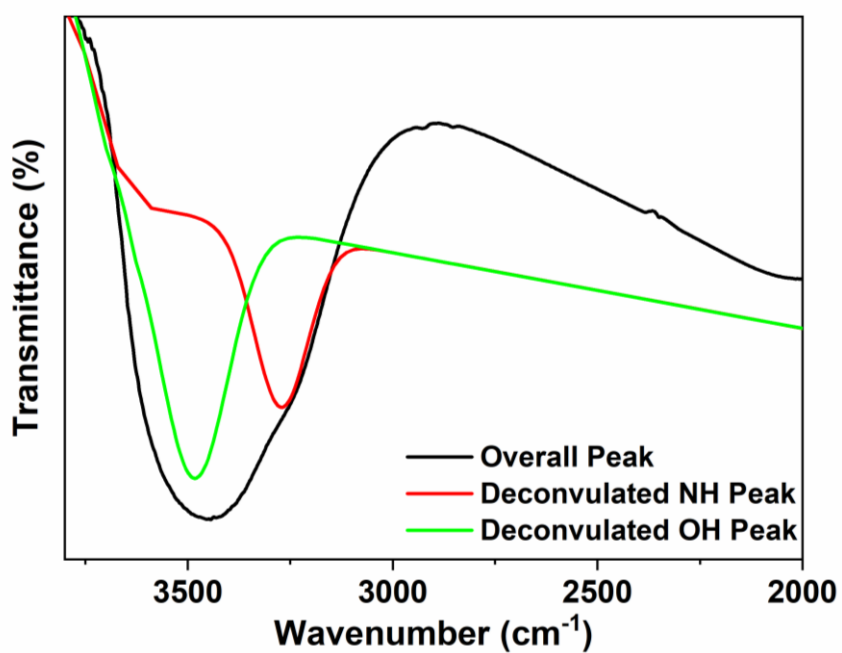


Figure 7.2 Deconvoluted peaks of N-H and O-H stretching in NH₂-GQD.

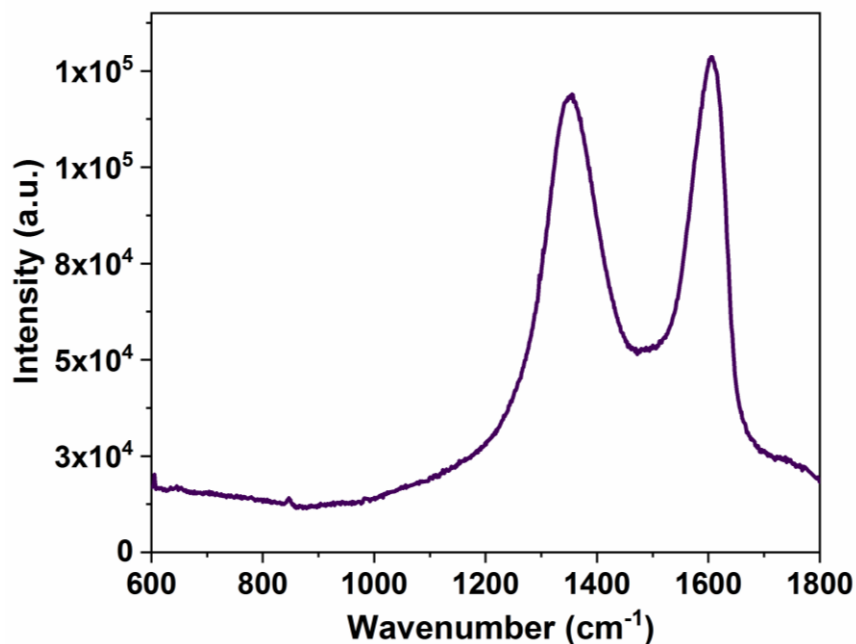


Figure 7.3 Raman spectrum of NH₂-GQD.

The bonding in NH₂-GQD were further determined by XPS analysis. The survey scan of NH₂-GQD was observed with peaks at 284 eV, 400 eV, and 532 eV corresponding to C, N, and O atoms, respectively (Figure 7.4). The low intensity of N peak suggests that fraction of N atom in quantum dot is low as compared to C and O which is the usual case with GQD. C and O atoms form core of the GQD whereas the functionalization with N just happen over few sites on the edge of the GQD and possibly as dopant in the GQD core. Hence in NH₂-GQD, the overall fraction of N will always be less than that of C and O which is supported by the survey scan. The C specific XPS scan and deconvoluted peaks are given in Figure 7.5. The peaks at 284 eV, 286 eV, and 288 eV are due to C-C, C-O-C, and C=O carbons of NH₂-GQD. The C available for C-C bonds being maximum leads to a highly intense peak followed by low intensity peak due to C=O. The GQDs are cut along C-O-C bonds present in graphene oxide, therefore, very few such bonds are left in NH₂-GQD hence a very low intensity peak. The N specific scan in given in Figure 7.6. The presence of N is ascertained by observing peak at 398 eV. This indicates that few C atoms in the GQD cores were replaced to N atom, resulting in N-doping of GQD. Further, the N atoms occupying C-NH₂ bonds at the edges of GQD were observed at 400 eV. The O specific scan of NH₂-GQD reaffirmed the presence of C-O and C=O bonds in the quantum dots by reflecting peaks at 529 eV

and 532 eV, respectively (Figure 7.7). The XPS analysis made the presence of the three primary atoms, C, N, and O evident in the NH₂-GQD sample along with the bond there are present in. Among all the bonds which were consistent with the FTIR spectra, presence of XPS peak corresponding to N at 398 eV, which can be attributed to the N occupying few positions in the all carbon skeleton of GQD lead to the conclusive evidence of N doping in the GQD via reported method.

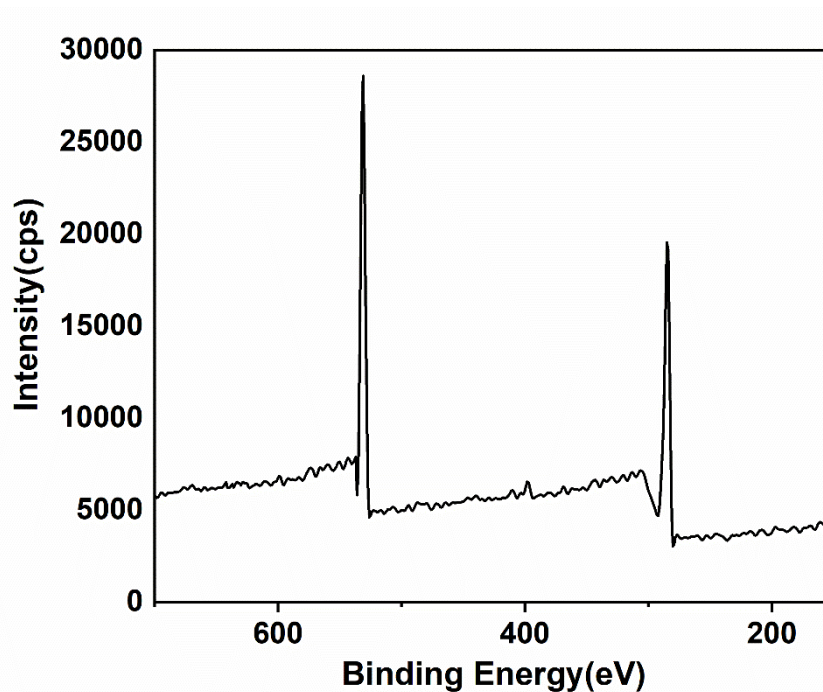


Figure 7.4 XPS survey scan of NH₂-GQD.

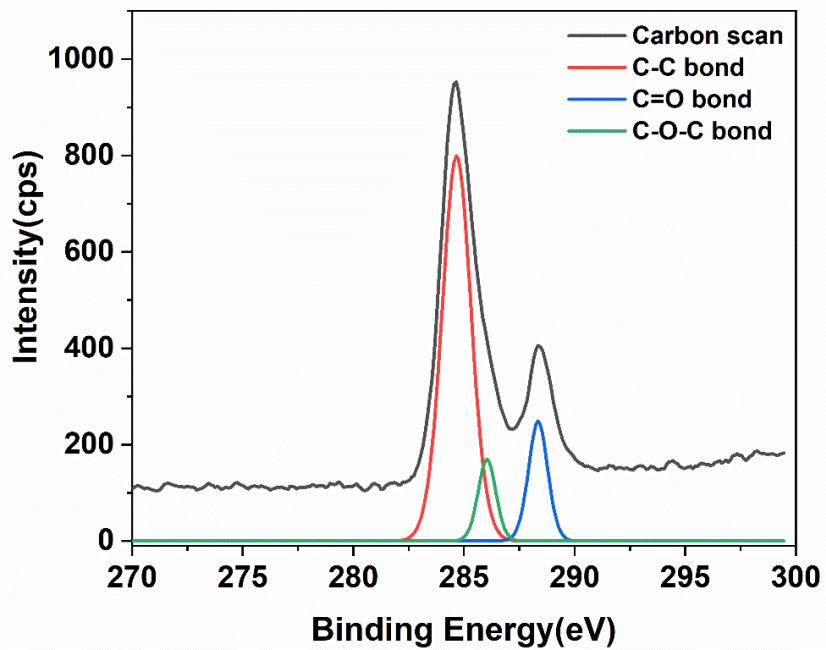


Figure 7.5 XPS C specific scan of NH₂-GQD.

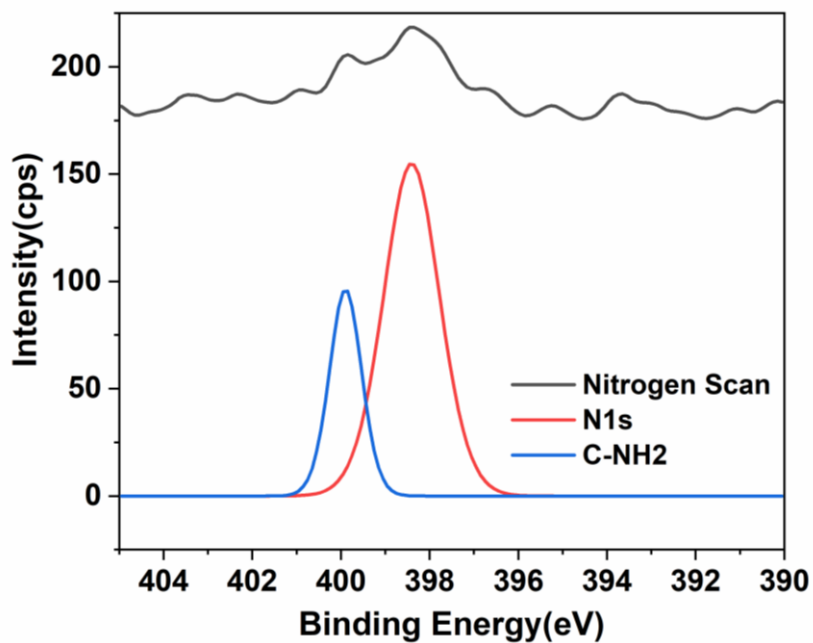


Figure 7.6 XPS N specific scan of NH₂-GQD.

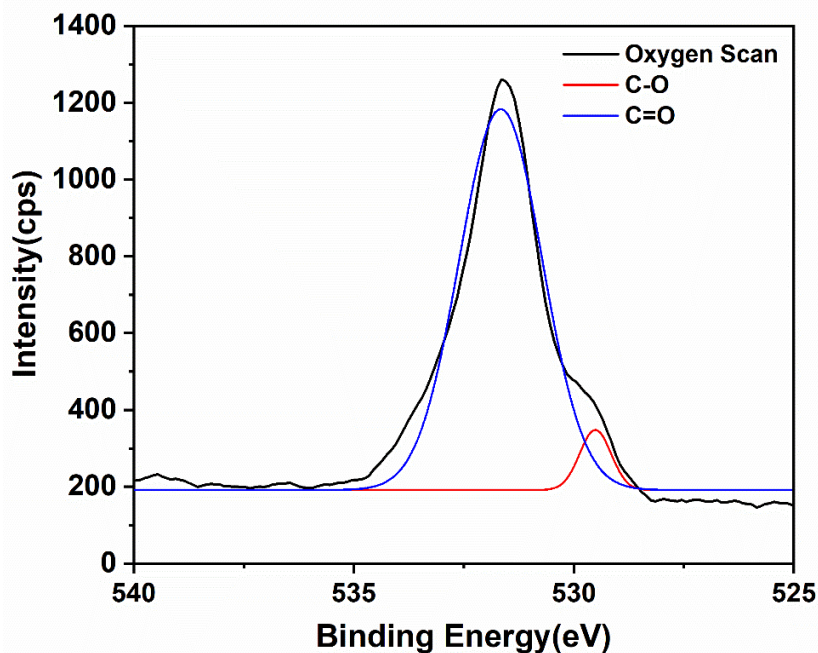


Figure 7.7 XPS O specific scan of NH₂-GQD.

The transmission electron micrograph of NH₂-GQD was recorded to analyze apparent thickness and size distribution of the quantum dots (Figure 7.8). The NH₂-GQD were of various atomic thickness which coupled with Raman analysis (as given in Figure 7.3) led to the conclusion to be of few atomic layers thick. The average particle size encountered for these quantum dots was 5 nm with 90% quantum dots being within 3 - 10 nm. The interaction of NH₂-GQD with glucose lead to aggregation of the quantum dots which can be visualized in Figure 7.9. The average particle size increased to 8 nm with 90% of the quantum dots being within 5 - 12 nm. Therefore, the NH₂-GQD bond to glucose molecule which leads to the larger size quantum dots. The size of the aggregated quantum dots is approximately double that of the as synthesized NH₂-GQD. This apparent doubling of the aggregate size leads to the conclusion that stoichiometric ration of NH₂-GQD to glucose in the aggregated quantum dots is 2:1. The possible mode of interaction between the NH₂-GQD and glucose is given in Figure 7.11. The apparent effect of this aggregation of quantum dots over the UV-Vis absorption and PL emission is further studied by recording respective spectra.

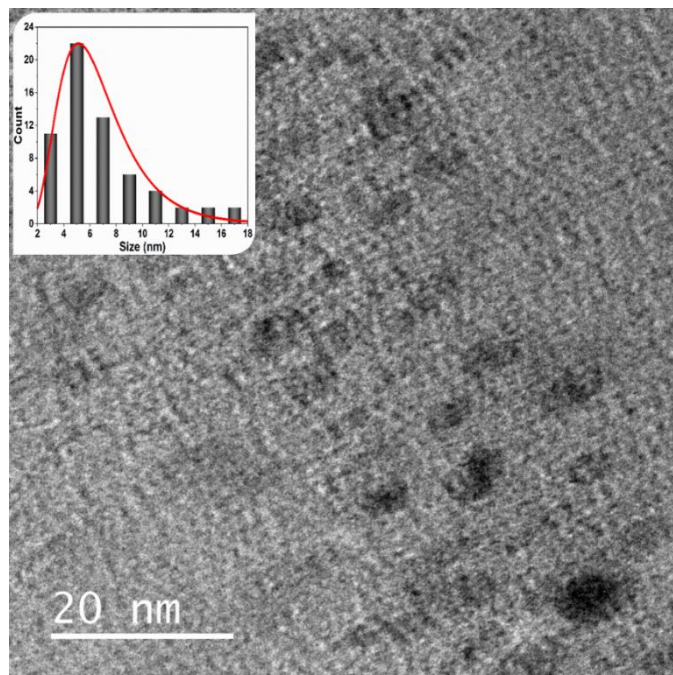


Figure 7.8 Transmission electron microscopic image of NH₂-GQD (Inset: Size distribution).

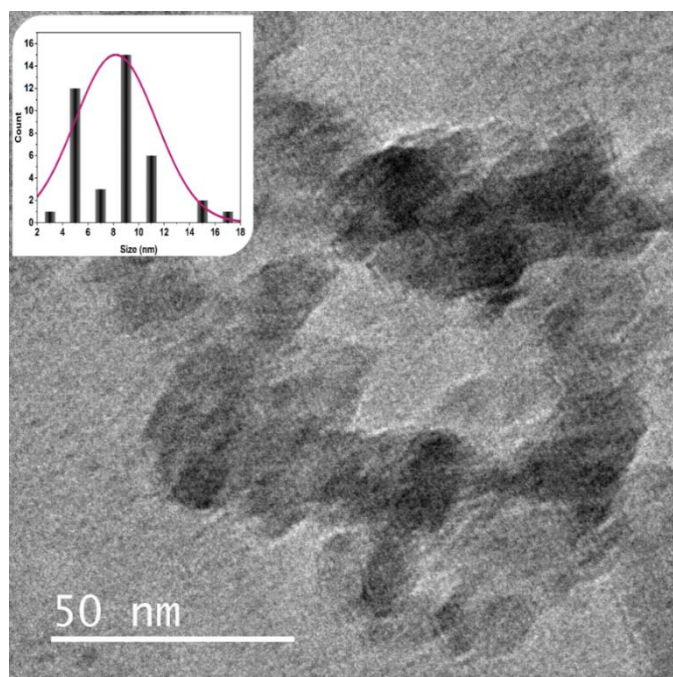


Figure 7.9 Transmission electron microscopic image of NH₂-GQD aggregated along glucose (Inset: Size distribution).

The UV-Vis absorption and PL spectra of NH₂-GQD are given in Figure 7.10. The UV-vis spectrum of NH₂-GQD showed that the onset of the absorption for the quantum dots

is at ~ 380 nm. Therefore, the bandgap of $\text{NH}_2\text{-GQD}$ is 3.26 eV. The maximum absorbance is observed at 260 nm (λ_{max}). This wavelength was used to study the UV-Vis absorbance-based sensing pattern of $\text{NH}_2\text{-GQD}$ for glucose. The PL spectra of $\text{NH}_2\text{-GQD}$ was recorded by exciting the quantum dot by an incident electromagnetic beam of wavelength 380 nm. This wavelength was chosen to observe the visible PL as any shorter wave leads to PL in shorter wave regions which is difficult to observe visually. The PL of the $\text{NH}_2\text{-GQD}$ if set in visible region makes observation of visual alteration in intensity possible. Hence, this can make qualitative determination of analytes possible. The highest intensity of the PL was observed at 480 nm for $\text{NH}_2\text{-GQD}$. Therefore, the intensity of PL was recorded at 480 nm was used to study the PL-based sensing pattern of $\text{NH}_2\text{-GQD}$ for glucose.

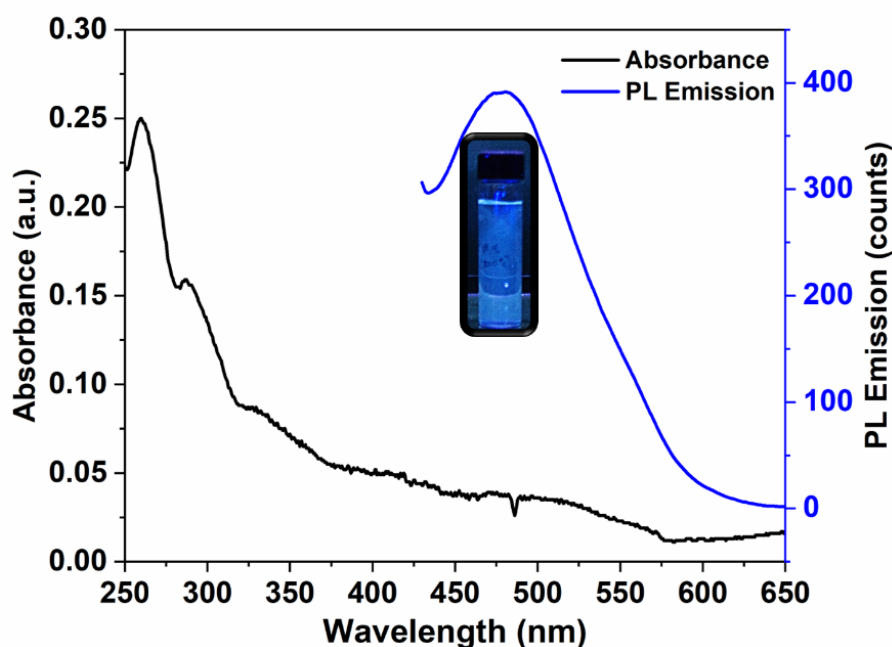


Figure 7.10 UV-Vis and photoluminescence spectra of $\text{NH}_2\text{-GQD}$ recorded within 250 - 650 nm and 420 - 650 nm, respectively. The photoluminescence spectrum was recorded for incident electromagnetic wave of wavelength 380 nm.

7.3.2 Mechanism of Aggregation induced photoluminescence emission in glucose-NH₂-GQD system

The mode of interaction between glucose and NH₂-GQD is given in Figure 7.11. The approximate 2-fold increase in the size of quantum dot aggregate w.r.t the size of NH₂-GQD hint towards the 2:1 stoichiometric ratio of NH₂-GQD to glucose in the highly luminescence quantum dot aggregate, wherein two NH₂-GQD are linked by a glucose linker. The chemical structure drawn in the schematic is for representation purpose to depict the position of active amine groups which plausibly binds to the hydroxyl groups of glucose. NH₂-GQD does not have a well-defined chemical formula as it is more of a functional material than a molecule. The apparent increase in the intensity of PL emission of NH₂-GQD when interacted with glucose is also due to the NH₂-GQD glucose aggregates. Zhang *et al.* earlier reported that cis-5,6-diol units of glucose binds to two functionalized GQD (Zhang *et al.* 2014). The intramolecular rotation of the luminescence center in the aggregates involves simultaneous movements of the glucose linker and another neighboring luminescence center. The high energy barrier of such motions rigids the aggregate thereby blocking the nonradiative relaxation channels, and populating the radiative decay, in turn making the luminescence center highly emissive (Liu *et al.* 2011b; Hong *et al.* 2009; Zhao *et al.* 2009). Additionally, the PL emission of the NH₂-GQD is highest in pH 10 which was made stable by the addition of glycine-sodium hydroxide buffer (0.08M). The glucose-NH₂-GQD aggregate also returned highest emission in pH 10.

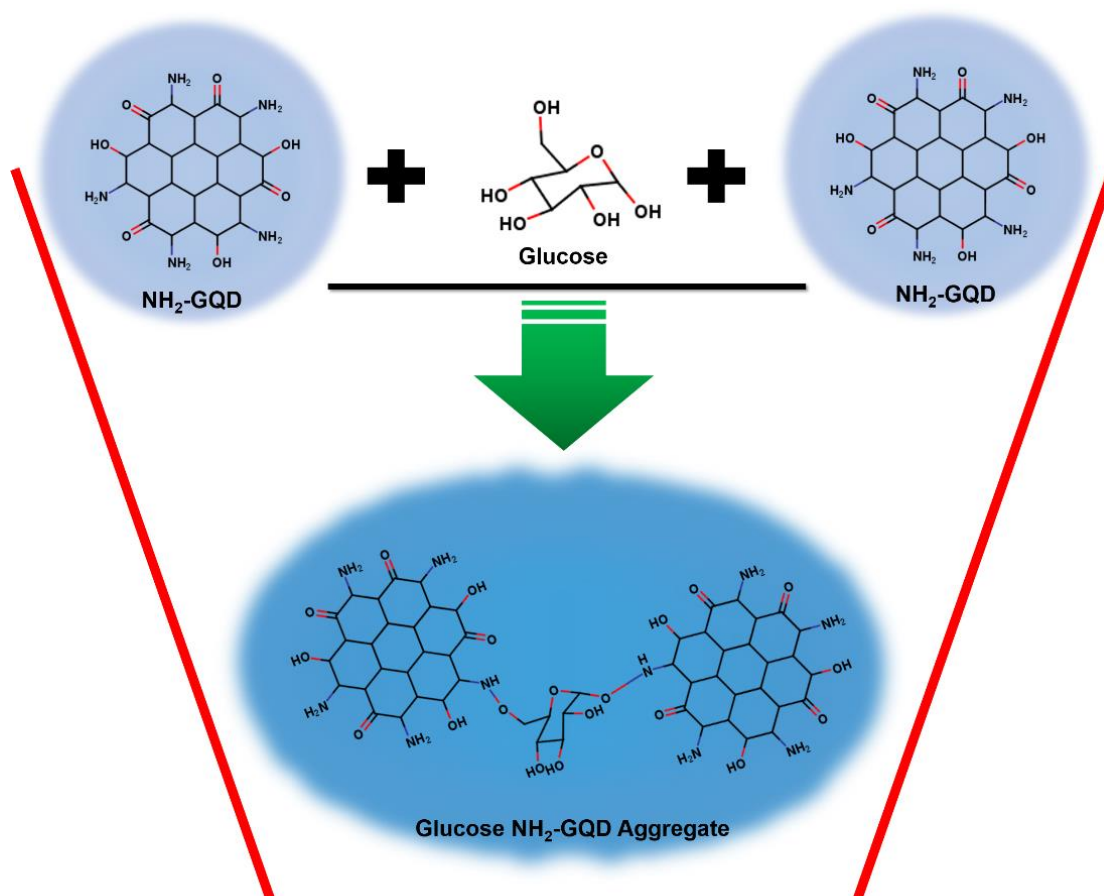


Figure 7.11 The plausible mode of interaction between NH₂-GQD and glucose in 2:1 stoichiometric ratio in aggregated quantum dot.

7.3.3 A Comparison of UV-Vis Absorbance and PL Emission Method on Determination of Glucose

The variation of the intensity of absorbance with respect to the concentration of glucose (C_{glucose}) is given in Figure 7.12. The marginal increase in the absorption was observed when the C_{glucose} was increased. The maximum absorption for the glucose NH₂-GQD system was found to be at 260 nm. All the absorption intensities of various glucose NH₂-GQD system were recorded at 260 nm. There was a relatively sharp increase in the intensity as the C_{glucose} is increased from 0.1 mM to 10 mM as compared to 50 mM to 500 mM. The transition in sensitivity was observed for C_{glucose} within 10 mM to 50 mM (Figure 7.13). The stark difference in sensitivities is evident from the difference in

slopes of the calibration curve. The calibration curve for the C_{glucose} from 0.1 mM to 10 mM determined with slope of 0.014 with R-square value of 0.9909 and most of the points being in the 95% confidence band of the linear trend (Figure 7.14). Compared to this, the calibration curve for the C_{glucose} from 50 mM to 500 mM determined with slope of 0.00026 with R-square value of 0.99305, again most of the points being in the 95% confidence band of the linear trend (Figure 7.15). The apparent increase in the absorbance intensity is higher for C_{glucose} within 0.1 mM to 10 mM. Hence, this will be the suitable range for the determination of glucose. However, the absolute range of the variation of absorption intensity is ~ 0.3 a.u is low. Therefore, this may induce a larger error in the measurement of C_{glucose} in real sample and hamper the sensitivity. To overcome these limitations, the PL of the NH_2 -GQD was considered to be a viable alternative. NH_2 -GQD showed absorbance at 260, 280, 325 and 380 nm. The absorbance of 380 nm radiation leads to visible PL at 480 nm in the NH_2 -GQD as observed in Figure 7.10. The 380 nm absorbance was also found to be increasing with the increase in the C_{glucose} , therefore the PL intensity was also increasing. The selection of the excitation wavelength of 380 nm while recording the emission spectra within the range of 430 to 650 nm was to eliminate the PL of water that is observed at 430 nm when excited with a wavelength of 350 nm.

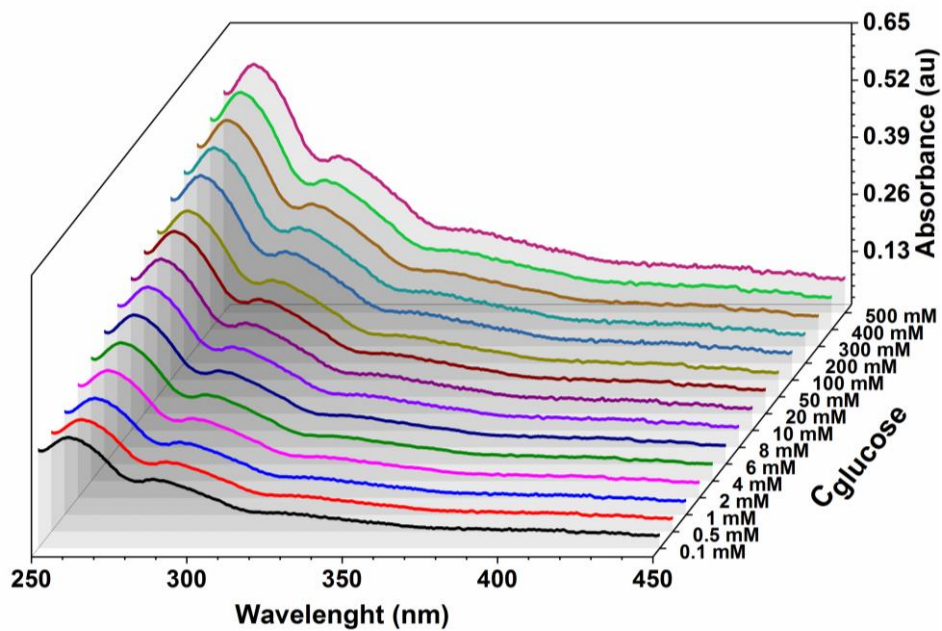


Figure 7.12 The variation on the UV-Vis absorbance spectra of NH₂-GQD at varying concentrations of glucose (0.1 mM to 500 mM).

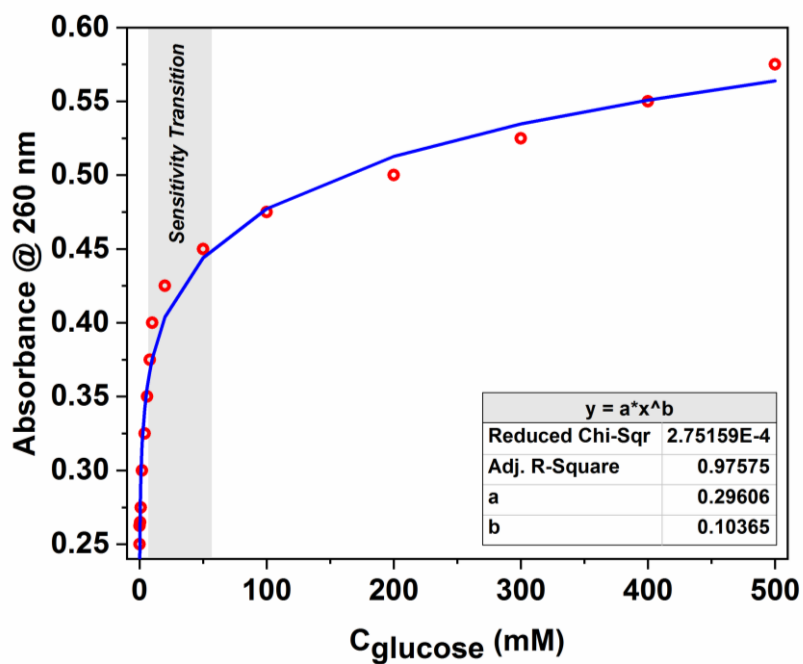


Figure 7.13 The variation of UV-Vis absorbance at 260 nm for varying concentrations of glucose (0.1 mM to 500 mM).

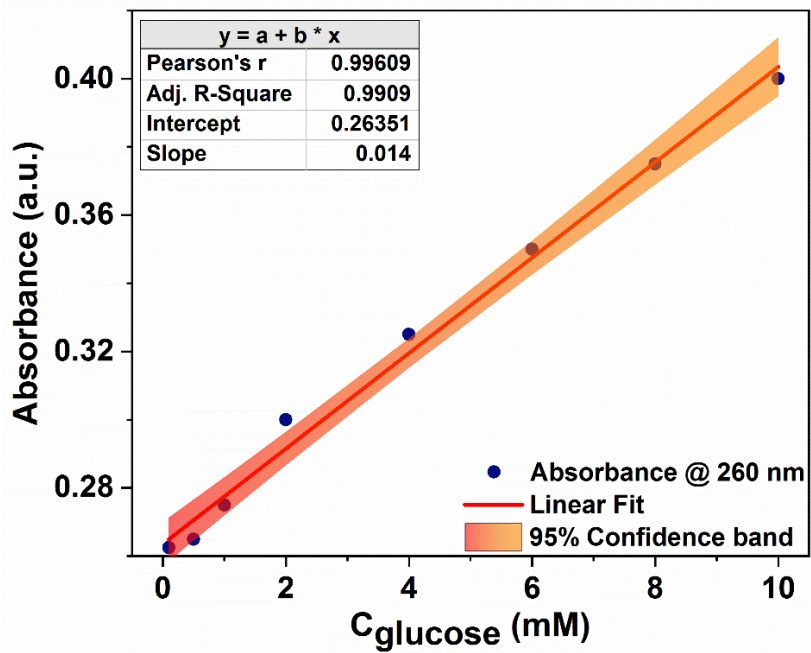


Figure 7.14 The variation of UV-Vis absorbance at 260 nm for varying concentrations of glucose (0.1 mM to 10 mM).

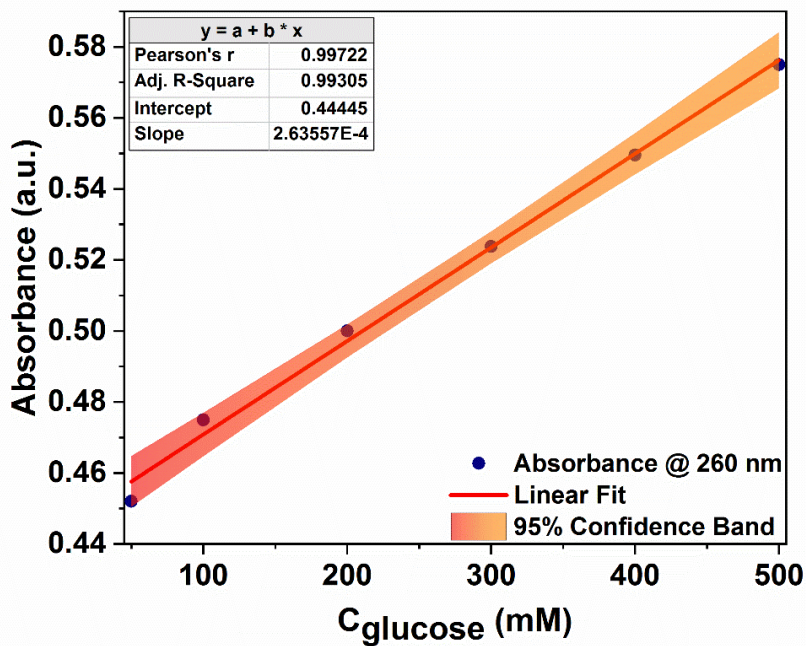


Figure 7.15 The variation of UV-Vis absorbance at 260 nm for varying concentrations of glucose (50 mM to 500 mM).

The variation of the intensity of PL emission spectra recorded at the excitation wavelength of 380 nm with respect to the C_{glucose} is given in Figure 7.16. The increase in the PL emission was observed when the C_{glucose} was increased. The variation in the intensity of absorbance spectra, the increase in the PL emission is observably more prominent due to the earlier described aggregation induced emission. The maximum PL emission for the glucose NH_2 -GQD system was found to be at 480 nm. Therefore, all the absorption intensities for various glucose NH_2 -GQD system were recorded at 480 nm. Again, as observed in the case of UV-Vis absorption spectra, there was a relatively sharp increase in the PL emission intensity as the C_{glucose} was increased from 0.1 mM to 10 mM as compared to 50 mM to 500 mM. The transition in sensitivity was again observed for C_{glucose} within 10 mM to 50 mM (Figure 7.17). The pronounced difference in sensitivities is evident from the difference in slopes of the calibration curve. The calibration curve for the C_{glucose} from 0.1 mM to 10 mM was determined with slope of 21.80384 with R^2 value of 0.99139 and most of the points being in the 95% confidence band of the linear trend (Figure 7.18). Compared to this, the calibration curve for the C_{glucose} from 50 mM to 500 mM determined with slope of 0.60315 with R^2 value of 0.98971, again with most of the points being in the 95% confidence band of the linear trend (Figure 7.19). The apparent increase in the PL intensity is higher for C_{glucose} within 0.1 mM to 10 mM. Hence, it is much more suitable range for the determination of glucose. Unlike the UV-Vis absorbance spectra, the absolute range of the variation of PL intensity is ~ 650 counts which is significantly higher. Therefore, this reduces the error in the measurement of C_{glucose} in real sample and improves the sensitivity.

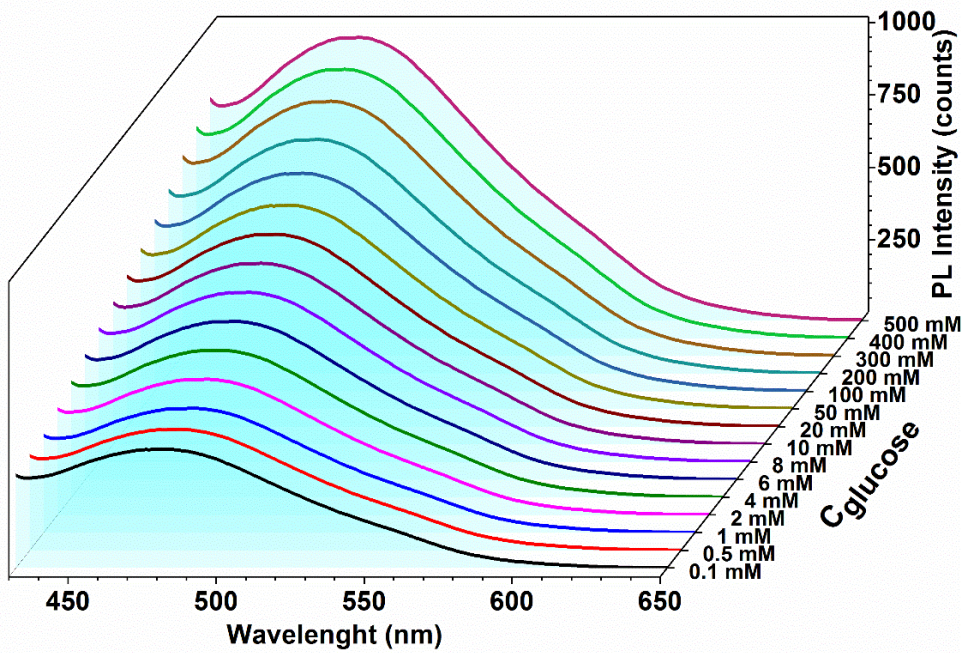


Figure 7.16 The variation on the photoluminescence spectra of NH₂-GQD at varying concentrations of glucose (0.1 mM to 500 mM).

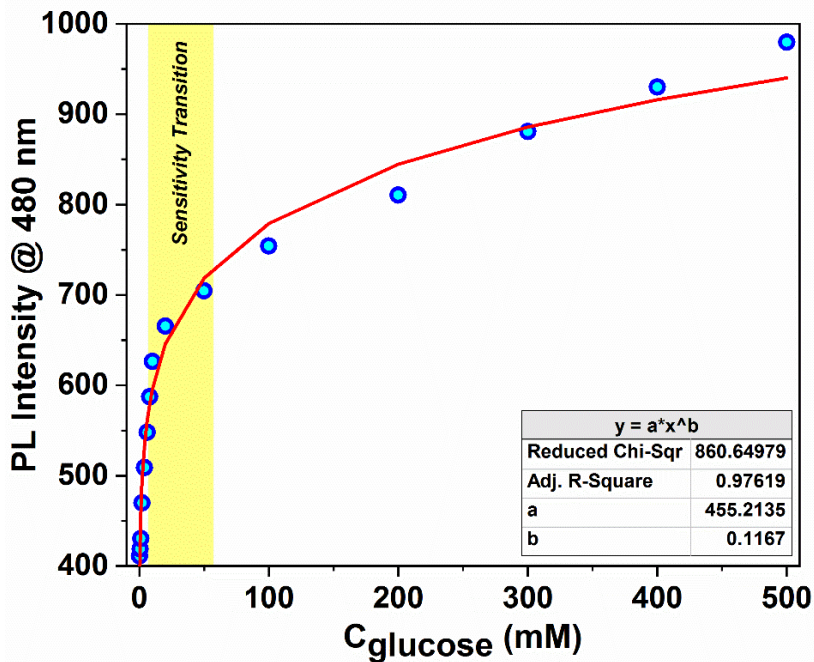


Figure 7.17 The variation of photoluminescence intensity at 480 nm for varying concentrations of glucose (0.1 mM to 500 mM).

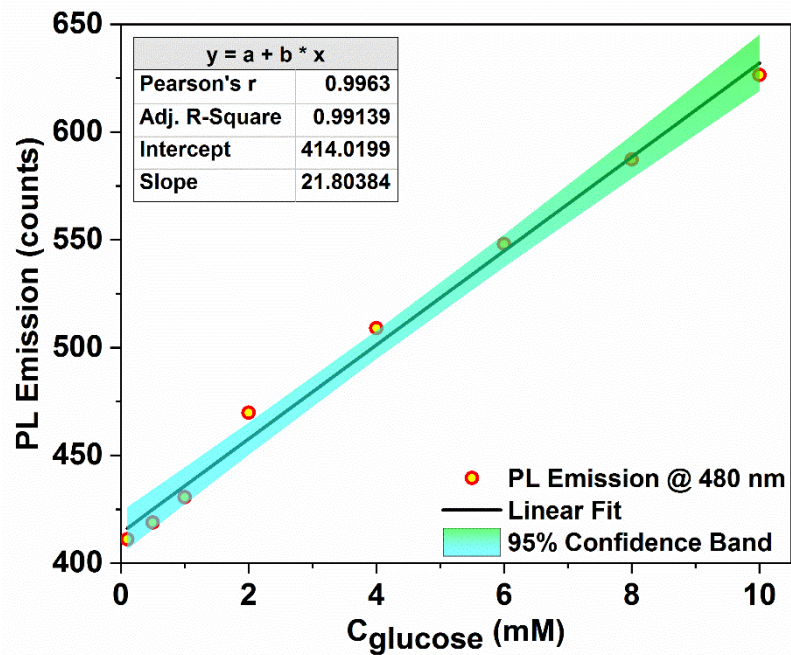


Figure 7.18 The variation of photoluminescence intensity at 480 nm for varying concentrations of glucose (0.1 mM to 10 mM).

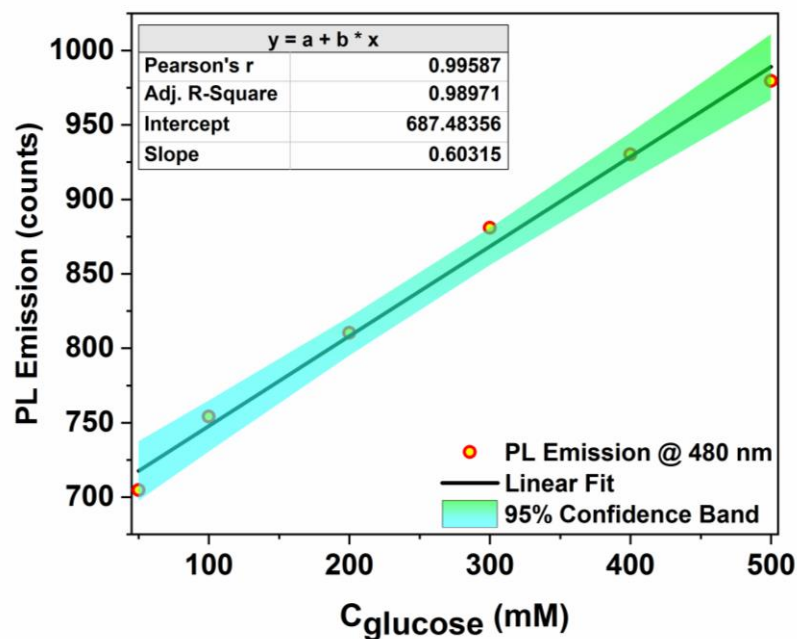


Figure 7.19 The variation of photoluminescence intensity at 480 nm for varying concentrations of glucose (50 mM to 500 mM).

7.3.4 Accuracy of the Determination of Glucose

The errors observed in the determination of C_{glucose} by both UV-Vis absorbance and PL emission methods along the concentration range 0.1 to 10 mM and 50 to 500 mM is given as Figure 7.20 – 7.22. As expected, the lower range of absolute variation within the least and highest UV-Vis absorbance observed for the glucose $\text{NH}_2\text{-GQD}$ system within lowest and highest C_{glucose} , showed larger error in measurement as compared to the measurement done by recording the PL emission (Figure 7.20 and 7.21). The slope for the variation of UV-Vis absorbance and PL emission was higher for the C_{glucose} varying from 0.1 mM to 10 mM than that of C_{glucose} varying from 50 mM to 500 mM, respectively. Therefore, the overall error in measurement was lower in the test samples which were within concentration 0.1 mM to 10 mM (Figure 7.22). The average % error for the absorbance method of determination of glucose were obtained as 6.60 % and 9.87 % for the C_{glucose} range of 0.1-10 mM and 50-500 mM, respectively. Therefore, the method returned an accuracy of 93.4 ± 6.60 % and 90.13 ± 9.87 % for C_{glucose} range of 0.1-10 mM and 50-500 mM, respectively. For the emission method of determination, the average % error obtained was 1.96 % and 2.67 % for the C_{glucose} between 0.1-10 mM and 50-500 mM, respectively. Hence the accuracy of PL emission method of sensing for C_{glucose} range of 0.1-10 mM and 50-500 mM are 98.04 ± 1.96 % and 97.33 ± 2.67 %, respectively. Therefore, the emission method for the quantitative analysis of glucose is more accurate in both the concentration regions. Additionally, careful selection of the concentration range suitable for linearity in PL emission makes glucose determination in wide concentration possible.

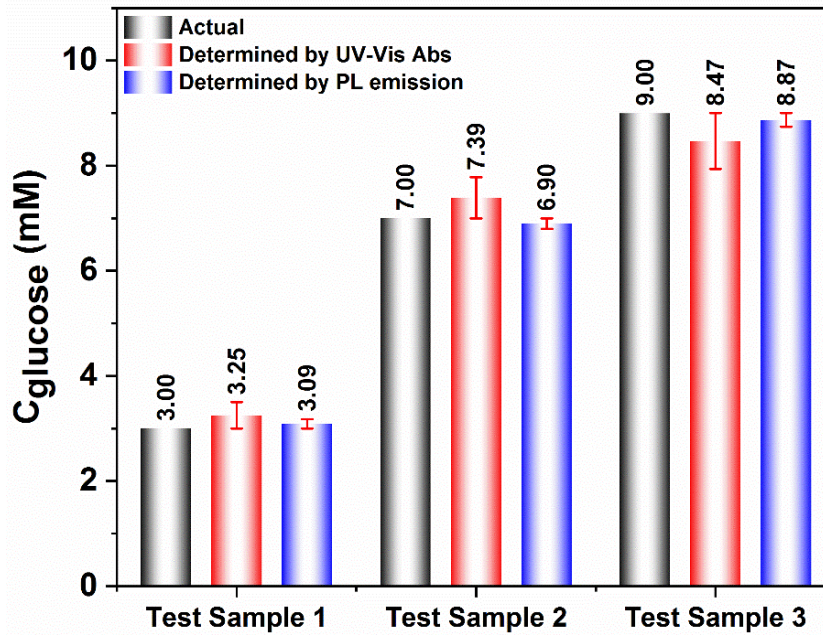


Figure 7.20 Determination of C_{glucose} in test sample 1 (3 mM), test sample 2 (7 mM) and test sample 3 (9 mM) using UV-Vis absorption calibration curve and PL intensity calibration curve.

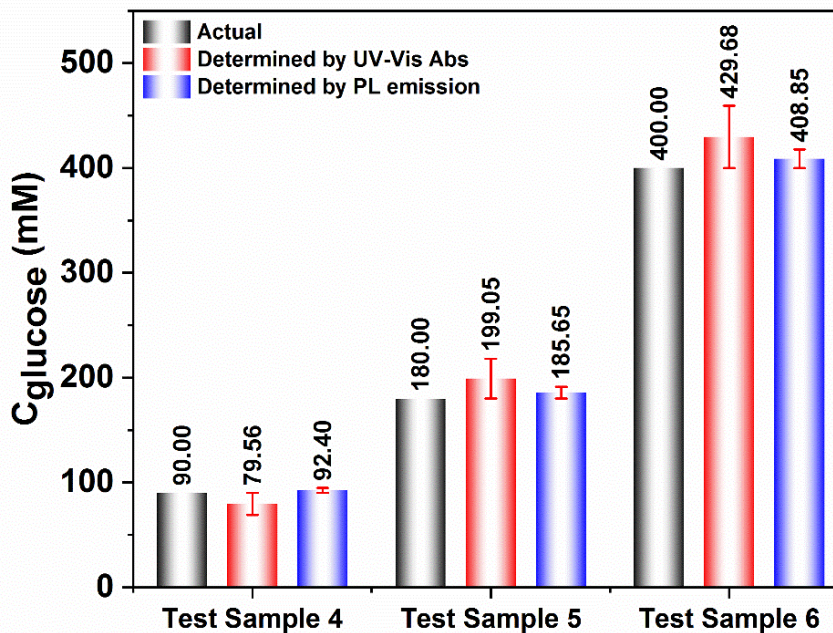


Figure 7.21 Determination of C_{glucose} in test sample 4 (90 mM), test sample 5 (180 mM), and test sample 6 (400 mM) using UV-Vis absorption calibration curve and PL intensity calibration curve.

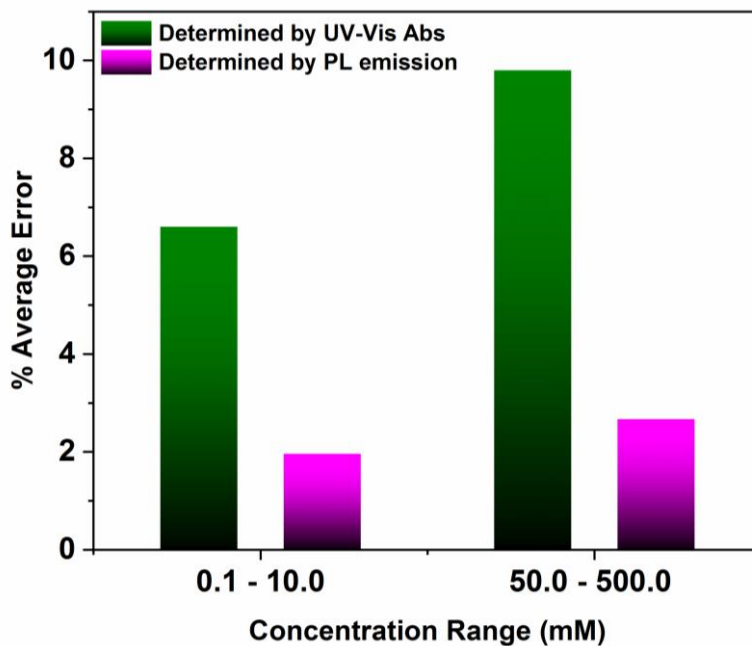


Figure 7.22 Average % Error for determination of C_{glucose} using UV-Vis absorption calibration curve and PL intensity calibration curve within the range of 0.1 – 10 mM and 50 – 500 mM.

7.3.5 Selectivity of Sensing methods

Figure 7.23 and 7.24 presents the relative absorbance and relative PL intensity of various sugars (Fructose, Galactose, mannose, Sucrose, Lactose and Maltose), respectively, in comparison to glucose at 10 mM concentration. The earlier comments made about the sensitivity of the probe for determination of the glucose in real samples can be again strengthened by the comparison of selectivity of the UV-Vis absorbance and PL emission-based determination of glucose in the sample in presence of other types of sugar. The relative absorbance of the glucose when compared to other sugars shows that the $\text{NH}_2\text{-GQD}$ is slightly selective towards glucose (Figure 7.23). The monosaccharides exhibit significant relative absorbance when compared to glucose as opposed to disaccharides. However, the relative PL intensity for glucose is significantly higher compared to both monosaccharides and disaccharides (Figure 7.24), which display highly selectivity nature of $\text{NH}_2\text{-GQD}$ as a PL sensory probe for the determination of glucose.

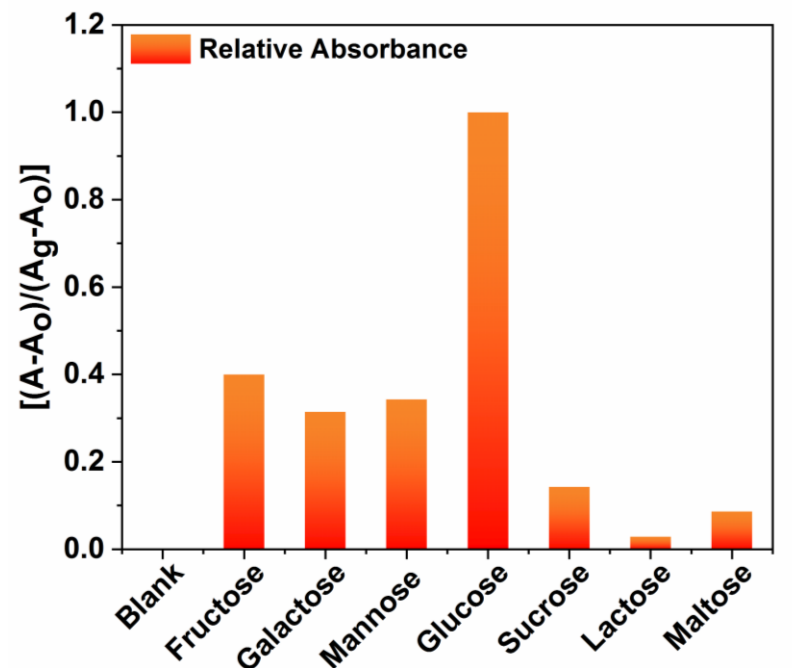


Figure 7.23 Relative absorbance of glucose in comparison to various sugars (10 mM).

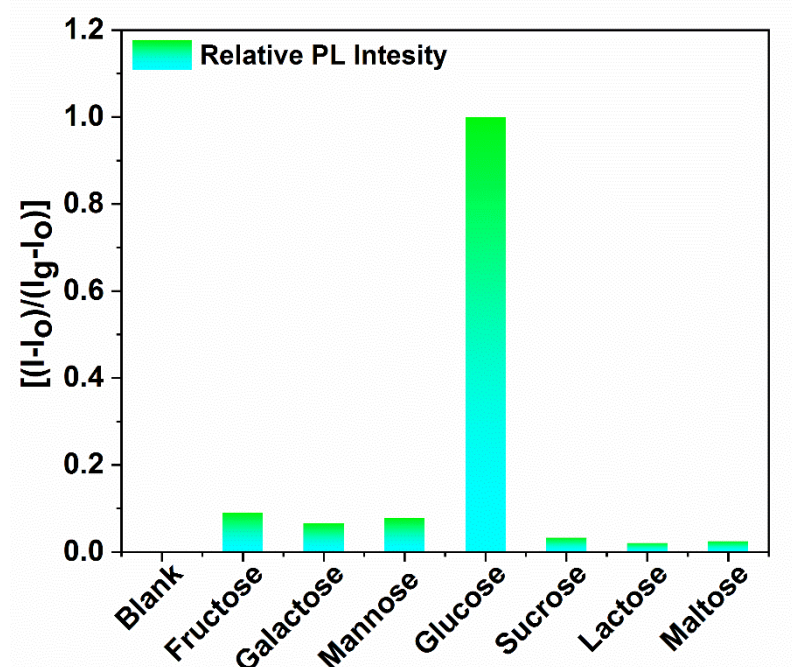


Figure 7.24 Relative photoluminescence intensity of glucose in comparison to various sugars (10 mM).

7.3.6 Determination of Glucose in Real Samples

The determination of glucose in real samples was performed using commercial Glucon D, Glucon D lime, and Glucon D orange, all manufactured by Kraft Heinz India. As per the nutritional fact, the glucose content in Glucon D, Glucon D lime, and Glucon D orange are 91 %, 47 % and 36 % w/w, respectively. The PL emission method was employed for the determination for all the samples. The samples were dissolved in distilled water to obtain sample concentration of 8 mM. The % composition of glucose by emission method for Glucon D, Glucon D lime, and Glucon D orange were obtained as 90.24 %, 45.98 % and 37.02 % w/w, respectively. These determinations are within ~ accuracy of $98 \pm 2\%$, which agrees with the earlier mentioned error analysis.

Table 7.1 Graphene Quantum Dots for PL detection of glucose.

S. No.	Type of GQD	Precursor	Linear Range (mM)	LOD (mM)	Error (%)	Sample	Ref
1	Carbon Dot	Willow bark	2 - 18	0.045	NM	Human blood serum	(Qin <i>et al.</i> 2013)
2	BBV-GQD	Graphene	1 - 60	NM	NM	Aqueous solution	(Liu <i>et al.</i> 2013)
3	B-GQD	Boron doped Graphene	0.1 - 10	0.03	NM	NM	(Zhang <i>et al.</i> 2014)
4	APBA-GQD	Graphene Oxide	0.1- 10	0.005	NM	Rat Brain Microdialysate	(Qu <i>et al.</i> 2013)
5	GQD	Glucose	5 - 50	NM	NM	NM	(Abdel-Fattah <i>et al.</i> 2016)
6	NH ₂ -GQD	Graphene Oxide	0.1 - 10 50 - 500	0.01	1.96 2.67	Commercial Glucose Mix	This work

The reported methods were compared with earlier reported literatures pertaining to the detection of glucose via photoluminescence emission method with various functionalized GQDs. The reported PL emission method of determining glucose was found to be superior in terms of the wide detection range of 0.1 mM to 500 mM (with

transition in sensitivity between 10-50 mM) with high accuracy of $98.04 \pm 1.96 \%$ and $97.33 \pm 2.67 \%$ for linear range of 0.1 – 10 mM and 50 – 500 mM, respectively. The determination of accuracy for the PL sensing ability of functionalized GQD is also presented for the first time to the best of author's information. Table 7.1 summarize the comparison of detection of glucose using few carbon dots or functionalized GQD reported in literature with the present study.

7.4 CONCLUSIONS

The amine functionalized graphene quantum dots were prepared in a one pot hydrothermal method using graphene oxide and hexamethylenetetramine. The obtained quantum dots exhibited all the predicted characteristics in the series of characterizations including FTIR, Raman, XPS, and TEM analysis. The enhancement of PL emission in the NH₂-GQD in presence of glucose was due to the formation of aggregate, which was well supported by the TEM analysis. This resulted in the significantly larger increase in PL intensity on addition of glucose in varying amounts. The UV-Vis absorbance and PL emission methods were evaluated for the determination of glucose. The PL emission method was significantly better with dual linear range 0.1-10 mM and 50-500 mM with an accuracy of $98.04 \pm 1.96 \%$ and $97.33 \pm 2.67 \%$, respectively. The LOD for the PL emission method was obtained to be 0.01 mM. The analysis of commercially available glucose instant mixes was analyzed, and the results were obtained with $\sim 98 \pm 2\%$ accuracy. Therefore, the NH₂-GQD was deemed to be a suited photoluminescent probe for the detection of glucose.

CHAPTER 8

**SYNTHESIS AND CHARACTERIZATION OF AMINE
FUNCTIONALIZED GRAPHENE QUANTUM DOTS AS CO-
SENSITIZER FOR HYBRID QUANTUM DOT SOLAR CELLS**

Abstract: This chapter discuss the application of amino functionalized graphene quantum dots (NH₂-GQD) synthesized via modified hydrothermal (HT) method as a co-sensitizer in conjunction with anthocyanin dye for hybrid quantum dot solar cell.

8.1. INTRODUCTION

The evolution of graphene after its discovery in 2004 (Novoselov *et al.* 2004) have seen a meteoric rise. A carbon-based nanomaterial is known for its different morphology and unique properties, is a two-dimensional nanomaterial having thickness of a single carbon atom. Graphene has characteristic features such as large surface area, high carrier mobility and superior mechanical flexibility, thermal and chemical stability (Lin *et al.* 2014). Thus, it is suitable for various applications in optoelectronic devices, energy storage media and drug delivery system. However, large area graphene is a zero-bandgap semimetal material, i.e., it is important for the devices with channels made of graphene to be switched off and hence, are not suitable for logic applications. Nevertheless, theoretical and experimental works revealed that the band structure of graphene can be tuned (Li *et al.* 2015c). It is possible to open a bandgap in graphene through several methods, for instance, biasing bilayer graphene, applying strain to graphene, constraining large area graphene in one dimension to form graphene nanoribbon or zero dimension to form Graphene quantum dots (GQD).

GQD are zero-dimensional material with characteristics derived from both graphene and carbon dots. Typically, GQD have diameters below 30 nm (Kim *et al.* 2012). Conversion of the 2D graphene sheets into 0D GQD results in functional phenomena such as quantum confinement leading to photoluminescence and edge effect (Pan *et al.* 2010). Unlike graphene, GQD show strong photoluminescence (Blanco *et al.* 2015; Sk *et al.* 2014; Xie *et al.* 2013). They are superior in terms of chemical inertness, ease of formation, low toxicity and excellent biocompatibility when compare to conventional semiconductor quantum dots makes them for great potential applications in next generation electronic and optoelectronic devices (Bacon *et al.* 2014). This prompted us to explore its applicability as a sensitizer in photovoltaic devices.

GQD have been explored in photovoltaics in different capacities. Pan et.al. reported heterojunction GQD/TiO₂ nanoarray for working electrode (Pan *et al.* 2013). Chen et.al. on the other hand, prepared GQD doped polypyrrole counter electrode for dye sensitized solar cells (DSSC) (Chen *et al.* 2013b). Li et.al. too reported GQD as electron acceptor in photovoltaic cells (Li *et al.* 2011). Kim et.al. reported similar use of GQD in bulk heterojunction cells (Kim *et al.* 2013a). Dutta et.al. fabricated ZnO/GQD solid state photovoltaic cells (Dutta *et al.* 2012). However, there have been very few reports on GQD as photo absorbers (Gupta *et al.* 2011; Yan *et al.* 2010a).

This chapter illustrates the synthesis and characterization amine functionalized graphene quantum dots (NH₂-GQD) and their application in photovoltaic devices as a co-sensitizer. Presented work is an exploratory route to understand the effect of parameters which pH and temperature on the synthesis of graphene quantum dots.

8.2. Experimental

8.2.1 Synthesis of NH₂-GQD

GQD was synthesized as per the method earlier described in Chapter 4. Functionalized GQDs were prepared using ammonium acetate (Amine functionalization) heated with dispersion of GQDs.

8.2.2 Extraction of Dye and Formulation of Sensitizer

Anthocyanin, a natural dye was extracted from hibiscus petals and was used as a sensitizer for this research. In a typical process, 25 g of Hibiscus *Rosa-Sinensis* flower petals were cut into small pieces and crushed using a mortar and pestle. The crushed petals were dispersed in 250 ml absolute ethanol at room temperature and kept overnight. The ethanolic extract was concentrated by heating at 40 °C for 2 hrs.

For fabrication of anthocyanin dye sensitized cell, 1 mL concentrated dye was diluted with 20 mL ethanol. For NH₂-GQD/Dye co-sensitized QDSC, the NH₂-GQD and dye was taken in 1:1 ratio, and further diluted with 20 mL ethanol.

8.2.3 Fabrication of the QDSC

The working electrode was prepared using a ITO glass slide with sheet resistance of 8 Ω/□. This slide was coated with TiO₂ of 300 mesh after forming a slurry in acetic acid.

The slide was annealed at 400 °C for 2 hrs. Further the dye or the NH₂-GQD/Dye mixture was adsorbed over the TiO₂ slide via solution dipping method. In this method the prepared slide was dipped in the sensitizer solution for 1 hour. During this stage, TiO₂ layer obtained a magenta shade which signified successful adsorption. Subsequently, the stained film was rinsed in water followed by ethanol. The counter electrode was prepared by applying silver paste over the slide of soda lime glass. The cell was assembled by bringing the working and counter electrode in contact from the coated side and securing them with the binder clip. The iodide/iodine electrolyte solution was added via edges of the slides. Figure 8.1 gives a schematic representation of the use of Anthocyanin dye and GQD mixture as photosensitizer for hybrid QDSC.

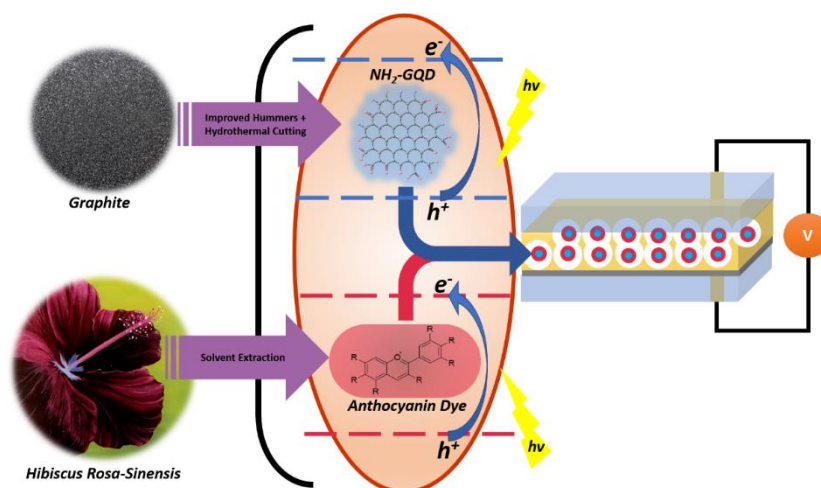


Figure 8.1 Schematic representation of the use of anthocyanin dye and NH₂-GQD as photosensitizer in a hybrid quantum dot sensitized solar cell.

8.3 RESULTS AND DISCUSSION

8.3.1 Characterization of NH₂-GQD

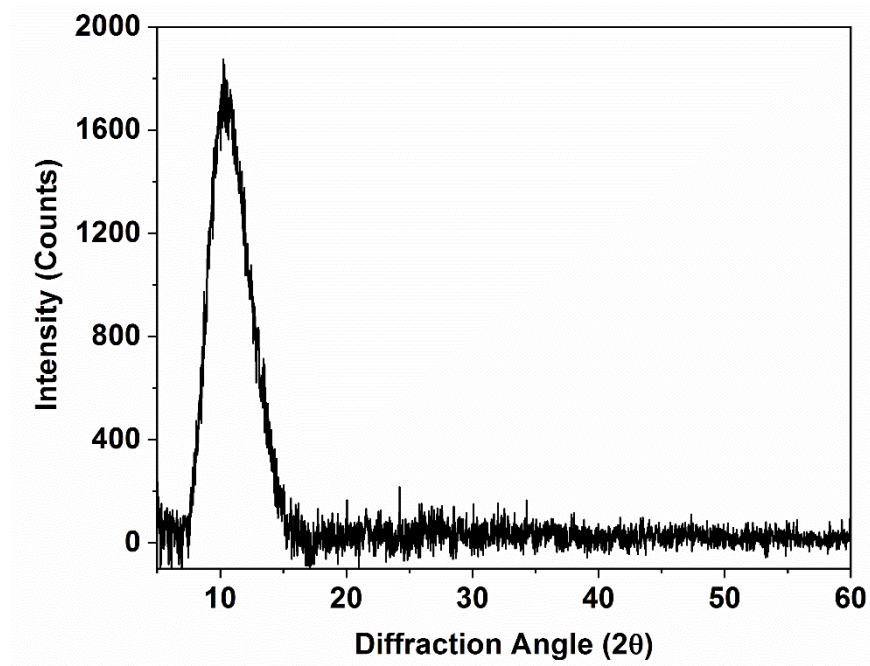


Figure 8.2 XRD Spectrum of graphene oxide

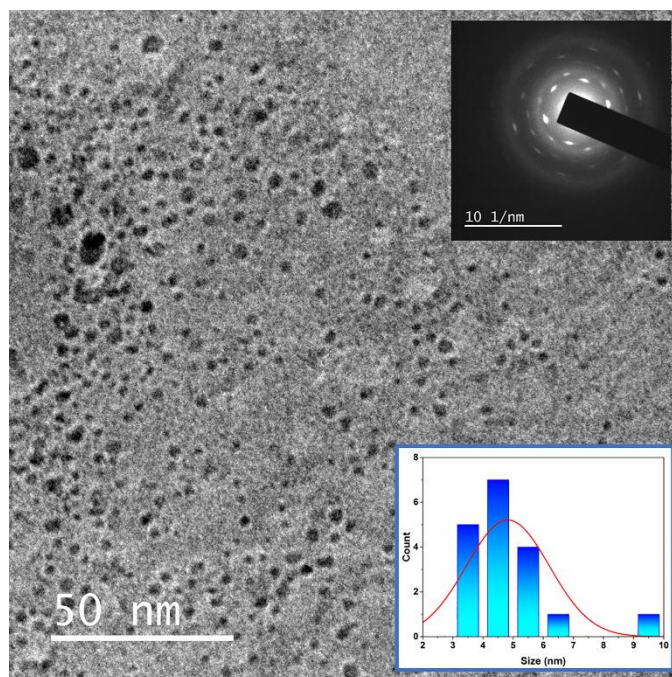


Figure 8.3 TEM image of NH₂-GQD (Inset: SED of NH₂-GQD, Particle size distribution, Image of Blue emission of NH₂-GQD).

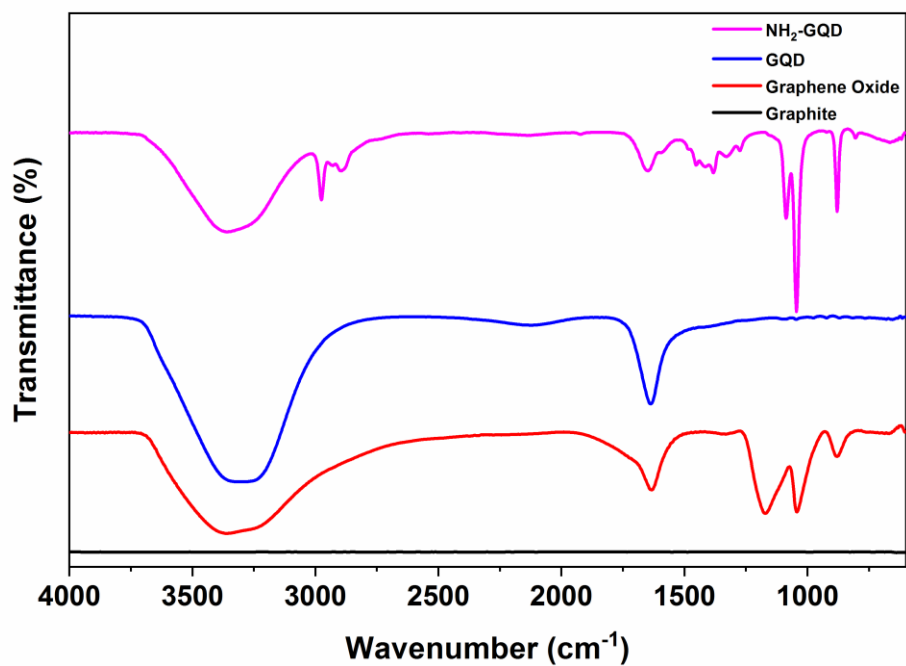


Figure 8.4 FTIR spectra of graphite, graphene oxide, GQD, and NH₂-GQD.

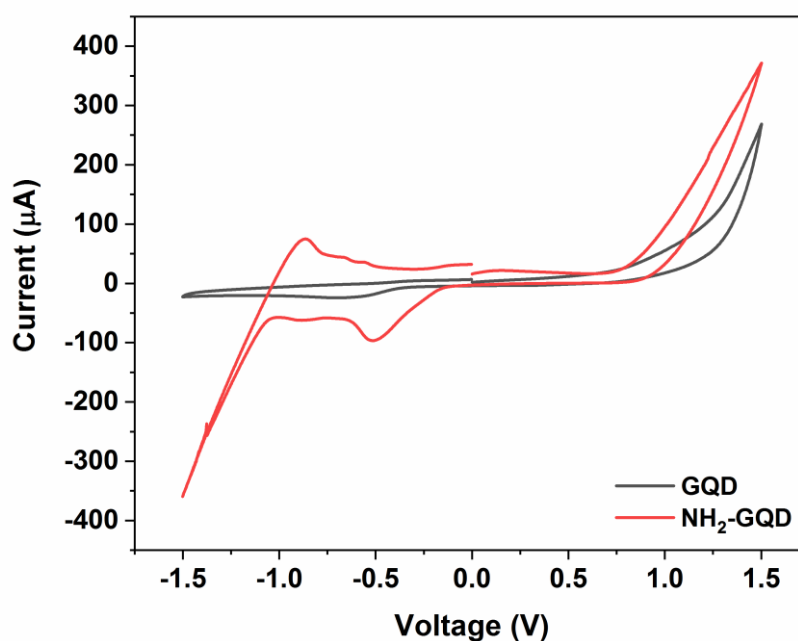


Figure 8.5 Cyclic voltammogram of GQD and NH₂-GQD.

Graphene oxide was analysed X-ray diffraction. It exhibited characteristic broad peak at 2θ of $7.5 - 15^\circ$ corresponding to the (002) plane of graphene oxide (Figure 8.2) signifying successful synthesis of graphene oxide.

The TEM imaging of the NH₂-GQD showed that the dots are of average particle size of 5 nm (Figure 8.3). The SAD pattern signifies that there still exist graphitic planes in the quantum dots which may be responsible for the effective charge transfer during sensitization discussed later. The quantum dots exhibited deep blue emission on excitation with wavelength of 365nm.

The FTIR spectra (Figure 8.4) of graphite, graphene oxide, GQD, and NH₂-GQD recorded from 4000-600 cm⁻¹. Generally, the spectra reveal the presence of oxygen containing functional groups attached to the all carbon structure. In the present graph, there are no peaks for graphite, which confirms the absence of oxygenated functional groups from the starting material. In graphene oxide, we observe characteristic peaks corresponding to the -OH at 3200-3600 cm⁻¹, C=O at 1670-1820 cm⁻¹, -COC at 1000-1300 cm⁻¹, which are the usual defects in graphene sheet present in graphene oxide. In GQD, we observe only peaks corresponding to the -OH at 3200-3600 cm⁻¹ and C=O at 1670-1820 cm⁻¹ which are indicative of -COOH terminating edges of GQD. These -COOH groups further play important role in binding with nitrogen in NH₂-GQD which is evident from the presence of doublet in the region of 1690-1630 cm⁻¹. This second peak is due to amide C=O stretching.

To evaluate the electrochemical properties of as-prepared amine functionalized GQDs, Cyclic Voltammetry was used. The apparatus consists of 3 electrodes with GQDs coated glassy carbon as working electrode, Pt as counter electrode and calomel electrode as reference electrode. We used 0.03 M NaOH solution as electrolyte. A potential sweep of -1.5 to 1.5 V at a scan rate of 100 mV.s⁻¹ was applied to sample and oxidation- reduction potential peaks were measured by a graph of current vs voltage. In Figure 8.5, amine-functionalized GQDs shows distinct cathodic and anodic peak at -0.8V and -0.5V respectively as opposed to as prepared GQDs. The peculiar nature of cathodic peak appearing before anodic peak in voltogram requires more attention to be fully understood. Hence, we can see potential in NH₂-GQD as material that can be used for further electrochemical applications.

8.3.2 Absorbance and Emission spectra of Sensitizers

The absorbance spectra of the dye, GQD, NH₂-GQD and NH₂-GQD/dye samples (Figure 8.6) suggests that NH₂-GQD/dye mixture have a wider absorption spectrum

compared to rest. This is indicative of the superior light absorbing capability of the mixture. The PL spectra of same samples suggest that NH₂-GQD/dye mixture have a wider emission profile which relates to the availability of different energy band gaps in the mixture (Figure 8.7). This could possibly be much more useful for the facilitation of charge transfer between sensitized molecule to TiO₂ layer in the working electrode of DSSC. The photoemission parameters of the dye and NH₂-GQD are given in Table 8.1.

Table 8.1 Photoemission parameters of NH₂-GQD

Quantum Yield	61 %
Band Gap	3.26 eV
HOMO	-5.84 eV
LUMO	-2.58 eV

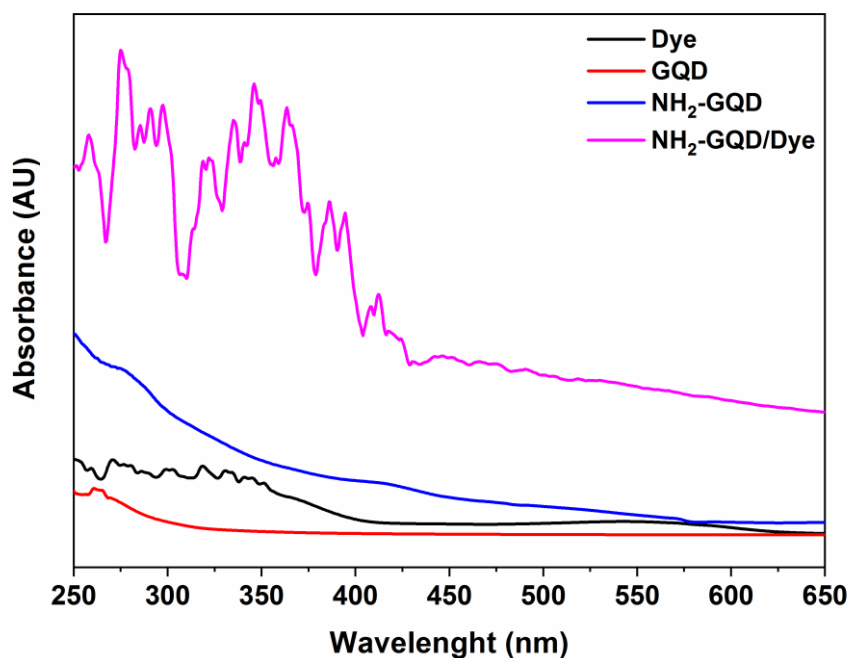


Figure 8.6 Absorbance spectra of dye, GQD, NH₂-GQD, and NH₂-GQD/Dye mixture.

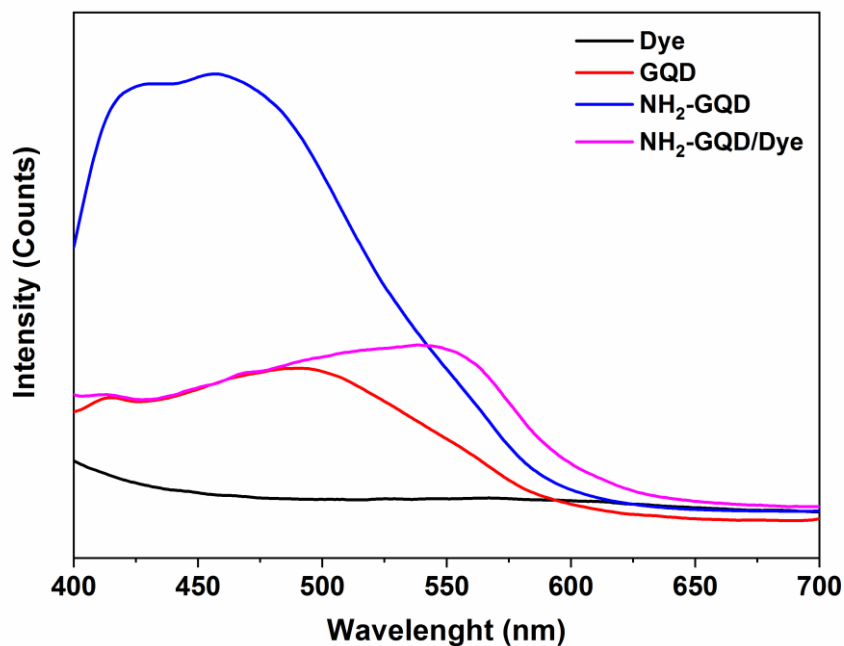


Figure 8.7 PL spectra of dye, GQD, NH₂-GQD, and NH₂-GQD/Dye mixture

8.3.3 Characterization of Photovoltaic Cells

Characterization of two cells with dye and NH₂-GQD/dye mixture as sensitizer are reported here. The UV and PL results indicated towards the better suitability of the mixture compared to dye for sensitization. This was further confirmed by studying the solar cell parameters. The parameters obtained for both the cells are given as Table 8.2. As evident from the presented data, the short circuit current (I_{sc}) of the cell increased by 29%, open circuit voltage (V_{oc}) by 20%, maximum power (P_{max}) by 56% and solar cell efficiency by 50%. These numbers are encouraging to establish the role of NH₂-GQD as a co-sensitizer in the hybrid DSSC. This may be because the graphene skeleton provides better electron transfer route to the oxide layer as opposed to the case in conventional DSSC. This is in addition to the quantum dots itself undergoing excitation on receiving visible light as evident from the absorption and PL spectra. The fill factor of both the cells remained largely unchanged which need further studies to improve.

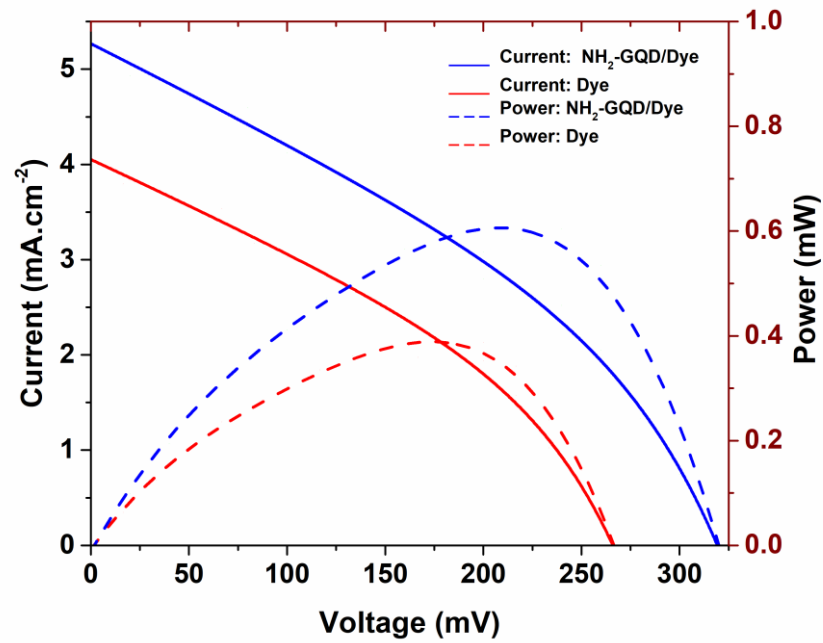


Figure 8.8 JV and output power curve of DSSC and NH₂-GQD/dye sensitized hybrid QDSC.

Table 8.2 Solar cell parameters.

Cell Parameters	Dye	NH ₂ -GQD/Dye
J_{sc} (mA/cm²)	4.08	5.30
V_{oc} (mV)	266.7	320
J_{max} (mA/cm²)	0.51	0.66
V_{max} (mV)	186.3	220
P_{max} (mW)	0.38	0.583
FF	0.376	0.375
PCE	1.863	2.8

8.4 CONCLUSIONS

Graphene quantum dots have received considerable attention because of their unique structural and optoelectronic properties. Unlike graphene, GQD possess band gaps and exhibit strong photoluminescence. Moreover, they are superior in chemical inertness, cytotoxicity and optical stability etc. NH₂-GQD synthesized from hydrothermal cutting method and its mixture with anthocyanin, natural dye was used to study its effect on hybrid QDSC. The reported results indicate that the quantum dots offer appreciable increase in the properties of the photovoltaic cells and thus is a worthy candidate to be tried in further studies. The fill factor of the cells however remains a point of concern and thus requires further research.

CHAPTER 9

SUMMARY AND CONCLUSIONS

Abstract: This chapter provides the summary of the thesis and important conclusions drawn from the undertaken research.

9.1 SUMMARY OF RESEARCH WORK

The motivation for the work presented in this thesis was to explore the ways in which the electronic transition happening in the GQD can be utilized. The excited electron in the band structure of GQD can be extracted directly from the LUMO of GQD by means of external circuit. Common applications associated with such extraction of electron are electrochemical sensors and photovoltaic devices. The extraction of electron was made possible by the introduction of graphene oxide which or TiO₂. Therefore, the work concentrated on the use of the so-called Even-D class of carbon nanostructures. Another fate the excited electron has in the band structure of GQD is to loss the energy in the form of visible electromagnetic wave and return of HOMO level. This phenomenon leads to the observed photoluminescence on GQD. This PL can be directly utilized for molecular and ionic sensing as demonstrated in the earlier chapters.

The work presented in thesis can be broadly classified in 3 major sections:

1. A new route for the top-down synthesis of GQD.
2. Application of GQD in Sensors.
 - a. GQD as PL Sensor.
 - b. GQD as Electrochemical Sensor.
3. Application of GQD in Photovoltaic Devices.

Hydrothermal cutting is the most common route to synthesize GQD from graphene oxide (GO). However, the poor control over the size of GQD obtained remains a major limitation of this method. Cleaving graphene sheets using highly focused electron beam have reportedly been used to fabricate graphene of desired dimensions. In similar approach, the use of focused metallic ion beam has been growing in popularity for producing highly uniform nanomaterials and metal-impregnated composite materials. Therefore, a new route to obtain the quantum dot by bombarding the graphene sheets with the swift heavy ions is reported in the thesis (Figure 9.1). The GQD obtained from this method exhibited all the properties typically associated with quantum dots. The

reduction in size of GO to yield GQD was reportedly due to the cleavage along the ethoxy (-C-O-C-) groups present in the GO.

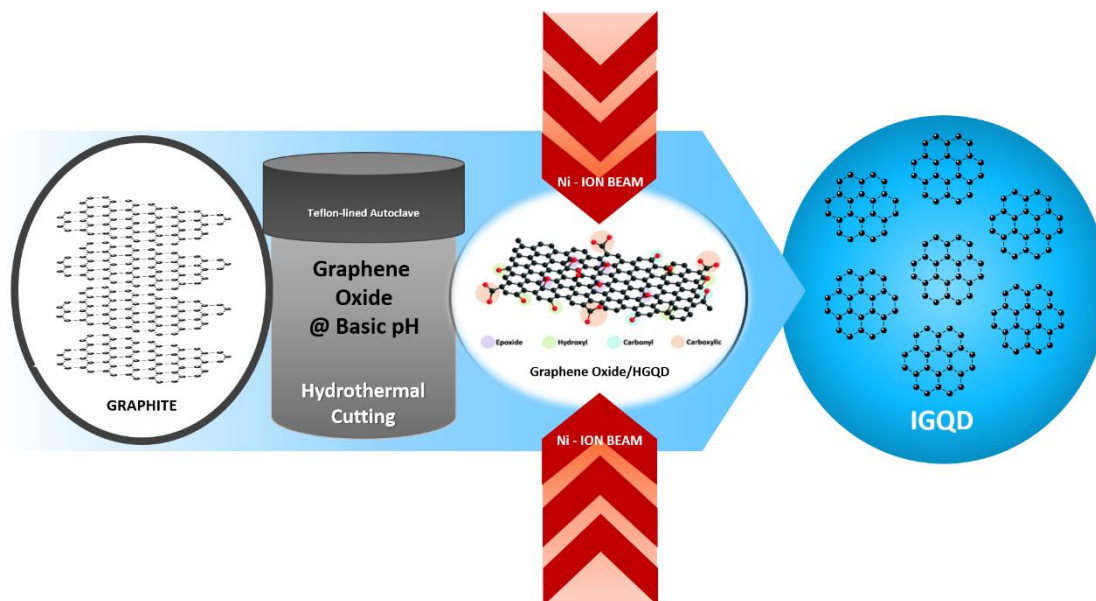


Figure 9.1 A schematic representation of synthesis of GQD using swift heavy ions.

Irrespective of the ability for the reported method to attain the highly uniform GQD as demonstrated in this work, the production of GQD in low yield was a major limitation. Therefore, hydrothermal cutting at relatively higher temperature was selected as principle method for the synthesis of GQD owing to its ability to return high yield. The hydrothermal route also makes one-pot synthesis of functionalized GQD possible. These GQD and functionalized GQD exhibited excellent PL. The ability of GQD to generated PL is highly suited for chemical sensing which was demonstrated in the reviewed literature. GQD in their native state were found to be highly useful in determining the metal cations like Ca^{2+} , Cu^{2+} and Co^{2+} with varying effect (Figure 9.2). These determination was made possible due to the PL quenching observed when GQD reacted with certain metal ions. Transition metals showed higher affinity towards GQD which was evident from the extent of PL quenching observed. This means that the transition metal ions cause lot of interference when present together in a solution. Therefore, the mode of detection for the transition metals and heavier metal cations can only be qualitative as the GQD exhibited detectable shift in the PL emission which can be associated with a metal cation.

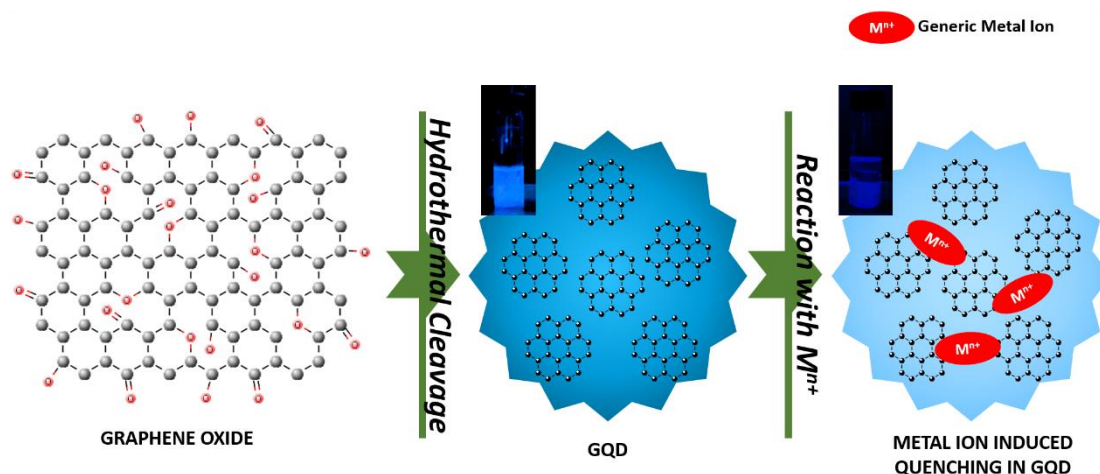


Figure 9.2 Photoluminescent quenching of the GQD on interaction with metal ions.

The determination of Ca^{2+} ions in the common hard water samples were quantitatively possible in the presence of interfering ions such as Al^{3+} , Na^+ and K^+ (Figure 9.3). The as-synthesized GQD were able to detect the concentration of Ca^{2+} ion in water as low as $5 \mu\text{M}$. The accuracy of determination was as high as 97% for linear range of detection between $5 - 250 \mu\text{M}$ of Ca^{2+} .

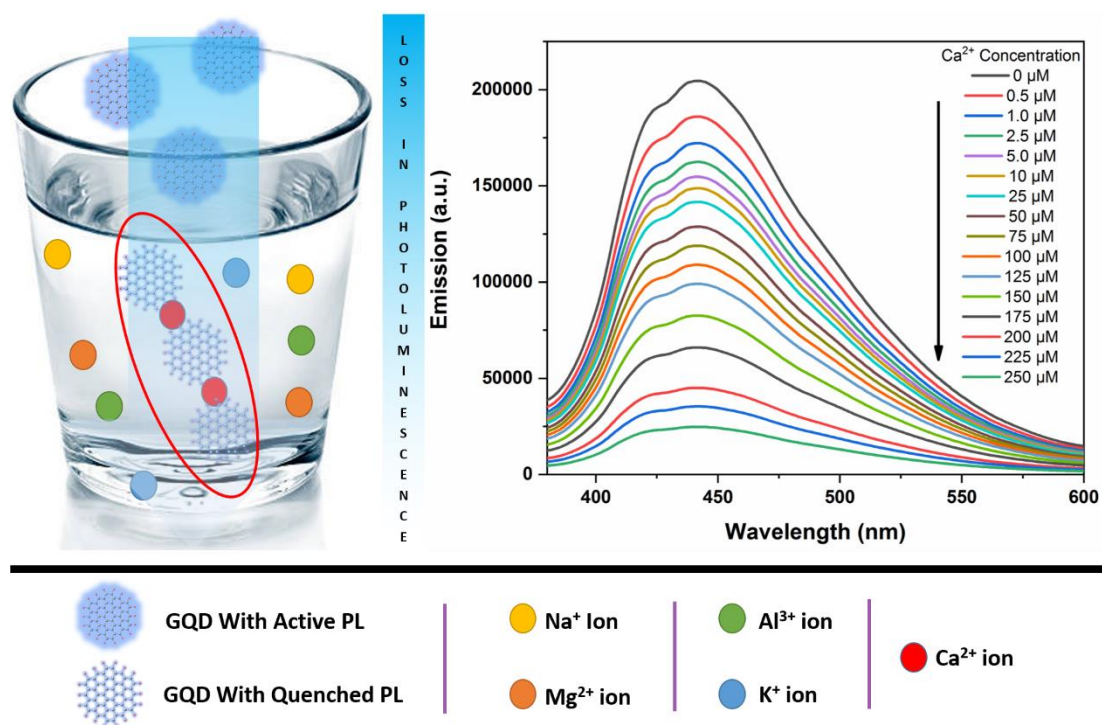


Figure 9.3 The detection of Ca^{2+} in presence of interfering ions using GQD.

The amine-functionalized GQD (NH₂-GQD) was prepared by refluxing GQD with 1M hexamethylenetetramine. NH₂-GQD resulted in the quantitative determination of glucose possible via aggregation induced PL enhancement (Figure 9.4). This mode of detection was a complete contrast to the one used for metal ions as the aggregation of GQD here increase the observed PL intensity. The reported sensing method showed a bi-range linearity with 0.1-10 mM and 50-500 mM of glucose being detected with the accuracy of 98 % and 97 % respectively.

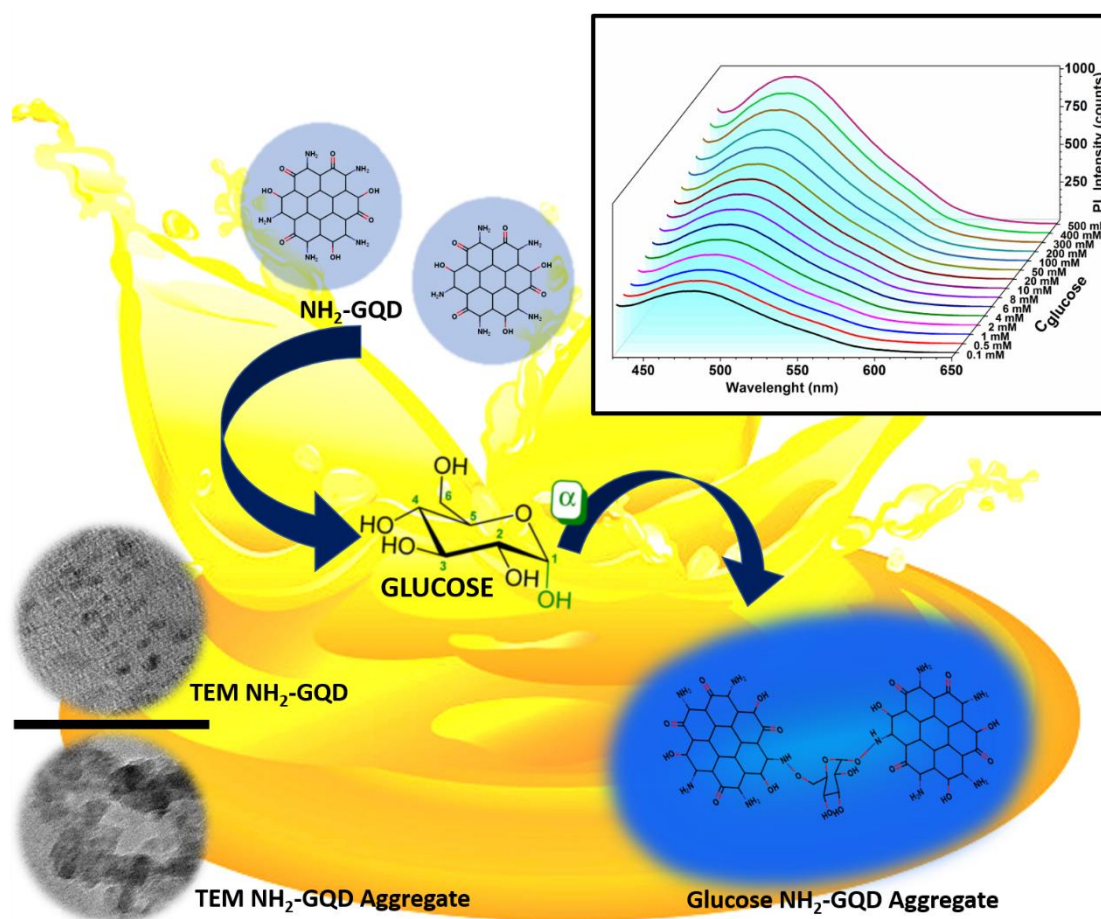


Figure 9.4 Intensification of photoluminescence of NH₂-GQD by aggregation in presence of glucose.

The NH₂-GQD also proved to be an active material for electrochemical determination of oxalic acid when composite with graphene oxide (GO) as NH₂-GQD-GO (Figure 9.5). The glassy carbon (GC) electrode coated with NH₂-GQD-GO returned the limit of detection of 50 μ M and the suitability of detection between 0.5 mM to 55 mM for oxalic acid. The electrochemical analysis of NH₂-GQD-GO composite showed a peak

in the cathodic current region which was enhanced in presence of oxalic acid in the media, which is an interesting deviation from the usually studied anodic current for the electrochemical sensors.

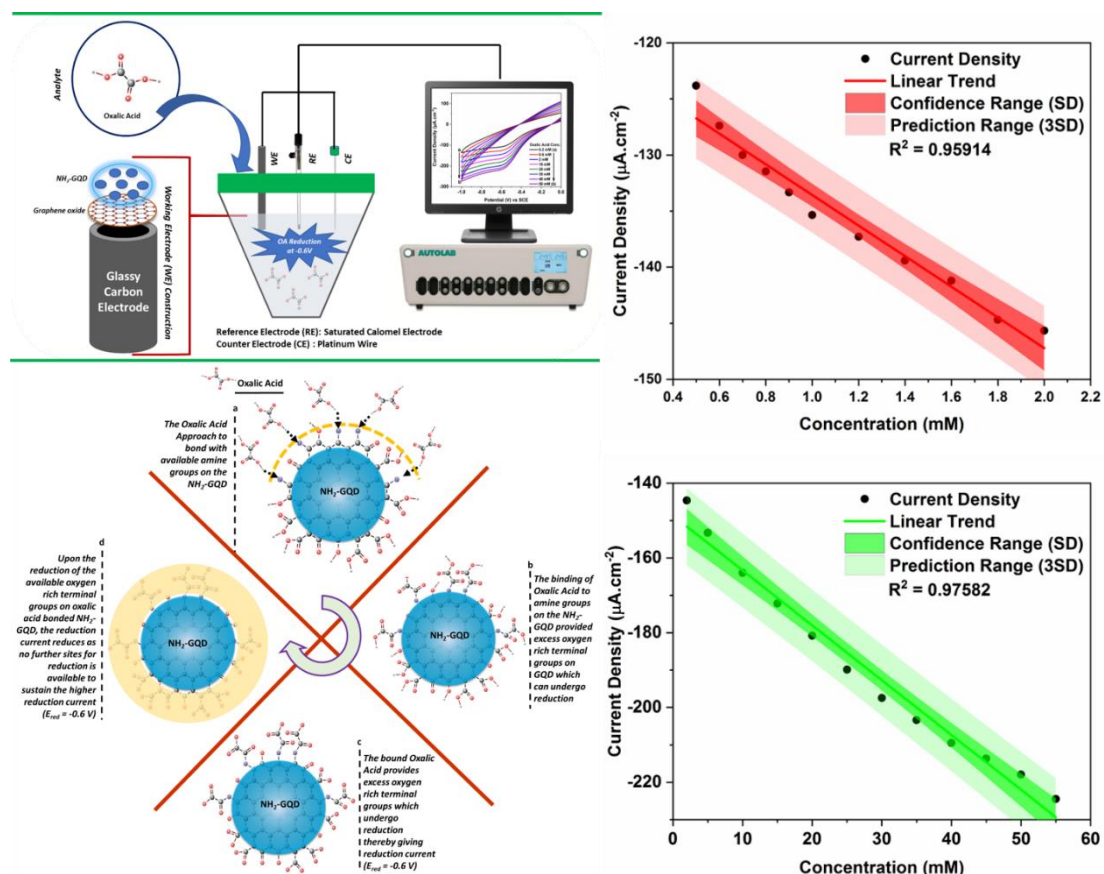


Figure 9.5 A schematic representation of oxalic acid sensing using NH₂-GQD-GO composite.

Table 9.1 Performance of GQD and modified GQD composites as sensors for various analytes.

S.No.	Material	Type of Sensor	Analyte	Linear Range	LoD	Accuracy
1	GQD	Photoluminescent Turn Off	Ca ²⁺	5 – 250 μM	5 μM	96.74 ± 3.26 %
2	NH ₂ -GQD	Photoluminescent Turn On	Glucose	0.1 – 10 mM 50- 500 mM	10 μM	98.04 ± 1.96 % 97.33 ± 2.67 %
3	NH ₂ -GQD-GO	Electrochemical Sensor	Oxalic Acid	0.5 - 2.0 mM 2.0 - 55.0 mM	50 μM	NA

Table 9.1 summarizes the performance of various iterations of GQD for sensing the above discussed analytes. The performance of the sensors was tested on real samples. The results obtained were consistent with the actual concentration of analytes within the error as reported in the table.

The NH₂-GQD also demonstrated to be an excellent co-sensitizer for the hybrid dye sensitized solar cell with the simple structure of the device as presented in Figure 9.6. NH₂-GQD in conjunction with anthocyanin dye acts as a performance enhancing co-sensitizer in a hybrid dye sensitized solar cell. Furthermore, the PCE was increased by 50.51% with appreciable rise in other parameters such as I_{sc}, V_{oc}, I_{max}, V_{max} and P_{max}.

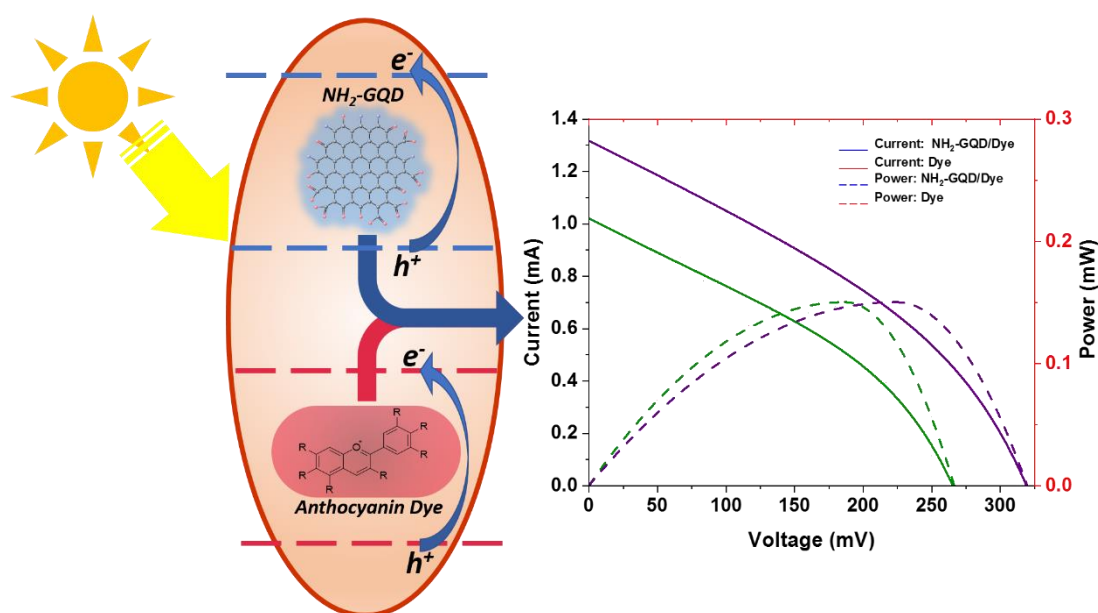


Figure 9.6 Anthocyanin and NH₂-GQD, a co-sensitization approach to hybrid quantum dots solar cells.

The work presented in the thesis demonstrates the utilization of the excited electrons brought about by the electromagnetic energy in the energy level of the graphene quantum dots. It is evident where the energy emitted by the electron returning to the ground state can be utilized for PL determination of various analytes, the extraction of excited electron through electrochemical route, opens up the possibility of using GQDs for electrochemical sensors and co-sensitizers in the photovoltaic devices.

9.2 CONCLUSIONS

The obtained results reflected over certain key points pertaining to the behaviour of graphene quantum dots and graphene oxide as a material for sensing and energy applications.

- The fragmentation of graphene oxide into GQD was due to the cleavage of the ethoxy ($-C-O-C-$) bonds as they are weakest bond present in the graphene oxide sheet. Therefore, these bonds can be easily broken by the bombardment of high kinetic energy ion beams.
- The interaction of GQD with metal ions happens among the electron rich atoms like O on the edge of the GQD and metal ions. This interaction leads to the relaxation of the quantum barrier therefore causing the observed PL quenching.
- Transition metal ions show higher extent of PL quenching with very little selectivity among them. However, interaction of GQD with transition metal ions lead to the shift in the PL emission. Thus, GQD is suitable for qualitative determination.
- The selectivity of the GQD was higher for Ca^{2+} ions among other few alkali and alkaline earth metals. This selectivity was attributed to the divalent nature and larger size of the Ca^{2+} ion among the tested cations. Hence, GQD can be an excellent sensor for the quantitative determination of Ca^{2+} ions.
- The PL quenching in GQD is dependent on the valency and the size of binding metal ions.
- The NH_2 -GQD exhibits higher PL intensity as compared to GQD. This PL is further increased by aggregation of NH_2 -GQD with glucose in 2:1 stoichiometric ratio. Hence, NH_2 -GQD makes an excellent PL sensor for the determination of glucose in various samples.
- Graphene oxide acts as an excellent substrate of NH_2 -GQD. The higher specific area of GO means that it allows more analytes to adsorb on the surface and interact with NH_2 -GQD. Additionally, GO also acts as an electron bridge between the NH_2 -GQD and current collector (electrode connected to external circuit).

- The NH₂-GQD-GO coated GC electrode exhibited a cathodic current at -0.6 V which increased in the presence of oxalic acid. The increase in the reduction current is linear with the increase in the concentration of oxalic acid thereby making direct electrochemical determination of oxalic acid feasible.
- The NH₂-GQD makes larger number of carboxylic group available for the reduction. This is because, NH₂-GQD binds with one carboxylic acid group of oxalic acid, and leaves other available of reduction at the electrode surface. Therefore, The NH₂-GQD-GO electrodes would be highly selective towards dibasic acids and tri-basic acids.
- The higher PL intensity of the NH₂-GQD is also reflected in better quantum yield of the material. This opens the ability of NH₂-GQD to absorb large quanta of light making it an excellent co-sensitizer for hybrid quantum dot solar cells. The direct sensitization using functionalized GQD still remains a challenge as there is still scope for optimisation of the fermi levels of the GQD.

9.3 FUTURE WORK

The principles of the properties exhibited by the quantum dots are well known. However, the same cannot be said for GQD. GQD in certain ways behave distinct of other quantum dots. Although we can assume the cause for such behaviour, a thorough investigation in the molecular and band structure is required to fully understand the behaviour of GQD. This would be an interesting research problem for the future work.

The applicability of Even-D carbon nanostructures, and specifically OD GQD was promising towards sensing applications. However, the use of GQD in the energy device is still at its infancy. The presented report over the use of GQD as a photosensitizer in PV device and few works in literature reflects over the potential the nanostructure have in such areas. OD carbon nanostructures are also not utilized to its potential in other electronics applications such as supercapacitors, batteries and light emitting diodes. Therefore, the applicability of GQD and its derivative would be explored in future.

REFERENCES

- Abdel-Fattah, T. M., Ebrahim, S., Soliman, M., and Shehab, M. (2016). "Graphene Quantum Dots As Optical Sensor for Glucose Detection", MA2016-02(50), 3782.
- Allen, M. J., Tung, V. C., and Kaner, R. B. (2010). "Honeycomb carbon: a review of graphene", Chem Rev, 110(1), 132-45.
- Alwarappan, S., Erdem, A., Liu, C., and Li, C.-Z. (2009). "Probing the Electrochemical Properties of Graphene Nanosheets for Biosensing Applications", The Journal of Physical Chemistry C, 113(20), 8853-57.
- Ananthanarayanan, A., Wang, X., Routh, P., Sana, B., Lim, S., Kim, D.-H., Lim, K.-H., Li, J., and Chen, P. (2014). "Facile Synthesis of Graphene Quantum Dots from 3D Graphene and their Application for Fe³⁺ Sensing", Advanced Functional Materials, 24(20), 3021-26.
- Ancillotti, F., Boschi, G., Perego, G., and Zazzetta, A. (1977). "Calcium binding capacity of carboxylic acids with an ethereal function. Crystal and molecular structure of calcium ethylenedioxydiacetate", Journal of the Chemical Society, Dalton Transactions(9), 901-05.
- Ao, Z. M., Yang, J., Li, S., and Jiang, Q. (2008). "Enhancement of CO detection in Al doped graphene", Chemical Physics Letters, 461(4-6), 276-79.
- Arsat, R., Breedon, M., Shafiei, M., Spizziri, P. G., Gilje, S., Kaner, R. B., Kalantar-zadeh, K., and Wlodarski, W. (2009). "Graphene-like nano-sheets for surface acoustic wave gas sensor applications", Chemical Physics Letters, 467(4-6), 344-47.
- Arunkumar, E., Ajayaghosh, A., and Daub, J. (2005). "Selective Calcium Ion Sensing with a Bichromophoric Squaraine Foldamer", Journal of the American Chemical Society, 127(9), 3156-64.
- Bacon, M., Bradley, S. J., and Nann, T. (2014). "Graphene Quantum Dots", Particle & Particle Systems Characterization, 31(4), 415-28.
- Bai, J.-M., Zhang, L., Liang, R.-P., and Qiu, J.-D. (2013). "Graphene Quantum Dots Combined with Europium Ions as Photoluminescent Probes for Phosphate Sensing", Chemistry – A European Journal, 19(12), 3822-26.
- Bala, T., Prasad, B. L. V., Sastry, M., Kahaly, M. U., and Waghmare, U. V. (2007). "Interaction of Different Metal Ions with Carboxylic Acid Group: A Quantitative Study", The Journal of Physical Chemistry A, 111(28), 6183-90.

Banks, C. E., Moore, R. R., Davies, T. J., and Compton, R. G. (2004). "Investigation of modified basal plane pyrolytic graphite electrodes: definitive evidence for the electrocatalytic properties of the ends of carbon nanotubes", *Chem Commun (Camb)*(16), 1804-5.

Bao, Q., Zhang, H., Wang, Y., Ni, Z., Yan, Y., Shen, Z. X., Loh, K. P., and Tang, D. Y. (2009). "Atomic-Layer Graphene as a Saturable Absorber for Ultrafast Pulsed Lasers", *Advanced Functional Materials*, 19(19), 3077-83.

Benitez-Martinez, S., Lopez-Lorente, A. I., and Valcarcel, M. (2014). "Graphene quantum dots sensor for the determination of graphene oxide in environmental water samples", *Anal Chem*, 86(24), 12279-84.

Benítez-Martínez, S., and Valcárcel, M. (2015). "Graphene quantum dots in analytical science", *TrAC Trends in Analytical Chemistry*, 72(Supplement C), 93-113.

Bergerman, J., and Elliot, J. S. (1955). "Method for Direct Colorimetric Determination of Oxalic Acid", *Analytical Chemistry*, 27(6), 1014-15.

Bertoluzza, A., Battaglia, M. A., Bonora, S., Monti, P., and Simoni, R. (1985). "Hydrogen bonds in calcium acid phosphates by infrared and Raman spectra", *Journal of Molecular Structure*, 127(1), 35-45.

Blanco, E., Blanco, G., Gonzalez-Leal, J. M., Barrera, M. C., Domínguez, M., and Ramirez-del-Solar, M. (2015). "Green and fast synthesis of amino-functionalized graphene quantum dots with deep blue photoluminescence", *Journal of Nanoparticle Research*, 17(5), 214.

Boehm, H. P., Clauss, A., Fischer, G. O., and Hofmann, U. (1962). "Das Adsorptionsverhalten sehr dünner Kohlenstoff-Folien", *Zeitschrift für anorganische und allgemeine Chemie*, 316(3-4), 119-27.

Cai, F., Liu, X., Liu, S., Liu, H., and Huang, Y. (2014). "A simple one-pot synthesis of highly fluorescent nitrogen-doped graphene quantum dots for the detection of Cr(vi) in aqueous media", *RSC Advances*, 4(94), 52016-22.

Celis, A., Nair, M. N., Taleb-Ibrahimi, A., Conrad, E. H., Berger, C., de Heer, W. A., and Tejeda, A. (2016). "Graphene nanoribbons: fabrication, properties and devices", *Journal of Physics D: Applied Physics*, 49(14), 143001.

- Chakraborti, H., Sinha, S., Ghosh, S., and Pal, S. K. (2013). "Interfacing water soluble nanomaterials with fluorescence chemosensing: Graphene quantum dot to detect Hg²⁺ in 100% aqueous solution", *Materials letters*, 97, 78-80.
- Chen, C.-M., Huang, J.-Q., Zhang, Q., Gong, W.-Z., Yang, Q.-H., Wang, M.-Z., and Yang, Y.-G. (2012). "Annealing a graphene oxide film to produce a free standing high conductive graphene film", *Carbon*, 50(2), 659-67.
- Chen, C., Xie, Q., Yang, D., Xiao, H., Fu, Y., Tan, Y., and Yao, S. (2013a). "Recent advances in electrochemical glucose biosensors: a review", *RSC Advances*, 3(14), 4473-91.
- Chen, J. H., Jang, C., Xiao, S., Ishigami, M., and Fuhrer, M. S. (2008). "Intrinsic and extrinsic performance limits of graphene devices on SiO₂", *Nat Nanotechnol*, 3(4), 206-9.
- Chen, L., Guo, C. X., Zhang, Q., Lei, Y., Xie, J., Ee, S., Guai, G., Song, Q., and Li, C. M. (2013b). "Graphene Quantum-Dot-Doped Polypyrrole Counter Electrode for High-Performance Dye-Sensitized Solar Cells", *ACS Applied Materials & Interfaces*, 5(6), 2047-52.
- Chen, R. B., Chang, C. P., and Lin, M. F. (2010). "Electric-field-tunable electronic properties of graphene quantum dots", *Physica E: Low-dimensional Systems and Nanostructures*, 42(10), 2812-15.
- Chen, X., Cai, Z., Huang, Z., Oyama, M., Jiang, Y., and Chen, X. (2013c). "Non-enzymatic oxalic acid sensor using platinum nanoparticles modified on graphene nanosheets", *Nanoscale*, 5(13), 5779-83.
- Chen, Z., Meng, H., Xing, G., Chen, C., Zhao, Y., Jia, G., Wang, T., Yuan, H., Ye, C., Zhao, F., Chai, Z., Zhu, C., Fang, X., Ma, B., and Wan, L. (2006). "Acute toxicological effects of copper nanoparticles in vivo", *Toxicology Letters*, 163(2), 109-20.
- Choe, M., Lee, B. H., Jo, G., Park, J., Park, W., Lee, S., Hong, W.-K., Seong, M.-J., Kahng, Y. H., and Lee, K. (2010). "Efficient bulk-heterojunction photovoltaic cells with transparent multi-layer graphene electrodes", *Organic Electronics*, 11(11), 1864-69.
- Choi, W., Lahiri, I., Seelaboyina, R., and Kang, Y. S. (2010). "Synthesis of Graphene and Its Applications: A Review", *Critical Reviews in Solid State and Materials Sciences*, 35(1), 52-71.

Choudhary, R., Koppala, S., and Swamiappan, S. (2015). "Bioactivity studies of calcium magnesium silicate prepared from eggshell waste by sol-gel combustion synthesis", *Journal of Asian Ceramic Societies*, 3(2), 173-77.

Chua, C. K., Sofer, Z., Simek, P., Jankovsky, O., Klimova, K., Bakardjieva, S., Hrdlickova Kuckova, S., and Pumera, M. (2015). "Synthesis of strongly fluorescent graphene quantum dots by cage-opening buckminsterfullerene", *ACS Nano*, 9(3), 2548-55.

Cooper, D. R., D'Anjou, B., Ghattamaneni, N., Harack, B., Hilke, M., Horth, A., Majlis, N., Massicotte, M., Vandsburger, L., Whiteway, E., and Yu, V. (2012). "Experimental Review of Graphene", *ISRN Condensed Matter Physics*, 2012, 1-56.

Costa, V. C., Amorim, F. A. C., de Babos, D. V., and Pereira-Filho, E. R. (2019). "Direct determination of Ca, K, Mg, Na, P, S, Fe and Zn in bivalve mollusks by wavelength dispersive X-ray fluorescence (WDXRF) and laser-induced breakdown spectroscopy (LIBS)", *Food Chemistry*, 273, 91-98.

Costello, J., Hatch, M., and Bourke, E. (1976). "An enzymic method for the spectrophotometric determination of oxalic acid", *The Journal of Laboratory and Clinical Medicine*, 87(5), 903-08.

Dan, Y., Lu, Y., Kybert, N. J., Luo, Z., and Johnson, A. T. (2009). "Intrinsic response of graphene vapor sensors", *Nano Lett*, 9(4), 1472-5.

De Raedt, H., and Katsnelson, M. I. (2009). "Electron energy level statistics in graphene quantum dots", *JETP Letters*, 88(9), 607-10.

Demchenko, A. P., and Dekaliuk, M. O. (2016). "The origin of emissive states of carbon nanoparticles derived from ensemble-averaged and single-molecular studies", *Nanoscale*, 8(29), 14057-69.

Diouf, A., Bouchikhi, B., and El Bari, N. (2019). "A nonenzymatic electrochemical glucose sensor based on molecularly imprinted polymer and its application in measuring saliva glucose", *Materials Science and Engineering: C*, 98, 1196-209.

Dong, Y., Li, G., Zhou, N., Wang, R., Chi, Y., and Chen, G. (2012). "Graphene Quantum Dot as a Green and Facile Sensor for Free Chlorine in Drinking Water", *Analytical Chemistry*, 84(19), 8378-82.

Du, X., Skachko, I., Barker, A., and Andrei, E. Y. (2008). "Approaching ballistic transport in suspended graphene", *Nat Nanotechnol*, 3(8), 491-5.

- Du, Y., He, Y., Zheng, Z., Shen, X., Zhou, Y., Wang, T., Zhu, Z., and Wang, C. (2019). "A Renewable Platform for High-Performance Glucose Sensor Based on Co(OH)₂ Nanoparticles/Three-Dimensional Graphene Frameworks", *Journal of the Electrochemical Society*, 166(2), B42-B48.
- Dutta, M., Sarkar, S., Ghosh, T., and Basak, D. (2012). "ZnO/Graphene Quantum Dot Solid-State Solar Cell", *The Journal of Physical Chemistry C*, 116(38), 20127-31.
- Fan, Z., Li, Y., Li, X., Fan, L., Zhou, S., Fang, D., and Yang, S. (2014). "Surrounding media sensitive photoluminescence of boron-doped graphene quantum dots for highly fluorescent dyed crystals, chemical sensing and bioimaging", *Carbon*, 70(Supplement C), 149-56.
- Fry, I. D. R., and Starkey, B. J. (1991). "The Determination of Oxalate in Urine and Plasma by High Performance Liquid Chromatography", *Annals of Clinical Biochemistry*, 28(6), 581-87.
- Fu, C., Yang, W., Chen, X., and Evans, D. G. (2009). "Direct electrochemistry of glucose oxidase on a graphite nanosheet–Nafion composite film modified electrode", *Electrochemistry Communications*, 11(5), 997-1000.
- Fujita, M., Wakabayashi, K., Nakada, K., and Kusakabe, K. (1996). "Peculiar Localized State at Zigzag Graphite Edge", *Journal of the Physical Society of Japan*, 65(7), 1920-23.
- Gadipelli, S., and Guo, Z. X. (2015). "Graphene-based materials: Synthesis and gas sorption, storage and separation", *Progress in Materials Science*, 69, 1-60.
- Geim, A., and MacDonald, A. H. (2007). "Graphene: Exploring carbon flatland", *Physics Today*, 60(8), 35-41.
- Geim, A. K., and Novoselov, K. S. (2007). "The rise of graphene", *Nat Mater*, 6(3), 183-91.
- Ghosh, R., Midya, A., Santra, S., Ray, S. K., and Guha, P. K. (2013). "Chemically reduced graphene oxide for ammonia detection at room temperature", *ACS Appl Mater Interfaces*, 5(15), 7599-603.
- Gryniewicz, G., Poenie, M., and Tsien, R. Y. (1985). "A new generation of Ca²⁺ indicators with greatly improved fluorescence properties", *Journal of Biological Chemistry*, 260(6), 3440-50.

Güçlü, A. D., Potasz, P., and Hawrylak, P. (2011). "Electric-field controlled spin in bilayer triangular graphene quantum dots", *Physical Review B*, 84(3), 035425.

Guo, C. X., Yang, H. B., Sheng, Z. M., Lu, Z. S., Song, Q. L., and Li, C. M. (2010). "Layered graphene/quantum dots for photovoltaic devices", *Angew Chem Int Ed Engl*, 49(17), 3014-7.

Gupta, V., Chaudhary, N., Srivastava, R., Sharma, G. D., Bhardwaj, R., and Chand, S. (2011). "Luminescent Graphene Quantum Dots for Organic Photovoltaic Devices", *Journal of the American Chemical Society*, 133(26), 9960-63.

Gupta, V. K., Jain, A. K., Maheshwari, G., Lang, H., and Ishtaiwi, Z. (2006). "Copper(II)-selective potentiometric sensors based on porphyrins in PVC matrix", *Sensors and Actuators B: Chemical*, 117(1), 99-106.

Guttinger, J., Frey, T., Stampfer, C., Ihn, T., and Ensslin, K. (2010). "Spin states in graphene quantum dots", *Phys Rev Lett*, 105(11), 116801.

Hallaj, T., Amjadi, M., Manzoori, J. L., and Shokri, R. (2015). "Chemiluminescence reaction of glucose-derived graphene quantum dots with hypochlorite, and its application to the determination of free chlorine", *Microchimica Acta*, 182(3), 789-96.

Hamilton, I. P., Li, B., Yan, X., and Li, L.-s. (2011). "Alignment of Colloidal Graphene Quantum Dots on Polar Surfaces", *Nano Letters*, 11(4), 1524-29.

He, Z., and Gao, H. (1997). "Simultaneous Determination of Oxalic and Tartaric Acid With Chemiluminescence Detection", *Analyst*, 122(11), 1343-46.

Hewageegana, P., and Apalkov, V. (2008). "Electron localization in graphene quantum dots", *Physical Review B*, 77(24), 245426.

Hong, Y., Lam, J. W. Y., and Tang, B. Z. (2009). "Aggregation-induced emission: phenomenon, mechanism and applications", *Chemical Communications*(29), 4332-53.

Hu, C., Liu, Y., Yang, Y., Cui, J., Huang, Z., Wang, Y., Yang, L., Wang, H., Xiao, Y., and Rong, J. (2013). "One-step preparation of nitrogen-doped graphene quantum dots from oxidized debris of graphene oxide", *Journal of Materials Chemistry B*, 1(1), 39-42.

Huang, H., Liao, L., Xu, X., Zou, M., Liu, F., and Li, N. (2013). "The electron-transfer based interaction between transition metal ions and photoluminescent graphene quantum dots (GQDs): A platform for metal ion sensing", *Talanta*, 117(Supplement C), 152-57.

Hummers, W. S., and Offeman, R. E. (1958). "Preparation of Graphitic Oxide", *Journal of the American Chemical Society*, 80(6), 1339-39.

Ihm, K., Lim, J. T., Lee, K.-J., Kwon, J. W., Kang, T.-H., Chung, S., Bae, S., Kim, J. H., Hong, B. H., and Yeom, G. Y. (2010). "Number of graphene layers as a modulator of the open-circuit voltage of graphene-based solar cell", *Applied Physics Letters*, 97(3), 032113.

Iijima, S. (1991). "Helical microtubules of graphitic carbon", *Nature*, 354(6348), 56-58.

Iijima, S., and Ichihashi, T. (1993). "Single-shell carbon nanotubes of 1-nm diameter", *Nature*, 363(6430), 603-05.

Jagtap, A. M., Varade, V., Konkena, B., Ramesh, K. P., Chatterjee, A., Banerjee, A., Pendyala, N. B., and Rao, K. S. R. K. (2016). "Interactions between photoexcited NIR emitting CdHgTe quantum dots and graphene oxide", *Journal of Applied Physics*, 119(7), 074306.

Jang, M. H., Ha, H. D., Lee, E. S., Liu, F., Kim, Y. H., Seo, T. S., and Cho, Y. H. (2015). "Is the Chain of Oxidation and Reduction Process Reversible in Luminescent Graphene Quantum Dots?", *Small*, 11(31), 3773-81.

Jayasumana, C., Gunatilake, S., and Senanayake, P. (2014). "Glyphosate, Hard Water and Nephrotoxic Metals: Are They the Culprits Behind the Epidemic of Chronic Kidney Disease of Unknown Etiology in Sri Lanka?", *International Journal of Environmental Research and Public Health*, 11(2)

Jin, S. H., Kim da, H., Jun, G. H., Hong, S. H., and Jeon, S. (2013). "Tuning the photoluminescence of graphene quantum dots through the charge transfer effect of functional groups", *ACS Nano*, 7(2), 1239-45.

Jo, G., Na, S.-I., Oh, S.-H., Lee, S., Kim, T.-S., Wang, G., Choe, M., Park, W., Yoon, J., Kim, D.-Y., Kahng, Y. H., and Lee, T. (2010). "Tuning of a graphene-electrode work function to enhance the efficiency of organic bulk heterojunction photovoltaic cells with an inverted structure", *Applied Physics Letters*, 97(21), 213301.

Ju, J., and Chen, W. (2014). "Synthesis of highly fluorescent nitrogen-doped graphene quantum dots for sensitive, label-free detection of Fe (III) in aqueous media", *Biosensors and Bioelectronics*, 58, 219-25.

Justino, C. I. L., Gomes, A. R., Freitas, A. C., Duarte, A. C., and Rocha-Santos, T. A. P. (2017). "Graphene based sensors and biosensors", *TrAC Trends in Analytical Chemistry*, 91, 53-66.

Kang, X., Wang, J., Wu, H., Liu, J., Aksay, I. A., and Lin, Y. (2010). "A graphene-based electrochemical sensor for sensitive detection of paracetamol", *Talanta*, 81(3), 754-9.

Kim, C. O., Hwang, S. W., Kim, S., Shin, D. H., Kang, S. S., Kim, J. M., Jang, C. W., Kim, J. H., Lee, K. W., Choi, S. H., and Hwang, E. (2014). "High performance graphene quantum dot photodetectors", *Sci Rep*, 4, 5603.

Kim, J. K., Park, M. J., Kim, S. J., Wang, D. H., Cho, S. P., Bae, S., Park, J. H., and Hong, B. H. (2013a). "Balancing Light Absorptivity and Carrier Conductivity of Graphene Quantum Dots for High-Efficiency Bulk Heterojunction Solar Cells", *ACS Nano*, 7(8), 7207-12.

Kim, K. B., Lee, W.-C., Cho, C.-H., Park, D.-S., Cho, S. J., and Shim, Y.-B. (2019). "Continuous glucose monitoring using a microneedle array sensor coupled with a wireless signal transmitter", *Sensors and Actuators B: Chemical*, 281, 14-21.

Kim, S., Hwang, S. W., Kim, M.-K., Shin, D. Y., Shin, D. H., Kim, C. O., Yang, S. B., Park, J. H., Hwang, E., Choi, S.-H., Ko, G., Sim, S., Sone, C., Choi, H. J., Bae, S., and Hong, B. H. (2012). "Anomalous Behaviors of Visible Luminescence from Graphene Quantum Dots: Interplay between Size and Shape", *ACS Nano*, 6(9), 8203-08.

Kim, S., Shin, D. H., Kim, C. O., Kang, S. S., Joo, S. S., Choi, S.-H., Hwang, S. W., and Sone, C. (2013b). "Size-dependence of Raman scattering from graphene quantum dots: Interplay between shape and thickness", *Applied Physics Letters*, 102(5), 053108.

Kim, W., Lee, J. S., Shin, D. H., and Jang, J. (2018). "Platinum nanoparticles immobilized on polypyrrole nanofibers for non-enzyme oxalic acid sensor", *Journal of Materials Chemistry B*, 6(8), 1272-78.

Koch, G. H., and Strong, F. M. (1969). "Determination of oxalate in urine", *Analytical Biochemistry*, 27(1), 162-71.

Kosynkin, D. V., Higginbotham, A. L., Sinitskii, A., Lomeda, J. R., Dimiev, A., Price, B. K., and Tour, J. M. (2009). "Longitudinal unzipping of carbon nanotubes to form graphene nanoribbons", *Nature*, 458(7240), 872-6.

Kotakoski, J., Brand, C., Lilach, Y., Cheshnovsky, O., Mangler, C., Arndt, M., and Meyer, J. C. (2015). "Toward Two-Dimensional All-Carbon Heterostructures via Ion Beam Patterning of Single-Layer Graphene", *Nano Letters*, 15(9), 5944-49.

Kroto, H. W., Heath, J. R., O'Brien, S. C., Curl, R. F., and Smalley, R. E. (1985). "C₆₀: Buckminsterfullerene", *Nature*, 318(6042), 162-63.

Kuang, H., Zhao, Y., Ma, W., Xu, L., Wang, L., and Xu, C. (2011). "Recent developments in analytical applications of quantum dots", *TrAC Trends in Analytical Chemistry*, 30(10), 1620-36.

Kumar, S., Tripathi, A., Khan, S. A., Pannu, C., and Avasthi, D. K. (2014a). "Radiation stability of graphene under extreme conditions", *Applied Physics Letters*, 105(13), 133107.

Kumar, S., Tripathi, A., Singh, F., Khan, S. A., Baranwal, V., and Avasthi, D. K. (2014b). "Purification/annealing of graphene with 100-MeV Ag ion irradiation", *Nanoscale Research Letters*, 9(1), 126.

Lauwerys, R., and Lison, D. (1994). "Health risks associated with cobalt exposure — an overview", *Science of The Total Environment*, 150(1), 1-6.

Lee, I., Loew, N., Tsugawa, W., Ikebukuro, K., and Sode, K. (2019). "Development of a third-generation glucose sensor based on the open circuit potential for continuous glucose monitoring", *Biosensors and Bioelectronics*, 124-125, 216-23.

Lee, J., Kim, K., Park, W. I., Kim, B.-H., Park, J. H., Kim, T.-H., Bong, S., Kim, C.-H., Chae, G., Jun, M., Hwang, Y., Jung, Y. S., and Jeon, S. (2012). "Uniform Graphene Quantum Dots Patterned from Self-Assembled Silica Nanodots", *Nano Letters*, 12(12), 6078-83.

Li, B., Nan, Y., Zhang, P., and Song, X. (2016). "Structural characterization of individual graphene sheets formed by arc discharge and their growth mechanisms", *RSC Advances*, 6(24), 19797-806.

Li, H., Kang, Z., Liu, Y., and Lee, S.-T. (2012). "Carbon nanodots: synthesis, properties and applications", *Journal of Materials Chemistry*, 22(46), 24230.

Li, L., Li, L., Wang, C., Liu, K., Zhu, R., Qiang, H., and Lin, Y. (2015a). "Synthesis of nitrogen-doped and amino acid-functionalized graphene quantum dots from glycine, and their application to the fluorometric determination of ferric ion", *Microchimica Acta*, 182(3), 763-70.

- Li, L., Wu, G., Yang, G., Peng, J., Zhao, J., and Zhu, J. J. (2013a). "Focusing on luminescent graphene quantum dots: current status and future perspectives", *Nanoscale*, 5(10), 4015-39.
- Li, S., Li, Y., Cao, J., Zhu, J., Fan, L., and Li, X. (2014). "Sulfur-doped graphene quantum dots as a novel fluorescent probe for highly selective and sensitive detection of Fe³⁺", *Analytical Chemistry*, 86(20), 10201-07.
- Li, X., Rui, M., Song, J., Shen, Z., and Zeng, H. (2015b). "Carbon and Graphene Quantum Dots for Optoelectronic and Energy Devices: A Review", *Advanced Functional Materials*, 25(31), 4929-47.
- Li, X., Zhu, H., Wang, K., Cao, A., Wei, J., Li, C., Jia, Y., Li, Z., Li, X., and Wu, D. (2010). "Graphene-on-silicon Schottky junction solar cells", *Adv Mater*, 22(25), 2743-8.
- Li, Y.-H., Zhang, L., Huang, J., Liang, R.-P., and Qiu, J.-D. (2013b). "Fluorescent graphene quantum dots with a boronic acid appended bipyridinium salt to sense monosaccharides in aqueous solution", *Chemical Communications*, 49(45), 5180-82.
- Li, Y., Hu, Y., Zhao, Y., Shi, G., Deng, L., Hou, Y., and Qu, L. (2011). "An Electrochemical Avenue to Green-Luminescent Graphene Quantum Dots as Potential Electron-Acceptors for Photovoltaics", *Advanced Materials*, 23(6), 776-80.
- Li, Y., Shu, H., Wang, S., and Wang, J. (2015c). "Electronic and Optical Properties of Graphene Quantum Dots: The Role of Many-Body Effects", *The Journal of Physical Chemistry C*, 119(9), 4983-89.
- Li, Y., Xie, M., Zhang, X., Liu, Q., Lin, D., Xu, C., Xie, F., and Sun, X. (2019). "Co-MOF nanosheet array: A high-performance electrochemical sensor for non-enzymatic glucose detection", *Sensors and Actuators B: Chemical*, 278, 126-32.
- Lim, S. Y., Shen, W., and Gao, Z. (2015). "Carbon quantum dots and their applications", *Chem Soc Rev*, 44(1), 362-81.
- Lin, L., Rong, M., Luo, F., Chen, D., Wang, Y., and Chen, X. (2014). "Luminescent graphene quantum dots as new fluorescent materials for environmental and biological applications", *TrAC Trends in Analytical Chemistry*, 54, 83-102.
- Liu, G., Nguyen, Q. T., Chow, E., Böcking, T., Hibbert, D. B., and Gooding, J. J. (2006). "Study of Factors Affecting the Performance of Voltammetric Copper Sensors

Based on Gly-Gly-His Modified Glassy Carbon and Gold Electrodes", *Electroanalysis*, 18(12), 1141-51.

Liu, J.-J., Zhang, X.-L., Cong, Z.-X., Chen, Z.-T., Yang, H.-H., and Chen, G.-N. (2013). "Glutathione-functionalized graphene quantum dots as selective fluorescent probes for phosphate-containing metabolites", *Nanoscale*, 5(5), 1810-15.

Liu, R., Wu, D., Feng, X., and Müllen, K. (2011a). "Bottom-Up Fabrication of Photoluminescent Graphene Quantum Dots with Uniform Morphology", *Journal of the American Chemical Society*, 133(39), 15221-23.

Liu, X., Gao, W., Zhou, X., and Ma, Y. (2014). "Pristine graphene quantum dots for detection of copper ions", *Journal of Materials Research*, 29(13), 1401-07.

Liu, Y., Deng, C., Tang, L., Qin, A., Hu, R., Sun, J. Z., and Tang, B. Z. (2011b). "Specific Detection of d-Glucose by a Tetraphenylethene-Based Fluorescent Sensor", *Journal of the American Chemical Society*, 133(4), 660-63.

Liu, Y., Huang, J., Wang, D., Hou, H., and You, T. (2010). "Electrochemical determination of oxalic acid using palladium nanoparticle-loaded carbon nanofiber modified electrode", *Analytical Methods*, 2(7), 855-59.

Lu, J., Yeo, P. S., Gan, C. K., Wu, P., and Loh, K. P. (2011). "Transforming C60 molecules into graphene quantum dots", *Nat Nanotechnol*, 6(4), 247-52.

Ma, L., Zeng, Q., Zhang, M., Wang, L., and Cheng, F. (2016). "Direct determination of oxalic acid by a bare platinum electrode contrasting a platinum nanoparticles-modified glassy carbon electrode", *Journal of Experimental Nanoscience*, 11(16), 1242-52.

Maity, D., Manna, A. K., Karthigeyan, D., Kundu, T. K., Pati, S. K., and Govindaraju, T. (2011). "Visible–Near-Infrared and Fluorescent Copper Sensors Based on Julolidine Conjugates: Selective Detection and Fluorescence Imaging in Living Cells", *Chemistry – A European Journal*, 17(40), 11152-61.

Majumder, T., and Mondal, S. P. (2016). "Advantages of nitrogen-doped graphene quantum dots as a green sensitizer with ZnO nanorod based photoanodes for solar energy conversion", *Journal of Electroanalytical Chemistry*, 769, 48-52.

Marcano, D. C., Kosynkin, D. V., Berlin, J. M., Sinitskii, A., Sun, Z., Slesarev, A., Alemany, L. B., Lu, W., and Tour, J. M. (2010). "Improved Synthesis of Graphene Oxide", *ACS Nano*, 4(8), 4806-14.

Mohanty, N., Moore, D., Xu, Z., Sreeprasad, T. S., Nagaraja, A., Rodriguez, A. A., and Berry, V. (2012). "Nanotomy-based production of transferable and dispersible graphene nanostructures of controlled shape and size", *Nat Commun*, 3, 844.

Mouras, S., Hamm, A., Djurado, D., and Cousseins, J. C. (1987). "Synthesis of first stage graphite intercalation compounds with fluorides", *Journal of Fluorine Chemistry*, 24(5), 572-82.

Ng, Y. H., Lightcap, I. V., Goodwin, K., Matsumura, M., and Kamat, P. V. (2010). "To What Extent Do Graphene Scaffolds Improve the Photovoltaic and Photocatalytic Response of TiO₂Nanostructured Films?", *The Journal of Physical Chemistry Letters*, 1(15), 2222-27.

Ngo, Y.-L. T., Choi, W. M., Chung, J. S., and Hur, S. H. (2019). "Highly biocompatible phenylboronic acid-functionalized graphitic carbon nitride quantum dots for the selective glucose sensor", *Sensors and Actuators B: Chemical*, 282, 36-44.

Novoselov, K. S., Geim, A. K., Morozov, S. V., Jiang, D., Zhang, Y., Dubonos, S. V., Grigorieva, I. V., and Firsov, A. A. (2004). "Electric Field Effect in Atomically Thin Carbon Films", *Science*, 306(5696), 666.

Ohno, Y., Maehashi, K., and Matsumoto, K. (2010). "Label-free biosensors based on aptamer-modified graphene field-effect transistors", *J Am Chem Soc*, 132(51), 18012-3.

Ohno, Y., Maehashi, K., Yamashiro, Y., and Matsumoto, K. (2009). "Electrolyte-gated graphene field-effect transistors for detecting pH and protein adsorption", *Nano Lett*, 9(9), 3318-22.

Oliver, N. S., Toumazou, C., Cass, A. E. G., and Johnston, D. G. (2009). "Glucose sensors: a review of current and emerging technology", *Diabetic Medicine*, 26(3), 197-210.

Ozbek, N., Tinas, H., and Atespare, A. E. (2019). "A procedure for the determination of trace metals in rice varieties using microwave induced plasma atomic emission spectrometry", *Microchemical Journal*, 144, 474-78.

Pacios Pujadó, M. (2012). "Carbon Nanotubes as Platforms for Biosensors with Electrochemical and Electronic Transduction"

Pan, D., Guo, L., Zhang, J., Xi, C., Xue, Q., Huang, H., Li, J., Zhang, Z., Yu, W., Chen, Z., Li, Z., and Wu, M. (2012). "Cutting sp² clusters in graphene sheets into colloidal

graphene quantum dots with strong green fluorescence", *Journal of Materials Chemistry*, 22(8), 3314-18.

Pan, D., Xi, C., Li, Z., Wang, L., Chen, Z., Lu, B., and Wu, M. (2013). "Electrophoretic fabrication of highly robust, efficient, and benign heterojunction photoelectrocatalysts based on graphene-quantum-dot sensitized TiO₂ nanotube arrays", *Journal of Materials Chemistry A*, 1(11), 3551-55.

Pan, D., Zhang, J., Li, Z., and Wu, M. (2010). "Hydrothermal Route for Cutting Graphene Sheets into Blue-Luminescent Graphene Quantum Dots", *Advanced Materials*, 22(6), 734-38.

Pan, F., Chen, D., Zhuang, X., Wu, X., Luan, F., Zhang, S., Wei, J., Xia, S., and Li, X. (2018). "Fabrication of gold nanoparticles/l-cysteine functionalized graphene oxide nanocomposites and application for nitrite detection", *Journal of Alloys and Compounds*, 744, 51-56.

Patil, A. J., Vickery, J. L., Scott, T. B., and Mann, S. (2009). "Aqueous Stabilization and Self-Assembly of Graphene Sheets into Layered Bio-Nanocomposites using DNA", *Advanced Materials*, 21(31), 3159-64.

Pérez-López, B., and Merkoçi, A. (2012). "Carbon nanotubes and graphene in analytical sciences", *Microchimica Acta*, 179(1-2), 1-16.

Pfeiffer, K., Berg, W., Bongartz, D., and Hesse, A. (1997). "The Direct Determination of Urinary Oxalate by Non-Suppressed Ion Chromatography." In.: *Kooperation de Gruyter*.

Ponomarenko, L. A., Schedin, F., Katsnelson, M. I., Yang, R., Hill, E. W., Novoselov, K. S., and Geim, A. K. (2008). "Chaotic Dirac Billiard in Graphene Quantum Dots", *Science*, 320(5874), 356.

Prasad, R., Ganesh, V., and Bhat, B. R. (2016). "Nickel-oxide multiwall carbon-nanotube/reduced graphene oxide a ternary composite for enzyme-free glucose sensing", *RSC Adv.*, 6(67), 62491-500.

Pundir, C. S., and Sharma, M. (2010). "Oxalate biosensor: a review", *Journal of Scientific & Industrial Research*, 69, 489-94.

Qazi, M., Vogt, T., and Koley, G. (2007). "Trace gas detection using nanostructured graphite layers", *Applied Physics Letters*, 91(23), 233101.

Qin, X., Lu, W., Asiri, A. M., Al-Youbi, A. O., and Sun, X. (2013). "Green, low-cost synthesis of photoluminescent carbon dots by hydrothermal treatment of willow bark and their application as an effective photocatalyst for fabricating Au nanoparticles–reduced graphene oxide nanocomposites for glucose detection", *Catalysis Science & Technology*, 3(4), 1027-35.

Qu, Z.-b., Zhou, X., Gu, L., Lan, R., Sun, D., Yu, D., and Shi, G. (2013). "Boronic acid functionalized graphene quantum dots as a fluorescent probe for selective and sensitive glucose determination in microdialysate", *Chemical Communications*, 49(84), 9830-32.

Razbirin, B. S., Rozhkova, N. N., Sheka, E. F., Nelson, D. K., and Starukhin, A. N. (2014). "Fractals of graphene quantum dots in photoluminescence of shungite", *Journal of Experimental and Theoretical Physics*, 118(5), 735-46.

Razmi, H., and Mohammad-Rezaei, R. (2013). "Graphene quantum dots as a new substrate for immobilization and direct electrochemistry of glucose oxidase: Application to sensitive glucose determination", *Biosensors and Bioelectronics*, 41, 498-504.

Razzino, C. A., Sgobbi, L. F., Marciano, F. R., and Lobo, A. O. (2019). 'Graphene-Based Sensors: Applications in Electrochemical (Bio) sensing.' in, *Handbook of Graphene: Biosensors and Advanced Sensors*.

Reina, A., Jia, X., Ho, J., Nezich, D., Son, H., Bulovic, V., Dresselhaus, M. S., and Kong, J. (2009). "Large area, few-layer graphene films on arbitrary substrates by chemical vapor deposition", *Nano Lett*, 9(1), 30-5.

Ritter, K. A., and Lyding, J. W. (2009). "The influence of edge structure on the electronic properties of graphene quantum dots and nanoribbons", *Nat Mater*, 8(3), 235-42.

Robinson, J. T., Perkins, F. K., Snow, E. S., Wei, Z., and Sheehan, P. E. (2008). "Reduced graphene oxide molecular sensors", *Nano Lett*, 8(10), 3137-40.

Romanovsky, I., Yannouleas, C., and Landman, U. (2009). "Edge states in graphene quantum dots: Fractional quantum Hall effect analogies and differences at zero magnetic field", *Physical Review B*, 79(7), 075311.

Roushani, M., and Abdi, Z. (2014). "Novel electrochemical sensor based on graphene quantum dots/riboflavin nanocomposite for the detection of persulfate", *Sensors and Actuators B: Chemical*, 201(Supplement C), 503-10.

Roy, P., Chen, P.-C., Periasamy, A. P., Chen, Y.-N., and Chang, H.-T. (2015). "Photoluminescent carbon nanodots: synthesis, physicochemical properties and analytical applications", *Materials Today*, 18(8), 447-58.

Ruess, G., and Vogt, F. (1948). "Hochstlamellarer Kohlenstoff aus Graphitoxhydroxyd", *Monatshefte für Chemie*, 78(3-4), 222-42.

Salehnia, F., Faridbod, F., Dezfuli, A. S., Ganjali, M. R., and Norouzi, P. (2017). "Cerium (III) ion sensing based on graphene quantum dots fluorescent turn-off", *Journal of fluorescence*, 27(1), 331-38.

Schedin, F., Geim, A. K., Morozov, S. V., Hill, E. W., Blake, P., Katsnelson, M. I., and Novoselov, K. S. (2007). "Detection of individual gas molecules adsorbed on graphene", *Nat Mater*, 6(9), 652-5.

Sciortino, A., Marino, E., Dam, B., Schall, P., Cannas, M., and Messina, F. (2016). "Solvatochromism Unravels the Emission Mechanism of Carbon Nanodots", *J Phys Chem Lett*, 7(17), 3419-23.

Shan, C., Yang, H., Song, J., Han, D., Ivaska, A., and Niu, L. (2009). "Direct electrochemistry of glucose oxidase and biosensing for glucose based on graphene", *Analytical Chemistry*, 81(6), 2378-82.

Shang, N. G., Papakonstantinou, P., McMullan, M., Chu, M., Stamboulis, A., Potenza, A., Dhesi, S. S., and Marchetto, H. (2008). "Catalyst-Free Efficient Growth, Orientation and Biosensing Properties of Multilayer Graphene Nanoflake Films with Sharp Edge Planes", *Advanced Functional Materials*, 18(21), 3506-14.

Shen, J., Zhu, Y., Chen, C., Yang, X., and Li, C. (2011). "Facile preparation and upconversion luminescence of graphene quantum dots", *Chem Commun (Camb)*, 47(9), 2580-2.

Shen, J., Zhu, Y., Yang, X., Zong, J., Zhang, J., and Li, C. (2012). "One-pot hydrothermal synthesis of graphene quantum dots surface-passivated by polyethylene glycol and their photoelectric conversion under near-infrared light", *New J. Chem.*, 36(1), 97-101.

Shi, Y., Kim, K. K., Reina, A., Hofmann, M., Li, L. J., and Kong, J. (2010). "Work function engineering of graphene electrode via chemical doping", *ACS Nano*, 4(5), 2689-94.

Shinde, D. B., Debgupta, J., Kushwaha, A., Aslam, M., and Pillai, V. K. (2011). "Electrochemical unzipping of multi-walled carbon nanotubes for facile synthesis of high-quality graphene nanoribbons", *J Am Chem Soc*, 133(12), 4168-71.

Silvestrov, P. G., and Efetov, K. B. (2007). "Quantum dots in graphene", *Phys Rev Lett*, 98(1), 016802.

Singh, A. K., Singh, R. P., and Saxena, P. (2006). "Cobalt(II)-selective electrode based on a newly synthesized macrocyclic compound", *Sensors and Actuators B: Chemical*, 114(2), 578-83.

Sk, M. A., Ananthanarayanan, A., Huang, L., Lim, K. H., and Chen, P. (2014). "Revealing the tunable photoluminescence properties of graphene quantum dots", *Journal of Materials Chemistry C*, 2(34), 6954-60.

Song, E. J., Kang, J., You, G. R., Park, G. J., Kim, Y., Kim, S.-J., Kim, C., and Harrison, R. G. (2013). "A single molecule that acts as a fluorescence sensor for zinc and cadmium and a colorimetric sensor for cobalt", *Dalton Transactions*, 42(43), 15514-20.

Stobinski, L., Lesiak, B., Malolepszy, A., Mazurkiewicz, M., Mierzwa, B., Zemek, J., Jiricek, P., and Bieloshapka, I. (2014). "Graphene oxide and reduced graphene oxide studied by the XRD, TEM and electron spectroscopy methods", *Journal of Electron Spectroscopy and Related Phenomena*, 195(Supplement C), 145-54.

Sun, H., Gao, N., Wu, L., Ren, J., Wei, W., and Qu, X. (2013). "Highly photoluminescent amino-functionalized graphene quantum dots used for sensing copper ions", *Chemistry—A European Journal*, 19(40), 13362-68.

Sun, X., Liu, Z., Welsher, K., Robinson, J. T., Goodwin, A., Zaric, S., and Dai, H. (2008). "Nano-Graphene Oxide for Cellular Imaging and Drug Delivery", *Nano Res*, 1(3), 203-12.

Suzuki, K., Tohda, K., Tanda, Y., Ohzora, H., Nishihama, S., Inoue, H., and Shirai, T. (1989). "Fiber-optic magnesium and calcium ion sensor based on a natural carboxylic polyether antibiotic", *Analytical Chemistry*, 61(4), 382-84.

Syshchyk, O., Skryshevsky, V. A., Soldatkin, O. O., and Soldatkin, A. P. (2015). "Enzyme biosensor systems based on porous silicon photoluminescence for detection of glucose, urea and heavy metals", *Biosensors and Bioelectronics*, 66, 89-94.

Tadi, K. K., and Motghare, R. V. (2013). "Potentiometric selective recognition of oxalic acid based on molecularly imprinted polymer", *International Journal of Electrochemical Science*, 8, 3197-211.

Tam, T. V., Trung, N. B., Kim, H. R., Chung, J. S., and Choi, W. M. (2014). "One-pot synthesis of N-doped graphene quantum dots as a fluorescent sensing platform for Fe³⁺ ions detection", *Sensors and Actuators B: Chemical*, 202, 568-73.

Tan, F., Cong, L., Li, X., Zhao, Q., Zhao, H., Quan, X., and Chen, J. (2016). "An electrochemical sensor based on molecularly imprinted polypyrrole/graphene quantum dots composite for detection of bisphenol A in water samples", *Sensors and Actuators B: Chemical*, 233, 599-606.

Tang, L., Ji, R., Cao, X., Lin, J., Jiang, H., Li, X., Teng, K. S., Luk, C. M., Zeng, S., Hao, J., and Lau, S. P. (2012). "Deep Ultraviolet Photoluminescence of Water-Soluble Self-Passivated Graphene Quantum Dots", *ACS Nano*, 6(6), 5102-10.

Tang, L., Ji, R., Li, X., Teng, K. S., and Lau, S. P. (2013). "Size-Dependent Structural and Optical Characteristics of Glucose-Derived Graphene Quantum Dots", *Particle & Particle Systems Characterization*, 30(6), 523-31.

Tang, L., Wang, Y., Li, Y., Feng, H., Lu, J., and Li, J. (2009). "Preparation, Structure, and Electrochemical Properties of Reduced Graphene Sheet Films", *Advanced Functional Materials*, 19(17), 2782-89.

Tkachev, S. V., Buslaeva, E. Y., Naumkin, A. V., Kotova, S. L., Laure, I. V., and Gubin, S. P. (2012). "Reduced graphene oxide", *Inorganic Materials*, 48(8), 796-802.

Trauzettel, B., Bulaev, D. V., Loss, D., and Burkard, G. (2007). "Spin qubits in graphene quantum dots", *Nature Physics*, 3(3), 192-96.

Trevaskis, M., and Trenerry, V. C. (1996). "An investigation into the determination of oxalic acid in vegetables by capillary electrophoresis", *Food Chemistry*, 57(2), 323-30.

Tyagi, C., Lakshmi, G. B. V. S., Kumar, S., Tripathi, A., and Avasthi, D. K. (2016). "Structural changes in graphene oxide thin film by electron-beam irradiation", *Nuclear Instruments and Methods in Physics Research Section B: Beam Interactions with Materials and Atoms*, 379(Supplement C), 171-75.

Valeur, B., and Leray, I. (2000). "Design principles of fluorescent molecular sensors for cation recognition", *Coordination Chemistry Reviews*, 205(1), 3-40.

Van Slyke, D. D., and Sendroy, J. (1929). "Gasometric determination of oxalic acid and calcium, and its application to serum analysis", *Journal of Biological Chemistry*, 84(1), 217-32.

Van Tam, T., Trung, N. B., Kim, H. R., Chung, J. S., and Choi, W. M. (2014). "One-pot synthesis of N-doped graphene quantum dots as a fluorescent sensing platform for Fe³⁺ ions detection", *Sensors and Actuators B: Chemical*, 202, 568-73.

Wallace, P. R. (1947). "The Band Theory of Graphite", *Physical Review*, 71(9), 622-34.

Wang, B., Zhuo, S., Chen, L., and Zhang, Y. (2014a). "Fluorescent graphene quantum dot nanoprobe for the sensitive and selective detection of mercury ions", *Spectrochimica Acta Part A: Molecular and Biomolecular Spectroscopy*, 131, 384-87.

Wang, F., Gu, Z., Lei, W., Wang, W., Xia, X., and Hao, Q. (2014b). "Graphene quantum dots as a fluorescent sensing platform for highly efficient detection of copper (II) ions", *Sensors and Actuators B: Chemical*, 190, 516-22.

Wang, J. (2008). "Electrochemical Glucose Biosensors", *Chemical Reviews*, 108(2), 814-25.

Wang, L., Peng, C., Yang, H., Miao, L., Xu, L., Wang, L., and Song, Y. J. J. o. M. S. (2019). "Ni@carbon nanocomposites/macroporous carbon for glucose sensor", *Journal of Materials Science*, 54(2), 1654-64.

Wang, L., Wang, Y., Xu, T., Liao, H., Yao, C., Liu, Y., Li, Z., Chen, Z., Pan, D., Sun, L., and Wu, M. (2014c). "Gram-scale synthesis of single-crystalline graphene quantum dots with superior optical properties", *Nat Commun*, 5, 5357.

Wang, S., Goh, B. M., Manga, K. K., Bao, Q., Yang, P., and Loh, K. P. (2010). "Graphene as atomic template and structural scaffold in the synthesis of graphene-organic hybrid wire with photovoltaic properties", *ACS Nano*, 4(10), 6180-6.

Wang, X., Cheng, Y., You, Z., Sha, H., Gong, S., Liu, J., and Sun, W. (2015). "Sensitive electrochemical determination of oxalic acid in spinach samples by a graphene-modified carbon ionic liquid electrode", *Ionics*, 21(3), 877-84.

- Wang, Y., Chen, X., Zhong, Y., Zhu, F., and Loh, K. P. (2009a). "Large area, continuous, few-layered graphene as anodes in organic photovoltaic devices", *Applied Physics Letters*, 95(6), 063302.
- Wang, Y., and Hu, A. (2014). "Carbon quantum dots: synthesis, properties and applications", *Journal of Materials Chemistry C*, 2(34), 6921-39.
- Wang, Y., Li, Y., Tang, L., Lu, J., and Li, J. (2009b). "Application of graphene-modified electrode for selective detection of dopamine", *Electrochemistry Communications*, 11(4), 889-92.
- Wang, Y., Zhao, S., Li, M., Li, W., Zhao, Y., Qi, J., and Cui, X. (2017). "Graphene quantum dots decorated graphene as an enhanced sensing platform for sensitive and selective detection of copper(II)", *Journal of Electroanalytical Chemistry*, 797, 113-20.
- Wu, X., Tian, F., Wang, W., Chen, J., Wu, M., and Zhao, J. X. (2013). "Fabrication of highly fluorescent graphene quantum dots using L-glutamic acid for / imaging and sensing", *J Mater Chem C Mater Opt Electron Devices*, 1(31), 4676-84.
- Wu, Z. L., Gao, M. X., Wang, T. T., Wan, X. Y., Zheng, L. L., and Huang, C. Z. (2014). "A general quantitative pH sensor developed with dicyandiamide N-doped high quantum yield graphene quantum dots", *Nanoscale*, 6(7), 3868-74.
- Xie, M., Su, Y., Lu, X., Zhang, Y., Yang, Z., and Zhang, Y. (2013). "Blue and green photoluminescence graphene quantum dots synthesized from carbon fibers", *Materials letters*, 93, 161-64.
- Xu, H., Zhou, S., Xiao, L., Wang, H., Li, S., and Yuan, Q. (2015). "Fabrication of a nitrogen-doped graphene quantum dot from MOF-derived porous carbon and its application for highly selective fluorescence detection of Fe³⁺", *Journal of Materials Chemistry C*, 3(2), 291-97.
- Xu, T.-T., Yang, J.-X., Song, J.-M., Chen, J.-S., Niu, H.-L., Mao, C.-J., Zhang, S.-Y., and Shen, Y.-H. (2017). "Synthesis of high fluorescence graphene quantum dots and their selective detection for Fe³⁺ in aqueous solution", *Sensors and Actuators B: Chemical*, 243, 863-72.
- Xu, X., Ray, R., Gu, Y., Ploehn, H. J., Gearheart, L., Raker, K., and Scrivens, W. A. (2004). "Electrophoretic analysis and purification of fluorescent single-walled carbon nanotube fragments", *J Am Chem Soc*, 126(40), 12736-7.

- Yan, X., Cui, X., Li, B., and Li, L.-s. (2010a). "Large, Solution-Processable Graphene Quantum Dots as Light Absorbers for Photovoltaics", *Nano Letters*, 10(5), 1869-73.
- Yan, X., Cui, X., and Li, L.-s. (2010b). "Synthesis of Large, Stable Colloidal Graphene Quantum Dots with Tunable Size", *Journal of the American Chemical Society*, 132(17), 5944-45.
- Yang, J., Deng, S., Lei, J., Ju, H., and Gunasekaran, S. (2011). "Electrochemical synthesis of reduced graphene sheet–AuPd alloy nanoparticle composites for enzymatic biosensing", *Biosensors and Bioelectronics*, 29(1), 159-66.
- Yang, W., Chow, E., Willett, G. D., Hibbert, D. B., and Gooding, J. J. (2003). "Exploring the use of the tripeptide Gly–Gly–His as a selective recognition element for the fabrication of electrochemical copper sensors", *Analyst*, 128(6), 712-18.
- Yeh, T.-Y., Wang, C.-I., and Chang, H.-T. (2013). "Photoluminescent C-dots@RGO for sensitive detection of hydrogen peroxide and glucose", *Talanta*, 115, 718-23.
- Yi, Y., Deng, J., Zhang, Y., Li, H., and Yao, S. (2013). "Label-free Si quantum dots as photoluminescence probes for glucose detection", *Chemical Communications*, 49(6), 612-14.
- Yoon, T., Shin, W. C., Kim, T. Y., Mun, J. H., Kim, T. S., and Cho, B. J. (2012). "Direct measurement of adhesion energy of monolayer graphene as-grown on copper and its application to renewable transfer process", *Nano Lett*, 12(3), 1448-52.
- Zaremski, P. M., and Hodgkinson, A. (1962). "The determination of oxalic acid in food", *Analyst*, 87(1038), 698-702.
- Zaremski, P. M., and Hodgkinson, A. (1965). "The fluorimetric determination of oxalic acid in blood and other biological materials", *Biochemical Journal*, 96(3), 717-21.
- Zhang, H., Virally, S., Bao, Q., Ping, L. K., Massar, S., Godbout, N., and Kockaert, P. (2012a). "Z-scan measurement of the nonlinear refractive index of graphene", *Opt Lett*, 37(11), 1856-8.
- Zhang, L., Zhang, Z.-Y., Liang, R.-P., Li, Y.-H., and Qiu, J.-D. (2014). "Boron-Doped Graphene Quantum Dots for Selective Glucose Sensing Based on the "Abnormal" Aggregation-Induced Photoluminescence Enhancement", *Analytical Chemistry*, 86(9), 4423-30.

Zhang, M., Bai, L., Shang, W., Xie, W., Ma, H., Fu, Y., Fang, D., Sun, H., Fan, L., Han, M., Liu, C., and Yang, S. (2012b). "Facile synthesis of water-soluble, highly fluorescent graphene quantum dots as a robust biological label for stem cells", *Journal of Materials Chemistry*, 22(15), 7461-67.

Zhang, Y., Wu, C., Zhou, X., Wu, X., Yang, Y., Wu, H., Guo, S., and Zhang, J. (2013). "Graphene quantum dots/gold electrode and its application in living cell H₂O₂ detection", *Nanoscale*, 5(5), 1816-9.

Zhang, Y. H., Chen, Y. B., Zhou, K. G., Liu, C. H., Zeng, J., Zhang, H. L., and Peng, Y. (2009). "Improving gas sensing properties of graphene by introducing dopants and defects: a first-principles study", *Nanotechnology*, 20(18), 185504.

Zhao, Z., Wang, Z., Lu, P., Chan, C. Y. K., Liu, D., Lam, J. W. Y., Sung, H. H. Y., Williams, I. D., Ma, Y., and Tang, B. Z. (2009). "Structural Modulation of Solid-State Emission of 2,5-Bis(trialkylsilylethynyl)-3,4-diphenylsiloles", *Angewandte Chemie*, 48(41), 7608-11.

Zhou, L., Geng, J., and Liu, B. (2013). "Graphene quantum dots from polycyclic aromatic hydrocarbon for bioimaging and sensing of Fe³⁺ and hydrogen peroxide", *Particle & Particle Systems Characterization*, 30(12), 1086-92.

Zhou, M., Zhai, Y., and Dong, S. (2009). "Electrochemical sensing and biosensing platform based on chemically reduced graphene oxide", *Analytical Chemistry*, 81(14), 5603-13.

Zhu, S., Zhang, J., Liu, X., Li, B., Wang, X., Tang, S., Meng, Q., Li, Y., Shi, C., Hu, R., and Yang, B. (2012). "Graphene quantum dots with controllable surface oxidation, tunable fluorescence and up-conversion emission", *RSC Advances*, 2(7), 2717-20.

Zhu, S., Zhang, J., Qiao, C., Tang, S., Li, Y., Yuan, W., Li, B., Tian, L., Liu, F., Hu, R., Gao, H., Wei, H., Zhang, H., Sun, H., and Yang, B. (2011). "Strongly green-photoluminescent graphene quantum dots for bioimaging applications", *Chem Commun (Camb)*, 47(24), 6858-60.

Zhu, X., Zuo, X., Hu, R., Xiao, X., Liang, Y., and Nan, J. (2014). "Hydrothermal synthesis of two photoluminescent nitrogen-doped graphene quantum dots emitted green and khaki luminescence", *Materials Chemistry and Physics*, 147(3), 963-67.

Zhu, Y., Wang, G., Jiang, H., Chen, L., and Zhang, X. (2015). "One-step ultrasonic synthesis of graphene quantum dots with high quantum yield and their application in sensing alkaline phosphatase", *Chem Commun (Camb)*, 51(5), 948-51.

Zhuo, S., Shao, M., and Lee, S. T. (2012). "Upconversion and downconversion fluorescent graphene quantum dots: ultrasonic preparation and photocatalysis", *ACS Nano*, 6(2), 1059-64.

PUBLICATIONS

LIST OF JOURNAL PUBLICATIONS

1. Praveen Mishra and Badekai Ramachandra Bhat (2017) “Photoluminescence Quenching in Metal Ion (Cu^{2+} , Co^{2+}) Interacted Graphene Quantum Dots” *Macromolecular Symposia*, 376, 1600200 (1-4); DOI: 10.1002/masy.201600200
2. Praveen Mishra and Badekai Ramachandra Bhat (2018) “Synthesis and characterization of graphene quantum dots and their size reduction using swift heavy ion beam” *Radiation Effects and Defects in Solids*, 173, 232-238; DOI: 10.1080/10420150.2018.1424850
3. Praveen Mishra and Badekai Ramachandra Bhat (2019) “Aggregative ways of graphene quantum dots with nitrogen-rich edges for direct emission spectrophotometric estimation of glucose” *Spectrochimica Acta A*, 223, 117325 (1-9); DOI: 10.1016/j.saa.2019.117325
4. Praveen Mishra and Badekai Ramachandra Bhat (2019) “Calcium-Induced Photoluminescence Quenching of Graphene Quantum Dots in Hard Water: A Quick Turn-Off Sensing Approach” *ChemistrySelect*, 4, 8682-8688
5. Praveen Mishra and Badekai Ramachandra Bhat (2019) “A study on the electro-reductive cycle of amino-functionalized graphene quantum dots immobilized on graphene oxide for amperometric determination of oxalic acid” *Microchimica Acta*, 186:646 (1-10); DOI: <https://doi.org/10.1007/s00604-019-3745-6>
6. Praveen Mishra and Badekai Ramachandra Bhat “Synthesis and Characterization of Amine Functionalized Graphene Quantum Dots as Sensitizer for Anthocyanin Sensitized Hybrid Dye Sensitized Solar Cells” *Materials Research Express* (**Communicated**)
7. Praveen Mishra and Badekai Ramachandra Bhat “Graphene quantum dots as an avenue for analytical science” (**Manuscript under preparation**)
8. Praveen Mishra and Badekai Ramachandra Bhat “Even-D carbon nanostructures in photovoltaic devices” (**Manuscript under preparation**)

LIST OF CONFERENCES

1. Praveen Mishra and Badekai Ramachandra Bhat (2016). "Photoluminescence quenching in metal ion (Cu^{2+} , Co^{2+}) interacted graphene quantum dots" International Conference on Soft Materials (ICSM 2016). 12-16 December 2016, MNIT, Jaipur, Rajasthan, India.
2. Praveen Mishra and Badekai Ramachandra Bhat (2017). "Synthesis and study of photoluminescence and electrochemical properties of graphene quantum dots" International Conference on Emerging Trends in Nanomaterials Science & Technology (ICETNMST - 2017). 04-06 January 2017, NIT Nagaland, Dimapur, Nagaland, India.
3. Praveen Mishra and Badekai Ramachandra Bhat (2017). "An Investigation of Graphene Quantum Dots" International Conference on Recent Trends in Chemical Science (ICRCS-17). 12-13 January 2017, Govt. Engg. College, Bikaner, Rajasthan, India.
4. Chethana. A, Praveen Mishra, Badekai Ramachandra Bhat (2017). "Synthesis and Characterization of Graphene Quantum Dots" International Conference on Recent Advances in Material Chemistry (ICRAMC 2017), 15-17th February 2017, SRM University, Kattankulathur, Tamil Nadu, India.
5. Praveen Mishra and Badekai Ramachandra Bhat (2017). "Photoluminescence Quenching in Calcium Interacted Graphene Quantum Dots" 6th International Engineering Symposium - IES 2017. March 1-3, 2017, Kumamoto University, Japan.
6. Praveen Mishra and Badekai Ramachandra Bhat (2017). "Electrochemical Detection of Oxalic acid in aqueous solution using Graphene Quantum Dots" 5th International Conference of Indian Council of Chemist (ICC 2017), 7-9 June 2017, Kuta, Bali, Indonesia
7. Praveen Mishra and Badekai Ramachandra Bhat (2017). "Effect of ion beam exposure on graphene quantum dots" International Conference on 'Accelerators in Materials and Medical Sciences' 2017 (ICAMMS'17). 5-7 October 2017, Amity University Dubai, Dubai, UAE.
8. Praveen Mishra and Badekai Ramachandra Bhat (2018). "Oxalic acid and graphene oxide quantum dots in aqueous medium: an electrochemical

- perspective” International Conference on Science and Engineering of Materials (ICSEM 2018). 06-08 January 2018, Sharda University, Greater Noida, Uttar Pradesh, India.
9. Praveen Mishra and Badekai Ramachandra Bhat (2018). “Calcium Induced Photoluminescence Quenching in Graphene Quantum Dots” International Conference on Recent Trends in Engineering & Sciences (ICRTES 2018). 20-21 February 2018, Visakhapatnam, Andhra Pradesh, India
 10. Praveen Mishra and Badekai Ramachandra Bhat (2018). “Graphene quantum dots and its biological applications” National Conference on Convergence of Pharmaceutical Sciences and Biomedical Technology (CPSBT - 2018). 21-23 March 2018, NIPER Ahmedabad, Gujarat, India
 11. Praveen Mishra and Badekai Ramachandra Bhat (2018). “Synthesis and Characterization of Amine Functionalized Graphene Quantum Dots” Materials & Technologies for Energy Conversion and Storage (M-TECS 2018). 26-29 September 2018, BARC, Mumbai, India
 12. Praveen Mishra and Badekai Ramachandra Bhat (2018). “Synthesis and Characterization of Polymer Based Graphene Quantum Dots, Graphene Oxide Composite” APA International Conference on Advances in Polymer Science & Technology (APA 2018). 1-3 November 2018, Kathmandu, Nepal
 13. Praveen Mishra and Badekai Ramachandra Bhat (2018). “A study of the supercapacitor performance of NiO/CNT/Graphene oxide composite” 27th National Conference of Indian Council of Chemists (ICC 2018). 12-14 December 2018, NITK Surathkal, Mangalore, Karnataka, India

LIST OF WORKSHOPS

1. GIAN workshop on “Nanotechnology: From Fundamentals to Practice”. 13-17 June, 2016, IISER Thiruvananthapuram, Kerala, India.
2. GIAN workshop on “Novel Functional Materials for Energy Conversion”. 4-7 October 2016, NITK Surathkal, Karnataka, India.
3. GIAN workshop on “Modern Perspectives on Renewable Energy and Biorefinery”. 6-10 November 2017, NITK Surathkal, Karnataka, India.

CURRICULUM VITAE

Praveen Mishra

201, Sri Nilaya Apartment
Church Street, Murugeshpalya
Bangalore, Karnataka
Pin – 560017

Mobile: +91-8105110897

+91-9971626373

e-mail: praveenmishra25@hotmail.com

vicky.18.97@gmail.com

Scopus ID: 57199688441 | WOS Research ID: O-3653-2019



Objective:

A continuous pursuit to achieve research excellence by means of enhancing knowledge, skills & expertise, and to provide original contribution to the scientific community and society.

Research Interest:

- Carbon-based Nanomaterials and their applications.
- Environmentally sustainable materials development.
- Energy Storage and Conversion devices.
- Condensed Matter Physics.

Education Qualification:

- *Ph.D. Chemistry* from *National Institute of Technology Karnataka*, Surathkal, Mangaluru, Karnataka, in 2020.
- *M.Sc. Industrial Chemistry* from *Amity University* Uttar Pradesh (CGPA = 9.2) in 2010. Second in University
- *B.Sc. Industrial Chemistry* from *Deshbandhu College, Delhi University* (69%) in 2008. Stood first in college.
- *AISSCE* from *CBSE* (78%) in 2005.
- *AISSE* from *CBSE* (78%) in 2003.

Ph.D. Thesis Title:

Even-D Carbon Nanostructures for Sensing and Energy Applications

Professional Experience:

- Post-Doctoral Consultant at Momentive Performance Materials (CRD), Bangalore from November 2019 onwards.

Experience (Research Studentship: 5 year 00 months):

- Research Scholar at Malaviya National Institute of Technology, Jaipur, India, from January 2013 to January 2015
- JRF in DRDO sponsored project in School of Engineering and Technology, Sharda University, from March 2012 to July 2013.
- JRF in MTRDC, DRDO sponsored project in School of Engineering and Technology, Sharda University, October 2010 to February 2012.
- As a project trainee in Department of Phytochemistry, Analytical Chemistry and Toxicology (PACT), DIPAS, DRDO for a period of six months, January 2010 to June 2010.
- Two months training as a trainee chemical analyst at Unichem Laboratories, Ghaziabad.

Projects as Research Fellow and Intern:

- **Development and characterization of Ionic Polymer Blend Membrane Metal Composites for the application of Actuation Devices.** P.I.: Prof. R. M. Mehra, Professor Emeritus, Sharda University; Co P.I.: Dr. P. K. Singh, Associate Professor, Sharda University.
- **Development of High Dielectric Polymer composite for Pulse Powered System.**
P.I.: Prof. B. Bhattacharya, Dean SET, Sharda University; Co P.I.: Prof. R. M. Mehra, Professor Emeritus, Sharda University
- **Antioxidant activity of Flavonoid rich fraction of Sea buckthorn leaves in chemical & biological system.** Guide: M. S. Yogendra Kumar, Sc B, DIPAS DRDO.

Publications:

- **Mishra, P.,** Bhat, B.R., A Study on the Electro-Reductive Cycle of Amino-Functionalized Graphene Quantum Dots Immobilized on Graphene Oxide for Amperometric Determination of Oxalic Acid (2019) *Microchimica Acta*, 186:646, <https://doi.org/10.1007/s00604-019-3745-6>.
- **Mishra, P.,** Bhat, B.R., Calcium-Induced Photoluminescence Quenching of Graphene Quantum Dots in Hard Water: A Quick Turn-Off Sensing Approach (2019) *ChemistrySelect*, 4(29), pp. 8682-8688 <https://doi.org/10.1002/slct.201901850>.
- **Mishra, P.,** and Bhat, B.R., Aggregative ways of Graphene Quantum Dots with Nitrogen-Rich Edges for Direct Emission Spectrophotometric Estimation of Glucose (2019) *Spectrochimica Acta A*, 223, 117325 <https://doi.org/10.1016/j.saa.2019.117325>.
- Kumar, L.M., **Mishra, P.,** Bhat, B.R., Fe–PNP Pincer Complex Immobilized on Graphene Oxide as a Catalyst for Suzuki–Miyaura Coupling Reactions (2019) *Catalysis Letters*, 149 (4), pp. 1118-1124 <https://doi.org/10.1007/s10562-019-02652-7>.

- Anuma, S., **Mishra, P.**, Bhat, B.R., Copper complex with N-,O- architecture grafted graphene oxide nanosheet as a heterogeneous catalyst for Suzuki cross coupling reaction (2019) Journal of the Taiwan Institute of Chemical Engineers, 95, pp. 643-651 <https://doi.org/10.1016/j.jtice.2018.09.029>.
- Kumar, L.M., **Mishra, P.**, Bhat, B.R., Iron pincer complex and its graphene oxide composite as catalysts for Suzuki coupling reaction (2019) Journal of Saudi Chemical Society, 23(3), pp. 307-314 <https://doi.org/10.1016/j.jscs.2018.08.005>.
- **Mishra, P.**, Bhat, B.R., Bhattacharya, B., Mehra, R.M., Synthesis and Characterization of High-Dielectric-Constant Nanographite–Polyurethane Composite (2018) JOM, 70 (7), pp. 1302-1306 <https://doi.org/10.1007/s11837-018-2877-1>.
- **Mishra, P.**, Bhat, B.R., Synthesis and characterization of graphene quantum dots and their size reduction using swift heavy ion beam (2018) Radiation Effects and Defects in Solids, 173 (3-4), pp. 232-238 <https://doi.org/10.1080/10420150.2018.1424850>.
- **Mishra, P.**, Bhat, B.R., Photoluminescence Quenching in Metal Ion (Cu²⁺, Co²⁺) Interacted Graphene Quantum Dots (2017) Macromolecular Symposia, 376 (1), art. no. 1600200 <https://doi.org/10.1002/masy.201600200>.

Book Chapters:

- **Mishra, P.**, Bhat, B.R., Correlation Between Synthesis and Properties of Graphene (2019) Graphene as Energy Storage Materials for Supercapacitors, MRF, USA Press, *Accepted*
- **Mishra, P.**, Bhat, B.R., Zero-dimensional carbon nanostructures for supercapacitors (2019) Morphology Design Paradigm for Supercapacitor, CRC Press, *Accepted*

Conference and Workshops:

- 37th National Conference of Indian Council of Chemists (ICC-2018) 12-14 December 2018, NITK Surathkal, Mangalore, India
- International Conference on 'Advances in Polymer Science and Technology' 2018 (APA 2018), 1st – 3rd November, 2018, Kathmandu, Nepal
- Materials & Technologies for Energy Conversion and Storage (M-TECS 2018) September 26-29, 2018, BARC Mumbai, India
- National Conference on Convergence of Pharmaceutical Sciences and Biomedical Technology (CPSBT - 2018). 21-23 March 2018, NIPER Ahmedabad, Gujarat, India
- International Conference on Recent Trends in Engineering & Sciences (ICRTES 2018). 20-21 February 2018, Visakhapatnam, Andhra Pradesh, India
- International Conference on Science and Engineering of Materials (ICSEM 2018). 06-08 January 2018, Sharda University, Greater Noida, Uttar Pradesh, India.

- International Conference on 'Accelerators in Materials and Medical Sciences' 2017 (ICAMMS'17). 5-7 October 2017, Amity University Dubai, Dubai, UAE.
- 5th International Conference of Indian Council of Chemist (ICC 2017), 7-9 June 2017, Kuta, Bali, Indonesia.
- 6th International Engineering Symposium - IES 2017. March 1-3, 2017, Kumamoto University, Japan.
- International Conference on Recent Advances in Material Chemistry (ICRAMC 2017), 15-17th February 2017, SRM University, Kattankulathur, Tamil Nadu, India.
- International Conference on Recent Trends in Chemical Science (ICRCS-17). 12-13 January 2017, Govt. Engg. College, Bikaner, Rajasthan, India.
- International Conference on Emerging Trends in Nanomaterials Science & Technology (ICETNMST - 2017). 04-06 January 2017, NIT Nagaland, Dimapur, Nagaland, India.
- International Conference on Soft Materials (ICSM 2016). 12-16 December 2016, MNIT, Jaipur, Rajasthan, India.
- International conference on Science and Engineering of Materials (ICSEM-2014) (January 2014) (Organising Committee Member).
- Indo-Japan Conference on Frontier Nanomaterials for Energy (FNE-2012) (January 2012) (Organising Committee Member).
- GIAN workshop on “Modern Perspectives on Renewable Energy and Biorefinery”. 6-10 November 2017, NITK Surathkal, Karnataka, India.
- GIAN workshop on “Novel Functional Materials for Energy Conversion”. 4-7 October 2016, NITK Surathkal, Karnataka, India.
- GIAN workshop on “Nanotechnology: From Fundamentals to Practice”. 13-17 June, 2016, IISER Thiruvananthapuram, Kerala, India.
- National Workshop on Application of Nanotechnology for Defence (November 2011).
- National Conference on Futuristic Materials (September 2011).
- National Workshop on Experimental tools for characterization of Novel Materials (February 2011).

Invited Lectures:

- Guest lecture on *Understanding Electrochemical Energy Systems and Challenges* on 21st February 2019, at St. Agnes Centre for Post Graduate Studies and Research, Mangalore,

Acquired Skills:

Analytical/ Characterization Instruments:

- | | |
|-------------------------|-------------------------------|
| • HPLC. | • FTIR/IR spectrophotometer. |
| • Gas Chromatography. | • UV - Vis spectrophotometer |
| • HPTLC/TLC. | • Electrochemical Workstation |
| • SC-XRD and Powder XRD | • DSC and TGA. |

Computer/IT Skills:

- Proficient in Computer applications pertaining to the academic uses with software like MS Office, OriginPro, Chemical Drawing Suits etc. to name a few.

Soft Skills:

- Trained in Behavioural Science.
- Excellent Communication Skills.
- Elementary level knowledge of French Language.

Achievements and Awards:

- **Young Scientist Award** for Best Oral presentation in Inorganic Section at 37th ICC 2018, NITK Surathkal, Mangalore, Karnataka
- **2nd best poster** presented in Indo-Japan Conference on Frontier Nanomaterials for Energy (FNE-2012).
- **Second** in CGPA in **M.Sc. Industrial Chemistry** from **Amity University, Noida-125** in 2010.
- **First** in 3rd semester, **Second** in 4th semester and **Third** in first and 2nd semester in **M.Sc Industrial Chemistry** from **Amity University, Noida-125** during 2008-10.
- **First rank** in 1st, 3rd, and Cumulative aggregate (Year 2006 and 2008) in **B.Sc Industrial Chemistry** from **Deshbandhu College, University of Delhi**.

Other Activities:

- **Paragliding** in **Sohanam** conducted by **NEFA** in year 2003.
- Qualified **UN** and **UNESCO** information test with **48%** and **45%** marks respectively in year 2002.
- **Adventure Camp** in **Manali** with A-Grade certificate in year 2002.
- **1st prize** in **Science Quiz Competition** at school level in year 2000.

Personal Details:

Father's Name : Yatindra Nath Mishra
Mother's Name : Pranita Mishra
Date of Birth : 25th July 1987
Nationality : Indian
Sex : Male
Blood Group : B+
Language Known : Hindi, English, French (elementary)
Interests : Photography, Reading, Music, Dance and Sports.